Copyright Warning & Restrictions

The copyright law of the United States (Title 17, United States Code) governs the making of photocopies or other reproductions of copyrighted material.

Under certain conditions specified in the law, libraries and archives are authorized to furnish a photocopy or other reproduction. One of these specified conditions is that the photocopy or reproduction is not to be "used for any purpose other than private study, scholarship, or research." If a, user makes a request for, or later uses, a photocopy or reproduction for purposes in excess of "fair use" that user may be liable for copyright infringement,

This institution reserves the right to refuse to accept a copying order if, in its judgment, fulfillment of the order would involve violation of copyright law.

Please Note: The author retains the copyright while the New Jersey Institute of Technology reserves the right to distribute this thesis or dissertation

Printing note: If you do not wish to print this page, then select "Pages from: first page # to: last page #" on the print dialog screen

Protein Separation

With

Mathematical Modeling For Chromatographic Operation

By

Hsien-Chih Ma

Dissertation Submitted to the Faculty of the Graduate School of the New Jersey Institute of Technology in Partial fulfillment of the requirements for the degree of Doctor of Engineering Science

1989

Approval Sheet

Title of Dissertation

Protein Separation

With

Mathematical Modeling for Chromatographic Operation

Name of Candidate

Hsien-Chih Ma

Doctor of Engineering Science, 1989

Thesis and Abstract Approved :

Dr. Ching-Rong Huang, Professor Department of Chemical Engineering, Chemistry and Environmental Science	Date

Vita

Name : Hsien-Chih Ma

Secondary education : Kwei Sun High School, Taipei, Taiwan, 1967

Institution attended	Date	Degree
Taipei Institute of Technology	1970 - 1975	B.S. Ch.E.
New Jersey Institute of Technology	1980 - 1982	M.S. Ch.E.
New Jersey Institute of Technology	1982 - 1989	D. Eng. Sc.

Major : Chemical Engineering

Minor : Computer Science

Publications

1. "Parametric Pumping with pH and Electric Field : Protein Separations," M.S. Thesis, 1981, NJIT
2. "Parametric Pumping with pH and Electric Field : Protein Separations," Industrial & Engineering Chemistry Fundamentals, 21, 1982, p. 205 - 214

ABSTRACT

Title of Thesis: Protein Separation with Mathematical Modeling for Chromatographic Operation

Hsien-Chih Ma, Doctor of Engineering Science, 1989

Thesis directed by: Dr. Ching-Rong Huang

We have performed experiments and derived mathematical models for packed bed columns used for liquid phase chromatographic separations of proteins with impulse input of feed solutions. These models can now be used to describe the relationships between the elution characteristics (peak height, peak position, and shapes) and the operating conditions (flow rate, and buffer conditions) of ion exchange and gel permeation column chromatography for protein separations.

The surface adsorption model was discussed relative to the nature of the mobile and stationary phases in ion exchange column chromatography for two distinct cases: with and without pore diffusion. For large solute molecules, such as proteins and enzymes, the surface adsorption model without pore diffusion is adequate for prediction of elution profiles from ion exchange columns. This model is shown to be sufficient, since the solute molecules can not readily diffuse into the solid matrix of column packings. For smaller solute molecules, such as amino acids and peptides, one must consider both the pore diffusion in the solid

matrix and the axial dispersion in the mobile phase. A separate gel permeation model for chromatography was developed to focus on the diffusion of solute molecules involving no adsorption on the solid phase.

The retention times of the large solute molecules are less than that of smaller molecules because of the lower probability for diffusion into the solid matrix of column packings. Thus, the application of a specific model depends on the origin of packing materials in the chromatography column, the size of solute molecules, and the interactions between the solid and mobile phases. Effects of model parameters (column length, cross sectional area, flow rate, effective contact area, void fraction, particle size, axial dispersion, mass transfer coefficient, equilibrium constant, and pore diffusivity) on the calculated elution profiles are discussed based on the "series mass transfer mechanism". These effects are incorporated to describe the transport behaviors of solute molecules between the solid and liquid phases.

The model protein system of a hemoglobin and an albumin mixture was experimentally separated by cycling the change of pH in ion exchange column chromatography experiments, in order to study the transport relationship between the protein elution profile and transient pH wave. A pH phase lag within the column

is needed to define for the pH cyclic zone operation in order to verify the elution characteristics between the experimental and predicted elution profiles. The success of our cycling techniques and models is further shown on the real protein system where we purified alkaline phosphatase from human placenta on an ion exchange packed bed with cycling of the buffer concentration. The optimal protein separation technique resulted in a high recovery and high purity product for this real protein enzyme system. The concentration phase lag and iso-ionic points are defined and combined with the relationships between the buffer concentrations and model parameters in order to predict the elution characteristics. The calculated and the experimental profiles are shown to be in good agreement when using the surface adsorption model without pore diffusion.

The derived models can also be applied to determine the Number of Theoretical Plates (N) and Height Equivalent to Theoretical Plates (HETP) from the calculated profiles (peak height, peak width, retention time, and retention volume). The model parameters can be obtained from the limited experimental data for the desired operating conditions (mobile phase composition, flow rate, and column dimensions) in order to evaluate the column efficiency and optimization of column operation.

Dedication

To my parents, Mr. and Mrs. Ma

To my parents-in-law, Mr. and Mrs. Tien

To my wife, Mimi and lovely children

Acknowledgment

The author is eternally grateful to the guidance and help received from Dr. Ching-Rong Huang during the preparation of this dissertation. Without his great enthusiasm and advanced concepts in theoretical modeling and experimental work, this accomplishment would have been unreachable. The author also appreciates and recognizes the valuable training received from Dr. Hung-Tsung Chen (deceased) in aspects of experimental techniques and inspiring insight during his master thesis.

Most of all, the author would like to express his appreciation to his family members for their understanding and pertinent encouragement. Finally, the author wishes to dedicate the entire work to those who have been very helpful in making this dissertation possible.

TABLE OF CONTENTS

List of Figures

Figure Page

Figure Page

Figure Page

List of Tables

Table Page

Table Page

1. Introduction

Separation in general

A substantial number of unit operations in chemical engineering are concerned with the problem of changing the composition of solutions and mixtures through methods not involving chemical reactions. Usually, these operations are directed toward separating a substance into its component parts. There are few chemical processes which do not require a preliminary purification of raw materials or final separation of products from by products, and for such purposes the mass transfer operations are usually used.

Because of the variation of physical significance of materials or mixtures to be handled, there are many different categories of mass transfer operations designed for different systems. Such as, direct contact of immiscible phases, phases separated by a membrane, direct contact of miscible phases, use of surface phenomena by direct and indirect operations. The direct operations produce the two phases from a single phase solution by adding or removal of heat. The indirect operations involves addition of a foreign substance and include gas absorption and stripping, adsorption, drying, leaching, liquid extraction and certain type of fractional crystallization.

Nevertheless, the method of separation applied to the specific system will necessarily depend on specific physical characteristic of the material to be separated; for some reasons; it is required to modify or develope other alternatives at the very beginning of the separation. New separation techniques should be always investigated for further demand.

1.1 Significance of protein and enzyme purification and chromatographic operation process

Proteins and enzymes are found in nature in complex mixtures, usually in cells which contain different proteins of different biological functions. In most of cases some other enzymes will act to interfere with one another. In order to study the properties and behavior of an enzyme as a chemical catalyst or a means to a metabolic mechanism in the living cell or for its use in biotechnology, it is necessary to isolate the enzyme from the mixture. Because they originate in complex mixtures and due to the requirements of high purity, there is always a demand to develope new ideas and techniques to achieve such purification.

In general, proteins can be separated from each other and from other kinds of molecules on the basis of such

characteristics as size, solubility, charge, and binding affinity using such techniques as precipitation, crystallization, electrophoresis, and column chromatography.

The study of chromatographic techniques is a subject which has been rapidly developing for separation in science and engineering (Chemical engineering education, 1981). In recent years the purification of proteins by column chromatography has become the most effective of all the separation methods in both preparative and analytical applications. The mechanism of the separation in different cases depends on adsorption, ion exchange, specific affinity to immobilized ligands or gel permeation or partition between two phases. In practice the physical application technique is usually similar for all. In fact, the chromatographic processes are mild techniques that do not involve heat generation or shear forces and their application can bring about clinically significant improvements in the quality of pharmaceutical drugs and other related products.

Due to the rapid progress, modern biotechnology has produced an increasing list of substances that have previously been in short supply or simply not available (C&EN 1987). Genetically engineered enzymes, hormones, plasma proteins, vaccines and antiviral drugs, such as interferone, are all candidates for purification by large scale chromatography. It is therefore logical to develope a generalized chromatographic technique to

handle the enormous variety of proteins. The necessity of systematic method development applied to the specific properties of proteins for production scale chromatograpgy optimization is obvious.

1-2 Background of parametric pumping and cyclic zone

The basic principle of parametric pumping is to apply the chromatographic operation in the coupling of periodic change in some intensive variable (such as temperature, pressure, pH, polarity, ionic strength, or electric field) and periodic changes in flow direction to separate the components of a fluid which flow past a solid adsorbent. Techniques commonly used in the chromatographic operation include: ion exchange/adsorption-desorption, gel filtration with molecular sieves, affinity chromatography, normal phase or reverse phase chromatography. All of these might be adapted to parametric pumping. In practice, the adaptation could be made in those chromatographic operations by setting up a variation of an intensive variable in order to create a reversible mass distribution between a mobile and stationary phase.

A similar separation process was developed by cyclic variation of a cycling zone adsorption (Barker and Pigford,

1971). The experimental results were reported to have capacity of cyclic separation with higher production rate than the oscillating flow process (Wilhelm and Sweed, 1968). This process was compared experimentally for the purification of the enzyme alkaline phosphatase by Chen et.al., 1981b and Ahmed, 1981. Under identical operating conditions, parametric pumping gave a higher purification factor and larger percent enzyme activity recovered, while cycling zone adsorption had a higher throughput rate. The enzyme purity received from both processes was two to three times better than the commercial available products.

1-2-1 Parametric pumping

The idea of parametric pumping was first introduced by Wilhelm and his coworkers in 1966. In 1968 Wilhelm and Sweed separated toluene from n-heptane using silica gel as adsorbent and temperature as intensive variable. The parametric pumping can be classified into two categories, based on the method of variation of process variable. As shown in Figure 1, the "direct mode", the control variable in the entire column is changed completely with the change of fluid flow direction. One example is temperature change through an entire packed bed by changing the temperature of the jacket as applied in "thermal parametric pumping". The "recuperative mode", the control

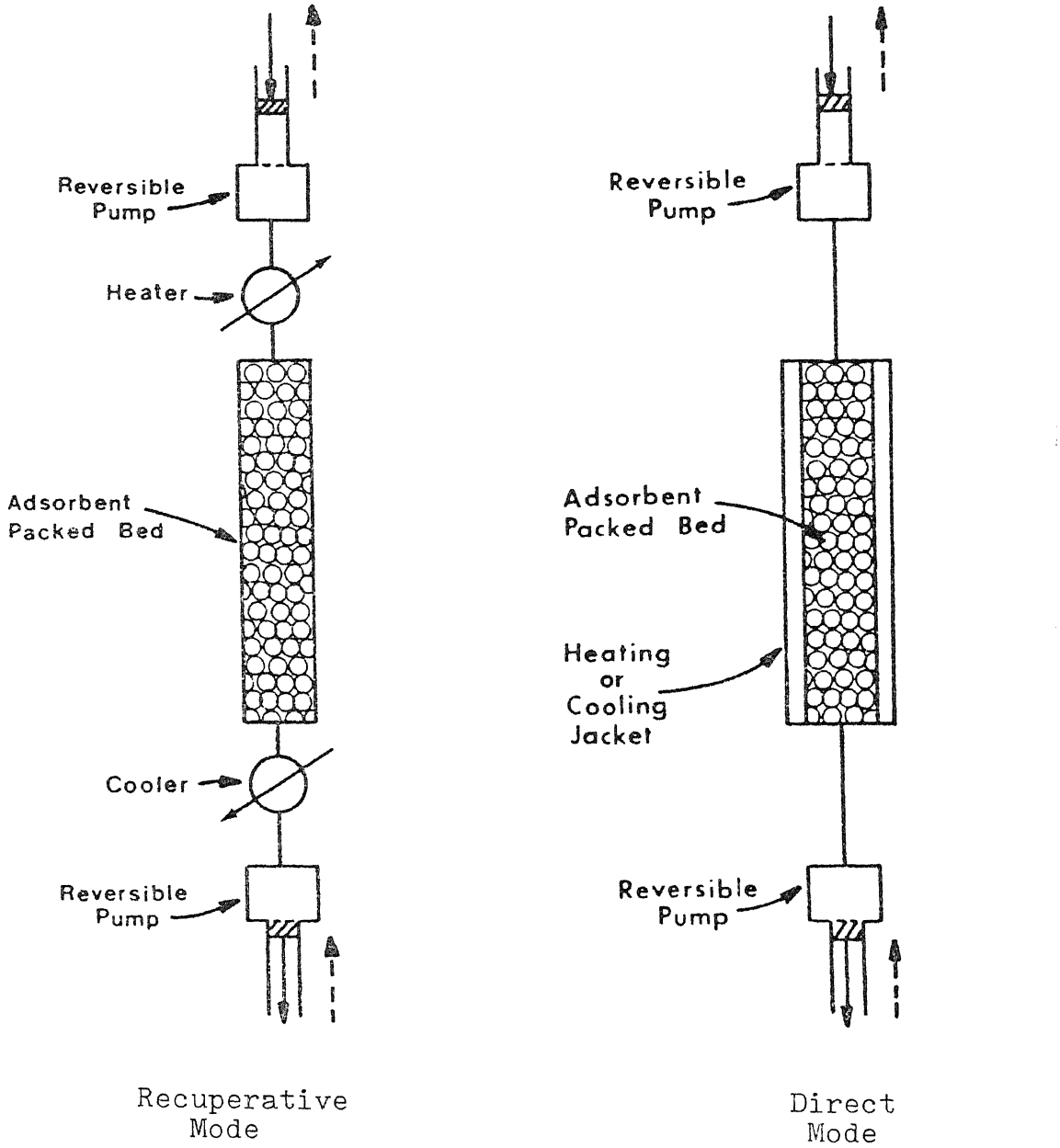

Fig. 1. Direct Mode and Recuperative Mode Operation

variable is changed from one end to the other end within the column after the change of fluid of direction. One example is to introduce hot fluid into top of a column and allow the cold fluid to emerge into a reservior during the first half cycle as shown in " thermal parametric pumping".

The work studied in thermal parametric pumping for directed mode are by Stokes in 1976, Stokes and Chen, 1979. The recuperative thermal mode are studied by Wilhelm et.al., 1966 and 1968; Rolke and Wilhelm, 1969; Gregory, 1974; Sweed and Rigaudeau, 1975; and Wankat, 1978b. The early study by Wilhelm; showed that the separation by direct mode is far superior to that of recuperative mode, due to the inefficiency of temperature swing response. Pressure swing adsorption has been wildly applied in separation of gas mixtures. Frank B. Hill and co-workers have developed pressure swing and thermal swing processes for the separation of hydrogen isotopes (Wong and Hill, 1979; Wong et.al., 1980; Chen et.al., 1981, and Hill et.al., 1982). Earlier work on the separation of hydrogen isotopes was done by Weaver and Hamrin, 1974. The separation of salt from water is of popular interest since the late 1960s. It has been studied by Wilhelm et.al., 1968; Rolke and Wilhelm, 1969; Chen et.al., 1976; Rice and Foo, 1981.

The protein separation of the model system Hemoglobin-Albumin was examined experimentally using recuperative mode pH

parametric pumping by Chen et.al., (1977, 1979a, 1980a, 1980b, 1981a). The incorporation of electric field and pH as separation parameter was studied by Huang et.al., 1982. The experimental separation in the region of over 100 have been achieved.

1-2-2 Cycling zone adsorption

Cycling zone adsorption may be operated in the "Standing Wave Mode" or the "Traveling Wave Mode". Those modes are analogous to the direct mode or the recuperative mode of parametric pumping respectively. The separation strategy and principle is identical to that of parametric pumping except that there is no change in flow direction in cyclic zone adsorption.

Cycling zone was first developed by Pigford in 1969 by examining cyclic changes in concentration of a fluid which flow through a fixed bed of solid adsorbent where the temperature of the bed is cycled. The separation is governed by the wave propagation properties of the bed. Gupta and Sweed in 1971, and Barker and Pigford in 1971 presented a theoretical explanation for temperature cyclic zone adsorption.

Van Der Vlist, E in 1971 applied the cyclic zone adsorption to the enrichment of oxygen and nitrogen in air. Wankat in 1974

published a review of cyclic separation processes. It covers heatless or pressure swing adsorption, parametric pumping and cycling zone adsorption as possible continuous preparative hromatographic separation method for ion exchange columns. Busbice and Wankat in 1975 applied the traveling pH wave for the separation of fructose and glucose from their aqueous solutions on an ion exchange resin. A countercurrent distribution theory was modified for pH waves and extended to Langmuir isotherms. Later, Nelson and Wankat in 1976 presented the application of cycling zone separation to preparative high pressure liquid chromatography. Dore and Wankat in 1976 applied multicomponent cycling zone adsorption to the glucose-fructose-water system by a discrete staged traveling pH wave mode of operation. Similar work in cyclic separation techniques was presented by Wankat in 1978. Ahmed and Chen in 1981, demonstrated the enzyme purification on a pH cycling zone adsorption process and compared the result with parametric pumping. Under the same buffer condition, cycling zone adsorption had a purification factor of 1.6 and parametric pumping had 2.8. However, cycling zone adsorption had higher product production rate.

The procedures involved in the separation of protein mixtures are generally tedious. The main concerns are the purity of the component of interest and the maintenance of its biological activity during the separation procedures. Parametric pumping and cycling zone adsorption have been shown

historically to be potential processes for protein separation. Thus, new separation methodologies applicable to chromatographic column operation are worthy of further study. However, there are many different protein systems in nature and each of them is biologically different in many ways. Obviously the way to separate them will be different. Cycling zone and parametric pumping are the useful means of separation which can be practiced as a favorable engineering process. Parametric pumping or the cycling zone can be scaled up for preparative purpose since the underlying strategy and principle are identical.

1-3 Review of packed bed

There are two theories, the plate theory and the rate theory, developed to study packed bed operation. It is obvious that when one understands the causes of peak spreading in terms of experimental conditions and physical parameters of the packed bed, he may be capable of operating the system more efficiently. The plate model was one of the earliest attempts to describe chromatography in a more mathematical manner. Starting from the assumption of a linear distribution isotherm, the separating efficiency of a chromatographic column is characterized by the height equivalent to a theoretical plate (H.E.T.P.). This H.E.T.P. is an empirical quantity and the theory does not deal with the mechanism which determine it. It is, however, of much practical value for column behavior evaluation.

The rate theory in principle provides all information on the influence of kinetic phenomena such as rate of mass transfer between phases, rate of adsorption, axial dispersion and flow behavior on the history of a band in the column. The basic difficulty lies in arranging an adequate physical concept to describe the phenomena of the movement of a solute molecule in and around the particles. This is why various authors differ in their way of treatment.

1-3-1 The plate theory

The various plate models apply the following simplifying assumptions.

1. As the name suggests, the chromatographic column is visualized as being divided into volume elements, or plates.
2. At each plate, the partition of the solute between the mobile and stationary phases is assumed to be fast so that it reaches equilibrium before moving on to the next plate.
3. The partition coefficient of the solute is the same in all plates, and are concentration independent.
4. Diffusion of the solute in the axial direction can be neglected.

5. The flow of the mobile phase is regarded as being discontinuous.

In some treatments, the flow proceeds in term of increments, each having the volume of one plate, while in others increments are infinitely similarly small. The plate model is schematically represented in Figure 2.

The plate model was first developed by Martin et.al in 1941. It was discussed by Gluechauf in 1955 and by Kenlemans in 1959. The application of plate model for ion exchange chromatography of amino acid was studied by Bogue et.al in 1960. The experiments were designed to study underlying mechanism and extend the usefulness of the theoretical approach for substance of biological interest. Snyder, 1967, 1969 and Steward, 1968 investigated the effect of packing particle diameter (d_p) on column efficiency in liquid-solid chromatography (LSC). They suggest that the use of porous adsorbents with d_p less than 40 micrometers should lead to improved performance due to increased rates of solute mass transfer. Knox and Saleem, 1972, studied the independent contribution to the plate height from process occurring in the mobile and stationary phases in GC. They found the plate height as a function of velocity under different column pressures, and with different carrier gases. Snyder, L.R. in

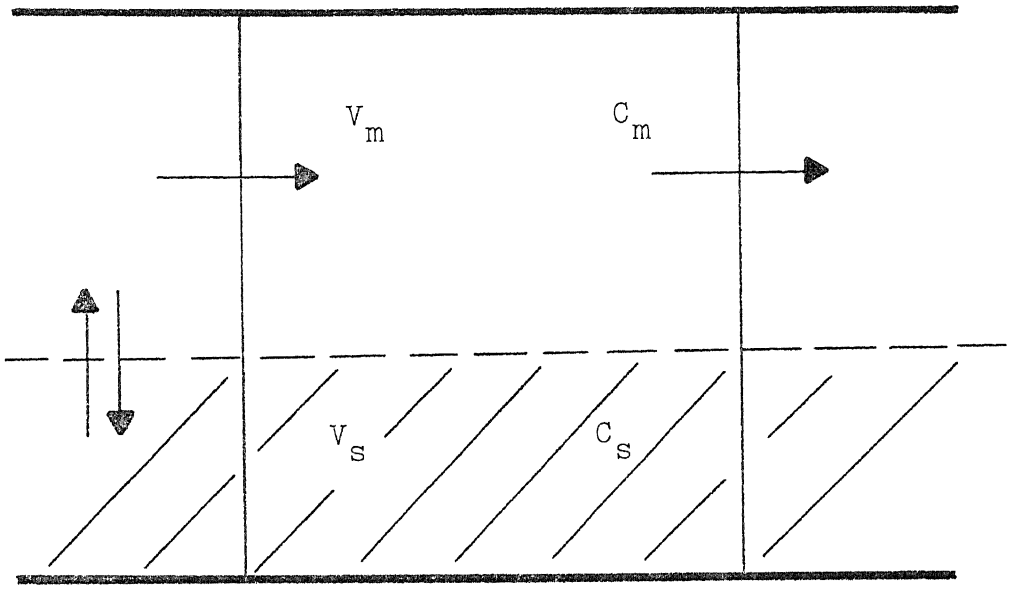

Fig. 2. A schematic diagram of the plate model.

C_m and C_s are the solute concentrations in the mobile and stationary phases.

V_m and V_s are the volumes of the mobile and stationary phases.

1972 developed a simple procedure applied to rapid selection of experimental conditions for achieving the optimum resolution in liquid column chromatography. Grushka, Snyder, and Knox in 1975 presented various theoretical and semi-theoretical approaches concerning zero dispersion in a chromatographic column. Similar work was done by Knox in 1977 to describe the basic principles of solute retention and band dispersion in chromatography by using the reduced parameter approach. Consideration of the problems in obtaining the optimum combination of elution speed, plate efficiency and economical use of pressure drop leads to the conclusion that column packing of d_p of around 5 micrometer or less in particle size. The column dimensions of 5mm bore and 100mm long, a plate number of between 7000 and 10000 should be obtained.

Kazuhiro et.al in 1983 presented a simple mathematical model for prediction of elution of proteins on an ion exchange column. Mainly, the model assumes two parameters: the distribution coefficient and number of plates. The distribution coefficient of proteins depends on ionic strength of the elution buffer. The number of plates is determined by the moment method. The peak position and peak width are predicted both by numerical calculation and a graphical method. Later, an article describing various proteins which are eluted both by stepwise and linear gradient elution on DEAE ion exchangers under a variety of experimental conditions was presented. The graphical method for

prediction of peak position was found to be applicable only when the elution curves were symmetrical.

The plate model is quite popular in chromatographic column efficiency evaluation due to the simple and compact algebra calculation. However, the model is developed based upon questionable assumptions. Those are listed as follows:

(1). Axial dispersion of the solute molecules can not be neglected. Since it contributes significantly to the broadening of the slow moving solute zone.
(2). The partition coefficient is concentration independent only for dilute concentrations.
(3). A discontinuous flow is obvious wrong in most chromatographic methods.
(4). The continuous flow also manifests itself in assuring that the chromatographic system is almost never in a state of true equilibrium.

In spite of these simplifications, the plate theory succeeds in several aspects. It is able to approximate, in some cases, the shape of the eluted peak, and it gives a measure of the system efficiency, namely the number of plates and plate height, H. However, the model did not indicate directly the connection between column processes and band spreading. The column efficiency mainly depends on carrier velocity, axial dispersion,

equilibrium relationships, mass transfer rate, particle size, and column dimensions, in addition to other parameters. The plate model does provide some simple equations based on mathematics of the Poisson distribution to account for individual share in plate height. As such it made an important contribution to the underlying chromatographic operation behavior.

Part of this work is to derive the governing equations describe the complexity of chromatographic operation based on the rate theory considering the combined operating mechanisms. The derived equations will be shown in Chapter 2, and the results are then explicitly related to the simple equations of plate theory to combine with the key phenomena and the column operating variables in a compact mathematical form. The results will be discussed in Chapter 6.

1-3-2 The rate theory

Many models have been developed to simulate the packed bed operation based upon rate theory. These models mostly apply the assumptions that the mass transfer rate between two phases is governed by one or more of the following mechanisms:

1. The axial dispersion of solute in the mobile phase.
2. The film resistance of solute molecule in the mobile phase to diffusion through the stagnant film of stationary phase.

3. The internal diffusion of solute molecules through the porous support of solid particles.
4. The equilibrium and rate of adsorption onto the solid particles.

Hougen and Marshall, 1947 presented a model to describe isothermal packed bed operation. They did not consider the axial dispersion in the mobile phase. However, they established the linear concentration relationship between the mobile and stationary phase, with mass transfer is controlled by external diffusion and surface adsorption. Similar work was done by Lapidus and Amundson in 1952 to examine the result of axial dispersion both in equilibrium and non-equilibrium cases. Van Deemter, Zniderweg and Klinkenberg, 1956, simplified the rigious treatment of Lapidus and Amundson and applied the empirical quantity of height equivalent to a theoretical plate (H.E.T.P) to examine the band broadening in linear and nonideal chromatography. The development of nonideality is caused by axial eddy diffusion and the fact that of transfer coefficient is finite and the assumption of linear isotherm. Chao and Hoelscher, 1966, used the method of moments to study the simultaneous axial dispersion and surface adsorption in a packed bed. Zwiebel et.al. 1971, 1972, 1974, investigated the external diffusion mechanism and attributed the difference between the adsorption and desorption to the nonlinearity of adsorption.

Bird et.al. 1960 and mickley et.al. 1957 developed the surface adsorption model by neglecting the axial dispersion and obtained an analytical solution in intergal form.

Rosen in 1952 was the first to propose that the adsorption process is governed simultaneously by internal and external diffusion. By assuming a linear equilibrium isotherm, unit imposed surface concentration on stationary phase, and ignoring the axial dispersion, Rosen obtained an analytic solution in a form of complicated infinite integral and determined by an approximation method. In addition, Rosen, 1954, carried out the integration by numerical method. Kasten et.al. 1952, studied the same mechanism as that of Rosen and obtain an analytic solution. In 1953, Deisler and Wilhelm examined all the mechanisms by using the steady state frequency response of a cosine input. They concluded that axial dispersion contributes a significant effect on adsorption process. Masamune and Smith, 1964, 1965, found that the internal surface adsorption occurred rapidly and the overall adsorption rate is governed by internal diffusion. They also presented an analytic solution in intergal form for the adsorption process controlled both by external and internal discussion. In 1968, Schneider and Smith evaluated the equilibrium constant, the adsorption rate constant, and internal diffusivities for light hydrocarbons by using the method of moments. Recently (1980, 1981), the pore diffusion model has been solved analytically by Rasmuson et.al.. This has also been solved numerically by Raghaven and Ruthven in 1983.

In a review of the development of rate theory, various attempts have been made to set up a simple model to complex model. However, there are still some disadvantages in establishing boundary conditions which are sufficiently related with the model itself and reality. Prior studies suggest that the concentration at the end of the column is assumed to be approximated as linear, or at infinite length of column is approaching to zero. These simplified conditions are not quite true according to actual operations.

In this work, an accurate and novel approach using the law of mass conservation for the fulfillment of rigorous treatment in setting up the boundary conditions is developed. Also, the derivation of unsteady state packed bed mass transfer equations, solved analytically by Laplace transform is presented. Those will be discussed as:

(1). The continuity equation considers the mass balance of solute in mobile phase.

(2). The rate equation of solute mass balance upon stationary phase.

(3). The linear equilibrium relationship accounts for the solute concentration linkage between mobile and stationary phase.

Those equations are derived in Sec. 2-1 for ion exchange chromatography. Within that section, the surface adsorption model and surface adsorption with pore diffusion model are

distinguished by the significance of diffusion in the solid phase. In the surface adsorption model, the stationary phase diffusion D_s is assumed to be negligible. The rate equation is expressed as the combined effects of stagnant film resistance and the driving force of the concentration difference between the solid and mobile phases. The pore diffusion model assumes the diffusion of solute molecules are significant in both fluid and solid phases. The rate equations both for the liquid and solid phase are expressed as a second order partial differential equations. It is reasonable to assume linear equilibrium isotherm for both models, because most of separations conducted by chromatography are under dilute feed input (especially, the biological mixtures or toxic wastes are employed).

In Sec. 2-2, the gel permeation model will be derived assuming solute diffusion is significant for both the mobile and stationary phase. No equilibrium relationship is evolved due to inertness of the solid phase. The separation is mainly achieved by the difference in diffusivity of solute molecules in both phases. Two continuity equations are set up to describe individually the behavior of the for the solute molecule in the two phases.

The models derived in Sec. 2-1 and 2-2 will be applied in Chapter 6 for application of chromatographic column evaluation by using the results of the derived model to calculate the elution

profile based on column parameters. From the calculated profile, the plate theory equations can be applied for the evaluation. The surface adsorption model will also be applied to the study of ion exchange chromatography separation of proteins and enzyme for elution prediction, separation strategy development, and optimization. The model protein system of hemoglobin and albumin will be discussed in Chapter 4 and real system alkaline phosphatase will be discussed in Chapter 5.

1-4 The ion exchange resin and protein purification

1-4-1 Ion exchange resin and its chromatography

An ion exchanger consists of an insoluable matrix to which charged groups have been covalently bound. The charged groups are associated with mobile counter ions. Those counter ions can be reversibly exchanged with other ions of the same charge without altering the matrix. It is possible to have both positive and negative ion exchangers. Positively charged exchangers have negatively charged counter ions (anions) available for exchanger and so are termed anion exchangers. Negatively charged exchangers have positively charged counter ions (cations) and are termed cation exchangers. The two types of ion exchangers can be further sub-divided into strong and weak depending on the dissociation constant of the inorganic groups of the resin.

The matrix may be based on inorganic compounds, synthetic

resins, polysaccharides etc. The nature of the matrix determines its physical properties such as its mechanical strength, flow characteristics, behavior towards biological substances, and to a certain extent, its capacity. Conventional resin beads are prepared by copolymerization of styrene and divinylbenzene with a degree of cross linking to provide mechanical stability. They may be of two types, microreticular (gel) and macroreticular (macroporous). From these original gel type ion exchangers, porous and pellicular bead material are developed. These have a solid polymer core which has ion exchange resin only on its surface, or from a glass bead with a skin of ion exchange material. The conventional resins can also be modified by using a porous surface with ion exchange properties. These bead structure are shown in Fig.3. The schematic of ion exchange resins structures in the demonstration model development will be discussed in Sec. 2-2-1 and 2-1-2.

Most ion exchange experiments are performed in two stages. The first stage is sample application and adsorption. Unbound substances can be washed out from the exchanger bed using a column volume of starting buffer. In the second stage, substances are eluted from the column, separated from each other. The separation is obtained since different substances have different affinities for the ion exchanger due to difference in their charges. These affinities can be controlled by varying conditions such as ionic strength and pH.

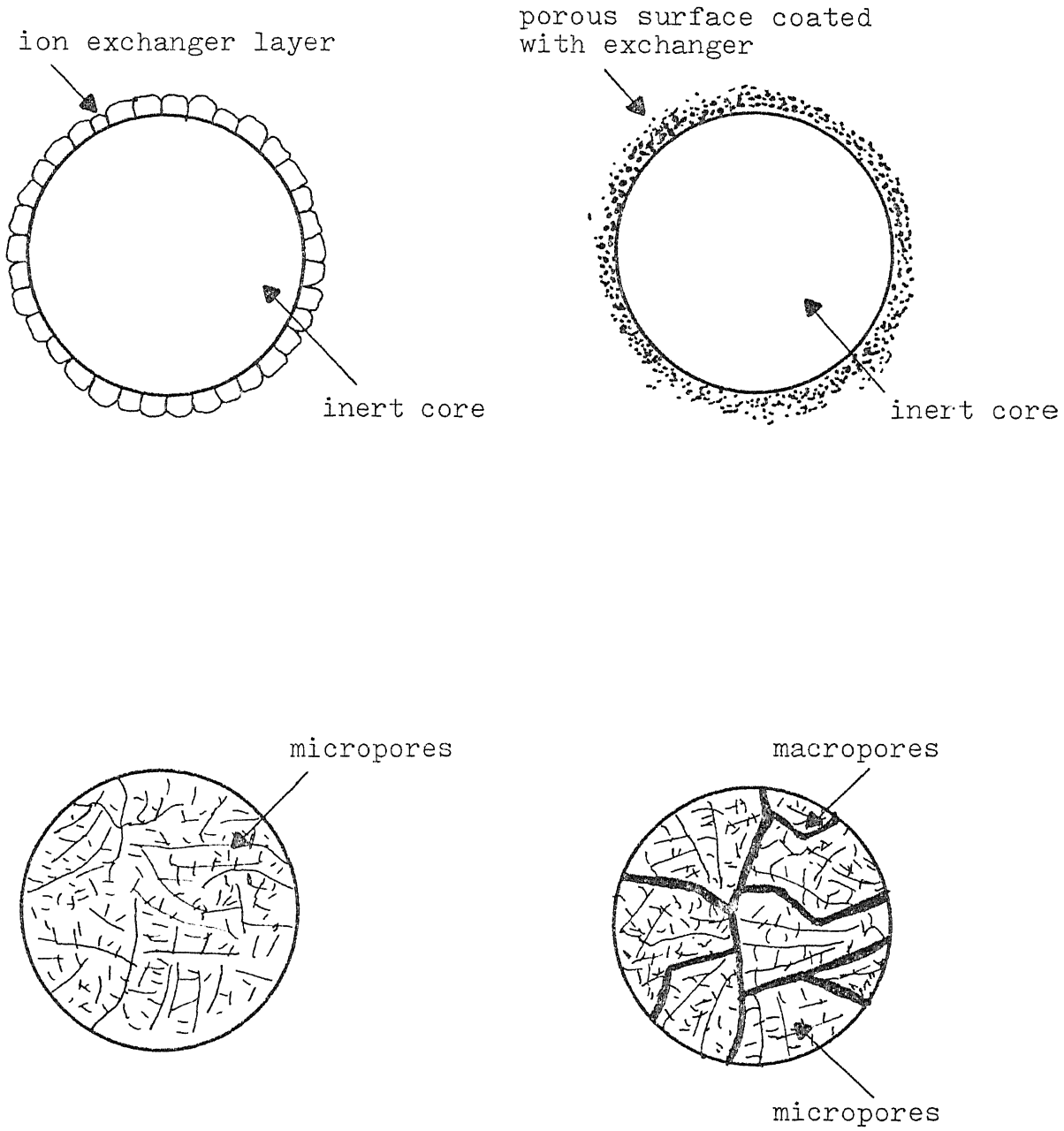

Fig. 3. Ion exchanger resins

pH dependence

Substances, proteins or enzymes, which carry both positively and negatively charged groups, however, are termed amphoteric and the charge they carry is depended on pH. At a certain pH value the substance will have zero net charge. This value is termed the isoelectric point (pI) and at this point substances are not bound to any type of ion exchanger. In principle, one could use either an anion or a cation exchanger to bind amphoteric samples by selecting the appropriate pH. This is illustrated in Fig. 4. Below its pI the protein has a net positive charge and could be adsorbed to cation exchanger. Above its pI the protein has a net negative charge and could be adsorbed to anion exchangers. In practice, however, there is a limiting factor, namely the stability. Many biological macromolecules become denatured outside a certain pH range and thus the choice of ion exchanger is limited by the stability of the sample. In summary:

1. If the sample are most stable below their pI's, a cation exchanger should be used.
2. If they are stable above their pI's, an anion exchanger should be used.
3. If stability is high over a wide pH range, either type of resin can be used.
4. The starting pH should be at least 1 pH unit above or below the pI of bound substances to facilitate adequate binding.

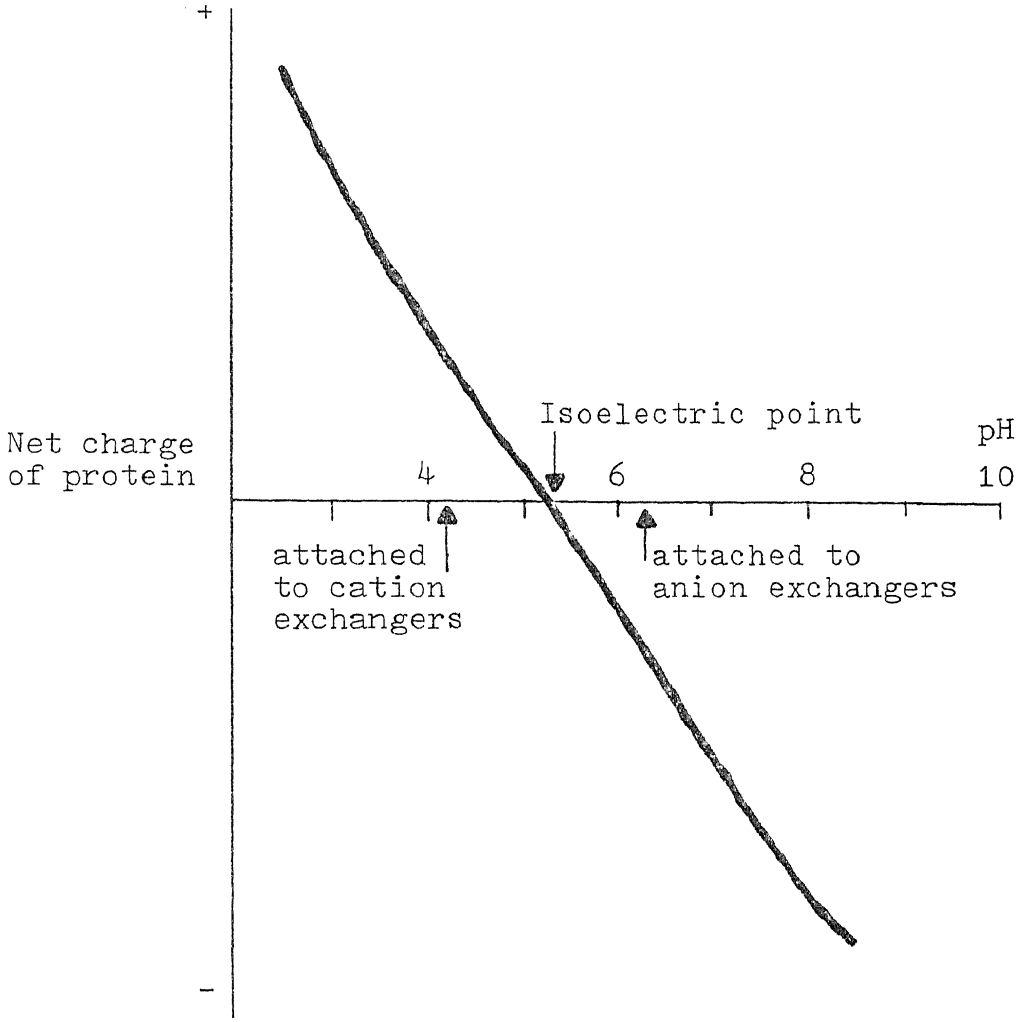

Fig. 4. The net charge of a protein as a function of pH

The application of pH dependence on protein separation will be discussed in Chapter 4.

Ionic strength dependence

After the feed solution was applied and adsorbed by an ion exchange column. At low ionic strength, generally, the competition among the charged groups for the adsorption site is low and components are bound strongly. With an increase in the buffer ionic strength, vigorous competition among charged ions for the adsorption site and reduced interaction between the ion exchanger and the sample substances may result. It will result the gradual elution depending upon the magnitude of affinity between the adsorbed component and resin. For the specific capacity of an ion exchanger, there is an ionic strength that is capable to elute one specific component of the adsorbed mixtures. Thus, other than the pI, every component has its cut off buffer concentration. In this work, the cut off point is defined as iso-ionic point or iso-concentration. To be more specific, the counter ion concentration for a ion exchanger is chosen as an index to indicate this value. For cation exchanger, the counter ion Na^+ is used and defined as pNa, similarly, the counter ion Cl^- for anion exchanger is defined as pCl. The definition of iso-concentration is illustrated in Fig. 5. In practice, buffer pH should be chosen such that sample components will carry opposite charge to that of the ion exchanger. The starting pH is

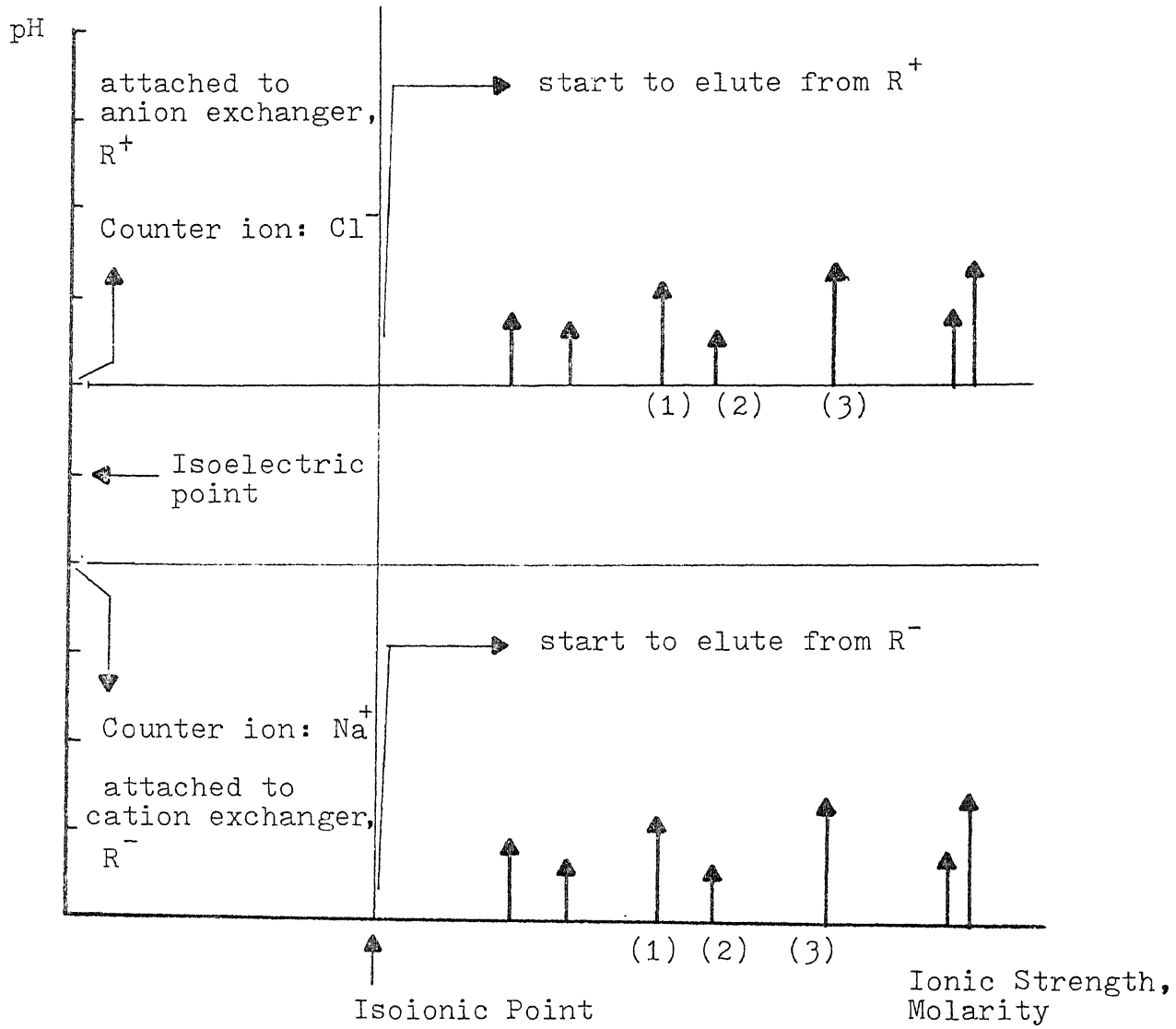

(1): 1st. isoionic point
(2): 2nd. isoionic point
(3): 3rd. isoionic point

Fig. 5. The ionic strength dependence for proteins elution

of about 1 pH unit above the pI of the substance of interest with anion exchanger and 1 pH unit below the pI for cation exchangers. Theoretically, an increase in ionic strength at constant pH (after adsorption), will start to elute the components of the mixtures individually. In general, the 2nd. isoionic point is the cut off buffer ionic strength to elute the component of interest. While the 1st. and 3rd. isoionic point are the ionic strength for the group components above and below the component of interest. In some cases, the component of interest may possibly be the first or the last one within the sample mixture so that only one isoionic point is needed for impurity elution.

1-4-2 pH cycling zone and concentration cycling zone

Cycling zone separation involves introduction of the fluid to be separated into a single column or a series of columns packed with a stationary adsorbent phase. The procedure consists primiarily of adsorption followed by desorption where the thermodynamic variables are periodically changed to force the separation to occur by every repeated adsorption/desorption. In this work, the pH and ionic strength are chosen as thermodynamic variables for ion exchange chromatography. They are named as pH cycling zone and concentration cycling zone as shown in Fig. 6. The pH cycling zone will be discussed in Chapter 4 and

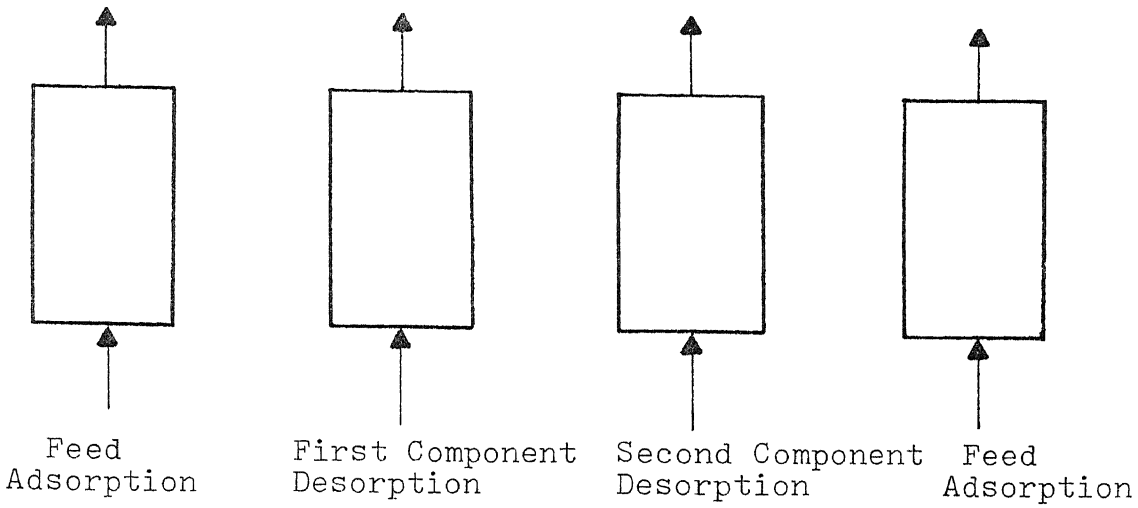

6a. pH cycling zone

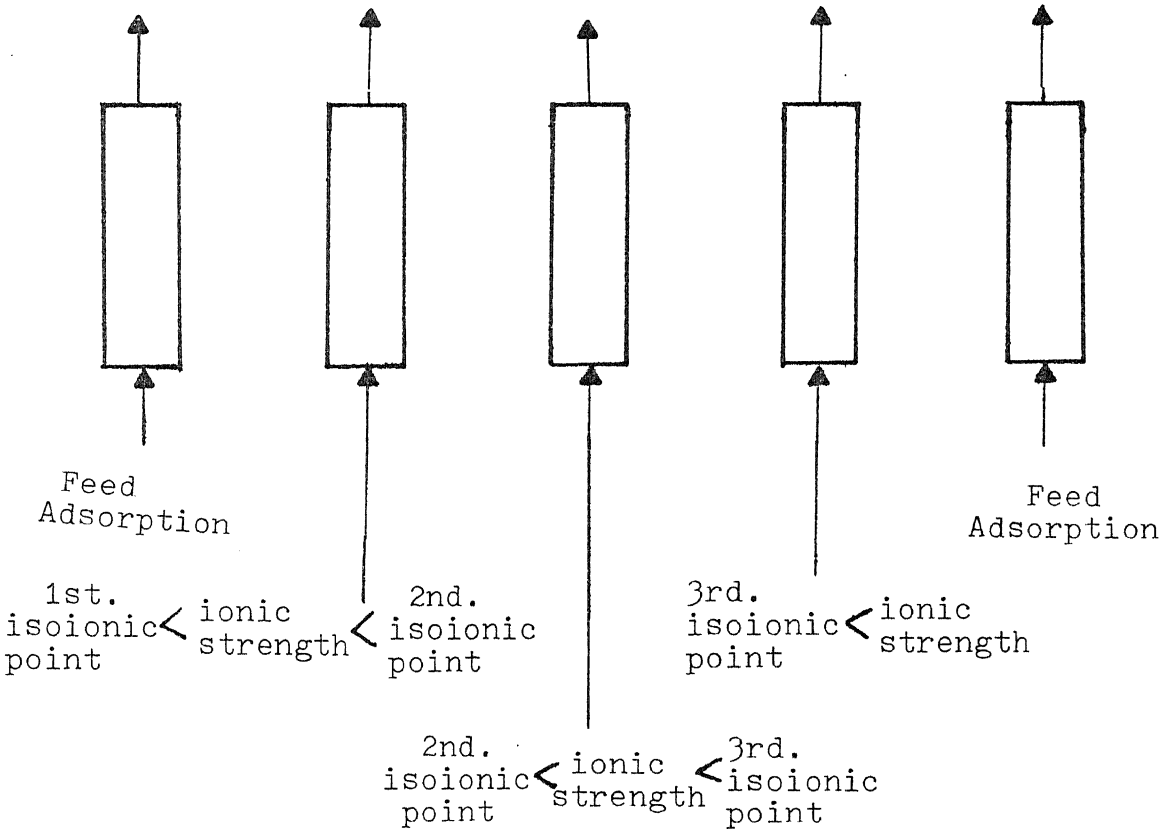

6b. Concentration cycling zone

Fig. 6. pH cycling zone and concentration cycling zone

concentration cycling zone in Chapter 5. For both example protein systems, the elution curves are predicted by the surface adsorption model and operating conditions are optimized.

pH cycling zone

Fig.6a shows the stages for pH cycling zone.

Stage 1: Adsorption. The pH of the feed solution is adjusted so that the components of interest will carry the opposite charge to that of the solid phase. The feed is then applied into the packed bed and displaces the solution at the other end of the bed. Due to the opposite charge between the sample components and the resin, the components are adsorbed onto the resin and the effluent is collected as waste. Usually, the feed volume should be applied at least one void volume of the packed bed in order to completely push out the waste.

Stage 2: Desorption. Actually, this stage may contain more than one substage depending on how many components of interest there are. If the process needs only one component, then two desorption substages are needed. The first one will only elute the component of interest. The second substage will take out the rest of components to a waste or recovery stream depending on how complete the component of interest is recovered during the first substage. Therefore, the pH value of the two incoming fluids for each substage should be adjusted so that the first

pH is just a little higher or lower than the pI value of the interested component depending on whether an anion or cation resin is used as the adsorbent. However, it should not be higher than the pH which will cause the elution of impurities. The second pH will be adjusted at a reasonable value to completely elute the rest of the components from solid phase. Thus, a cycle is completed.

Concentration cycling zone

Basically, the stages for separation are similar to that of pH cycling zone. However, the separation principles are completely different. The parameter for pH cycling zone is pH, which controls the charged group of proteins for adsorption and desorption. The parameter for concentration cycling zone, on the other hand, is the buffer ionic strength. The adsorption stage will occur for low ionic strength buffer and the desorption stage will occur for high ionic strength buffers.

The thermodynamic variable-ionic strength, will distinguish the affinity between adsorbed protein and resin into small discrete ranges. Within two consecutive buffer concentrations, the separation can be achieved by a similar strategy as that of pH cyclic zone. This methodology has an advantage for the separation of protein mixtures with very close isoelectric point and molecular weight distribution, when the conventional pH ion

exchange or size exclusion chromatography fails to achieve the satisfied separation. The illustrated separation strategy development will be discussed in Chapter 5.

Fig. 6b shows the stages for concentration cycling zone.

Stage 1: Adsorption. This stage is same as the pH cycling zone.

Stage 2: Desorption. The desorption strategy is similar to pH cycling zone but with elution buffer having higher ionic strength at the same pH value of the adsorption feed. The ionic strength of incoming fluid for first substage is close to the 2nd. isoionic point as defined in Fig. 5. This will elute the component of interest and keep the impurity from being eluted. The second substage will apply the buffer with higher ionic strength than the third isoionic point in order to completely elute the rest of the proteins. The effluent is treated as a recovery stream for Stage 1, thus, completing the cycle.

1-4-3 Comment for cycling zone and parametric pumping

As previous discussed, protein separations are wearisome procedures. The main concern of protein separation is how to obtain a satisfactory protein purity without losing its biological activity. The previous applications of parametric pumping and cycling zone on protein separation have shown that both are effective processes. There are however many protein systems in nature. Each of them is biologically and structurally

different in many ways and their separation strategy will be different also. Therefore, it is obvious that each system has to be examined individually in order to develope the proper purification methodology.

Cycling zone and parametric pumping are useful means of separation. Typical isolation processes, such as ion exchange and affinity and gel filtration chromatography, can be combined with the pre-procedures such as precipitation and crystallization and extraction for the purpose of crude protein generation and result in high purity proteins. The underlying strategy developed for bench scale purification will eventually scale up for mass production. Based on the same separation principles and strategies, the concept of parametric pumping and cycling zone may very well be candidates for scale up purposes. Actually, the cycling zone can provide the basic information for parametric pumping for method development. It will however depend on how complex the protein system is. In practice, one will have to select the right choice of solid phase and mobile phase, such as buffer system and ionic strength and pH level. In order to establish the most efficient separation procedures, sometimes, one may be content with using a series of different resins and cycling zone chromatography to achieve satisfactory results. From the running conditions derived for cycling zone, it is easy to extend the cyclic zone into a semicontinuous or continuous

parametric pumping procedure in order to obtain higher product purity. However, there is no absolute guideline to evaluate which method is superior. The cycling zone has low design cost and easy for maintenance. Parametric pumping, on the other hand, has the advantage of continuous feed input and product withdrawal but has higher design cost and complexity in operation.

2. Theory and mathematical models for packed column

The study of chromatographic packed bed operation by mathematical treatment is one of the great interests in process design. Prior development for the modeling of packed beds has been discussed in Sec. 1-3. Most of them emphasized the discussion of general mechanisms. However, very few of them have further discussion on the specific type, such as ion exchange or size exclusion column. For a given packed bed, one might be interested in the prediction of elution profile, which can be related with the operating conditions such as flow rate, column dimensions, pH and ionic strength of liquid phase and their effects on the solid phase. The models derived in this chapter will provide the application for such purpose.

Three mathematical models will be analytically solved and discussed in Sec. 2-1-1, 2-1-2, and 2-2. Two of them are for ion exchange chromatography and one is for gel permeation chromatography. For the reasons of clarity and simplicity, several common assumptions are described as following:

1. The physical and chemical stability of fluid and solid phase are held constant throughout the column.

2. The packing material are spherical particles with a narrow size distribution.

3. The end effects, caused by geometric shape at the

column inlet and outlet, are neglected.

4. Plug flow is valid within the column, so that the solute distribution in radial direction is even.

5. Impuse input is described by impuse function $\delta(t)$ with impuse strength c_I, i.e., $c_I \delta(t)$ is the input function at the column inlet at the time of zero.

2-1 Ion exchange chromatographic packed bed

In this section, two models are established for describing the ion exchange packed bed. The distinction between two models is the significance of pore diffusion within the solid matrix. The schematic diagram for two models is illustrated in Fig. 7. This figure shows the ion exchange chromatographic column operation in aspects of mobile phase transport dynamics and solute mass transfer mechanisms. Due to the insignificance of solute diffusion within the solid phase, the surface adsorption model discussed in Sec.2-1-1 will not consider pore diffusion. While the model developed in Sec. 2-1-2 will consider all mode of diffusion.

2-1-1 Surface adsorption model

model development

As shown in Fig.7, we select our system as a shell element of length Δz and cross sectional area S. We perform the mass

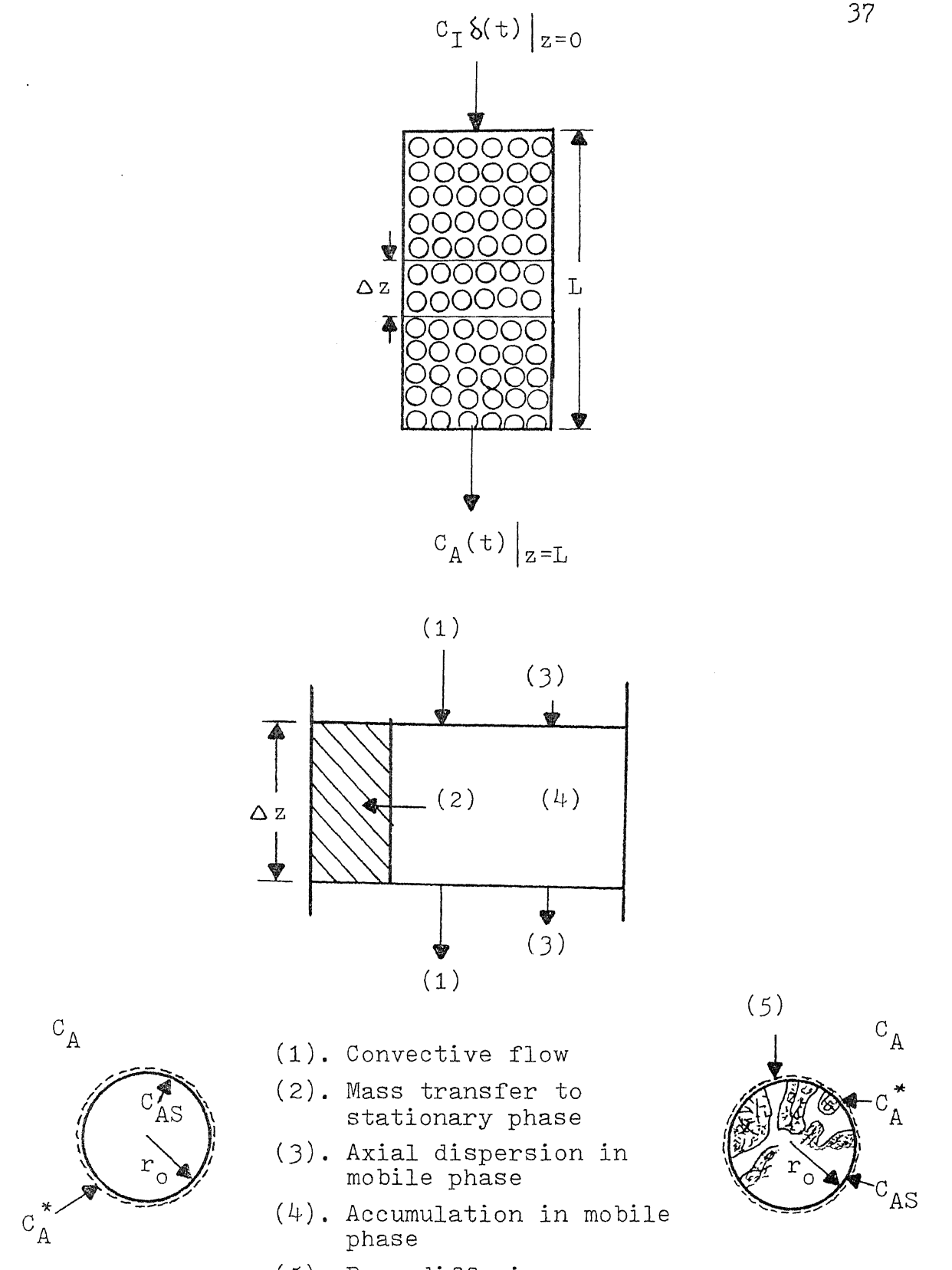

Fig. 7. Schematic diagram of ion exchange packed column

balance of component A in the Z direction. Accordingly, the following equations are set up. Material balance of component A in mobile phase:

$$S\epsilon\Delta z \frac{\partial c_A}{\partial t} = vS\, c_A\Big|_z - vSc_A\Big|_{z+\Delta z} - \frac{S\Delta z(1-\epsilon)}{4/3\pi r_o^3} 4\pi r_o^2 k_f (c_A - c_A^*) + \epsilon S N_{AZ}\Big|_z - \epsilon S N_{AZ}\Big|_{z+\Delta z}$$

where c_A is bulk concentration, c_A^* is bulk concentration at interface, ϵ is the bed porosity, r_o is the average particle size, k_f is the mass transfer coefficient, v is superficial velocity and $N_{AZ} = -E_d \frac{\partial c_A}{\partial t}$ is the mass flux due to the axial dispersion. Divide the equation by $S\epsilon\Delta Z$ and let ΔZ approach to zero. The above equation reduces to

$$\frac{\partial c_A}{\partial t} = -\frac{v}{\epsilon}\frac{\partial c_A}{\partial z} + E_d \frac{\partial^2 c_A}{\partial z^2} - \frac{ak_f}{\epsilon}(c_A - c_A^*) \qquad \text{(A-1)}$$

The terms stand for accumulation in the fluid phase, convective transport, transport by axial dispersion, and mass transfer between two phases. The symbol "a" is the effective constant surface area within per $S\Delta Z$ bed volume, and defined as

$$a = \frac{S\Delta z\ (1-\epsilon)}{4/3\,\pi r_o^3} 4\pi r_o^2 = \frac{3(1-\epsilon)}{r_o}$$

The material balance of solid phase:

$$4\pi r_o^2 \frac{\partial c_{AS}}{\partial t} = 4\pi r_o^2 k_f (c_A - c_A^*)$$

$$\text{or} \quad \frac{\partial c_{AS}}{\partial t} = k_f (c_A - c_A^*) \qquad \text{(A-2)}$$

where C_{AS} is the solid phase concentration, and Eq. A-2 stands

for surface-averaged accumulation on the spherical porous particles through the film mass transfer resistance. Under isothermal and isobaric condition, a linear relationship between the solid and liquid phase is assumed for most dilute concentration.

$$c_A^* = mc_{AS} \qquad (A-3)$$

where "m" is the slope of plot of c_A^* v.s. c_{AS} and defined as equilibrium constant which is a function of pH and ionic strength of liquid phase. Two boundary conditions and initial condition for Eq. A-1 are:

B.C. 1

$$vSc_I\delta(t)\Big|_{z=\Delta z} - vSc_A\Big|_{z=\Delta z} - S\epsilon N_{AZ}\Big|_{z=\Delta z} - \frac{S\Delta z(1-\epsilon)}{4/3\,\pi r_o^3}4\pi r_o^2 k_f(c_A - c_A^*) = \epsilon S\Delta z\frac{\partial C_A}{\partial t}$$

where $N_{AZ} = -E_d\frac{\partial c_A}{\partial z}$. Let ΔZ approach to zero and define the bulk flow rate $Q = vs$, it reduces to:

$$(Qc_I\delta(t) - Qc_A)_{z=0} + S\epsilon E_d\frac{\partial c_A}{\partial z}\Big|_{z=0} = 0 \qquad (A-4)$$

It states the back mixing at the column inlet due to the axial dispersion.

B.C. 2,

$$Q\int_{t=0}^{t}(c_I\delta(t) - c_A\Big|_{z=L})dt = \epsilon S\int_{z=0}^{z=L}c_A dz + \frac{S(1-\epsilon)}{4/3\,\pi r_o^3}4\pi r_o^2\int_{z=0}^{z=L}c_{AS}dz$$

or

$$\int_{t=0}^{t}(c_I\delta(t) - c_A\Big|_{z=L})dt = \frac{S\epsilon}{Q}\int_{z=0}^{z=L}c_A dz + \frac{3S(1-\epsilon)}{r_o Q}\int_{z=0}^{z=L}c_{AS}dz \qquad (A-5)$$

The left hand side of the equation stands for total mass balance throughout time period, t, and right hand side of the equation stand for overall mass balance in both liquid and solid phase for the whole column.

I.C. at $t = t_o = 0$

$$c_A(z,t=0) = c_{A,t_o} \qquad \text{(A-6a)}$$

$$c_A^*(z,t=0) = c_{A,t_o}^* \qquad \text{(A-6b)}$$

$$c_{AS}(z,t=0) = c_{AS,t_o} \qquad \text{(A-6c)}$$

It describes the concentration of liquid, solid, and interface at $t = 0$ and be noted that $c_A(Z,t=0) = 0$; $c_A^*(Z,t=0) = 0$; and $c_{AS}(Z,t=0) = C$ are the special cases for Eq. (A-6) and so are the following conditions are true at $t \leq 0$,

$$\int_{t=0}^{t} (0 - c_{A,t_o}\Big|_{z=L})dt = \frac{S\epsilon}{Q}\int_{z=0}^{z=L} c_{A,t_o}\,dz + \frac{3S(1-\epsilon)}{r_o Q}\int_{z=0}^{z=L} c_{AS,t_o}\,dz \qquad \text{(A-7a)}$$

equilibrium relationship;

$$c_{A,t_o}^* = m c_{AS,t_o} \qquad \text{(A-7b)}$$

and liquid concentration;

$$c_{A,t_o}^* = c_{A,t_o} \qquad \text{(A-7c)}$$

Introducing the dimensionless variables:

$$C_A = \frac{c_A - c_{A,t_o}}{c_I \frac{L^2}{E_d}}, \quad C_A^* = \frac{c_A^* - c_{A,t_o}^*}{c_I \frac{L^2}{E_d}}, \quad C_{AS} = \frac{c_{AS} - c_{AS,t_o}}{c_I \frac{L^2}{E_d}}$$

$$\tau = \frac{E_d t}{L^2}, \quad \eta = \frac{z}{L}, \quad r = \frac{m\epsilon}{a}$$

With the aid of Eq. A-7, eqns A-1 to A-6 are reduced to:

liquid phase,

$$\frac{\partial C_A}{\partial \tau} = \frac{\partial^2 C_A}{\partial \eta^2} - \frac{ak_f L^2}{\epsilon E_d}(C_A - C_A^*) - \frac{QL}{S\epsilon E_d}\frac{\partial C_A}{\partial \eta} \qquad \text{(A-8)}$$

solid phase,

$$\frac{\partial C_{AS}}{\partial \tau} = \frac{k_f L^2}{E_d}(C_A - C_A^*) \qquad \text{(A-9)}$$

equilibrium relationship,

$$C_A^* = \frac{ar}{\epsilon} C_{AS} \qquad \text{(A-10)}$$

B.C. 1

$$\frac{E_d}{L^2}\delta\left(\frac{L^2}{E_d}\tau\right) - C_A\Big|_{\eta=0} + \frac{S\epsilon E_d}{QL}\frac{\partial C_A}{\partial \eta}\Big|_{\eta=0} = 0 \qquad \text{(A-11)}$$

B.C. 2

$$\frac{E_d}{L^2}\int_0^\tau \delta\left(\frac{L^2}{E_d}\tau\right)d\tau - \int_0^\tau C_A\Big|_{\eta=1} d\tau = \frac{S\epsilon E_d}{QL}\int_{\eta=0}^{\eta=1} C_A d\eta + \frac{aSE_d}{QL}\int_{\eta=0}^{\eta=1} C_{AS} d\eta \qquad \text{(A-12)}$$

I.C. at

$$C_A(\eta, \tau=0) = 0 \qquad \text{(A-13a)}$$

$$C_A^*(\eta, \tau=0) = 0 \qquad \text{(A-13b)}$$

$$C_{AS}(\eta, \tau=0) = 0 \qquad \text{(A-13c)}$$

Taking the Laplace transform with respect to τ from Eqns. A-8 to A-12, respectively,

$$p\overline{C_A} = \frac{d^2\overline{C_A}}{d\eta^2} - \frac{ak_f L^2}{E_d}(\overline{C_A} - \overline{C_A}^*) - \frac{QL}{S\epsilon E_d}\frac{d\,\overline{C_A}}{d\eta} \qquad \text{(A-14)}$$

$$p\,\overline{C_{AS}} = \frac{k_f L^2}{E_d}(\overline{C_A} - \overline{C_A}^*) \qquad \text{(A-15)}$$

$$\overline{C_{AS}} = \frac{\epsilon}{ar}\overline{C_A}^* \qquad \text{(A-16)}$$

where "p" stands for Lapalce domain. By substituting Eq. A-16 into A-15,

$$\frac{\epsilon p}{ar}\,\overline{C_A}^{*} = \frac{k_f L^2}{E_d}\,(\,\overline{C_A} - \overline{C_A}^{*})$$

or

$$\overline{C_A}^{*} = \frac{ark_f L^2}{\epsilon p E_d + k_f L^2 ar}\,\overline{C_A} \qquad \text{(A-17)}$$

Substitute Eq. A-17 into A-14, and combine as,

$$\frac{d^2\overline{C_A}}{d\eta^2} - \left(\, p + \frac{ak_f L^2}{E_d}\,\frac{p}{(p+mk_f L^2/E_d)}\right)\overline{C_A} - \frac{QL}{S\epsilon E_d}\,\frac{d\overline{C_A}}{d\eta} = 0$$

or

$$\frac{d^2\overline{C_A}}{d\eta^2} - A\,\frac{d\overline{C_A}}{d\eta} - F(p)\,\overline{C_A} = 0 \qquad \text{(A-18)}$$

where

$$A = \frac{QL}{S\epsilon E_d},, \quad F(p) = p + \frac{Bp}{p+(mk_f L^2/E_d)}\,, \quad B = \frac{ak_f L^2}{E_d} \qquad \text{(A-18a)}$$

B.C. 1

$$\left(\frac{E_d}{L^2}\right)^2 - \overline{C_A}\Big|_{\eta=0} + \frac{1}{A}\,\frac{d\overline{C_A}}{d\eta}\Big|_{\eta=0} = 0 \qquad \text{(A-19)}$$

B.C.2

$$A\left(\left(\frac{E_d}{L^2}\right)^2 - \overline{C_A}\Big|_{\eta=1}\right) = F(p)\int_{\eta=0}^{\eta=1}\overline{C_A}\,d\eta \qquad \text{(A-20)}$$

Eq. A-18 is a second order ordinary equation and can be solved as,

$$\overline{C_A}(p,\eta) = e^{A\eta/2}\left(\, C_1 \sinh\frac{\sqrt{\Gamma}}{2}\eta + C_2\cosh\frac{\sqrt{\Gamma}}{2}\eta\right) \qquad \text{(A-21)}$$

where $\sqrt{\Gamma} = \sqrt{A^2+4F}$

Eq. A-21 is then substituted into Eqns A-19 and A-20 to set up

simultaneous equations for solving the constant C_1 and C_2, so

$$C_1 = -\left(\frac{A\cosh\frac{\sqrt{}}{2} + \sqrt{}\sinh\frac{\sqrt{}}{2}}{\cosh\frac{\sqrt{}}{2} + (A+\frac{2F}{A})\sinh\frac{\sqrt{}}{2}}\right)\left(\frac{E_d}{L^2}\right)^2 \qquad \text{(A-22)}$$

$$C_2 = \left(\frac{\sqrt{}\cosh\frac{\sqrt{}}{2} + A\sinh\frac{\sqrt{}}{2}}{\sqrt{}\cosh\frac{\sqrt{}}{2} + (A+\frac{2F}{A})\sinh\frac{\sqrt{}}{2}}\right)\left(\frac{E_d}{L^2}\right)^2 \qquad \text{(A-23)}$$

Constant C_1 and C_2 are then substitute into Eq.A-21 to have final solution of , thus,

$$\overline{C_A}(p,\eta) = e^{\frac{A\eta}{2}}\left(\frac{\frac{A}{\sqrt{}}\sinh(1-\eta)\frac{\sqrt{}}{2} + \cosh(1-\eta)\frac{\sqrt{}}{2}}{\cosh\frac{\sqrt{}}{2} + \frac{(A+2F/A)}{\sqrt{}}\sinh\frac{\sqrt{}}{2}}\right)\left(\frac{E_d}{L^2}\right)^2 \qquad \text{(A-24)}$$

Eq. A-24 is in the Laplace domain, so the next step is to take the inverse Laplace transform to get the final answer. Before taking the inverse transform, we have to examine the validity of the Eq. A-24. According to Heaviside's expansion, if the J(p)/L(p) are two polynominals such that L(p) has the higher degree and contains the factor p-a that is not repeated, then the inverse transform will be, $L^{-1}\left(\frac{J(p)}{L(p)}\right) = \sum_{n=1}^{\infty}\frac{J(p_n)}{L(p_n)}e^{p_n t}$

where p_n is any complex number. So, we have to make sure that

$$L(p) = \cosh\frac{\sqrt{}}{2} + \frac{(A+2F/A)}{\sqrt{}}\sinh\frac{\sqrt{}}{2} \qquad \text{(A-25)}$$

has higher degree than

$$J(p) = \frac{A}{\sqrt{}}\sinh(1-\eta)\frac{\sqrt{}}{2} + \cosh(1-\eta)\frac{\sqrt{}}{2} \qquad \text{(A-26)}$$

where $\sqrt{} = \sqrt{A^2+4F}$.

By expansion of hyperbolic function in terms of infinite series,

$$\cosh\frac{\sqrt{\ }}{2} = \sum_{n=0}^{\infty}(A^2+4F)^n\frac{(\frac{1}{2})^{2n}}{(2n)!} \quad , \quad \cosh\frac{1-\eta}{2}\sqrt{\ } = \sum_{n=0}^{\infty}(A^2+4F)^n\frac{(\frac{1-\eta}{2})^{2n}}{(2n)!}$$

$$\frac{1}{\sqrt{\ }}\sinh\frac{\sqrt{\ }}{2} = \sum_{n=0}^{\infty}(A^2+4F)^n\frac{(\frac{1}{2})^{2n+1}}{(2n+1)!} \quad , \frac{1}{\sqrt{\ }}\sinh\frac{\sqrt{\ }}{2}(1-\eta)=\sum_{n=0}^{\infty}(A^2+4F)^n\frac{(\frac{1-\eta}{2})^{2n+1}}{(2n+1)!}$$

and substitute into Eq. A-24 to have,

$$\overline{C_A}(p,\eta) = e^{A\eta/2}\left(\frac{\sum_{n=0}^{\infty}(A^2+4F)^n\left(\frac{(\frac{1-\eta}{2})^{2n}}{(2n)!} + A\sum_{n=0}^{\infty}\frac{(\frac{1-\eta}{2})^{2n+1}}{(2n+1)!}\right)}{\sum_{n=0}^{\infty}(A^2+4F)^n\left(\frac{(\frac{1}{2})^{2n}}{2n!} + (A+2F/A)\frac{(\frac{1}{2})^{n+1}}{(2n+1)!}\right)}\right)\frac{E_d^2}{L^4} \qquad \text{(A-27)}$$

Furthermore, express A^2+4F and $A+2F/A$ in terms of p,

$$A^2+4F = \frac{a_0p^2+a_1p+a_2}{p+a_3} \quad , \quad A+2F/A = \frac{b_0p^2+b_1p+b_2}{A(p+a_3)}$$

where,

$$a_3 = \frac{k_fL^2m}{E_d} = \alpha r \ , \ a_0=4 \ , \ a_1=4\alpha r+4B+A^2 \ , \ a_2 = A^2\alpha r \ , \ b_0=2 \ , \ b_1=2B+2\alpha r+A^2$$

$$b_2= A^2\alpha r$$

so, Eq.A-27 becomes,

$$\overline{C_A}(p,\eta) = e^{\frac{A\eta}{2}}\left(\frac{\sum_{n=0}^{\infty}\left(\frac{a_0p^2+a_1p+a_2}{p+a_3}\right)^n\left(\frac{(\frac{1-\eta}{2})^{2n}}{2n!} + A\frac{(\frac{1-\eta}{2})^{2n+1}}{(2n+1)!}\right)}{\sum_{n=0}^{\infty}\left(\frac{b_0p^2+b_1p+b_2}{p+a_3}\right)^n\left(\frac{(\frac{1}{2})^{2n}}{2n!} + \frac{b_0p^2+b_1p+b_2}{p+a_3}\frac{(\frac{1}{2})^{n+1}}{(2n+1)!}\right)}\right) \qquad \text{(A-28)}$$

From Eqns A-27 and A-28, we have the following conclusions:

1. L(p) has higher power than that of J(p).

2. No branch cut exists in Eq. A-27.

3. It has only simple poles at L(p).

Eq. A-24 becomes,

$$\overline{C_A}(p,\eta) = \frac{J(p)}{L(p)} e^{A\eta/2} \frac{E_d^2}{L^4} \qquad (A-29)$$

By the application of Residue Theorem and Heasivide's expansion, we have the inverse transform, i.e.,

$$L^{-1}(\overline{C_A}(p,\eta)) = \sum_{n=0}^{\infty} \text{residue of } e^{p_n\tau}\overline{C_A}(p,\eta) \text{ at poles } p_n$$

$$= \sum_{n=0}^{\infty} e^{A\eta/2} e^{p_n\tau} \frac{J(p_n)}{L'(p_n)} \frac{E_d^2}{L^4} \qquad (A-30)$$

Residues at

$$\cosh\frac{\sqrt{\ }}{2} + \frac{A+\frac{2F}{A}}{\sqrt{\ }}\sinh\frac{\sqrt{\ }}{2} = 0$$

Rearrange Eq. A-25 to become,

$$\tanh\frac{\sqrt{\ }}{2} = -\frac{A\sqrt{\ }}{A^2+2F} \qquad (A-31)$$

and let $A^2 + 4F = \beta_n^2$ (A-32)

Case 1: $A^2 + 4F \geq 0$

Since $\sqrt{A^2+4F} = \beta_n$ and Eq. A-31 becomes,

$$\tanh\frac{\beta_n}{2} = -\frac{2A\beta_n}{A^2+\beta_n^2} \qquad (A-33)$$

It can be shown that there is no suitable solution for Eq. A-32 except at $\beta_n = 0$.

Case 2: $A^2 + 4F < 0$

Since $\sqrt{A^2+4F}=i\beta_n$ and Eq. A-31 reduces to

$$\tanh\frac{i\beta_n}{2} = -\frac{i\beta_n}{(A^2-\beta_n^2)/2A} \quad \text{or} \quad \tan\frac{\beta_n}{2} = -\frac{2A\beta_n}{A^2-\beta_n^2} \qquad \text{(A-34)}$$

Since the "tan" is a periodic function. Thus, the eigenvalue can be solved numerically from Eq. A-34 within each $n\pi/2$ and $(n+1)\pi/2$ interval, where n is ranged from 0 to infinity. Once the β_n is obtained, each β_n is then substituted into Eq. A-32 for solving p_{nm}, where m = 1 or 2.

i.e., $A^2 + 4F = -\beta_n^2$, or $F(p) = -(A^2+\beta_n^2)/4$

and define $\varphi = (A^2 + \beta_n^2)/4$. Connecting with Eq. A-18A, we have

$$F(p) = p + \frac{Bp}{p+(mk_fL^2/E_d)} = p+\frac{Bp}{p+\alpha r} = -\varphi, \quad \text{where } \alpha r = \frac{k_fL^2m}{E_d}$$

Solved for $P_{nm} = -\frac{-G \pm \sqrt{G^2-4H}}{2}$, $\quad m=1,2 \quad 1\le n\le\infty$ (A-35)

where

$$G= \alpha r + B + \varphi, \quad H= r\alpha\varphi$$

Now, the residues at $p = p_{nm}$ or Eq. A-30 can be changed as,

$$L^{-1}(\overline{C_A}(p,\eta)) = e^{A\eta/2}\sum_{m=1}^{2}\sum_{n=0}^{\infty} e^{p_{nm}\tau}\frac{J(p_{nm})\ E_d^2}{L'(p_{nm})\ L^4} \qquad \text{(A-36)}$$

The denominator can be expressed as,

$$L'(p_{nm}) = \frac{d}{dp}\left(\cosh\frac{\sqrt{\ }}{2} + \frac{(A+\frac{2F}{A})}{\sqrt{\ }}\sinh\frac{\sqrt{\ }}{2}\right)$$

or

$$L'(p_{nm}) = \left(\frac{dF}{dp}\right)* \left(\left(\frac{1+\frac{2}{A}-2\left(\frac{A+2F/A}{A^2+4F}\right)}{\sqrt{\ }}\right)\sinh\frac{\sqrt{\ }}{2} + \frac{A+\frac{2F}{A}}{A^2+4F}\cosh\frac{\sqrt{\ }}{2}\right) \qquad \text{(A-37)}$$

where $dF/dp = \frac{d}{dp}\left(p+\frac{Bp}{\alpha r+p}\right) = 1 + \frac{B\alpha r}{(p+\alpha r)^2}$ (A-38)

However, at $p = p_{mn}$, $A^2+4F = -\beta_n^2$ and $\sqrt{A^2+4F} = i\beta_n$;

such that

$$J(p_{nm}) = \cos\frac{(1-\eta)}{2}\beta_n + \frac{A}{\beta_n}\sin\frac{(1-\eta)}{2}\beta_n \qquad \text{(A-39)}$$

$$L'(p_{nm}) = \left(1+\frac{B\alpha r}{(p_{nm}+\alpha r)^2}\right)\left(\frac{\beta_n^2(A+1)+A^2}{A\beta_n^3}\sin\frac{\beta_n}{2} - \frac{A^2-\beta_n^2}{2A\beta_n^2}\cos\frac{\beta_n}{2}\right) \qquad \text{(A-40)}$$

Substitute Eqns A-39 and A-40 into Eq. A-36 we get the final solution. Thus,

$$C_A(\eta,\tau) = \sum_{m=1}^{2}\sum_{n=0}^{\infty} e^{\left(\frac{A\eta}{2}+p_{nm}\tau\right)} \frac{\left(\beta_n\cos\frac{(1-\eta)}{2}\beta_n + A\sin\frac{(1-\eta)}{2}\beta_n\right)*\frac{E_d^2}{L^4}}{\left(1+\frac{B\alpha r}{(p_{nm}+\alpha r)^2}\right)\left(\frac{\beta_n^2(A+1)+A^2}{A\beta_n^2}\sin\frac{\beta_n}{2} - \frac{A^2-\beta_n^2}{2A\beta_n}\cos\frac{\beta_n}{2}\right)} \qquad \text{(A-41)}$$

Eq. A-41 described the concentration profile of component A at any position and instant time within the packed column for an impulse feed input. Therefore, the elution profile of component A can be obtained from Eq. A-41 for $\eta = 1$; i.e.,

$$C_A(\tau,1) = \sum_{m=1}^{2}\sum_{n=1}^{\infty} e^{\left(\frac{A}{2}+p_{nm}\tau\right)} \frac{B_n^2E_d^2}{\left(1+\frac{B\alpha r}{(p_{nm}+\alpha r)^2}\right)\left(\frac{\beta_n^2(A+1)+A^2}{A\beta_n}\sin\frac{\beta_n}{2} - \frac{A^2-\beta_n^2}{2A}\cos\frac{\beta_n}{2}\right)L^4} \qquad \text{(A-42)}$$

Note: $\beta_o = 0$

Discussion

The result of surface adsorption model Eq. A-42 describes the concentration profile at the end of the column. The calculated results are plotted individually for the effect of variation of parameters vs. concentration, such as flow rate, column length or cross sectional area and so on.

Fig.8 shows the effect of volumetric flow rate, Q. For the same size of column, the mobile phase with higher flow rate will travel through the column in less time. Because of short duration, the elution peak will be sharp and narrow for high flow rate as compared with low flow rate. Fig. 9 and Fig. 10 demonstrate the effect of column length and cross sectional area. Obviously, the large column dimension will increase the residence time of mobile phase in the column, and the elution profile will become broad with a long tail due to the axial dispersion. It implies that the small column diameter and short column length will lead to better resolution for chromatographic operation.

As mentioned earlier, the mass transfer rate of solute with the solid phase is regulated by sequential mechanisms. In order to stimulate better mass transfer rate, the resistance between two phases has to be reduced to a minimum. The mass transfer

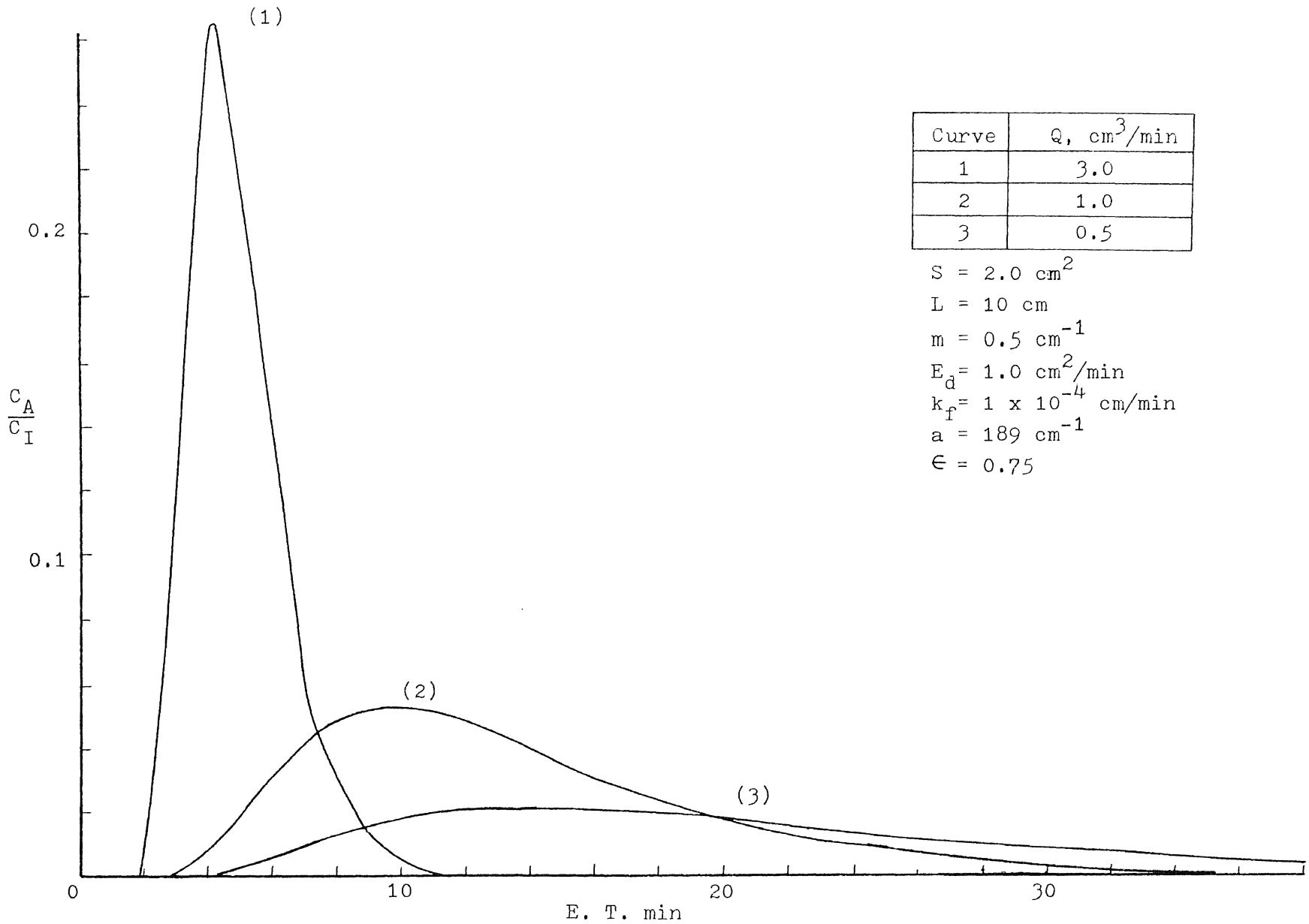

Curve	Q, cm^3/min
1	3.0
2	1.0
3	0.5

$S = 2.0\ cm^2$
$L = 10\ cm$
$m = 0.5\ cm^{-1}$
$E_d = 1.0\ cm^2/min$
$k_f = 1 \times 10^{-4}\ cm/min$
$a = 189\ cm^{-1}$
$\epsilon = 0.75$

Fig. 8 Effect of Volumetric flow rate, Q (Surface Adsorption Model)

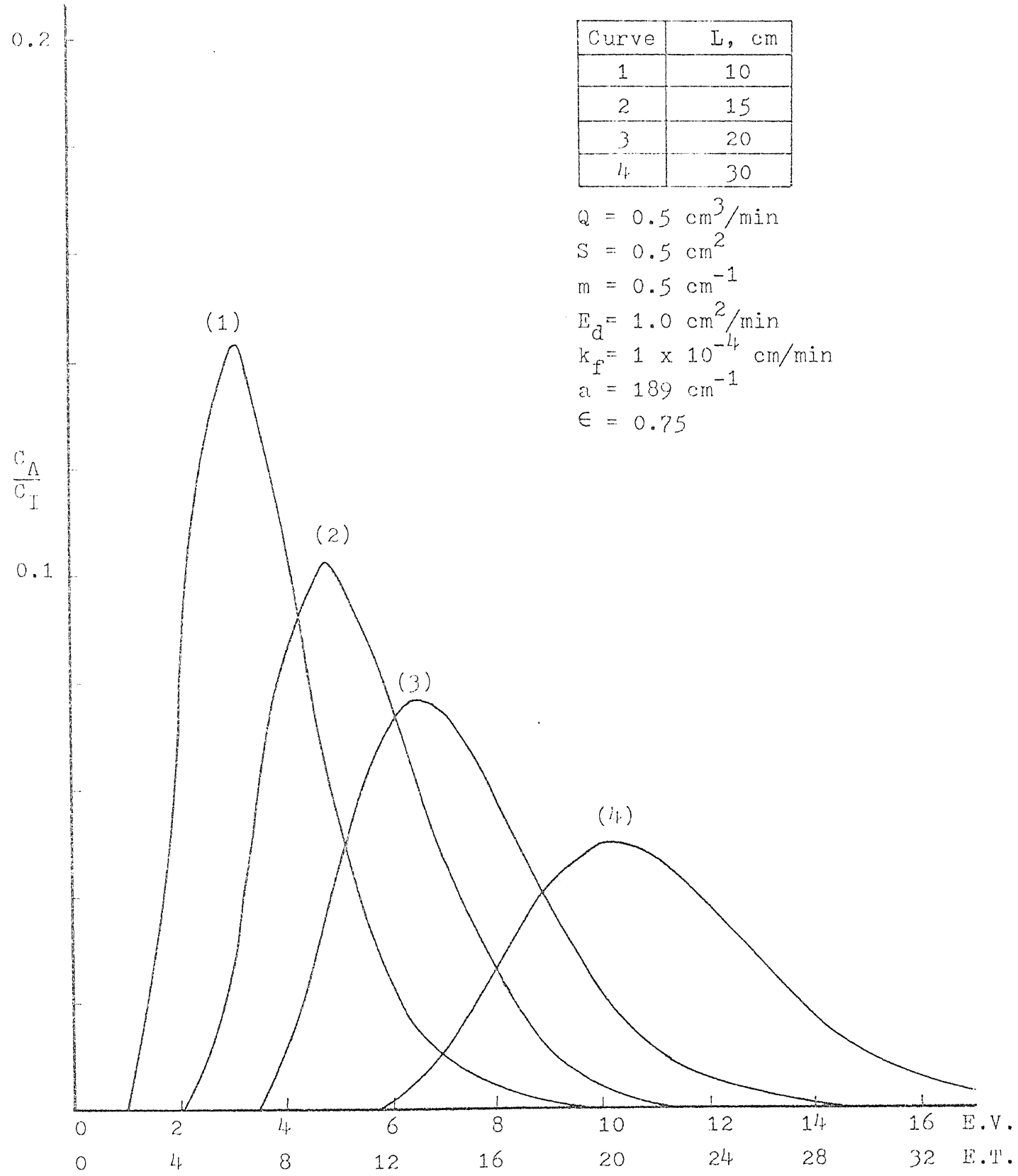

Curve	L, cm
1	10
2	15
3	20
4	30

$Q = 0.5\ cm^3/min$
$S = 0.5\ cm^2$
$m = 0.5\ cm^{-1}$
$E_d = 1.0\ cm^2/min$
$k_f = 1 \times 10^{-4}\ cm/min$
$a = 189\ cm^{-1}$
$\epsilon = 0.75$

Fig. 9 Effect of Column Length, L

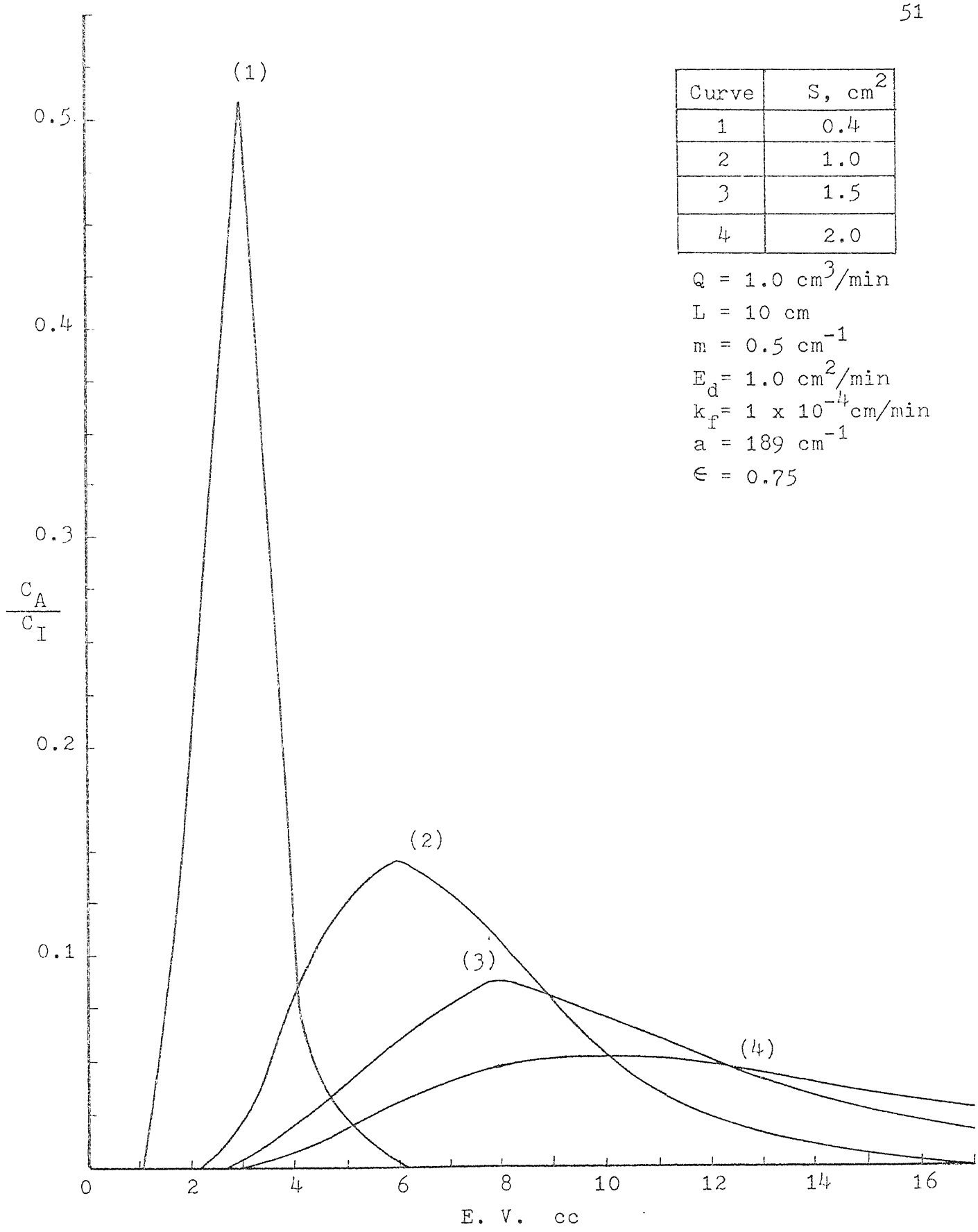

Curve	S, cm^2
1	0.4
2	1.0
3	1.5
4	2.0

Q = 1.0 cm^3/min
L = 10 cm
m = 0.5 cm^{-1}
E_d = 1.0 cm^2/min
k_f = 1 x 10^{-4} cm/min
a = 189 cm^{-1}
ϵ = 0.75

Fig. 10 Effect of Column Cross Sectional Area, S

is first governed by the film resistance for solute to diffuse across the interface with driving force of concentration difference. Then, the equilibrium constant will control the distribution of solute molecules between solid and liquid phases. For low equilibrium constant "m" means the affinity of solute molecule to the solid phase is strong. The solute molecule will be adsorbed by the solid phase since they have opposite charge in the low buffer ionic strength environment. For high values of the equilibrium constant "m", the solute molecule has a high tendency to stay in mobile phase and thus is less likely to be adsorbed by the solid phase. This relationship can be adequately explained by Eq. A-3 $C_A^* = m\ C_{AS}$. It states that solute concentration is a linear relationship between the solid and liquid phase and is regulated by the equilibrium constant "m". This equilibrium constant results from the combined effects of buffer pH, buffer ionic strength, feed concentration, and the adsorption capacity of solid phase.

Fig.11 shows the effect of mass transfer coefficient on the elution profile. Under the same operating conditions, the k_f is varied according to strong affinity, m = 1. It can be easily shown that small values of k_f will represent high mass transfer resistance for solute to diffuse through the interface. As a result, the solute will be more likely to stay in liquid phase and to have high elution peak area as shown by curve 3 and 4.

Curve	k_f, cm/min
1	1×10^{-3}
2	1×10^{-4}
3	1×10^{-5}
4	1×10^{-6}

$Q = 1.0\ cm^3/min$
$S = 1.0\ cm^2$
$L = 10\ cm$
$*m = 1.0\ cm^{-1}$
$E_d = 1.0\ cm^2/min$
$a = 189\ cm^{-1}$
$\epsilon = 0.75$

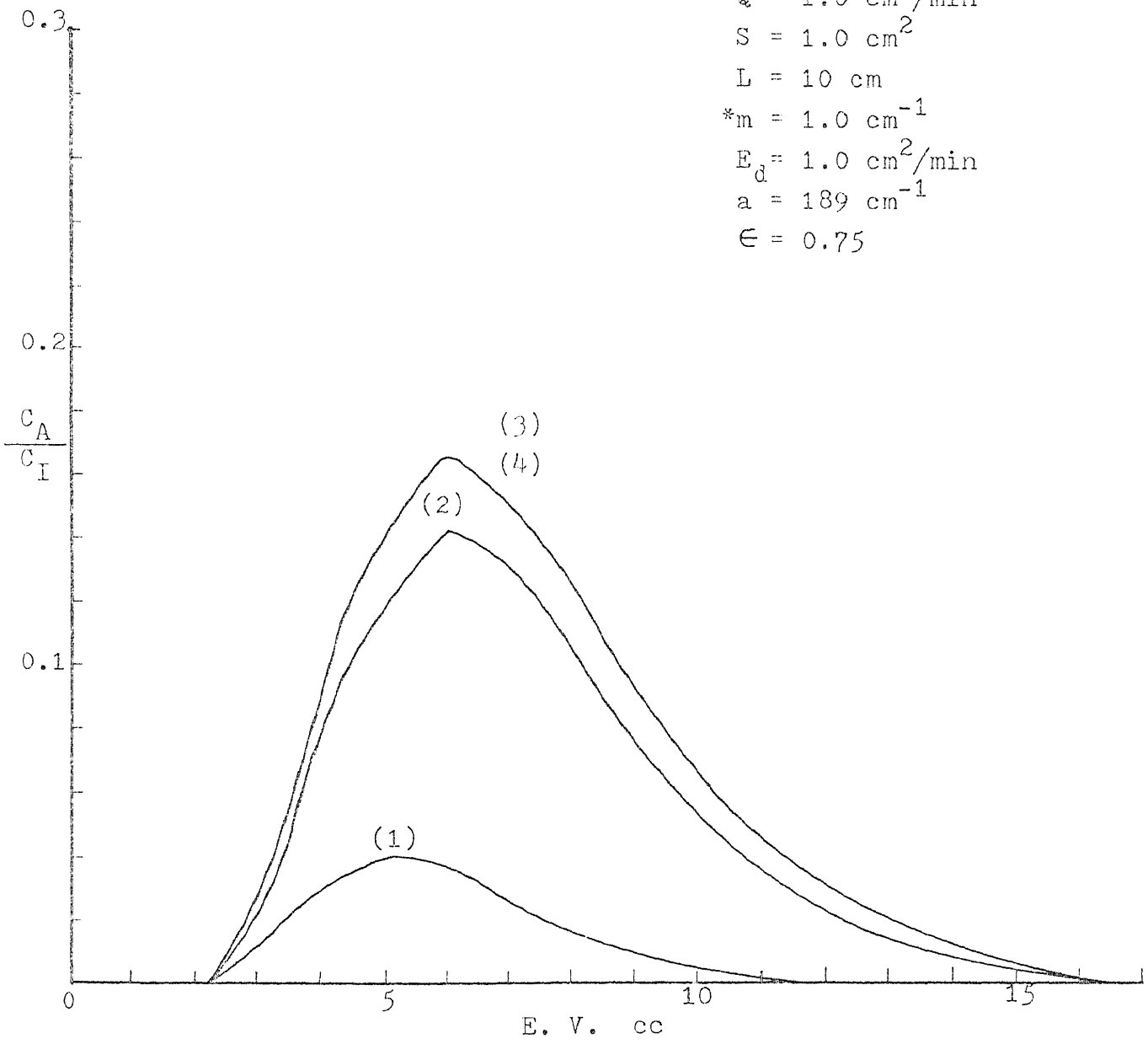

Fig. 11 Effect of Mass Transfer Coefficient, k_f

Curves 1 and 2 show that low mass transfer resistance results in low elution area for bigger value of K_f. The solute molecule can easily easy to overcome the film resistance to approach the solid phase. The strong affinity, m=1, also enhances the adsorption between solid and liquid phases.

Figures 12 and 13 show the effect of equilibrium constant for high and low mass transfer resistance k_f equal $1x10^{-4}$ and $1x10^{-3}$ respectively. A high values of k_f implies small resistance to mass transfer. Figure 12, therefore, shows that the equilibrium constant is the dominant parameter which controls the solute distribution between two two phases. A large "m" value means that the solute has less affinity for the stationary phase will therefore result in larger elution area. The opposite behavior is observed for small values of "m". Figure 13 shows that when k_f is small and the resistance is substantial the solute can not readily diffuse across the boundary to be adsorbed by the solid phase. As aresult, most of solute will stay in the liquid phase. Obviously, k_f is the dominant factor and variation of the equilibrium constant "m" does not create a large difference in peak shape. If resistance is large, the peak shape is insensitive to variations in the equilibrium constant. However, when the film resistance is small, the peak shape is substantially effected by the equilibrium constant. This demonstrates the validity of the sequential mass transfer mechanism.

Curve	m, cm^{-1}
1	0.5
2	10.0
3	1000
4	1×10^5

$Q = 1.0\ cm^3/min$
$S = 1.0\ cm^2$
$L = 10\ cm$
$E_d = 0.75\ cm^2/min$
$*k_f = 1 \times 10^{-3} cm/min$
$a = 189\ cm^{-1}$
$\epsilon = 0.75$

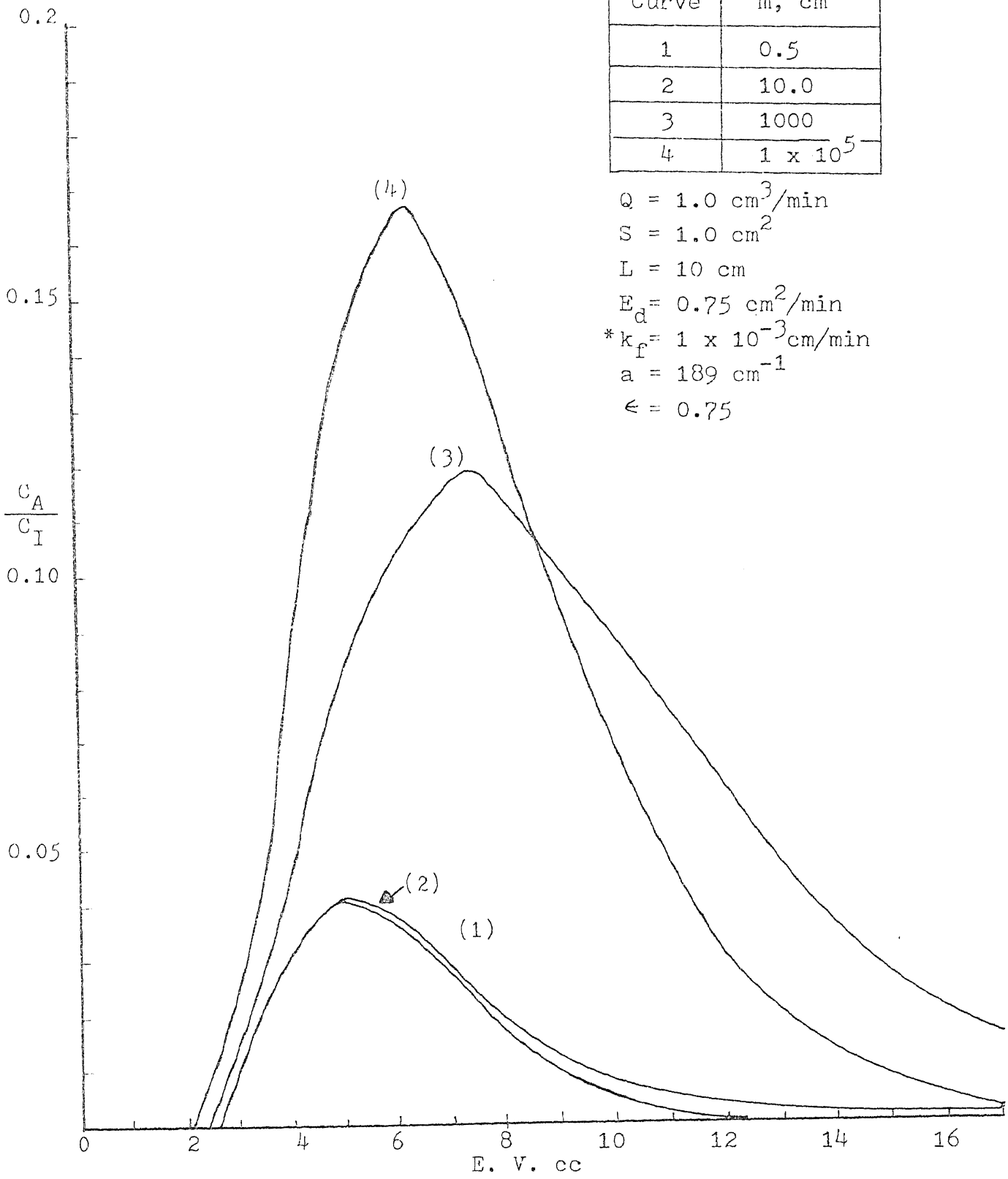

Fig. 12 Effect of Equilibrium Constant, m

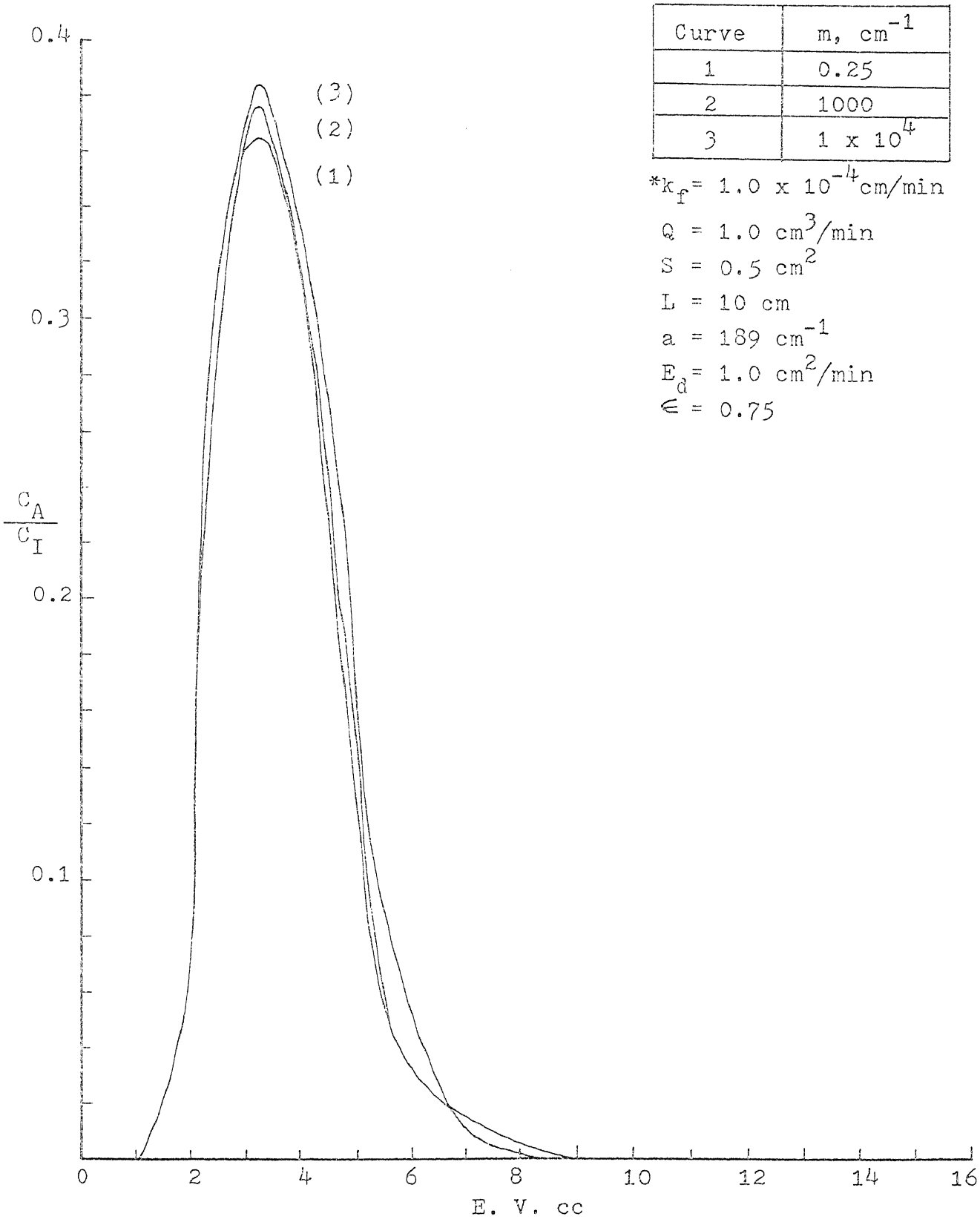

Curve	m, cm^{-1}
1	0.25
2	1000
3	1×10^4

*$k_f = 1.0 \times 10^{-4}$ cm/min

Q = 1.0 cm^3/min

S = 0.5 cm^2

L = 10 cm

a = 189 cm^{-1}

E_d = 1.0 cm^2/min

ϵ = 0.75

Fig. 13 Effect of Equilibrium Constant, m

According to the definition, the axial dispersion is the result of eddy diffusion and molecular diffusion. An increase in axial dispersion will cause the superposition of the axial flow and thus the elution profile will be deviated more from a normal bell shape distribution, i.e., broad and long tail peak. Such deviation will reduce the resolution and efficiency of chromatographic column. Figure 14 shows the effect of axial dispersion. For E_d = 0.5 or less, the elution profile is close to normal frequency distribution. And as E_d increases, it means the axial dispersion effect is significant and leads the solute elution profile to break through the column earlier and with long tail.

Figure 15 shows the effect of contact area, $a=3(1-\epsilon)/r_o$, which is a function of void fraction and solid particle radius. In this figure the void fraction is constant, so that high contact surface area means small particle size. Under high mass transfer resistance $k_f = 1x10^{-4}$ and high affinity m=1, the elution profiles will be varied dramatically result from the changing of effective contact area. The low effective contact surface area will obviously has high resolution area and vice versa. Because of high mass transfer resistance and high affinity, it will result the solute to be adsorbed as long as the effective contact area is available.

Figure 16 shows the effect of void fraction. In this figure, the effective contact area, a=189, is constant. So, the

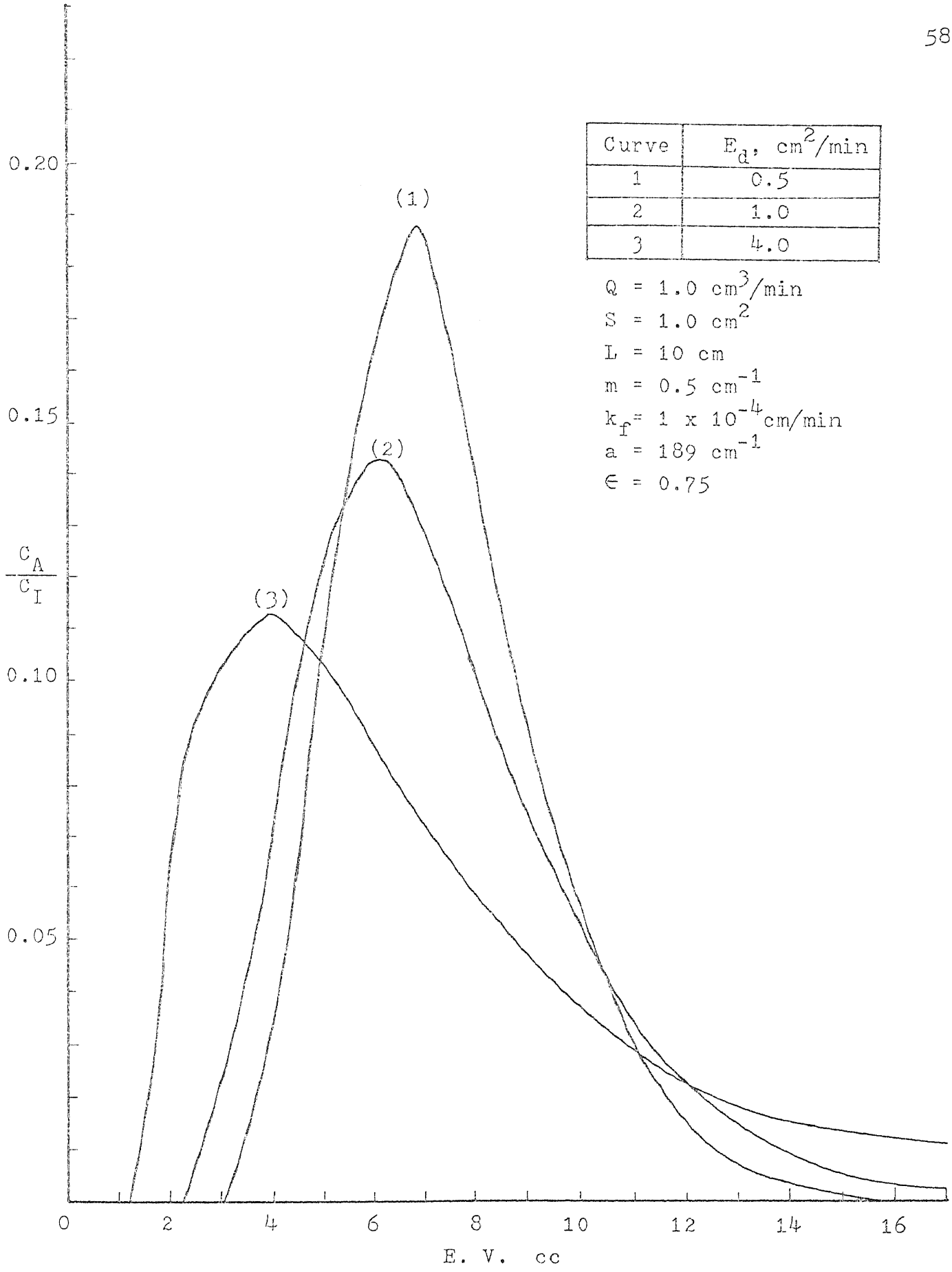

Fig. 14 Effect of Axial Dispersion, E_d

Curve	a, cm^{-1}
1	10
2	1000
3	1×10^{4}

$Q = 1.0\ cm^3/min$

$S = 1.0\ cm^2$

$L = 10\ cm$

$*m = 1.0\ cm^{-1}$

$E_d = 0.75\ cm^2/min$

$*k_f = 1 \times 10^{-4}\ cm/min$

$\epsilon = 0.75$

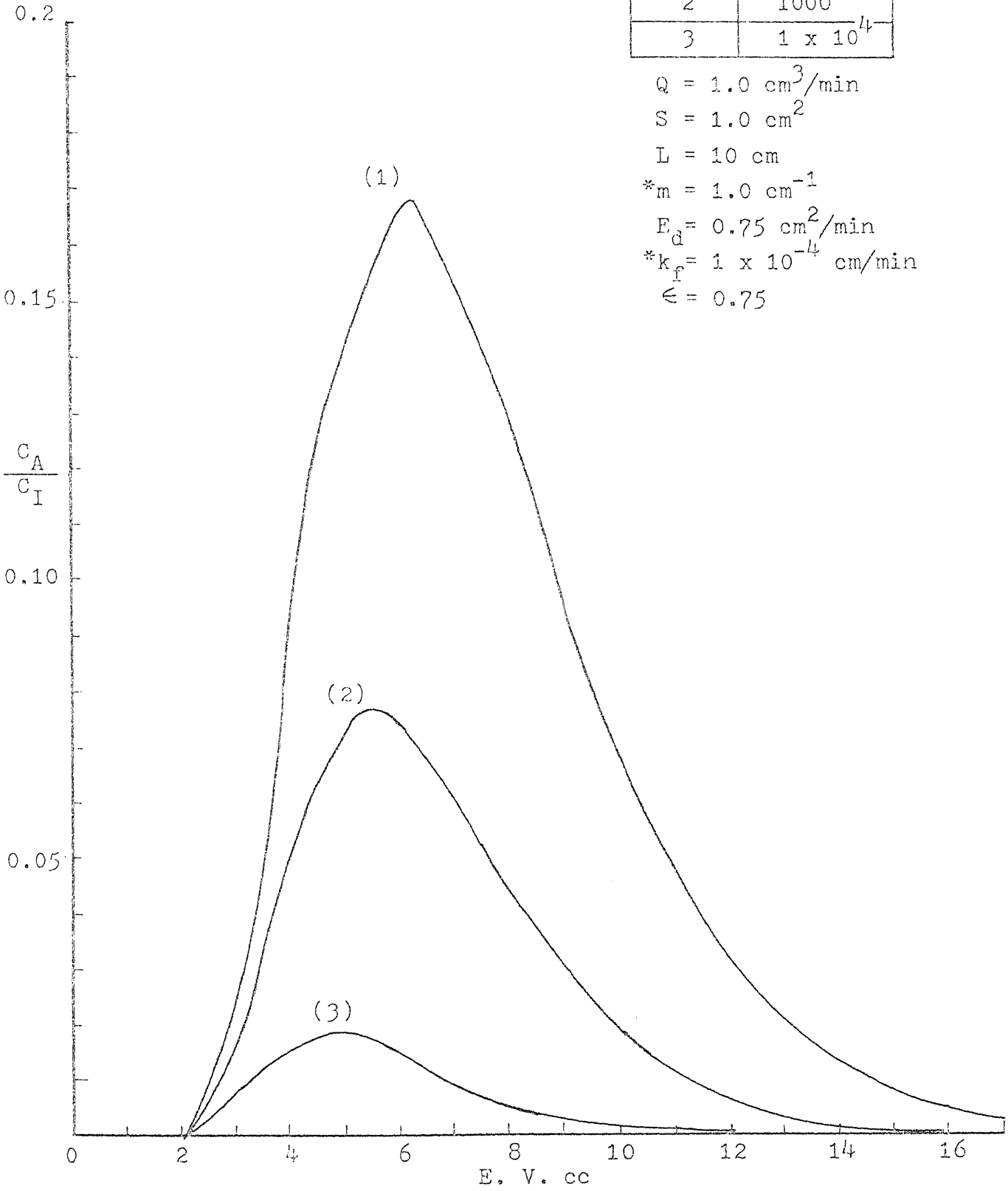

Fig. 15 Effect of Effective Contact Area, a

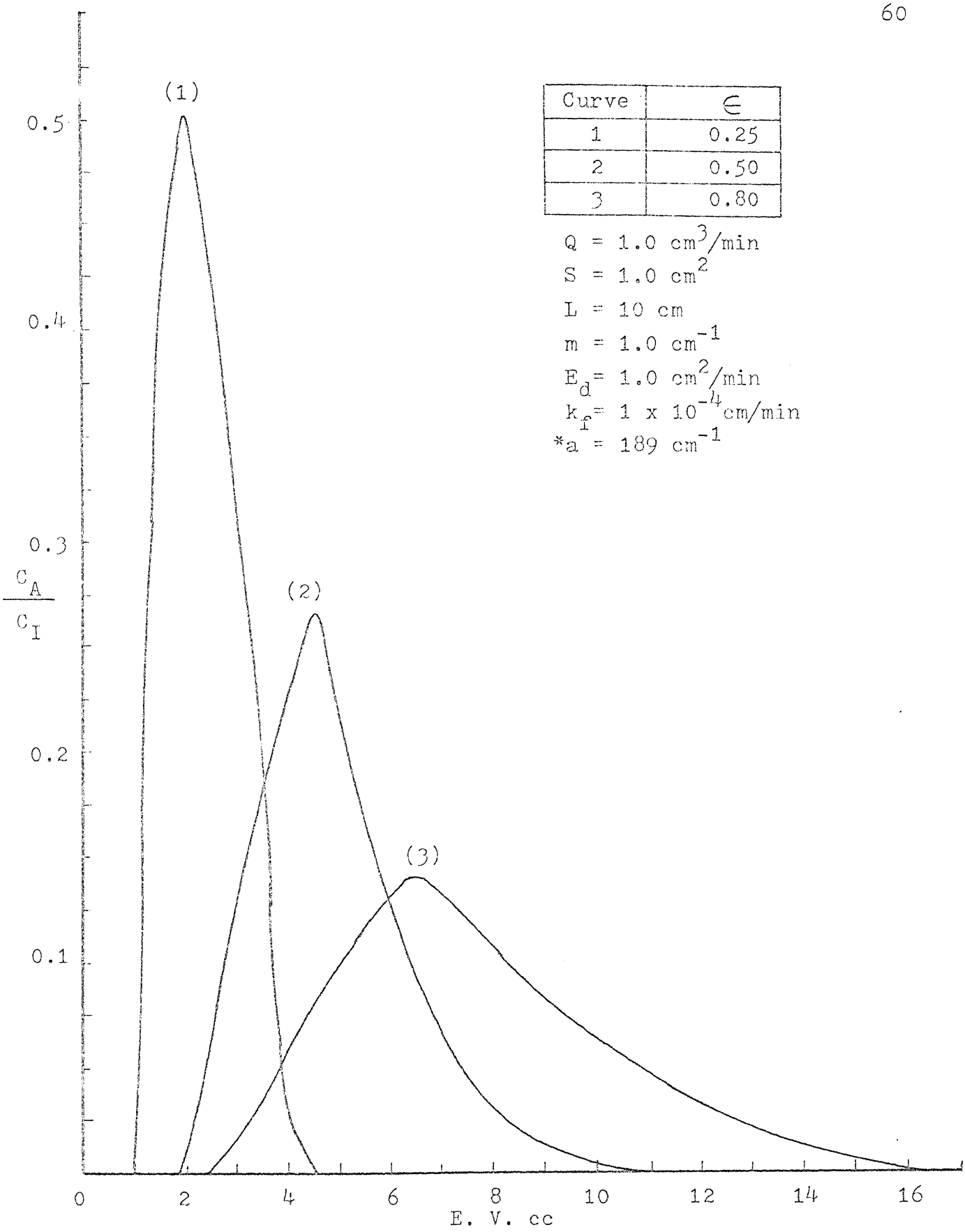

Curve	ϵ
1	0.25
2	0.50
3	0.80

$Q = 1.0\ cm^3/min$
$S = 1.0\ cm^2$
$L = 10\ cm$
$m = 1.0\ cm^{-1}$
$E_d = 1.0\ cm^2/min$
$k_f = 1 \times 10^{-4}\ cm/min$
$*a = 189\ cm^{-1}$

Fig. 16 Effect of Void Fraction, ϵ

small void fraction will require large particle radius and small solid phase volume. Since there is less solid for adsorption, there is a net reduction in the retention time of the solute in the bed. Therefore, this results to a sharp peak and a earlier break profile.

2-1-2 Surface adsorption with pore diffusion

As previously discussed, the mathematical model of ion exchange chromatographic operation are distinct as diffusion transport of solute between two phases. The nature of diffusion transport can be classified into two categories:

(i). the external diffusion in mobile phase, called axial dispersion.
(ii). the internal diffusion in stationary phase, called pore diffusion.

The significance of pore diffusion can be neglected in some cases which have been described in the surface adsorption model. In this section, both the internal and external diffusion are considered. The mass transfer rate is also controlled by a sequential mechanism which is same as that for the surface adsorption model. The mechanism mainly consists of film resistance, linear equilibrium relationship, pore diffusion, and effective contact area. The linear equilibrium relationship is dependent upon the relative magnitudes of the

internal and external diffusion. However, the illustration of equilibrium relationship as affinity of solute to the solid phase may be more appropriate in discussion such serial transfer mechanisms.

In addition to the earlier made assumptions, the following are set up for solid phase.

1. Within the homogeneous solid matrix, the diffusion of solute molecule obeys the Fick's law.
2. The diffusion transport is only a function of radial direction, there is no variation for any angular position.

Model development

According to Fig.7, the shell material balance is performed and the governing equation for this model may be formulated.

Mass balance of fluid phase

$$\frac{\partial c_A}{\partial t} = - \frac{Q}{S\epsilon} \frac{\partial c_A}{\partial z} - \frac{3(1-\epsilon)}{\epsilon r_o} k_f (c_A - c_A^*) + E_d \frac{\partial^2 c_A}{\partial z^2} \qquad (B\text{-}1)$$

Material balance of solid phase

Mass balance for solute A over a spherical shell of thickness Δr within a single solid particle.

$$4\pi r^2 N_{Ar}\Big|_r - 4\pi r^2 N_{Ar}\Big|_{r+\Delta r} = 4\pi r^2 \Delta r \frac{\partial c_{AS}}{\partial t}$$

where $N_{Ar} = -D_s \partial c_{AS}/\partial r$ is the mole flux for species A in the r direction, and D_s is the effective diffusivity for solute A within the porous matrix. Division by $4\pi\Delta r$, letting Δr approaching zero and substituting with $N_{Ar} = -D_s \partial c_{AS}/\partial r$ gives

$$D_s \frac{1}{r^2} \frac{\partial}{\partial r} \left(r^2 \frac{\partial c_{AS}}{\partial r}\right) = - \frac{\partial c_A}{\partial t} \qquad \text{(B-2)}$$

In general, the effective diffusivity in ion exchange pack bed depends on pH, ionic strength, and feed concentration, etc. However, D_s in practice is a constant as long as the running condition is fixed. Eq. B-2 is to be solved with the boundary conditions:

B.C. 1 $$\left.\frac{\partial c_{AS}}{\partial r}\right|_{r=0} = 0 \quad \text{or} \quad \left. c_{AS}\right|_{r=0} = \text{finite} \qquad \text{(B-3)}$$

B.C. 2 $$D_s \left.\frac{\partial c_{AS}}{\partial r}\right|_{r=r_o,z,t} = k_f (c_A - c_A^*) \qquad \text{(B-4)}$$

This equation states that the mass transfer of solute A from the bulk flow to particle surface ($r = r_o$) is equal to the mass flux of solute A at which it diffuses into solid particle.

Equilibrium relationship between liquid and solid phase

$$c_A^*(z,t) = m_v \, c_{AS}\,(r=r_o,z,t) \qquad \text{(B-5)}$$

where m_v is the volume based equilibrium constant.

Boundary and initial conditions for fluid phase:

B.C. 1

$$QC_I\delta(t) - Qc_A\Big|_{z=\Delta z} + S\epsilon E_d\frac{\partial c_A}{\partial z}\Big|_{z=\Delta z} = \Delta zS\epsilon\frac{\partial c_A}{\partial t}$$

letting Δz approaching zero, this equation reduces to

$$C_I\delta(t) - c_A\Big|_{z=0} + \frac{S\epsilon E_d}{Q}\frac{\partial c_A}{\partial t}\Big|_{z=0} = 0 \qquad \text{(B-6)}$$

Eq. B-6 states that the back mixing due to the axial dispersion.

B.C. 2

$$Q\int_{t=0}^{t}(C_I\delta(t) - c_A\Big|_{z=L})dt = \int_{z=0}^{z=L}\frac{(1-\epsilon)S}{4/3\ r_o^3}\left(\int_0^{2\pi}\int_0^{\pi}\int_0^{r_o} c_{AS}r^2 dr\sin\theta d\theta d\phi\right)dz + S\epsilon\int_{z=0}^{z=L} c_A dz$$

or,

$$\int_{t=0}^{t=t}(C_I\delta(t) - c_A\Big|_{z=L})dt = \frac{3(1-\epsilon)S}{Qr_o^3}\int_{z=0}^{z=L}\left(\int_{r=0}^{r=r_o} c_{AS}r^2dr\right)dz + \frac{S\epsilon}{Q}\int_{z=0}^{z=L} c_A dz \qquad \text{(B-7)}$$

Initial conditions;

$$c_A(Z, t=0) = c_{A,t_o} \qquad \text{(B-8a)}$$

$$c_{AS}(r,z,t=0) = c_{AS,t_o} \qquad \text{(B-8b)}$$

$$c_A^*(z,t=0) = c_A^*,t_o \qquad \text{(B-8c)}$$

If above concentrations are equal zero at time equal zero, this will be the special case for Eqns. B-8.

Noting that the following conditions are true;

For $t > 0$;

$$c_{A,t_o}\Big|_{z=0,t>0} = 0 \qquad \text{(B-9a)}$$

For $t < 0$; $\quad c^{*}_{A,t_o} = mc_{AS,t_o}$ (B-9b)

$$c^{*}_{A,t_o} = c_{A,t_o} \tag{B-9c}$$

and total material balance at $t \leq t_o$

$$\int_0^t (0-c_{A,t_o}\Big|_{z=L})dt = \frac{S}{Q}\int_{z=0}^{Z=L} c_{A,t_o}dz + \frac{3(1-\epsilon)S}{Qr_o^3}\int_{z=0}^{z=L}\int_{r=0}^{r=r_o} c_{AS,t_o} r^2 dr dz \tag{8-9d}$$

Introducing the dimensionless concentration and dimensionless terms as

$$C_A = \frac{c_A - c_{A,t_o}}{c_I \frac{L^2}{E_d}}, \quad C_{AS} = \frac{c_{AS} - c_{AS,t_o}}{c_I \frac{L^2}{E_d}}, \quad C_A^{*} = \frac{c_A^{*} - c_{A,t_o}^{*}}{c_I \frac{L^2}{E_d}}$$

$$\tau = \frac{tE_d}{L^2}, \quad \eta = \frac{z}{L}, \quad R = \frac{r}{r_o}$$

With the aid of Eqns. B-9, the equations from B-1 to B-8 may be converted into dimensionless form;

Liquid phase

$$\frac{\partial C_A}{\partial \tau} = \frac{\partial^2 C_A}{\partial \eta^2} - \frac{3(1-\epsilon)k_f}{r_o \epsilon}\frac{L^2}{E_d}(C_A - C_A^{*}) - \frac{QL}{S\epsilon E_d}\frac{\partial C_A}{\partial \eta} \tag{B-10}$$

Solid phase

$$\frac{D_s}{r_o^2}\frac{L^2}{E_d}\frac{1}{R^2}\frac{\partial}{\partial R}\left(R^2\frac{\partial C_{AS}}{\partial R}\right) = \frac{\partial C_{AS}}{\partial \tau} \tag{B-11}$$

B.c. 1

$$\left.\frac{\partial C_{AS}}{\partial R}\right|_{R=0} = 0 \quad \text{or,} \quad \left. C_{AS}\right|_{R=0} = \text{finite} \tag{B-12}$$

B.C. 2

$$\left.\frac{\partial C_{AS}}{\partial R}\right|_{R=1} = Bi\ (C_A - C_A^*) \qquad (B\text{-}13)$$

where $Bi = k_f r_o / D_s$; biot number, dimensionless terms.

Equilibrium relationship:

$$C_A^* = m_v C_{AS} \qquad (B\text{-}14)$$

Boundary conditions for Eq. B-10:

B.C. 1

$$\frac{E_d}{L^2}\delta\left(\frac{L^2}{E_d}\tau\right) - C_A\Big|_{\eta=0^+} + \frac{S\epsilon E_d}{QL}\left.\frac{\partial C_A}{\partial \eta}\right|_{\eta=0} = 0 \qquad (B\text{-}15)$$

B.C. 2

$$\frac{E_d}{L^2}\int_0^\tau \delta\left(\frac{L^2}{E_d}\tau\right)d\tau - \int_0^\tau C_A\Big|_{\eta=1} d\tau = \frac{3(1-\epsilon)E_d}{QL}\int_{\eta=0}^{\eta=1}\left(\int_{R=0}^{R=1} C_{AS}R^2 dR\right)d\eta + \frac{S\epsilon E_d}{QL}\int_{\eta=1}^{\eta=1} C_A d\eta \qquad (B\text{-}16)$$

I.C. becomes, $C_A(\eta, \tau = 0) = 0 \qquad (B\text{-}17a)$

$$C_A^*(\eta, \tau = 0) = 0 \qquad (B\text{-}17b)$$

$$C_{AS}(\eta, \tau = 0) = 0 \qquad (B\text{-}17c)$$

Taking the Laplace transform with respect to τ, we have

fluid phase

$$p\overline{C_A} = \frac{d^2\,\overline{C_A}}{d\eta^2} - w\,(\overline{C_A} - \overline{C_A}^*) - A\,\frac{d\overline{C_A}}{d\eta} \qquad (B\text{-}18)$$

with boundary conditions,

B.C. 1

$$\left(\frac{E_d}{L^2}\right)^2 - \overline{C_A}\Big|_{\eta=0} + \frac{1}{A}\left.\frac{dC_A}{d\eta}\right|_{\eta=0} = 0 \qquad (B\text{-}18a)$$

B.C. 2

$$\frac{1}{p}\left(\left(\frac{E_d}{L^2}\right)^2 - \overline{C_A}\Big|_{\eta=1}\right) = \frac{3(1-\epsilon)SE_d}{QL}\int_{\eta=0}^{\eta=1}\left(\int_{R=0}^{R=1}\overline{C_{AS}}\,R^2 dR\right)d\eta + 1/A\int_{\eta=0}^{\eta=1}\overline{C_A}\,d\eta \qquad \text{(B-18b)}$$

Solid phase

$$p\,\overline{C_{AS}} = \frac{D_s}{r_o^2}\frac{L^2}{E_d}\left(\frac{d^2\,\overline{C_{AS}}}{dR^2} + \frac{d\,\overline{C_{AS}}}{dR}\right) \qquad \text{(B-19)}$$

with boundary conditions,

B.C. 1

$$\left.\frac{d\,\overline{C_{AS}}}{d\,R}\right|_{R=0} \quad \text{or,} \quad \overline{C_{AS}} = \text{finite} \qquad \text{(B-19a)}$$

B.C. 2

$$\left.\frac{d\,\overline{C_{AS}}}{d\,R}\right|_{R=1} = Bi\,\left(\overline{C_A} - \overline{C_A}^*\right) \qquad \text{(B-19b)}$$

Equilibrium relationship at interface

$$C_A^* = m_v\,\overline{C_{AS}}\ (R=1, \eta, p) \qquad \text{(B-20)}$$

where $A = QL/S\epsilon E_d$, $w = ak_f L^2/E_d$, $Bi = k_f r_o/D_s$, $a = 3(1-\epsilon)/r_o$. Eq. B-19 can be simplified as

$$R^2\frac{d^2\,\overline{C_{AS}}}{d\,R^2} + 2R\,\frac{d\overline{C_{AS}}}{dR} - \frac{r_o^2 E_d}{D_s L^2}pR^2\overline{C_{AS}} = 0 \qquad \text{(B-21)}$$

The equation is a form of generalized bessel function,

$$x^2y'' + x(a+2bx^p)y' + (c+dx^{2q}+b(a+p-1)x^p + b^2x^{2p})y = 0$$

can be solved with a complete solution

$$y = x^{\alpha} e^{-\beta x^{p}} \left(C_1 J_v(\lambda x^{q}) + C_2 Y_v(\lambda x^{q}) \right)$$

where $$\alpha = \frac{1-a}{2} \quad , \quad \beta = \frac{b}{p} \quad , \quad \lambda = \frac{d}{q} \quad , \quad v = \frac{\sqrt{(1-a)^2 - 4c}}{2q}$$

such that Eq. B-21 can be solved as,

$$\overline{C_{AS}} = R^{-\frac{1}{2}} \left(C_1 I_{\frac{1}{2}}(\sqrt{pc}\, R) + C_2 I_{-\frac{1}{2}}(\sqrt{pc}\, R) \right) \qquad \text{(B-22)}$$

where $c = r_o^2 E_d^2 / L_s^2 D$

According to Eq. B-19a, $I_{-\frac{1}{2}}(pc\, R)_{R=0} \longrightarrow \infty$

the constant C_1 must be zero if the $\overline{C_{AS}}$ is not to be infinite, at R = 0, hence the Eq.B-22 is

$$\overline{C_{AS}} = R^{-\frac{1}{2}} \left(C_1 I_{\frac{1}{2}}(\sqrt{pc}\, R) \right) \qquad \text{(B-23)}$$

Substituting Eq. B-23 into Eq. B-19b to give to solve for C_1,

$$C_1 = \frac{Bi\ \overline{C_A}}{pc I_{3/2}(\sqrt{pc}) + Bi\ m_v I_{\frac{1}{2}}(\sqrt{pc})} \qquad \text{(B-24)}$$

Then, substitute Eq.B-23 into Eq.B-20 to give

$$\overline{C_A}^{*} = m_v\, C_1 I_{\frac{1}{2}}(\sqrt{pc}) \qquad \text{(B-25)}$$

With combination of Eq. B-24 and Eq. B-25 may give the connection between $\overline{C}_A^{*}$ and $\overline{C}_A$, Hence,

$$\overline{C_A}^{*}(\eta, p) = \left(\frac{Bi\ m_v\ I_{\frac{1}{2}}(\sqrt{pc})}{\sqrt{pc} I_{3/2}(\sqrt{pc}) + Bi\ m_v I_{\frac{1}{2}}(\sqrt{pc})} \right) \overline{C_A} \qquad \text{(B-26)}$$

Substitute Eq.B-26 into Eq. B-18 to give;

$$\frac{d^2\overline{C_A}}{d\eta^2} - A\frac{d\overline{C_A}}{d\eta} - F\overline{C_A} = 0 \qquad \text{(B-27)}$$

where $F(p) = p + D(p)$ and $D(p) = \dfrac{w\sqrt{pc}\, I_{3/2}(\sqrt{pc})}{\sqrt{pc}I_{3/2}(\sqrt{pc}) + Bim_v I_{\frac{1}{2}}(\sqrt{pc})}$ (B-29)

solve Eq.B-27 to give,

$$\overline{C_A} = e^{\frac{A}{2}\eta}\left(C_3\sinh\frac{\sqrt{\ }}{2} + C_4\cosh\frac{\sqrt{\ }}{2} \right), \text{ where } \sqrt{\ } = \sqrt{A^2+4F} \qquad \text{(B-30)}$$

The two constants C_3 and C_4 can be evaluated by substituting Eq.B-30 into Eq.B-18a and Eq. B-18b. By solving tedious and lengthy equations, we end up with;

$$C_3 = -\left(\frac{A\cosh\frac{\sqrt{\ }}{2} + \sinh\frac{\sqrt{\ }}{2}}{\cosh\frac{\sqrt{\ }}{2} + (A+\frac{2F}{A})\sinh\frac{\sqrt{\ }}{2}} \right)\frac{E_d^2}{L^4} \qquad \text{(B-31)}$$

and

$$C_4 = \left(\frac{\sqrt{\ }\cosh\frac{\sqrt{\ }}{2} + A\sinh\frac{\sqrt{\ }}{2}}{\sqrt{\ }\cosh\frac{\sqrt{\ }}{2} + (A+\frac{2F}{A})\cdot\sinh\frac{\sqrt{\ }}{2}} \right)\frac{E_d^2}{L^4} \qquad \text{(B-32)}$$

After solving C_3 and C_4, the Eq.B-30 will give:

$$\overline{C_A}(\eta,p) = e^{\frac{A}{2}\eta}\left(\frac{\frac{A}{\sqrt{\ }}\sinh(1-\eta)\frac{\sqrt{\ }}{2} + \sinh\frac{\sqrt{\ }}{2}}{\cosh\frac{\sqrt{\ }}{2} + (A+\frac{2F}{A})\frac{1}{\sqrt{\ }}\sinh\frac{\sqrt{\ }}{2}} \right)\frac{E_d^2}{L^4} \qquad \text{(B-33)}$$

Before taking the Laplace inverse transform for Eq.B-33 to get final solution, it is important to examine the validity for residue theorem. As discussed in Sec.2-1-1, we may conclude that

Eq.B-33 has no branch point and power of p at denominator is higher than that of numerator. Also, it only existsssimple poles which satisfy the denominator.

If we rewrite Eq.B-33 as:

$$\overline{C_A}(\eta,p) = e^{\frac{A}{2}\eta}\frac{E_d^2}{L^4}\frac{J(p)}{L(p)}$$

where

$$J(p) = \cosh(1-\eta)\frac{\sqrt{}}{2} + \frac{A}{\sqrt{}}\sinh(1-\eta)\frac{\sqrt{}}{2} \qquad \text{(B-34)}$$

$$L(p) = \cosh\frac{\sqrt{}}{2} + (A + \frac{2F}{A})\frac{1}{\sqrt{}}\sinh\frac{\sqrt{}}{2} \qquad \text{(B-35)}$$

By applying the residue theorem,

$$C_A(\tau,\eta)=L^{-1}(\overline{C_A}(p,\eta))= \sum_{n=0}^{\infty}\text{Residue of } e^{p_n\tau}\overline{C_A}(p,\eta) \text{ at simple poles } p_n$$

which p_n occurs at L(p) = 0, therefore,

$$\tanh\frac{\sqrt{}}{2} = -\frac{\sqrt{}}{A+\frac{2F}{A}} \qquad \text{(B-36)}$$

$$C_A(\tau,\eta) = e^{A\eta/2}\frac{E_d^2}{L^4}\sum_{n=0}^{\infty}\lim_{p\to p_n}\left(\frac{J(p)}{L'(p)}\right)e^{p\tau} \qquad \text{(B-37)}$$

where $L'(p) = d\,L(p)/dp$.

Residues of $\overline{C}_A(\tau,\eta)$ at $p = p_n$

As derived in Sec.2-1-A, we have the eigenvalues that only negative values may satisfy Eq.B-36 and hence reduce it to,

$$\tan\frac{\beta_n}{2} = -\frac{2A\beta_n}{A^2-\beta_n^2} \qquad \text{(B-38)}$$

where $\beta_n^2 = -(A^2 + 4F)$ (B-39)

The eigenvalues β_n can be solved from Eq.B-38. Once this is done,

the values of p_n can be evaluated from Eq.B-39 . Hence,

$$F = -\frac{A^2 + B_n^2}{4} = -\xi \quad \text{where} \quad \xi = \frac{A^2 + B_n^2}{4}$$

According to Eq.B-28 and Eq.B-29, the F(p) can be established as:

$$p + \frac{w\sqrt{pc}\, I_{3/2}\sqrt{pc}}{pc\, I_{3/2}(\sqrt{pc}) + Bi\, m_v I_{\frac{1}{2}}(\sqrt{pc})} + \xi = 0 \qquad \text{(B-40)}$$

Eq.B-40 may be solved numerically for p . Before doing so, Eq.B-40 needs further simplification. Thus, according to half order Bessel identies,

$$I_{\frac{1}{2}}(x) = \sqrt{\frac{2}{\pi x}}\sinh x \qquad \text{(B-40-1)}$$

$$I_{3/2}(x) = \sqrt{\frac{2}{\pi x}}\left(\cosh x - \frac{\sinh x}{x}\right) \qquad \text{(B-40-2)}$$

By substituting Eqns.B-41-1 and B-40-2 into Eq.B-40 and letting $p = -S_{mn}$ to give:

$$-S_{mn} + \xi + \frac{w\sqrt{S_{mn}c}\left(\cos\sqrt{S_{mn}c} - \frac{\sin\sqrt{S_{mn}c}}{\sqrt{S_{mn}c}}\right)}{\sqrt{S_{mn}c}\left(\cos\sqrt{S_{mn}c} - \frac{\sin\sqrt{S_{mn}c}}{\sqrt{S_{mn}c}}\right) + Bi\, m_v \sin\sqrt{S_{mn}c}} = 0$$

or may be simplified further as:

$$\tan\sqrt{S_{mn}c} = \frac{\sqrt{S_{mn}c}\,(\xi - S_{mn} + w)}{(\xi - S_{mn})(1 - Bi\, m_v) + w} \qquad \text{(B-41)}$$

Therefore, for every β_n where $1 \le n \le \infty$, there will have a set p_{mn} which satisfy the Eq.B-41 . By applying the residue theorem, such that Eq.B-38 becomes,

$$C_A(\tau,\eta) = e^{\frac{A}{2}\eta}\frac{E_d^2}{L^4}\sum_{n=1}^{\infty}\sum_{m=1}^{\infty}\lim_{p\to p_{mn}}\left(\frac{J(p)}{L'(p)}e^{p\tau}\right) \qquad \text{(B-42)}$$

where

$$J(p) = \cosh\frac{\sqrt{\ }}{2}(1-\eta) + \frac{A}{\sqrt{\ }}\sinh\frac{\sqrt{\ }}{2}(1-\eta) \qquad \text{(B-34)}$$

$$L(p) = \cosh\frac{\sqrt{\ }}{2} + (A + \frac{2F}{A})\frac{1}{\sqrt{\ }}\sinh\frac{\sqrt{\ }}{2} \qquad \text{(B-35)}$$

Note that $\sqrt{\ } = \sqrt{A^2+4F}$.

By differentiating L(p) with respect to p, we may have:

$$L'(p) = \frac{d\,L(p)}{d\,p} = \frac{dF}{dp}\left(\left(1 + \frac{2}{A} - \frac{2(A+\frac{2F}{A})}{A^2+4F}\right)\frac{1}{\sqrt{\ }}\sinh\frac{\sqrt{\ }}{2} + \frac{A+\frac{2F}{A}}{A^2+4F}\cosh\frac{\sqrt{\ }}{2}\right) \qquad \text{(B-43)}$$

where

$$\frac{dF}{dp} = 1 + w\left(\frac{\frac{m_v Bi\,c}{2}\left((\sinh\sqrt{pc})^2 - (\cosh\sqrt{pc} - \frac{\sinh\sqrt{pc}}{\sqrt{pc}})^2\right) - \frac{m_v Bi}{2}\sqrt{\frac{c}{p}}\sinh\sqrt{pc} * XW)}{(\sqrt{pc}(\cosh\sqrt{pc} - \frac{\sinh\sqrt{pc}}{\sqrt{pc}}) + m_v Bi\,\sinh\sqrt{pc}\,)^2}\right)$$

where $XW = \cosh\sqrt{pc} - \dfrac{\sinh\sqrt{pc}}{\sqrt{pc}}$ (B-44)

According to Eq.B-39 we have,

$$\beta_n^2 = -(A^2+4F) \quad , \quad \sqrt{A^2+4F} = i\,\beta_n$$

$$A + \frac{2F}{A} = \frac{A^2 - \beta_n^2}{2A} \quad \text{and} \quad p = -S_{mn}$$

By substituting these equations into Eq.B-34, B-43 and B-44 to give;

$$\frac{d\,F}{d\,p} = -\frac{dF}{dS_{mn}} = 1 + w\,\frac{\frac{Bim_v c}{2}\left((\sin\phi)^2 + XW^2 - \frac{m_v Bi}{2}\sqrt{\frac{c}{S_{mn}}}\sin\phi * XW\right))}{(\phi * XW + m_v Bi\,\sin\phi)^2} \qquad \text{(B-45)}$$

where $\phi = \sqrt{S_{mn}c}$ and $XW = \cos\phi - \dfrac{\sin\phi}{\phi}$.

$$\frac{d\,L(p)}{dp} = \left(\frac{dF}{dp}\right) * \left(\frac{\beta_n^{\,2}(A+1)+A^2}{A\beta_n^{\,3}} \sin\frac{\beta_n}{2} - \frac{A^2-\beta_n^{\,2}}{2A\beta_n^{\,2}}\cos\frac{\beta_n}{2} \right) \qquad \text{(B-46)}$$

$$J\,(p) = \cos\frac{\beta_n}{2}(1-\eta) + \frac{A}{\beta_n}\sin\frac{\beta_n}{2}(1-\eta) \qquad \text{(B-47)}$$

where $\phi = \sqrt{S_{mn}c}$

Substituting Eq.B-45, B-46 and B-47 into Eq.B-42 to have final inverse transform of $\overline{C}_A$. Hence,

$$C_A(\tau,\eta) = \sum_{n=1}^{\infty}\sum_{m=1}^{\infty} e^{\frac{A}{2}\eta+p_{mn}\tau}\left(\frac{\cos\frac{\beta_n}{2}(1-\eta) + \frac{A}{\beta_n}\sin\frac{\beta_n}{2}(1-\eta)}{\left(\frac{dF}{dp}\right)*\left(\frac{\beta_n^{\,2}(A+1)+A^2}{A\,\beta_n^{\,3}}\sin\frac{\beta_n}{2} - \frac{A^2-\beta_n^{\,2}}{2A\beta_n^{\,2}}\cos\frac{\beta_n}{2}\right)}\right)\frac{E_d^{\,2}}{L^4} \qquad \text{(B-48)}$$

The elution profile of component A at $\eta = 1$ is:

$$C_A(\tau,\eta) = \sum_{n=1}^{\infty}\sum_{m=1}^{\infty} e^{\frac{A}{2}\eta+p_{mn}\tau}\left(\frac{\beta_n^{\,2}}{\left(\frac{dF}{dp}\right)*\left(\frac{\beta_n^{\,2}(A+1)+A^2}{A\beta_n^{\,2}}\sin\frac{\beta_n}{2} - \frac{A^2-\beta_n^{\,2}}{2A}\cos\frac{\beta_n}{2}\right)}\right)\frac{E_d^{\,2}}{L^4} \qquad \text{(B-49)}$$

Again, note: $p_{mn} = -S_{mn}$, $dF/dp = -dF/dS_{mn}$ = Eq.B-45 .

The eigenvalues β_n and p_{mn} are obtained from Eq.B-38 and Eq. B-41 .

Discussion

Figures 17 to 27 illustrate the calculated elution profiles for the surface adsorption with pore diffusion model. Nine basic parameters as described in Eq. B-49 are individually plotted under different chromatographic operating column conditions to describe the transport behavior for impulse feed input.

The effect of volumetric flow rate and column dimensions are shown on Fig.17, 18, and 19. The elution profiles are consistent with the surface adsorption model in that the long resistence time of solute molecules within the packed column will cause the peak broadening due to the significant axial dispersion and pore diffusion effects.

Fig.20 and Fig.21 show the effect of mass transfer coefficient on elution profile. According to the previous discussion, the mass transfer coefficient represents the film transfer resistance of solute molecule between the solid and liquid phase. These two figures are similar in that both the calculated results have minimum elution area for specific k_f value, for example $k_f = 1x10^{-6}$. Figure 20 shows no elution at all (curve 6) while Fig.21 shows the lowest elution area (curve 6) among different k_f values. The difference between these two figures result from different particle size r_o, pore diffusion and equilibrium constant "m". The strong affinity case for m = 1

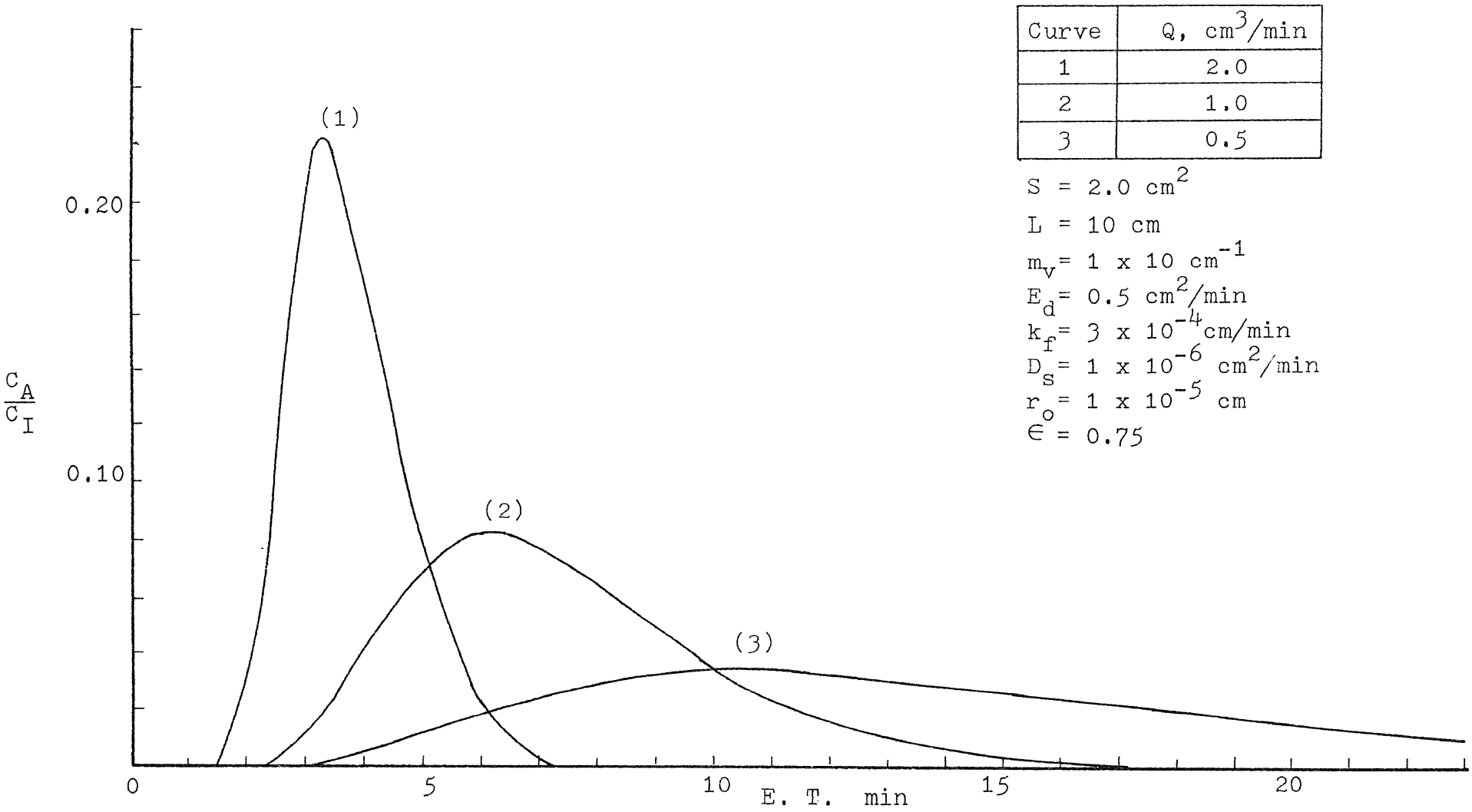

Fig. 17 Effect of Volumetric Flow Rate, Q (Surface Adsorption with Pore Diffusion Model)

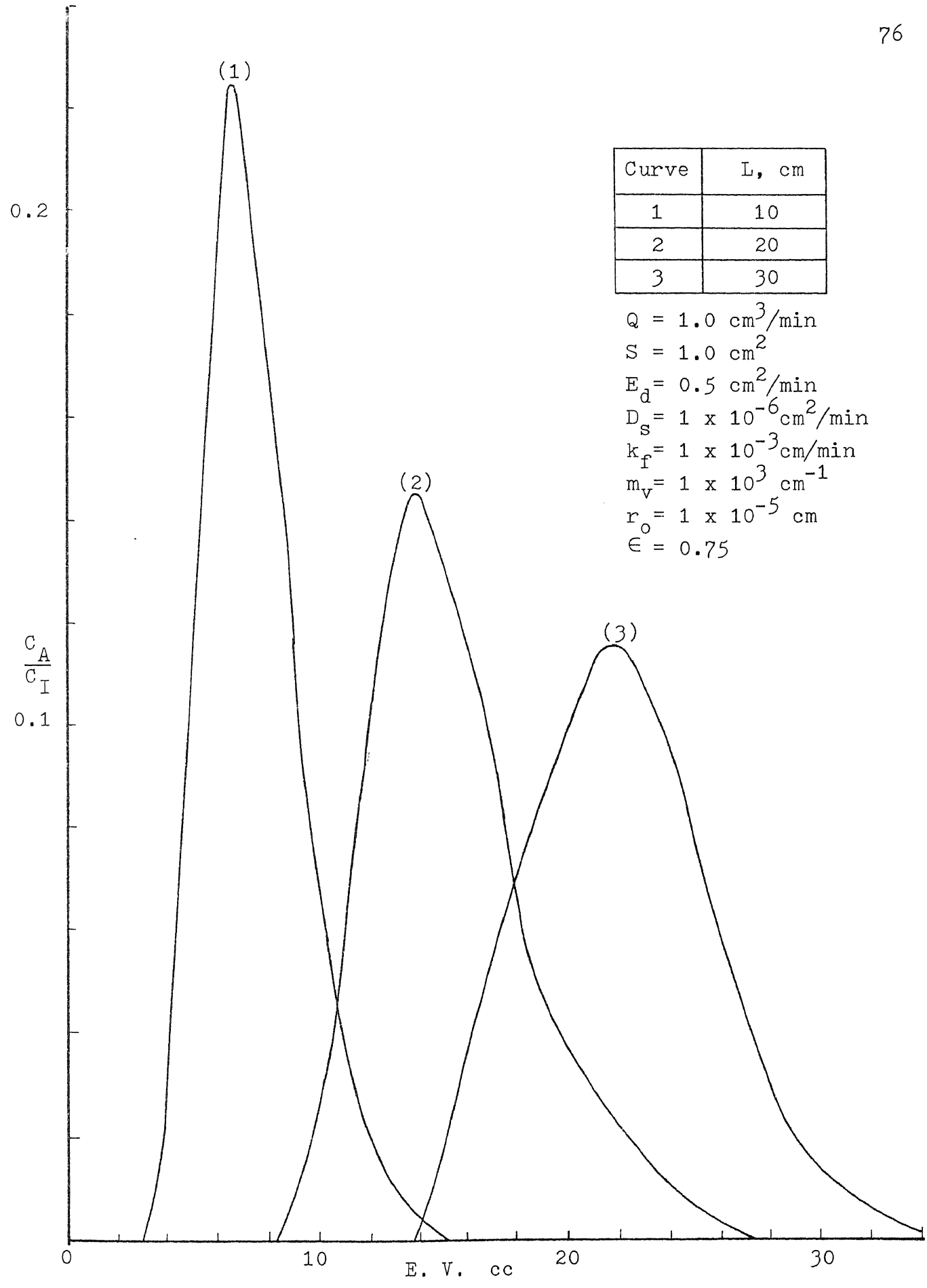

Curve	L, cm
1	10
2	20
3	30

$Q = 1.0\ cm^3/min$
$S = 1.0\ cm^2$
$E_d = 0.5\ cm^2/min$
$D_s = 1 \times 10^{-6} cm^2/min$
$k_f = 1 \times 10^{-3} cm/min$
$m_v = 1 \times 10^{3}\ cm^{-1}$
$r_o = 1 \times 10^{-5}\ cm$
$\epsilon = 0.75$

Fig. 18 Effect of Column Length, L

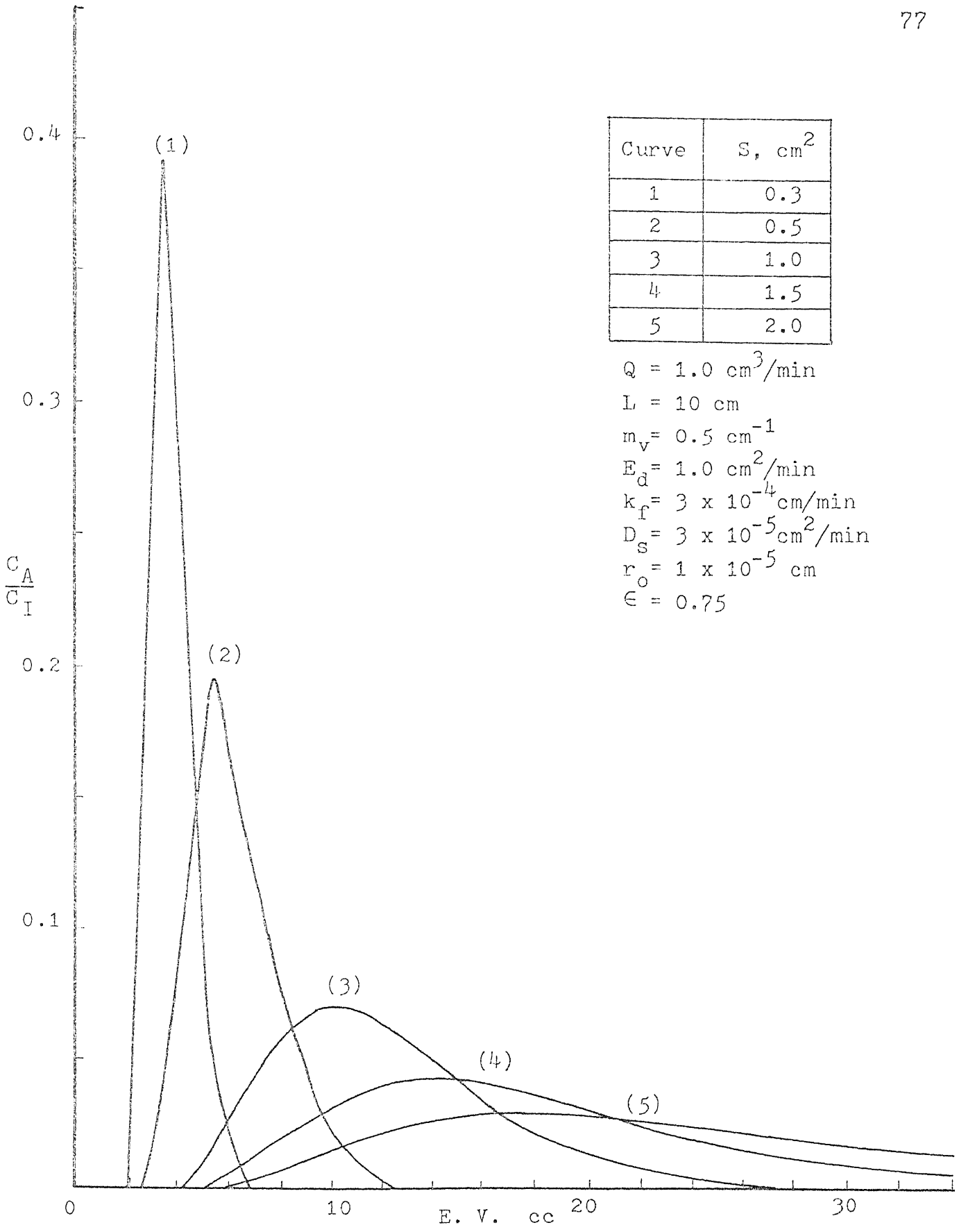

Curve	S, cm^2
1	0.3
2	0.5
3	1.0
4	1.5
5	2.0

$Q = 1.0\ cm^3/min$
$L = 10\ cm$
$m_v = 0.5\ cm^{-1}$
$E_d = 1.0\ cm^2/min$
$k_f = 3 \times 10^{-4} cm/min$
$D_s = 3 \times 10^{-5} cm^2/min$
$r_o = 1 \times 10^{-5}\ cm$
$\epsilon = 0.75$

Fig. 19 Effect of Cross Sectional Area, S

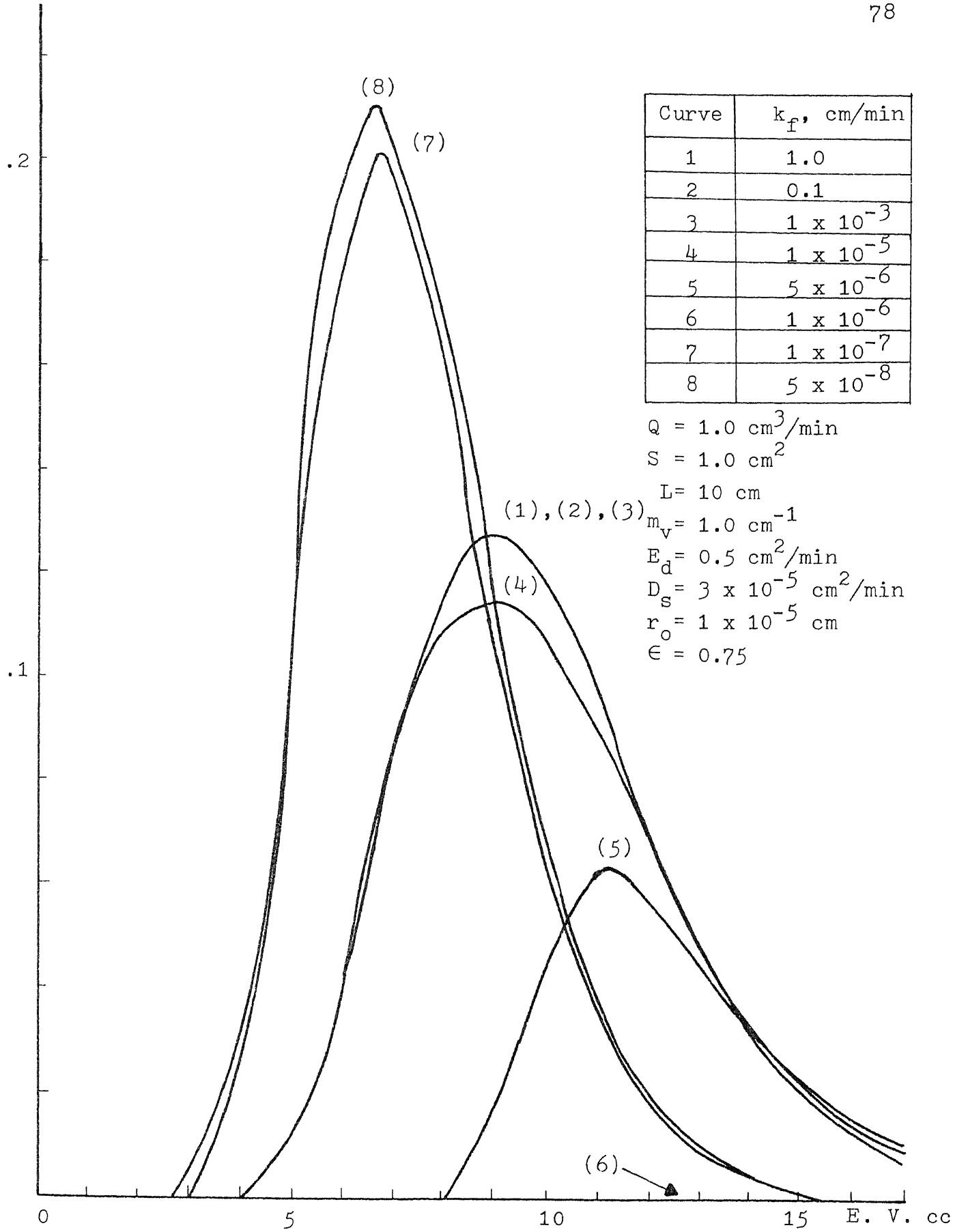

Curve	k_f, cm/min
1	1.0
2	0.1
3	1×10^{-3}
4	1×10^{-5}
5	5×10^{-6}
6	1×10^{-6}
7	1×10^{-7}
8	5×10^{-8}

$Q = 1.0$ cm^3/min
$S = 1.0$ cm^2
$L = 10$ cm
$m_v = 1.0$ cm^{-1}
$E_d = 0.5$ cm^2/min
$D_s = 3 \times 10^{-5}$ cm^2/min
$r_o = 1 \times 10^{-5}$ cm
$\epsilon = 0.75$

Fig. 20 Effect of Mass Transfer Coefficient, k_f

Curve	k_f, cm/min
1	1×10^{-3}
2	1×10^{-5}
3	5×10^{-6}
4	1×10^{-7}
5	8×10^{-7}
6	1×10^{-6}

$Q = 1.0\ cm^3/min$

$S = 1.5\ cm^2$

$L = 10\ cm$

$E_d = 0.5\ cm^2/min$

$D_s = 5 \times 10^{-7} cm^2/min$

$r_o = 1 \times 10^{-3}\ cm$

$m_v = 100\ cm^{-1}$, $\epsilon = 0.75$

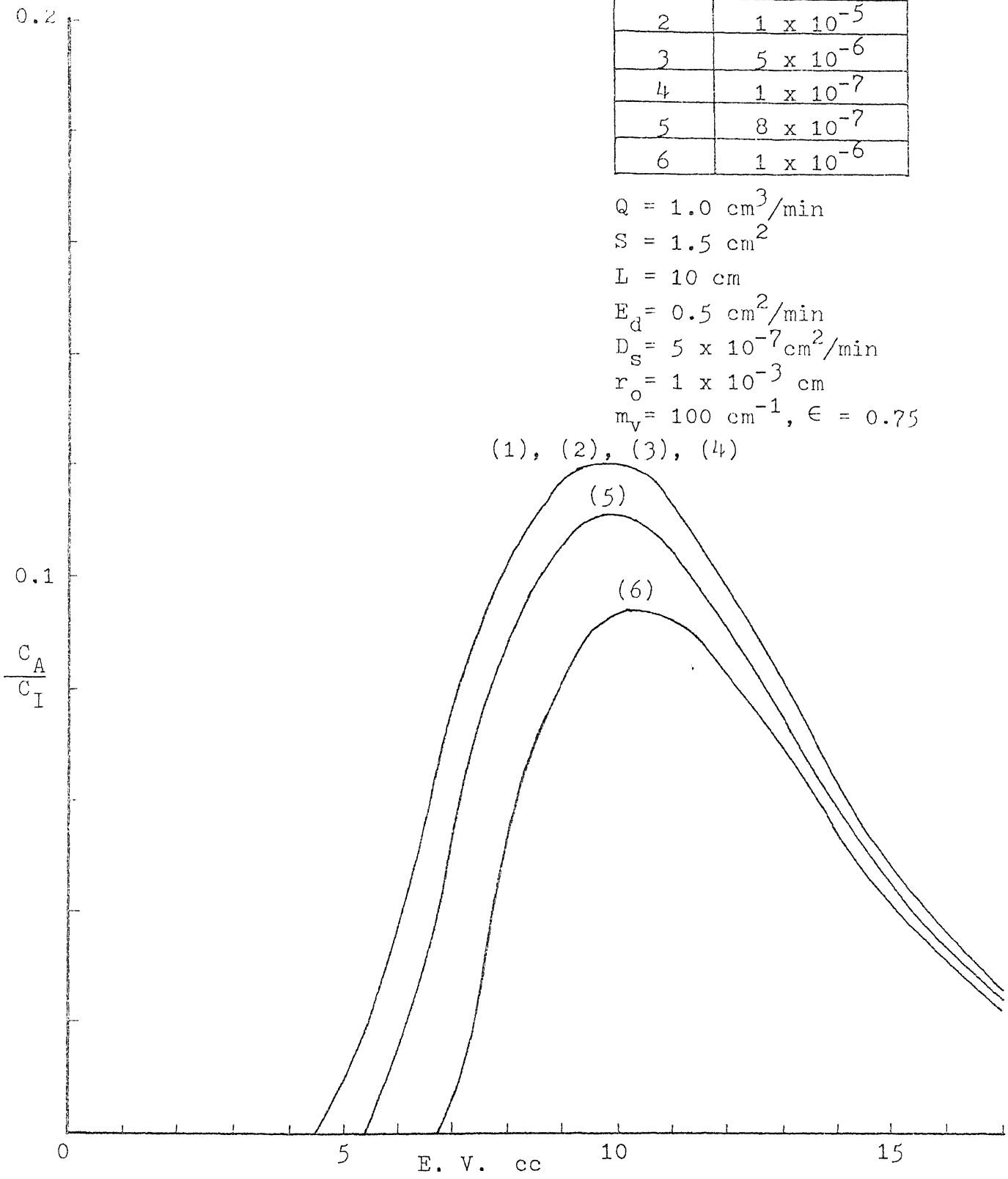

Fig. 21 Effect of Mass Transfer Coefficient, k_f

described in Fig.20 illustrated the results that the k_f variation seems to be more sensitive than that of weak affinity case as described in Fig.21 where m = 100. The elution profiles reach a minimum area for specific k_f value can be explained from Eq.B-4

$$D_s \frac{\partial c_{AS}}{\partial r}\Big|_{r=r_o,z,t} = k_f (c_A - c_A^*) \qquad (B-4)$$

It described the liquid phase concentration is equal to the first derivative of solid phase concentration c_{AS} with respect to particle radial distance, r.

The effect of affinity equilibrium constant between two phases are shown in Fig.22 . It demonstrates the consistency with the surface adsorption model that high value of m implies a weak affinity of solute molecule to solid phase, and the calculated result will show high elution profile. Again, the affinity between solute molecule and ion exchange resin is a function of buffer pH and buffer ionic strength and feed concentration. The charged group and competition between charged ions for adsorption site will regulate the solute equilibrium distribution between two phases.

Fig.23 shows the effect of axial dispersion. The efficiency of the packed bed decreases with the increase of the axial dispersion, and the elution profile becomes broad and with long tail.

Fig.24 and Fig.25 show the effect of pore diffusion. The difference between two figures is the choice of solid particle

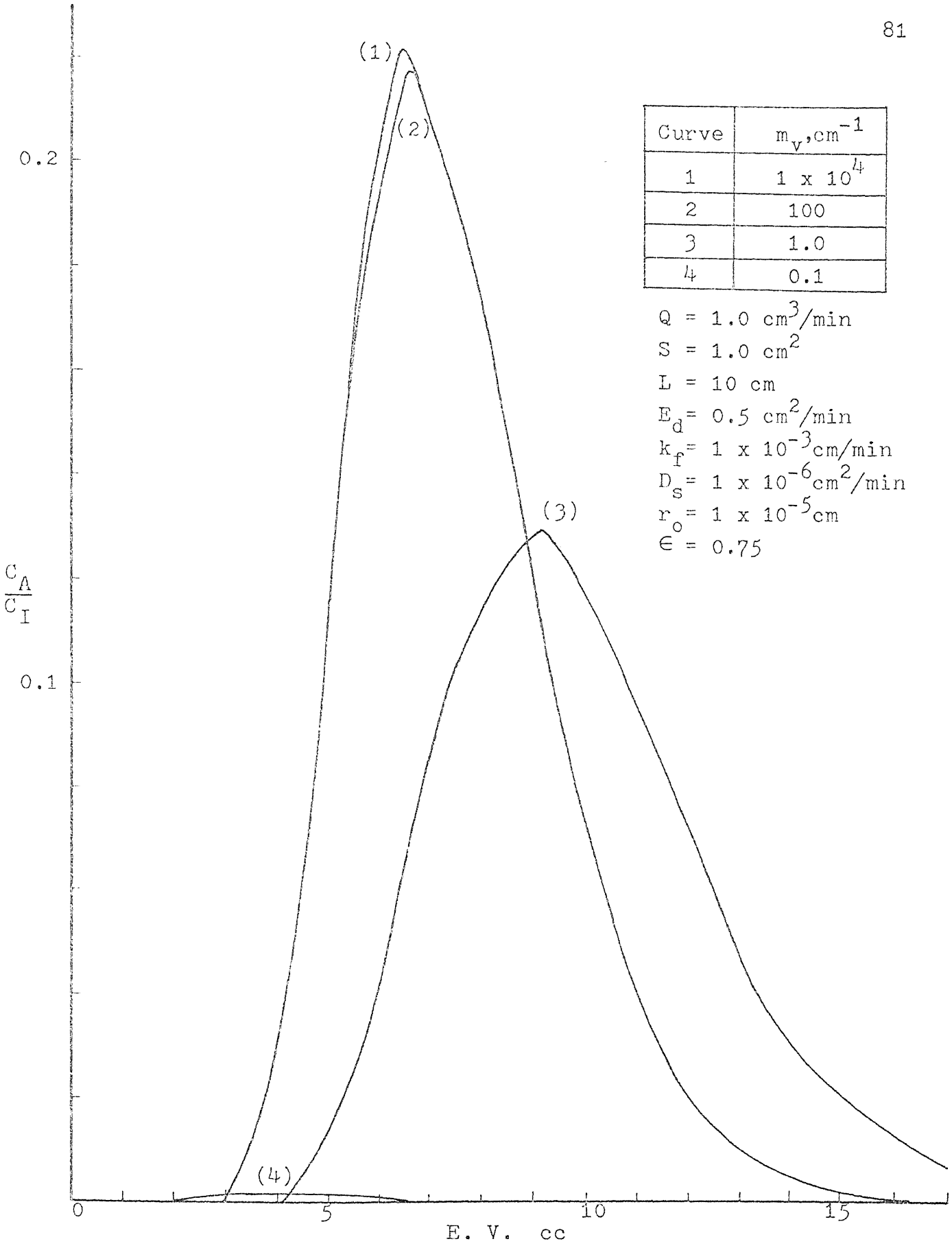

Curve	m_v, cm^{-1}
1	1×10^4
2	100
3	1.0
4	0.1

$Q = 1.0\ cm^3/min$
$S = 1.0\ cm^2$
$L = 10\ cm$
$E_d = 0.5\ cm^2/min$
$k_f = 1 \times 10^{-3}\ cm/min$
$D_s = 1 \times 10^{-6}\ cm^2/min$
$r_o = 1 \times 10^{-5}\ cm$
$\epsilon = 0.75$

Fig. 22 Effect of Equilibrium Constant, m_v

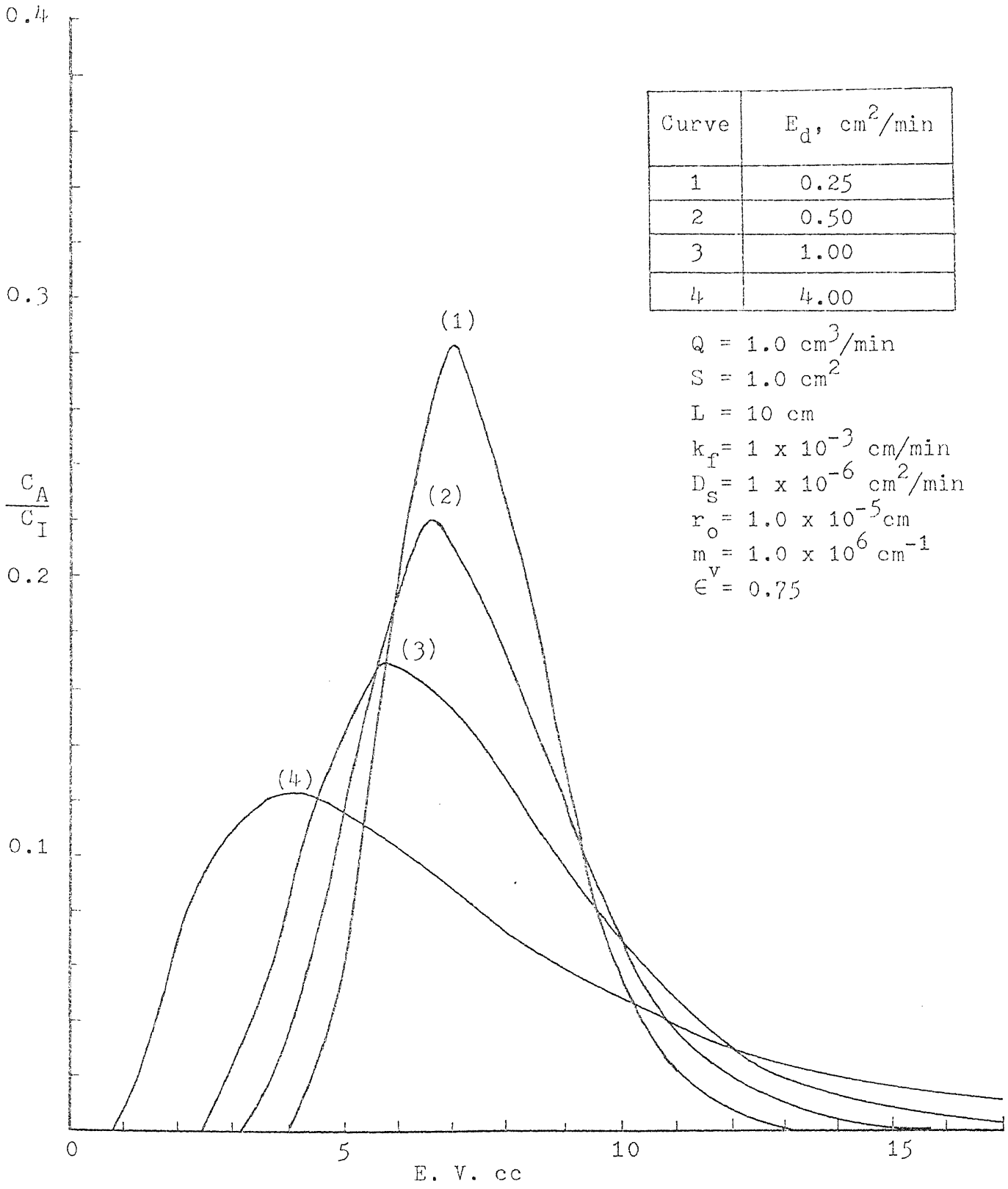

Curve	E_d, cm^2/min
1	0.25
2	0.50
3	1.00
4	4.00

$Q = 1.0\ cm^3/min$
$S = 1.0\ cm^2$
$L = 10\ cm$
$k_f = 1 \times 10^{-3}\ cm/min$
$D_s = 1 \times 10^{-6}\ cm^2/min$
$r_o = 1.0 \times 10^{-5}\ cm$
$m_v = 1.0 \times 10^{6}\ cm^{-1}$
$\epsilon = 0.75$

Fig. 23 Effect of Axial Dispersion, E_d

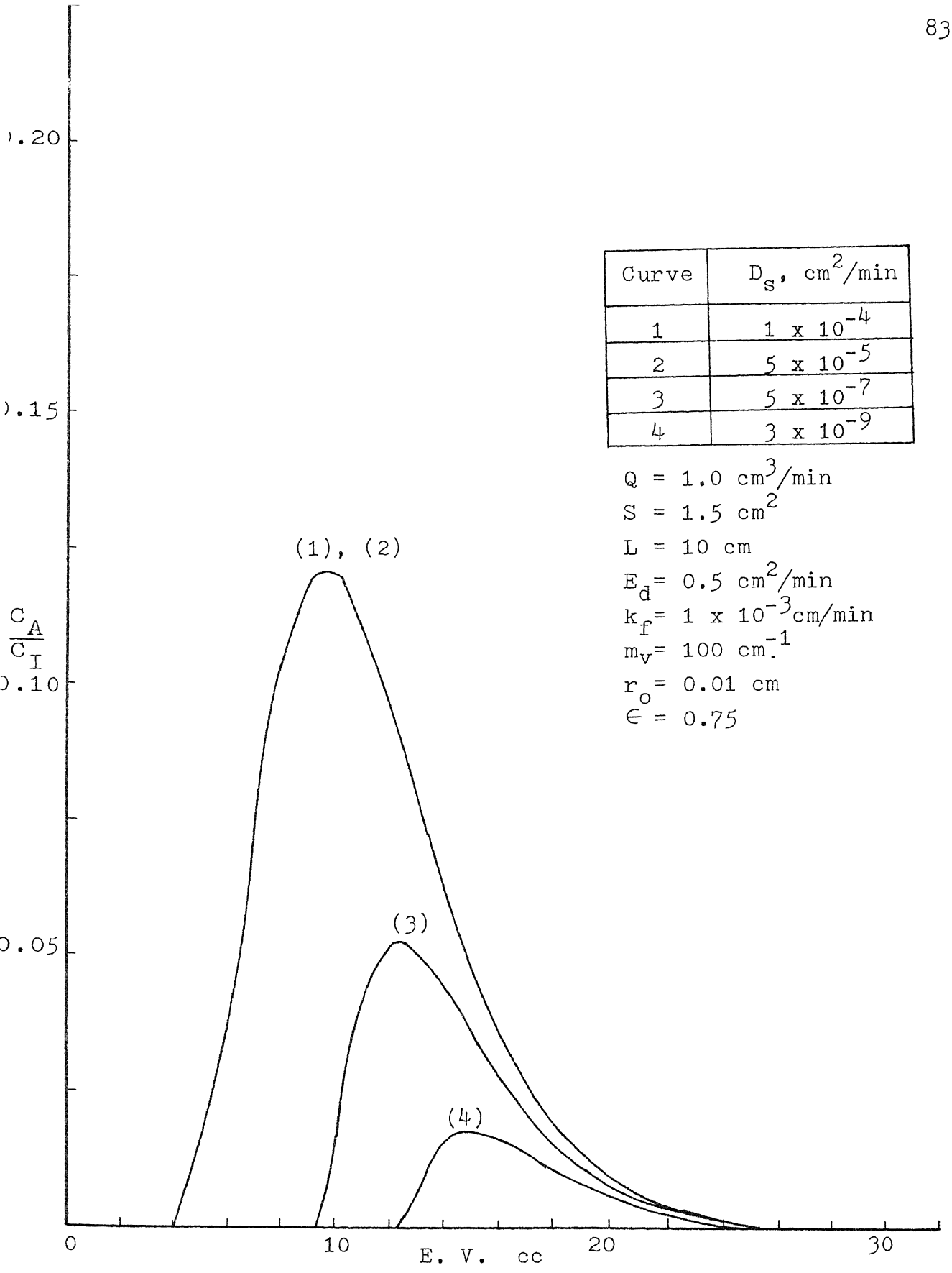

Curve	D_s, cm^2/min
1	1×10^{-4}
2	5×10^{-5}
3	5×10^{-7}
4	3×10^{-9}

$Q = 1.0\ cm^3/min$
$S = 1.5\ cm^2$
$L = 10\ cm$
$E_d = 0.5\ cm^2/min$
$k_f = 1 \times 10^{-3} cm/min$
$m_v = 100\ cm^{-1}$
$r_o = 0.01\ cm$
$\epsilon = 0.75$

Fig. 24 Effect of Pore Diffusion, D_s

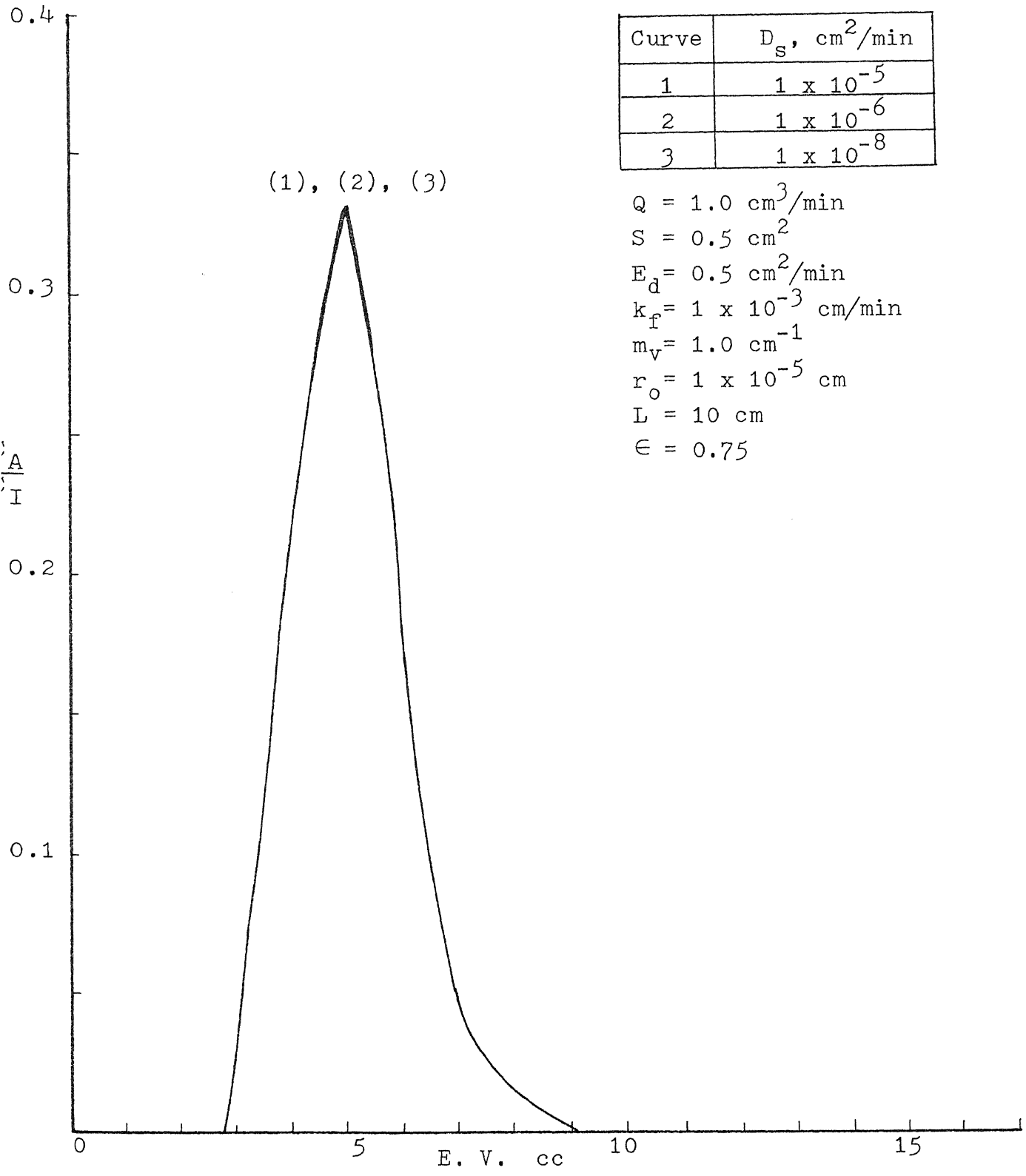

Curve	D_s, cm^2/min
1	1×10^{-5}
2	1×10^{-6}
3	1×10^{-8}

$Q = 1.0\ cm^3/min$
$S = 0.5\ cm^2$
$E_d = 0.5\ cm^2/min$
$k_f = 1 \times 10^{-3}\ cm/min$
$m_v = 1.0\ cm^{-1}$
$r_o = 1 \times 10^{-5}\ cm$
$L = 10\ cm$
$\epsilon = 0.75$

Fig. 25 Effect of Pore Diffusion, D_s

size, r_o. By definition, the large solute molecule has a small diffusivity and small solute molecule has a large diffusivity. The large molecule will travel faster than small solute molecule due to a lower tendency to diffuse into the solid matrix. Therefore, Fig.24 shows that a chromarographic column packed with large particle $r_o = 1x10^{-2}$ will have less effect on pore diffusion for large molecules. In contrast, a small molecule has higher probability of diffusing into the solid particle and this delays the break point. Figure 25, on the other hand, shows no difference in the elution profiles for both large and small pore diffusivity on column chromatography packed with small particle $r_o = 1x10^{-5}$.

Figure 26 shows the effect of particle size. The small solid particle gives better column efficiency. Figure 27 shows the effect of void fraction. Results are shown to be similar to the surface adsorption without pore diffusion model. The small void fraction column packing results in sharp and narrow peaks.

2-2 Gel Permeation Chromatographic column

Gel permeation chromatography is also referred to as gel filtration, size exclusion, or gel chromatography. The separation principles are based on the nature of the size and the shape of solute molecules. As a solute molecule passes through chromatographic column its movement depends upon the bulk flow of

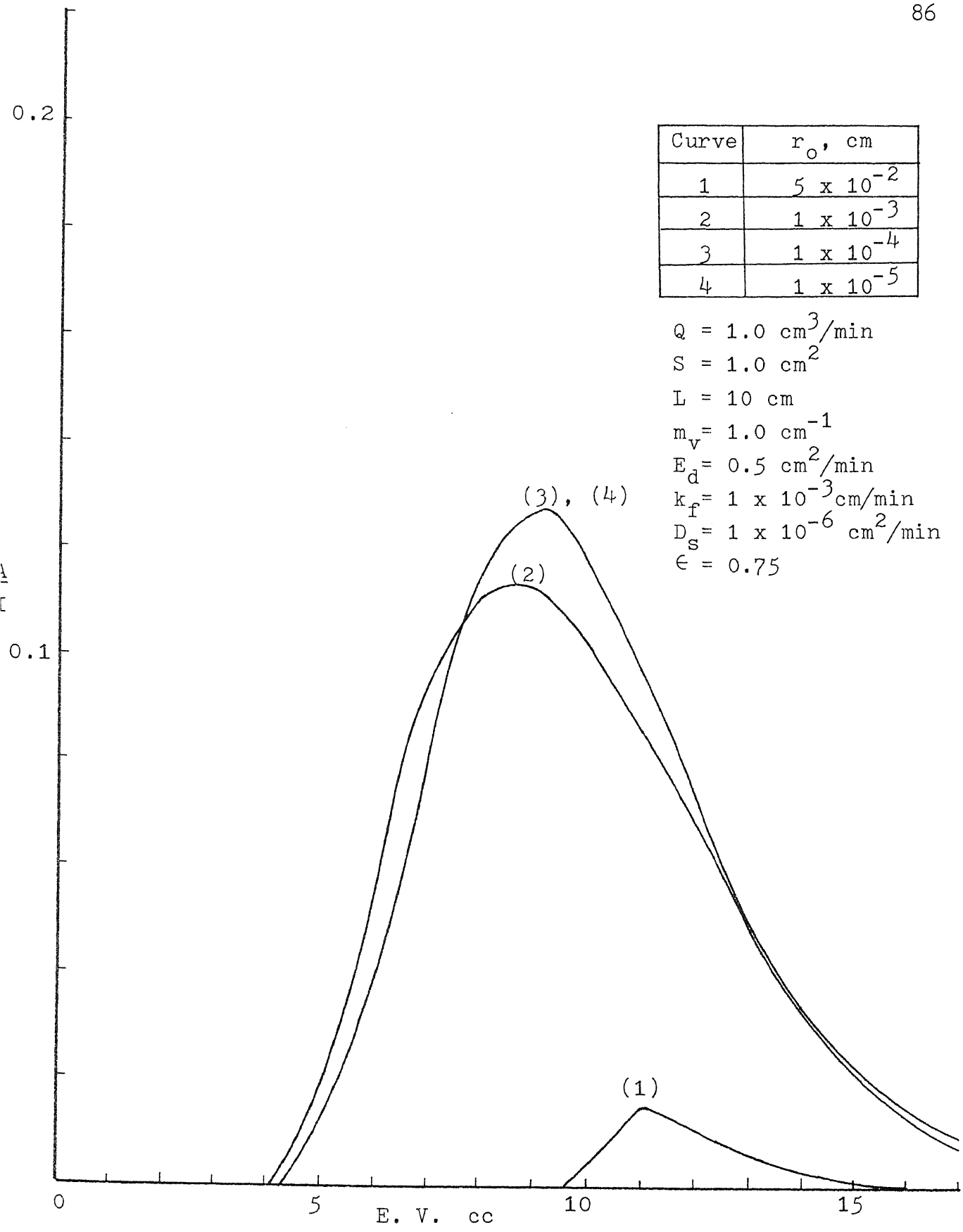

Curve	r_o, cm
1	5×10^{-2}
2	1×10^{-3}
3	1×10^{-4}
4	1×10^{-5}

$Q = 1.0\ cm^3/min$
$S = 1.0\ cm^2$
$L = 10\ cm$
$m_v = 1.0\ cm^{-1}$
$E_d = 0.5\ cm^2/min$
$k_f = 1 \times 10^{-3}\ cm/min$
$D_s = 1 \times 10^{-6}\ cm^2/min$
$\epsilon = 0.75$

Fig. 26 Effect of Particle Size, r_o

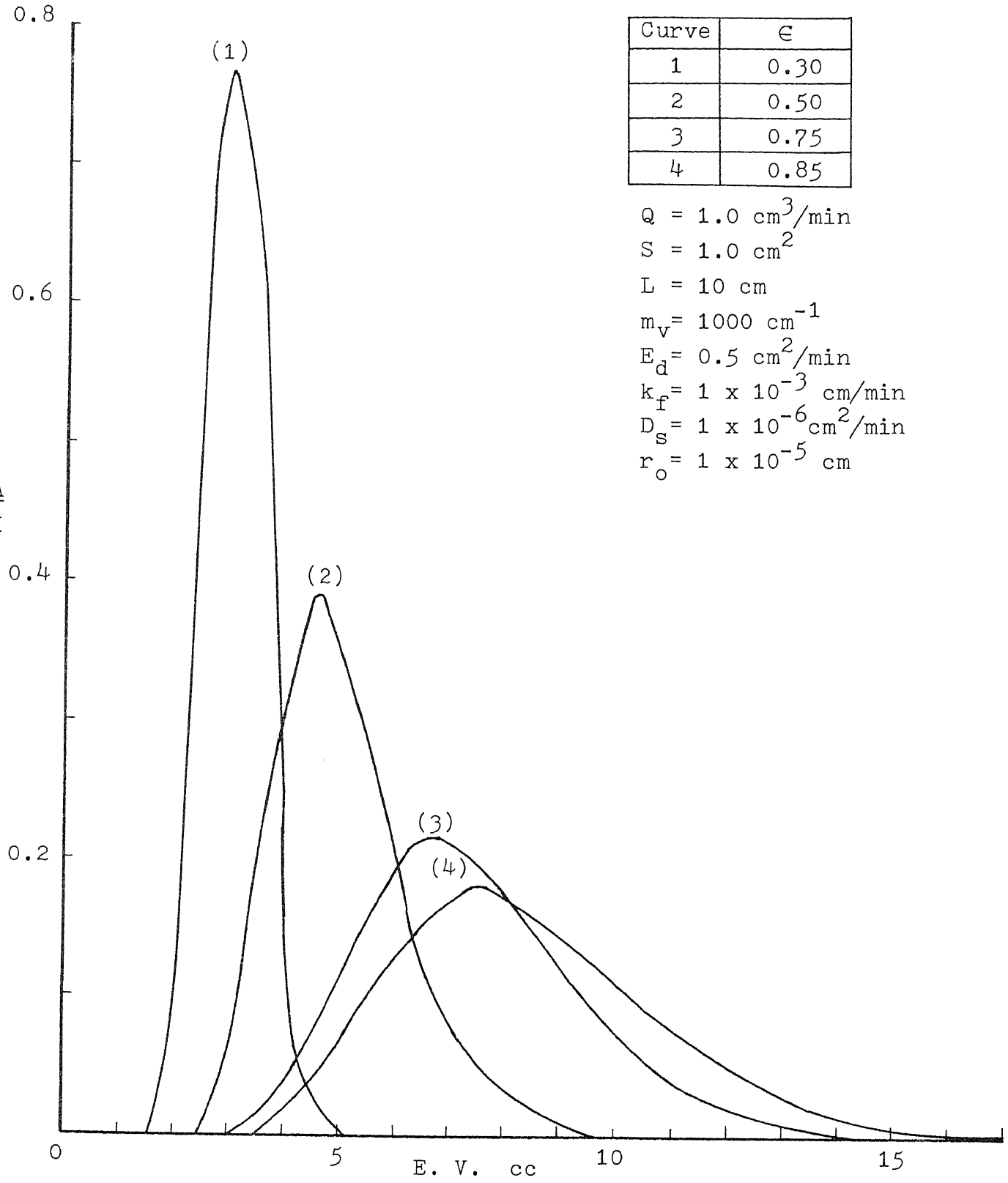

Curve	ϵ
1	0.30
2	0.50
3	0.75
4	0.85

$Q = 1.0\ cm^3/min$
$S = 1.0\ cm^2$
$L = 10\ cm$
$m_v = 1000\ cm^{-1}$
$E_d = 0.5\ cm^2/min$
$k_f = 1 \times 10^{-3}\ cm/min$
$D_s = 1 \times 10^{-6} cm^2/min$
$r_o = 1 \times 10^{-5}\ cm$

Fig. 27 Effect of Void Fraction, ϵ

the mobile phase and upon the internal and external diffusion of the solute molecule both into and out of the stationary phase. The separation principle of a gel filtration column relies on differences in diffusion of sample molecules into the pores of the the stationary phase. Unlike the ion exchange resin, the gel permeation resin is chemically and physically inert to the solute molecule. Large molecules never enter the stationary phase; therefore, they move through the chromatographic column quicker. Small molecules will enter the gel pores and move slowly through the column. The probability of diffusion into pores depends on the size and shape of the molecule in addition to the size of the pores in the solid phase. Therefore, different sized molecules will elute in order of decreasing molecular size.

As with the prior discussion of ion exchange chromatography, the elution profile is governed by the equilibrium constant; that is the magnitude of affinity between solute molecule and solid phase. Most likely, the mass transfer coefficient and internal/external diffusion are controlled by charge group interactions. In the other words, the equilibrium constant is the dominant parameter which controls the elution as an on/off system. However, the model development of gel permeation packed bed will not consider the equilibrium relationship, because of the inertness of solid phase. Thus, only mass transfer resistance, axial dispersion, and pore diffusion are considered.

Model development

We consider the gel permeation column packed with uniform porous particles, the fluid enters at inlet of the column traveling with constant superficial velocity across the fixed cross sectional area S and length L. The prior assumptions made in Sec. 2-1 are valid except that the equilibrium relationship is not exist.

Material balance of fluid phase

$$\frac{\partial c_A}{\partial t} = - \frac{Q}{S\epsilon} \frac{\partial c_A}{\partial z} - \frac{3(1-\epsilon)}{\epsilon r_o} k_f (c_A - c_A \Big| r=r_o) + E_d \frac{\partial^2 c_A}{\partial z^2} \qquad (C-1)$$

Material balance of solid phase

$$D_s \frac{\partial}{\partial r} (r^2 \frac{\partial c_A}{\partial r}) = r^2 \frac{\partial c_A}{\partial t} \qquad (C-2)$$

Note that the concentration of component A in bulk fluid within the porous particle use the same notation c_A. It suggests that the inertness of porous particle enacts the solute molecule to be identical within two phases. The two boundary conditions related with Eq.C-2 are:

B.C. 1 $r = 0$, c_A = finite or $\frac{\partial c_A}{\partial r} = 0$ (C-3)

B.C. 2 $r = r_o$ $-N_{Ar} = D_s \frac{\partial c_A}{\partial r} = k_f (c_A - c_A \Big|_{r=0})$ (C-4)

I.C. and B.C. related with Eq.C-1:

I.C. at $t = t_o = 0$, $0 \leq z \leq L$

$$c_A\ (z,\ r>r_o,\ t=t_o) = c_{A,\ t_o} \qquad (C\text{-}5\text{-}1)$$

$$c_A\ (z,\ r=r_o,\ t=t_o) = c_{A,t_o}\Big|_{r=r_o} \qquad (C\text{-}5\text{-}2)$$

Note that $c_{A,t_o} = c_{A,\ t_o}\Big|_{r=r_o}$ at $t \leq t_o$

B.C. 1

$$C_I\delta(t) - c_A\Big|_{z=0} + \frac{S\epsilon E_d}{Q}\frac{\partial c_A}{\partial z}\Big|_{z=0} = 0 \qquad (C\text{-}6)$$

B.C. 2

$$\int_0^t (C_I\delta(t) - c_A\Big|_{z=L})dt = \frac{S\epsilon}{Q}\int_{z=0}^{z=L} c_A dz + \frac{3(1-\epsilon)S}{Qr_o^3}\int_{z=0}^{z=L}\int_{r=0}^{r=r_o} c_A r^2 dr dz \qquad (C\text{-}7)$$

Introducing the dimensionless form and substitute into Eq.C-1 to Eq.C-7.

$$C_A = \frac{c_A - c_{A,t_o}}{C_I\frac{L^2}{E_d}}\ ,\quad \tau = \frac{tE_d}{L^2}\ ,\quad \eta = \frac{z}{L}\ ,\quad R = \frac{r}{r_o}$$

Therefore, <u>fluid phase</u>:

$$\frac{\partial C_A}{\partial \tau} = \frac{\partial^2 C_A}{\partial \eta^2} - \frac{3(1-\epsilon)}{\epsilon r_o}k_f\frac{L^2}{E_d}(C_A - C_A\Big|_{R=1}) - \frac{QL}{S\epsilon E_d}\frac{\partial C_A}{\partial \eta} \qquad (C\text{-}8)$$

<u>Solid phase</u>:

$$\frac{D_s}{r_o^2}\frac{L^2}{E_d}\frac{1}{R^2}\left(R^2\frac{\partial C_A}{\partial R}\right) = \frac{\partial C_A}{\partial R} \qquad (C\text{-}9)$$

B.C. for solid phase become;

B.C. 1 at $R = 0$ C_A = finite or $\frac{\partial C_A}{\partial R} = 0$ (C-10)

B.C. 2 at $R = 1$ $\frac{\partial C_A}{\partial R} = Bi\ (C_A - C_A\big|_{R=1})$ (C-11)

I.C. and B.C. for fluid phase:

$$C_A(\eta\ ,\ R>1,\ \tau=0\ ) = 0 \qquad \text{(C-12-1)}$$

$$C_A(\eta\ ,\ R=1,\ \tau=0\ ) = 0 \qquad \text{(C-12-2)}$$

B.C. 1

$$\frac{E_d}{L^2}\,\delta\left(\frac{L^2}{E_d}\tau\right) - C_A\Big|_{\eta=0} + \frac{S\epsilon E_d}{Q\ L}\,\frac{\partial C_A}{\partial \eta}\Big|_{\eta=0} = 0 \qquad \text{(C-13)}$$

Note that total material balance at $\tau \leq 0$ (I.C.) is true.

$$0 - \frac{L^2}{E_d}\int_0^{\tau} c_{A,t_o}\Big|_{\eta=1} d\tau = \frac{S\epsilon L}{Q}\int_0^1 c_{A,t_o} d\eta + \frac{3(1-\epsilon)S}{Qr_o^3}\int_0^1\int_0^1 c_{A,t_o} R^2 r_o^3 dR * Ld \qquad \text{(C-14)}$$

With the aid of Eq.C-14, B.C. 2 becomes;

$$\frac{E_d}{L^2}\int_0^{\tau}\delta\left(\frac{L^2}{E_d}\tau\right)d\tau - \int_0^{\tau} C_A\Big|_{\eta=1} d\tau = \frac{S\epsilon E_d}{QL}\int_0^1 C_A d\eta + \frac{3(1-\epsilon)SE_d}{QL}\int_0^1\int_0^1 C_A R^2 dR\ d\eta \qquad \text{(C-15)}$$

Taking the Laplace transform with respect to τ from eqns. C-8 to C-15 except Eq.C-14;

Fluid phase;

$$p\,\overline{C_A} = \frac{d^2\,\overline{C_A}}{d\eta^2} - w\left(\overline{C_A} - \overline{C_A}\Big|_{R=1}\right) - A\,\frac{d\,\overline{C_A}}{d\eta} \qquad \text{(C-16)}$$

B.C. 1

$$\left(\frac{E_d}{L^2}\right)^2 - \overline{C_A}\Big|_{\eta=0} + \frac{1}{A}\,\frac{d\,\overline{C_A}}{d\eta}\Big|_{\eta=0} = 0 \qquad \text{(C-16-1)}$$

B.C. 2

$$\frac{1}{p}\left(\left(\frac{E_d}{L^2}\right)^2 - \overline{C_A}\Big|_{\eta=1}\right) = \frac{1}{A}\int_{\eta=0}^{\eta=1}\overline{C_A}\,d\eta + \frac{3(1-\epsilon)SE_d}{QL}\int_{\eta=0}^{\eta=1}\int_{R=0}^{R=1}\overline{C_A}R^2\,dR\,d\eta \qquad \text{(C-16-2)}$$

Solid phase:

$$p\overline{C_A} = \frac{D_s L^2}{r_o^2 E_d}\left(\frac{d^2\,\overline{C_A}}{dR^2} + \frac{2}{R}\,\frac{d\overline{C_A}}{dR}\right) \qquad \text{(C-17)}$$

B.C. 1 at R=0 $\quad \overline{C_A}$ = finite (C-18-1)

B.C. 2 at R=1 $\quad \dfrac{d\,\overline{C_A}}{dR} = Bi\left(\overline{C_A} - \overline{C_A}\Big|_{R=1}\right)$ (C-18-2)

Solving for Eq.C-17 and evaluated the two constants C_1 and C_2 by Eqns.C-18-1 and C-18-2, we have;

$$\overline{C_A} = R^{-\frac{1}{2}}\left(\frac{BiR^{-\frac{1}{2}}I_{\frac{1}{2}}(\sqrt{pc}R)}{\sqrt{pc}\,I_{3/2}(\sqrt{pc}) + Bi\cdot I_{\frac{1}{2}}(\sqrt{pc})}\right)\overline{C_A} \qquad \text{(C-19)}$$

where $c = r_o^2 E_d / D_s L^2$

substituting $R = 1$ into Eq.C-19 and the result is therefore substituted into Eq.C-16 to have;

$$\frac{d^2 \overline{C_A}}{d\eta^2} - A\frac{d \overline{C_A}}{d\eta} - F\overline{C_A} = 0 \qquad \text{(C-20)}$$

where $$F(p) = p + \frac{w\sqrt{pc}\, I_{3/2}(\sqrt{pc})}{\sqrt{pc}\, I_{3/2}(\sqrt{pc}) + Bi\, I_{\frac{1}{2}}(\sqrt{pc})} \qquad \text{(C-21)}$$

Solving for Eq. C-20 and evaluate the two constants C_3 and C_4 by two B.C. Eqns. C-16-1 and C-16-2, we may generate the dimensionless concentration in Laplace domain.

$$\overline{C_A}(\eta,p) = e^{\frac{A}{2}\eta}\left(\frac{A\sinh(1-\eta)\frac{\sqrt{\Gamma}}{2} + \sqrt{\Gamma}\cosh(1-\eta)\frac{\sqrt{\Gamma}}{2}}{\sqrt{\Gamma}\cosh\frac{\sqrt{\Gamma}}{2} + (A+\frac{2F}{A})\sinh\frac{\sqrt{\Gamma}}{2}}\right)\frac{E_d^2}{L^4} \qquad \text{(C-22)}$$

where $\sqrt{\Gamma} = \sqrt{A^2 + 4F}$.

After checking the validity of Eq.C-22, the inverse Laplace transform can be performed. The procedures are similar to Sec.2-1-A. We may conclude that Eq.C-22 has no branch points and the power of p at the denominator is higher than that of numerator. By the application of residue theorem, the similar procedures are discussed in Sec. 2-1-B, we will first solve for B_n from

the denominator of Eq.C-22 to have, $\tan\frac{\beta_n}{2} = -\frac{2A\beta_n}{A^2 - \beta_n^2}$ (C-23)
where $-\beta_n^2 = A^2 + 4F$ and substitute F(p), Eq.C-21 into Eq.C-24 for solving p_{mn}. Once the p_{mn} are obtained, we are ready for applying the residue theorem, i.e.,

$$L^{-1}(\overline{C_A}(\eta,p)) = \lim_{p\to p_{mn}}(p-p_{mn})e^{p_{mn}\tau}e^{\frac{A\eta}{2}}\frac{E_d^2}{L^4}\frac{J(p)}{L(p)} = e^{\frac{A\eta}{2}}\frac{E_d^2}{L^4}\sum_{m=1}^{\infty}\sum_{n=1}^{\infty}e^{p_{mn}\tau}\frac{J(p_{mn})}{L'(p_{mn})}$$

where $J(p_{mn}) = \cos\frac{\beta_n}{2}(1-\eta) + \frac{A}{\beta_n}\sin\frac{\beta_n}{2}(1-\eta)$

$$L'(p_{mn}) = \frac{d(L(p_{mn}))}{dp} = \frac{dF}{dp}\left(\frac{\beta_n^2(A+1)}{A\beta_n^3}\sin\frac{\beta_n}{2} - \frac{A^2-\beta_n^2}{2A\beta_n^2}\cos\frac{\beta_n}{2}\right)$$

$$\frac{dF}{dp} = 1 + w\frac{\frac{Bi\ c}{2}\left((\sin\phi)^2+(\cos\phi-\frac{\sin\phi}{\phi})^2\right) - \frac{Bi}{2}\sqrt{\frac{c}{S_{mn}}}\sin\phi(\cos\phi-\frac{\sin\phi}{\phi})}{\left(\phi(\cos\phi-\frac{\sin\phi}{\phi}) + Bi\sin\phi\right)^2} \qquad (C-25)$$

$$\phi = \sqrt{S_{mn}c}\ ,\quad S_{mn} = -p_{mn}\ ,\quad c = \frac{r_o^2E_d}{L^2D_s}$$

We may obtain the final solution $C_A(\eta,\tau)$ in expression as;

$$C_A(\eta,\tau) = \sum_{m=1}^{\infty}\sum_{n=1}^{\infty}e^{\frac{A}{2}\eta+p_{mn}\tau}\frac{\cos\frac{\beta_n}{2}(1-\eta) + \frac{A}{\beta_n}\sin\frac{\beta_n}{2}(1-\eta)}{\left(\frac{dF}{dp}\right)\left(\frac{\beta_n^2(A+1)+A^2}{A\beta_n^3}\sin\frac{\beta_n}{2} - \frac{(A^2-\beta_n^2)}{2A\beta_n^2}\cos\frac{\beta_n}{2}\right)}\frac{E_d^2}{L^4} \qquad (C-26)$$

It describes the concentration of component A at any distance measured from column inlet and at any instantaneous time. However, we are interested for the concentration profile at $\eta = 1$, i.e., the end of the column. By substituting $\eta = 1$ into Eq.C-26, we may have the final solution which describes the component A expressed as a function of time at the outlet of the column;

$$C_A(\tau,1) = \sum_{m=1}^{\infty} \sum_{n=1}^{\infty} e^{\frac{A}{2}\eta + p_{mn}\tau} \frac{\beta_n^2 E_d^2}{(\frac{dF}{dp})(\frac{B_n^2(A+1)+A^2}{A\beta_n}\sin\frac{\beta_n}{2} - \frac{A^2-B_n^2}{2A}\cos\frac{\beta_n}{2})\, L^4} \quad (C-27)$$

where dF/dp = Eq.C-25 .

Discussion

The calculated results of gel permeation packed bed, Eq.C-26, are plotted based on model parameters to study the individual effect of the elution profile.

Figures 28 to 30 illustrate effects of volumetric flow rate Q, column length L, and cross sectional area S. The conditions which may prolong the duration of solute molecule in the column are low volumetric flow rate, large column length, and large cross sectional area. Similar results as those obtained for ion exchange packed bed are obtained. Long duration of the solute molecule in the column will deteriorate the column efficiency, and result in peak broadening and tailing.

The effect of mass transfer coefficient k_f is shown in Figure 31. The film resistance will be the first obstacle that the solute molecule has to overcome in order to diffuse into the solid phase. The small k_f value means large film resistance for diffusion into the solid phase and will therefore result in narrow and sharp peaks. Large k_f values indicate small film resistance and will enable the molecule to spend more time in the solid phase. Therefore, the resulting peaks will be broad with significant tailing and the break point is delayed.

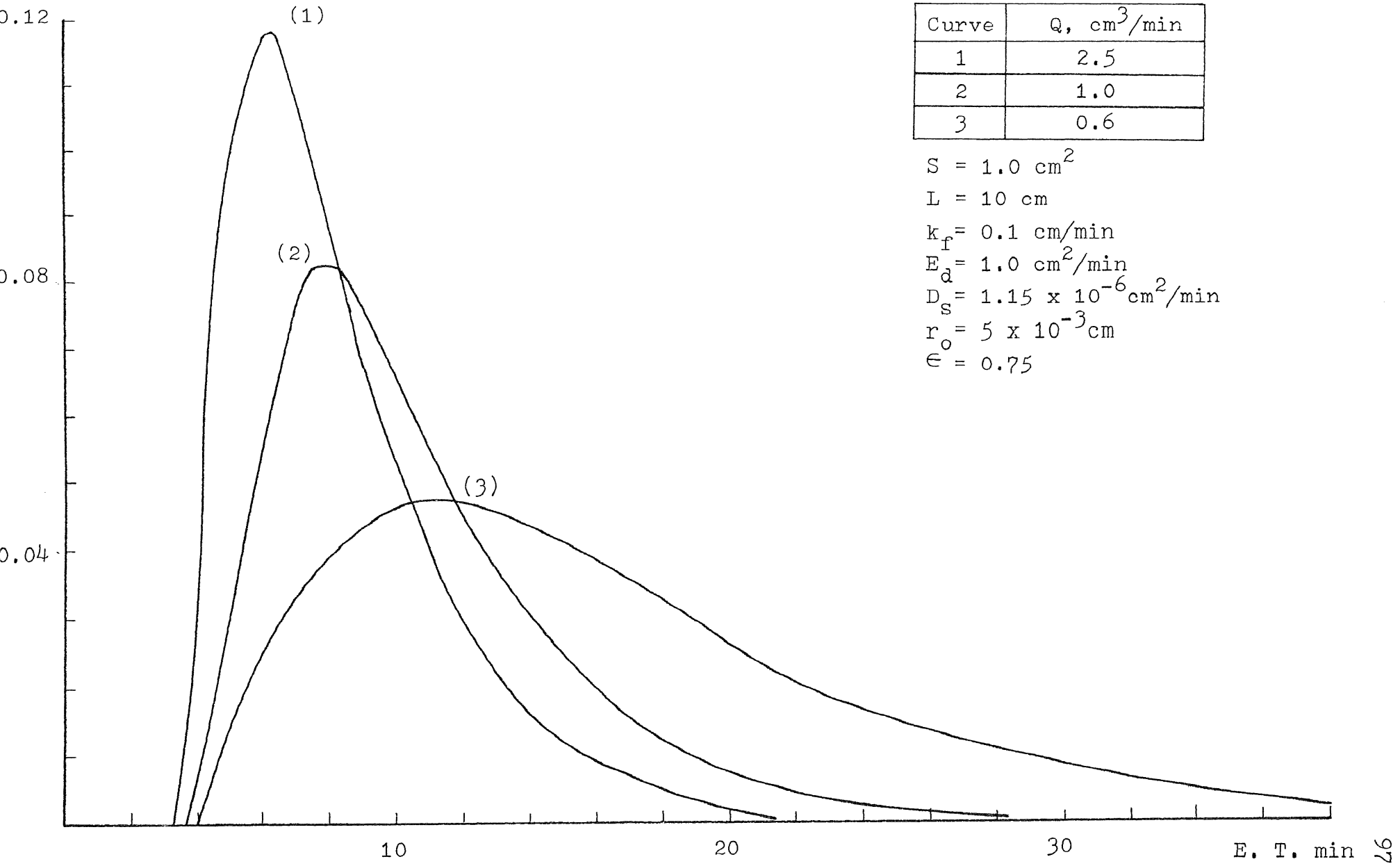

Curve	Q, cm^3/min
1	2.5
2	1.0
3	0.6

$S = 1.0\ cm^2$

$L = 10\ cm$

$k_f = 0.1\ cm/min$

$E_d = 1.0\ cm^2/min$

$D_s = 1.15 \times 10^{-6} cm^2/min$

$r_o = 5 \times 10^{-3} cm$

$\epsilon = 0.75$

Fig. 28 Effect of Volumetric Flow Rate, Q (GPC)

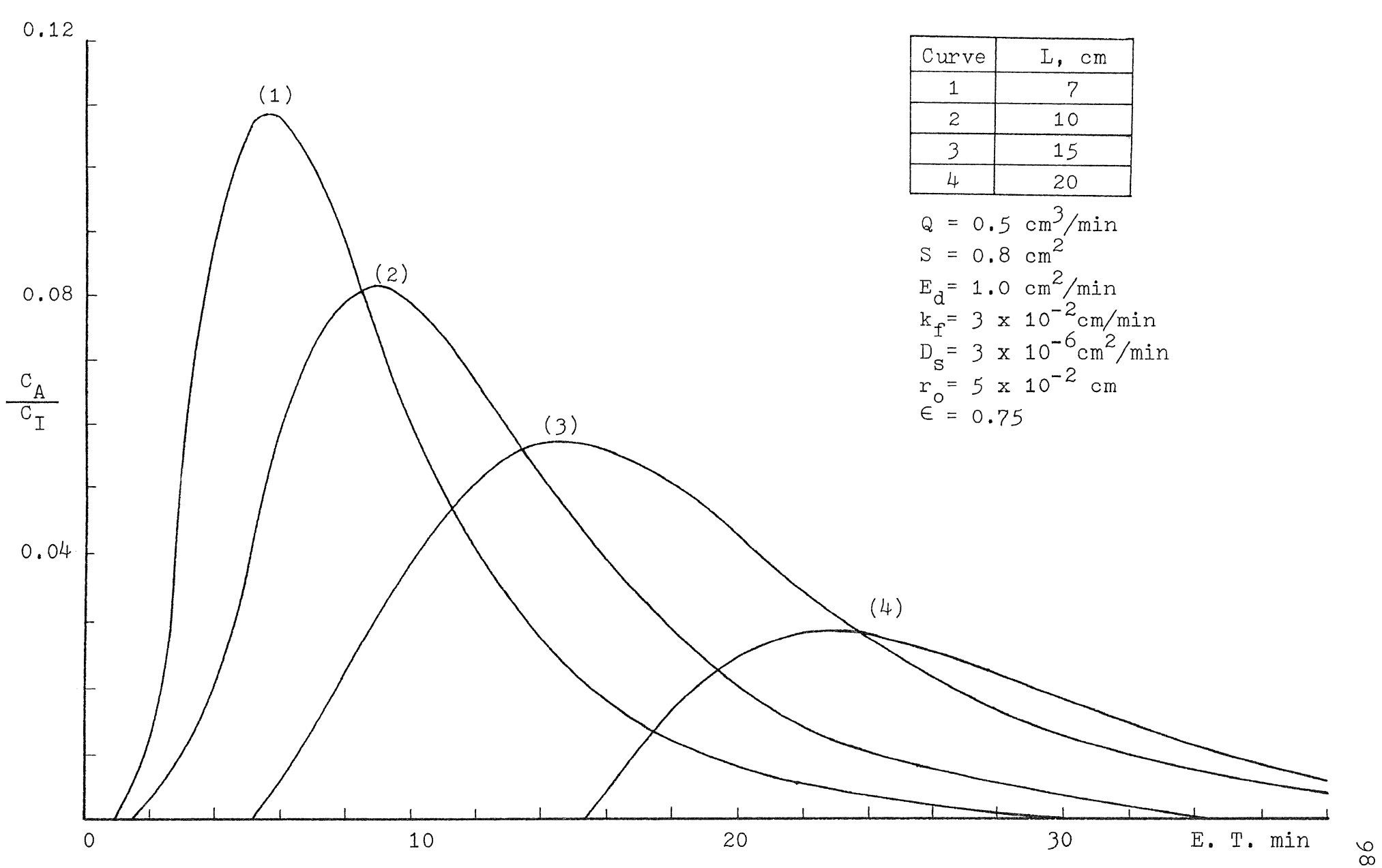

Fig. 29 Effect of Column Length, L

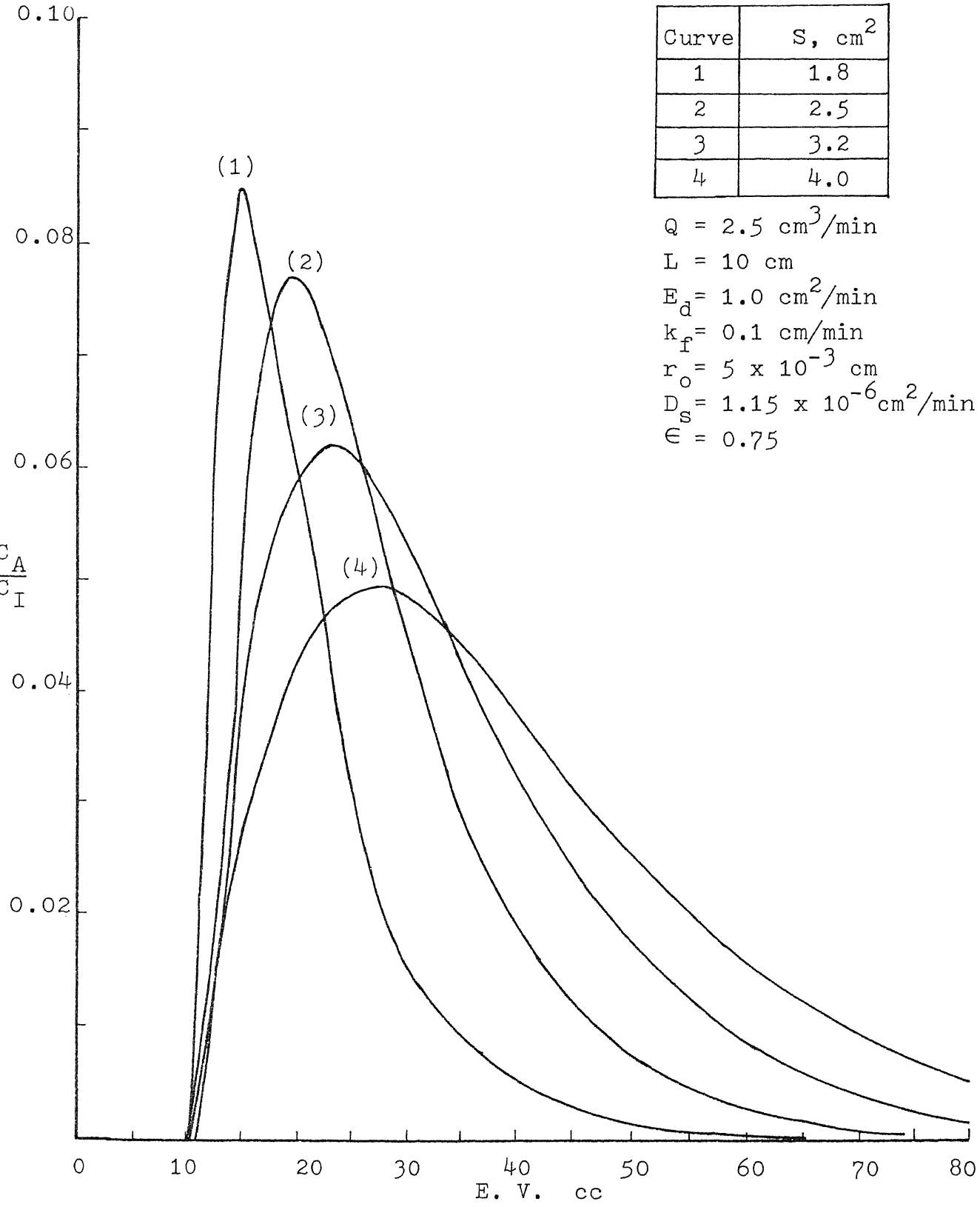

Curve	S, cm^2
1	1.8
2	2.5
3	3.2
4	4.0

$Q = 2.5\ cm^3/min$
$L = 10\ cm$
$E_d = 1.0\ cm^2/min$
$k_f = 0.1\ cm/min$
$r_o = 5 \times 10^{-3}\ cm$
$D_s = 1.15 \times 10^{-6} cm^2/min$
$\epsilon = 0.75$

Fig. 30 Effect of Cross Sectional Area, S

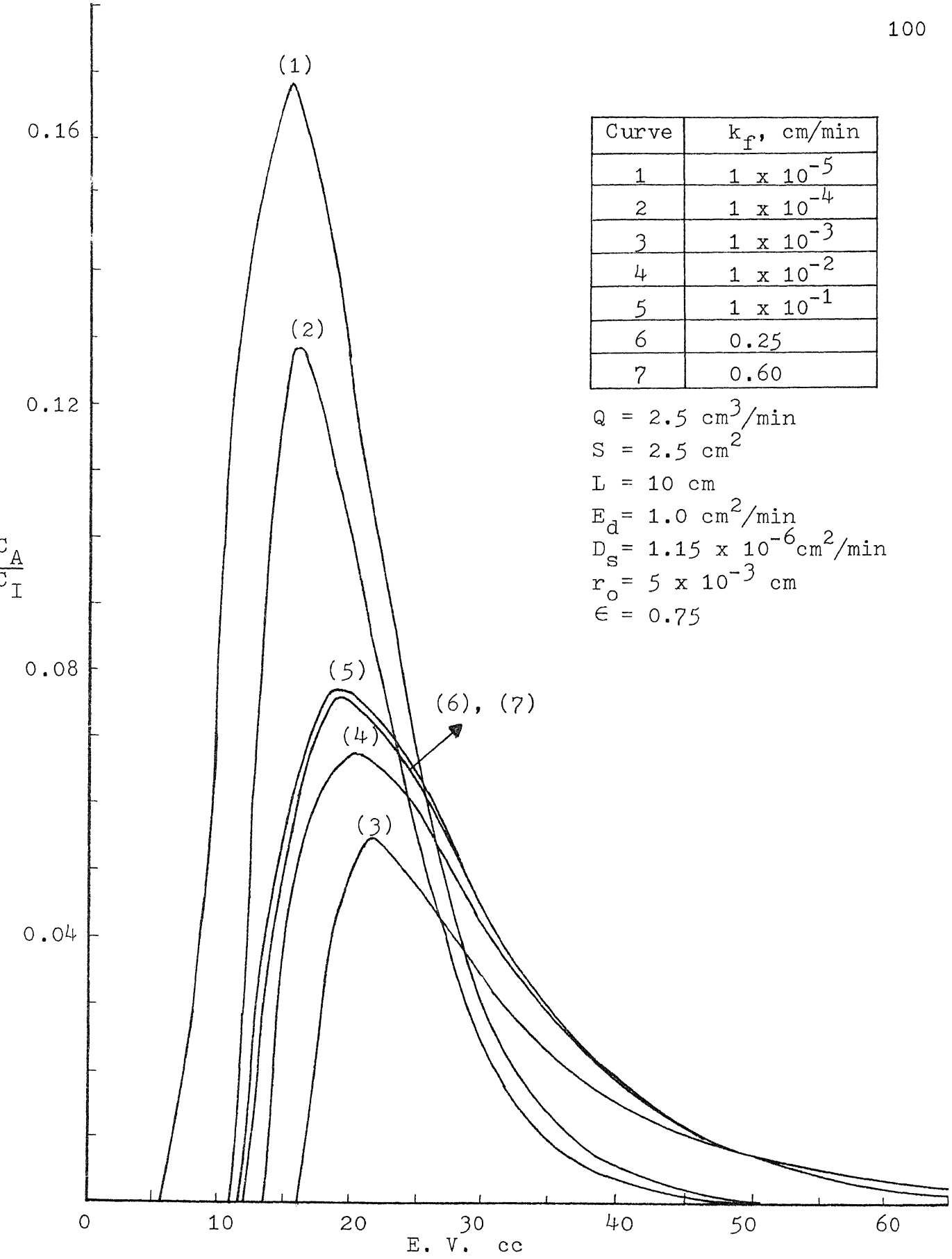

Curve	k_f, cm/min
1	1×10^{-5}
2	1×10^{-4}
3	1×10^{-3}
4	1×10^{-2}
5	1×10^{-1}
6	0.25
7	0.60

$Q = 2.5\ cm^3/min$
$S = 2.5\ cm^2$
$L = 10\ cm$
$E_d = 1.0\ cm^2/min$
$D_s = 1.15 \times 10^{-6} cm^2/min$
$r_o = 5 \times 10^{-3}\ cm$
$\epsilon = 0.75$

Fig. 31 Effect of Mass Transfer Coefficient, k_f

There is a break point for k_f shown in curve 3 of Fig. 31 ($k_f = 1x10^{-3}$). This peak is the flattest and with the longest tail when compared with smaller and large k_f curves. Similar results were also observed in Fig.20 and Fig.21 when the surface adsorption with pore diffusion model was discussed. The reason for this behavior is given in the discussion of Sec. 2-1-2.

Figure 32 illustrates the effect of axial dispersion E_d; that is the combination of molecular and eddy diffusivity in the fluid phase. Similar results are obtained as with the discussion in Sec.2-1. High E_d values will have early break and long tail peak. The efficiency of the chromatographic column decreases with an increase in axial dispersion.

Figure 33 shows the effect of pore diffusion D_s on the elution profile for a fixed k_f value. The small pore diffusivity will have sharp profile and earlier break point as compare with the large D_s value. As to the relation of molecular weight and pore diffusivity, the high molecular weight (large molecules) have small diffusivity and small molecules have large diffusivity. Also, large molecules have difficulty diffusing into the solid phase. Therefore, large molecules will have an early break point and sharp peak, while small molecules will elute later. This also illustrates the separation principle of a gel permeation column, and how it can separate different molecular weight mixtures.

Curve	E_d, cm^2/min
1	0.5
2	1.0
3	4.0

$Q = 0.5\ cm^3/min$
$S = 1.0\ cm^2$
$L = 10\ cm$
$k_f = 3 \times 10^{-2} cm/min$
$D_s = 3 \times 10^{-6} cm^2/min$
$r_o = 5 \times 10^{-2} cm$
$\epsilon = 0.75$

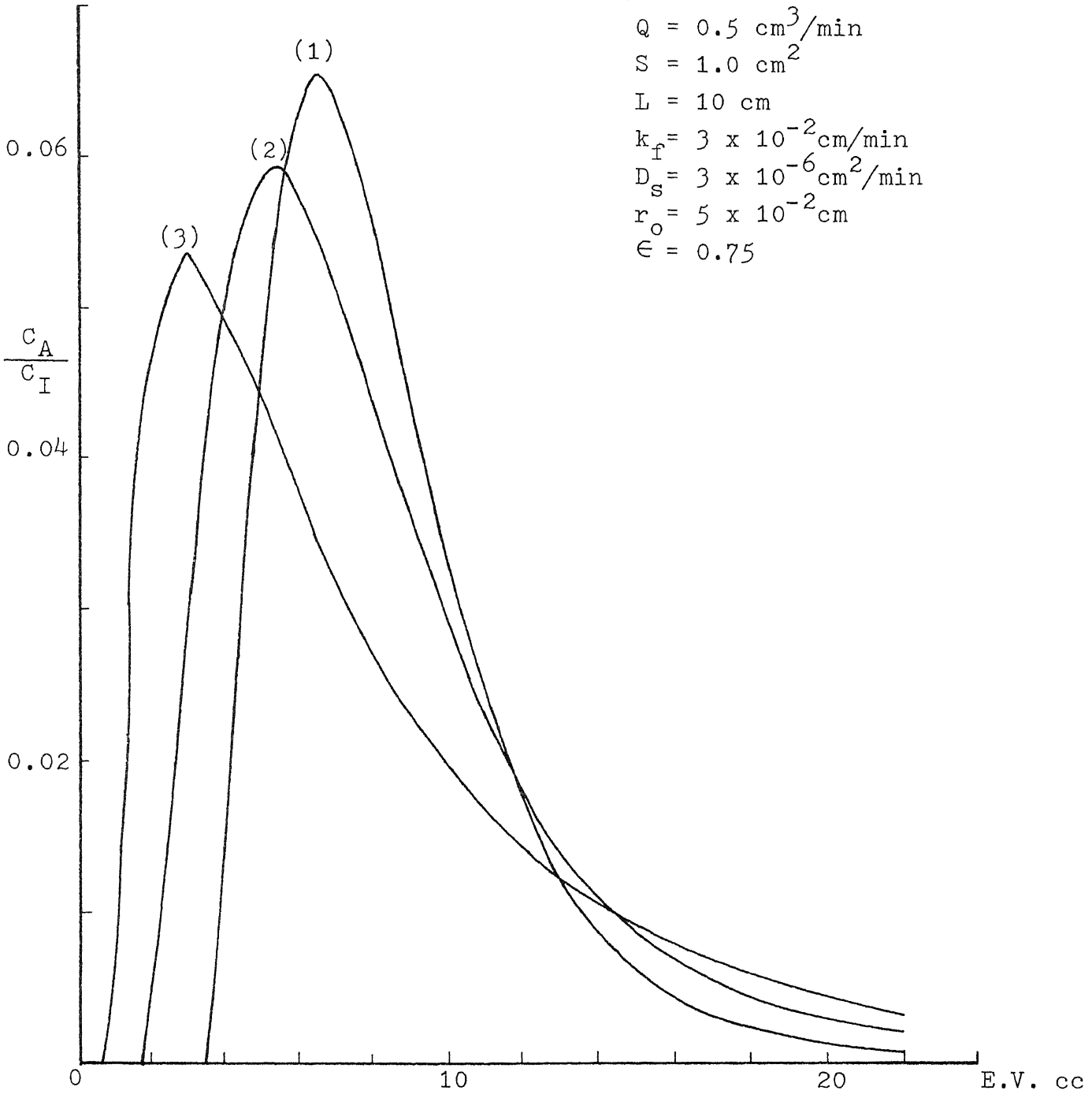

Fig. 32 Effect of Axial Dispersion, E_d

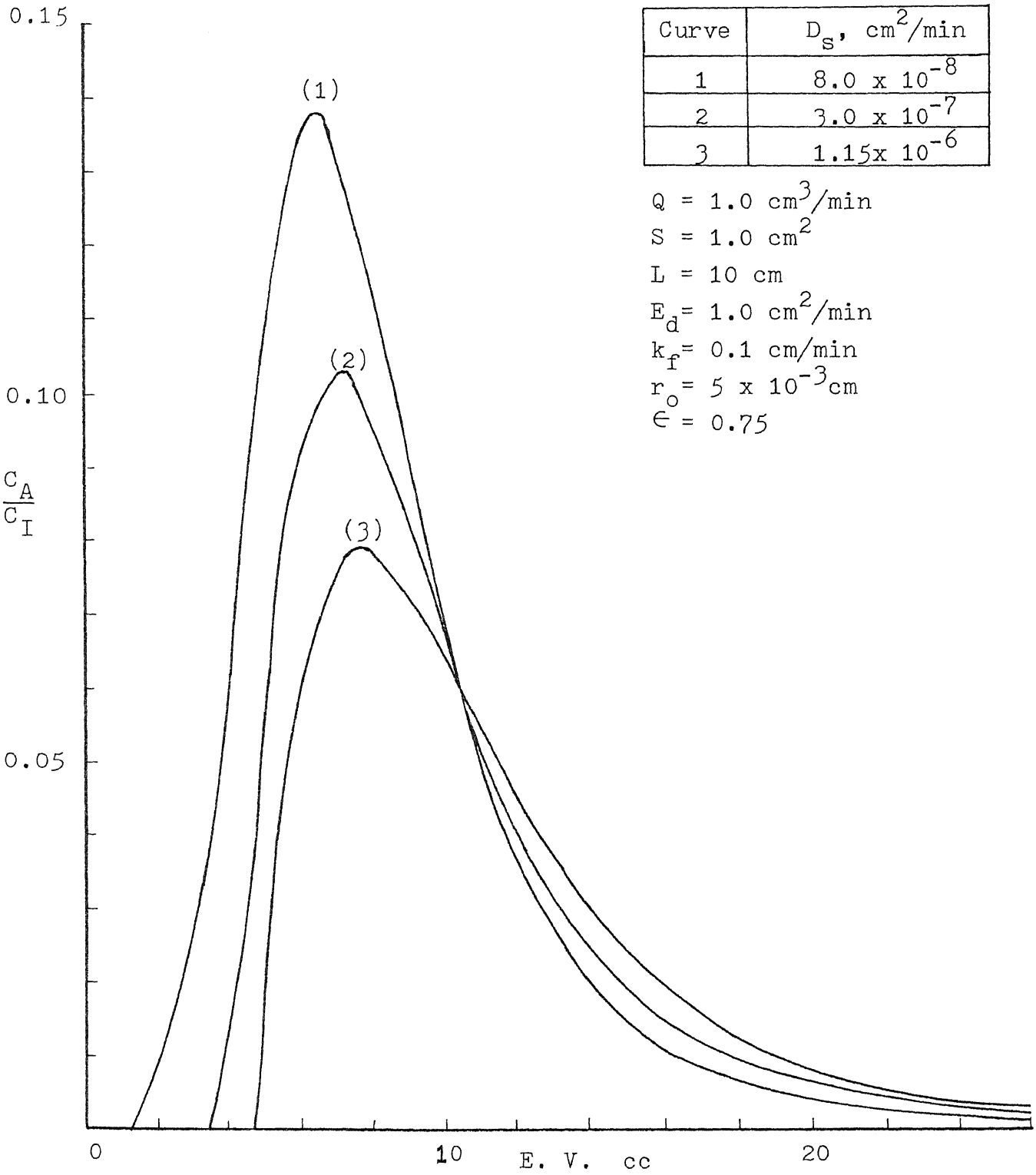

Curve	D_s, cm^2/min
1	8.0×10^{-8}
2	3.0×10^{-7}
3	1.15×10^{-6}

$Q = 1.0\ cm^3/min$
$S = 1.0\ cm^2$
$L = 10\ cm$
$E_d = 1.0\ cm^2/min$
$k_f = 0.1\ cm/min$
$r_o = 5 \times 10^{-3} cm$
$\epsilon = 0.75$

Fig. 33 Effect of Pore Diffusion, D_s

Figures 34 and 35 show the effect of solid particle size r_o. These two figures illustrate the basic principle that the large particles have less effective diffusion pore volume available. Therefore, the solute will have less opportunity to diffuse into the solid phase and result in earlier elution characterized by a sharp peak and short tail. In constrast, it is not difficult to infer that the small particle will deteriorate the elution profile due to more effective diffusion pore volumes. However, these two figures illustrate that there is a critical particle size which will result in the worst column efficiency and elution profile where $r_o = 1x10^{-3}$ cm. For those particles with size larger or smaller than the critical r_o, the peak tends to show better column efficiency but the difference is not significant. This implies that the particle size of the GPC packed bed is not so sensitive in affecting an adequate separation, except for particles larger than about $r_o = 0.01$cm. This also illustrates the basic GPC separation principle that the solute molecular weight and molecular shape are the fundamental factors which influence the resolution. Unlike the ion exchange packed bed, the separation by GPC is not an on/off control scheme by the variation of parameters such as buffer pH and/or buffer ionic strength. Therefore, a GPC separation can be performed in the presence of essential ion of cofactors, detergents, at biological temperature (37^{o}C), or other conditions where ion exchange

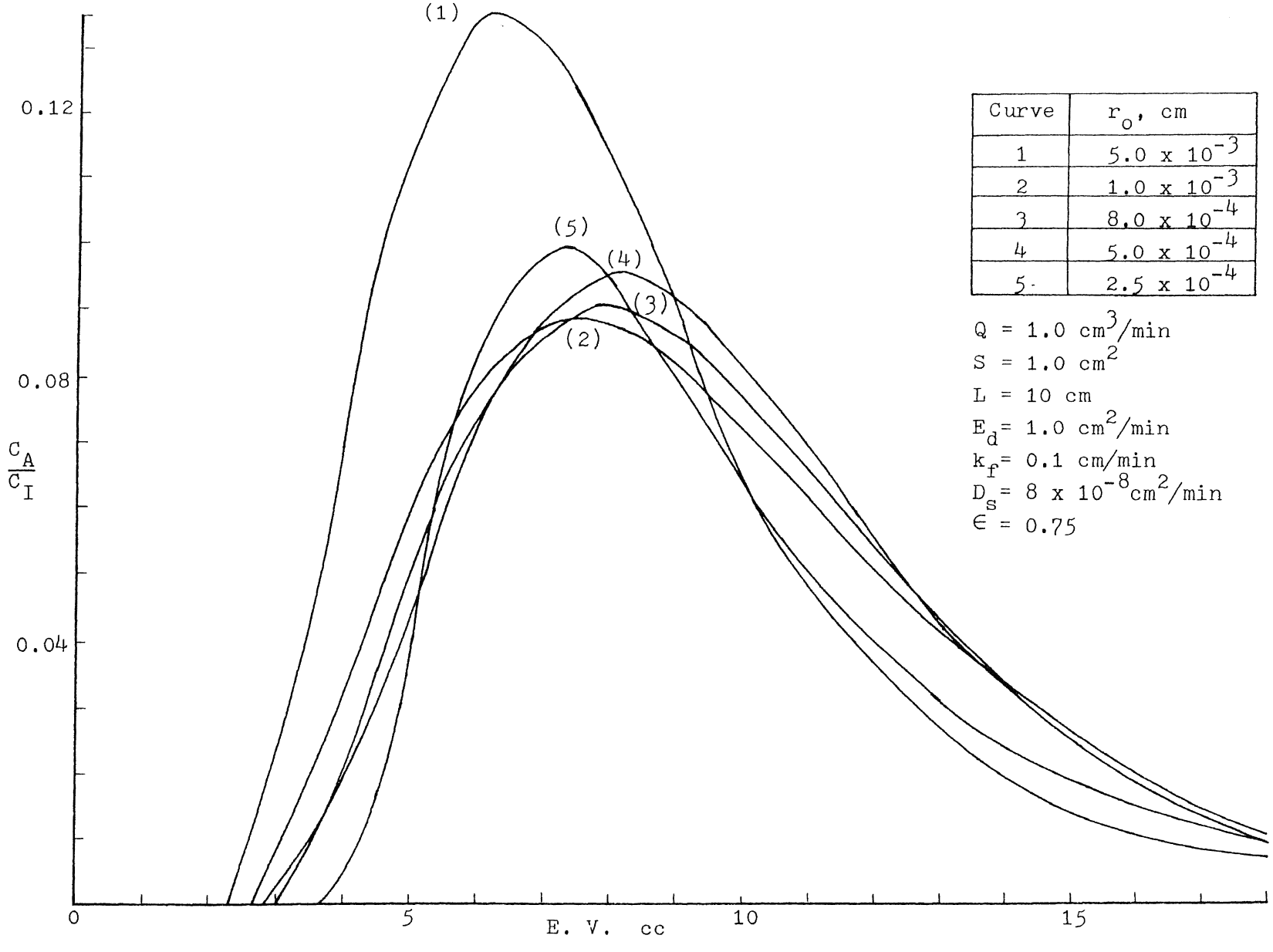

Fig. 34 Effect of Particle Size, r_o

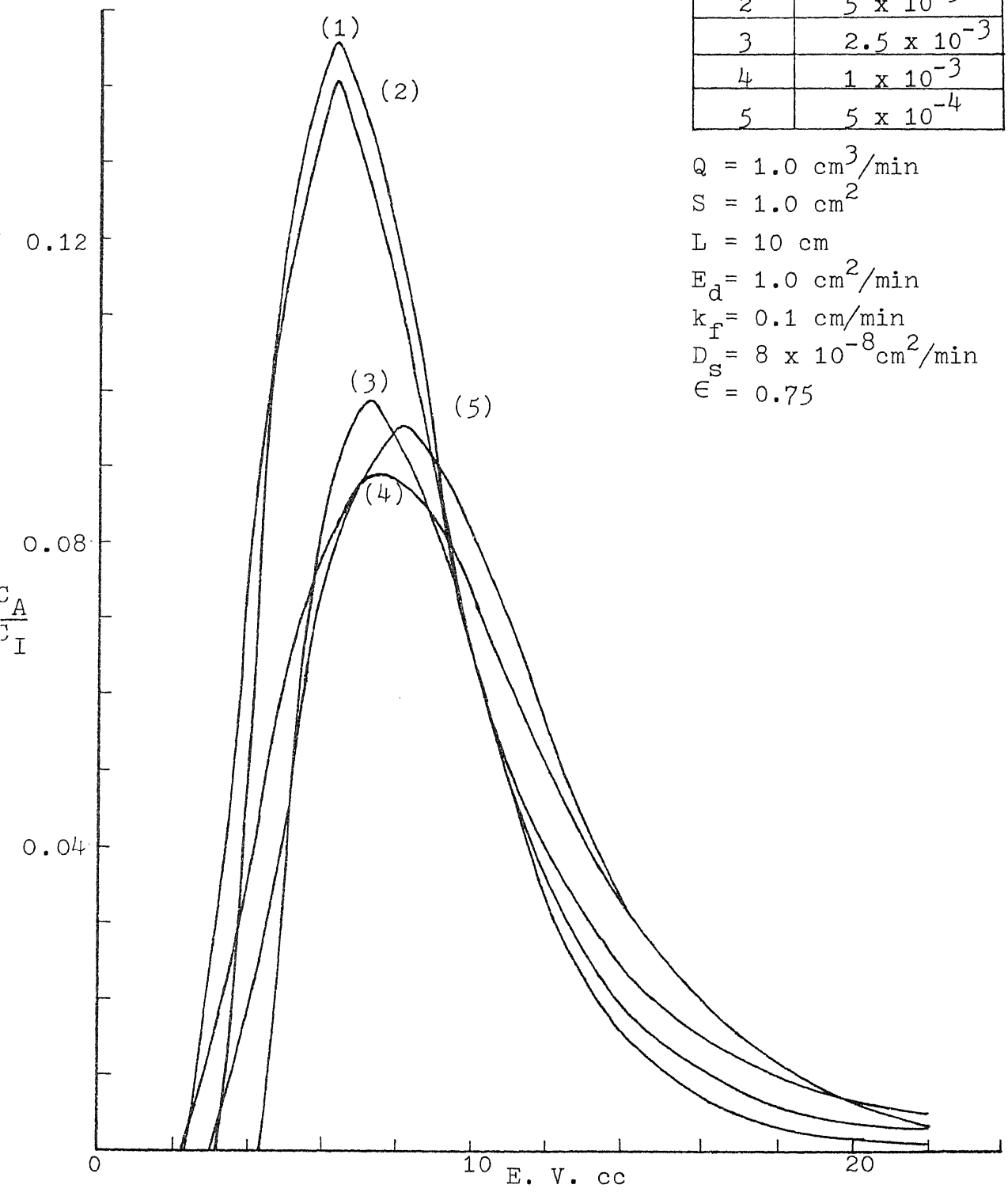

Curve	r_o, cm
1	1×10^{-2}
2	5×10^{-3}
3	2.5×10^{-3}
4	1×10^{-3}
5	5×10^{-4}

$Q = 1.0\ cm^3/min$
$S = 1.0\ cm^2$
$L = 10\ cm$
$E_d = 1.0\ cm^2/min$
$k_f = 0.1\ cm/min$
$D_s = 8 \times 10^{-8} cm^2/min$
$\epsilon = 0.75$

Fig. 35 Effect of Particle Size, r_o

separation is inappropriate. This is the main reason that GPC is a reliable and straight forward method for the separation of different molecular weight mixtures.

3. Experimental Study

Proceeding with the prior mathematical model development for a chromatographic column, two protein systems were experimentally studied on an ion exchange packed bed and the results are discussed in Ch.4 and Ch.5 to demonstrate the application of the surface adsorption model on the prediction of elution profile, optimization and purification method development. The content of this chapter will introduce the background of protein systems, equipment, strategy, set up, measurement of experimental parameters, and a discussion of the operation mode for cyclic zone separation.

3-1 Protein systems

A two component protein mixture was selected as a model system to examine the feasibility of separation on an ion exchange resin and to explore the dynamic behavior of column operation. The experimental study will emphasize the application of the surface adsorption model.

The crude enzyme alkaline phosphatase from human placenta was chosen as the real system, and the purification was performed such that the separation method and the application of

the surface adsorption model are combined in discussion of different aspects.

Model system- human hemoglobin and albumin

Worthington human hemoblobin and serium albumin are used. The hemoglobin is simulated as the protein of interest and albumin as impurity. Two proteins were equally weighted and dissolved in buffer solution and separated on a cation exchanger (R^-) by pH cyclic zone.

Hemoblobin functions as oxygen, carbon dioxide, and H^+ carrier in human blood cells. Its molecular weight is approximately 63,000 and isoelectric point is at pH 6.7. It is the best understood of the allosteric proteins. Hemoglobin consists of four polypeptide chains of about 574 amino acid residue.

Albumin is the most abundant of the plasma proteins and plays a functional role in osmotic regulation and in the binding and transport of substances of physiological and metabolic importance. It has a molecular weight of 65000 to 66000, and an isoelectric point at pH 4.6 - 4.7 . The albumin molecule at physiological pH is regarded as a compact, dense, negatively, charged molecule whose structure consists of a single polypeptide

chain of about 575 amino acids.

Real system: Alkaline phosphatase (Human placenta) - HPAP

Alkaline phosphatase is a broad term associated with nonspecific phosphomonesterases with activity optima at alkaline pH.

$$\text{orthophosphoric monoester} + H_2O \longrightarrow \text{Alcohol} + H_3PO_4$$

Isoenzymes of alkaline phosphatase were found in bacteria, beef kidney, chicken intestine, in addition to human placenta and liver. They all have different composition. Human placenta alkaline phosphatase (HPAP) is present in many mammalian tissues and is usually associated with intracellar lipoprotein membranes. HPAP catalyzes hydrolysis of phosphomonoesters. Alkaline phosphatase has an isoelectric point of pH 4.5 and a molecular weight approximately equal to 70,000. It is a znic metalloenzyme that probably exists as a dimer. Its amino acid composition has been reported by Ghosh and Fishman in 1968.

The crude (partially purified) enzyme HPAP is obtained from Sigma Chemical Co. Since the enzyme is extracted from the human placental fluid, some of the proteins are thought to be undesirable; the major impurity is albumin.

HPAP was presented in concentration of 0.02 wt% in buffer solution and purified on an anion exchanger (R^+) by concentration cyclic zone.

3-2 Experimental set up

The cyclic zone adsorption experimental apparatus is shown in Fig.36. Two different sizes of chromatographic column and two types ion exchanger were used. A low pressure Pharmacia chromatography K16/40 column (0.016 m ID and 0.4 m in height) was packed with 8cm height of CM Sepharose (a cation exchanger). The K16/40 column was used for small scale separation. The other semi-preparative scale column - LKB 7900 Uniphor column was modified for continuous operation by the addition of a second elution stopper. Minor modifications were made on the elution stopper and the filter in order to supply adequate support for the solid phase. The column (0.026 m ID and 0.15m in height) was fully loaded with CM Sepharose (a cation exchanger). Both the small scale column and semi- preparative scale column will be used for the separation of the model protein system. The results will be discussed in Ch. 4.

The column used to purify the real enzyme system alkaline phosphatase was a Pharmicia chromatography K16/40 column packed to an 8cm height of DEAE-Sepharose (a anion exchanger). The

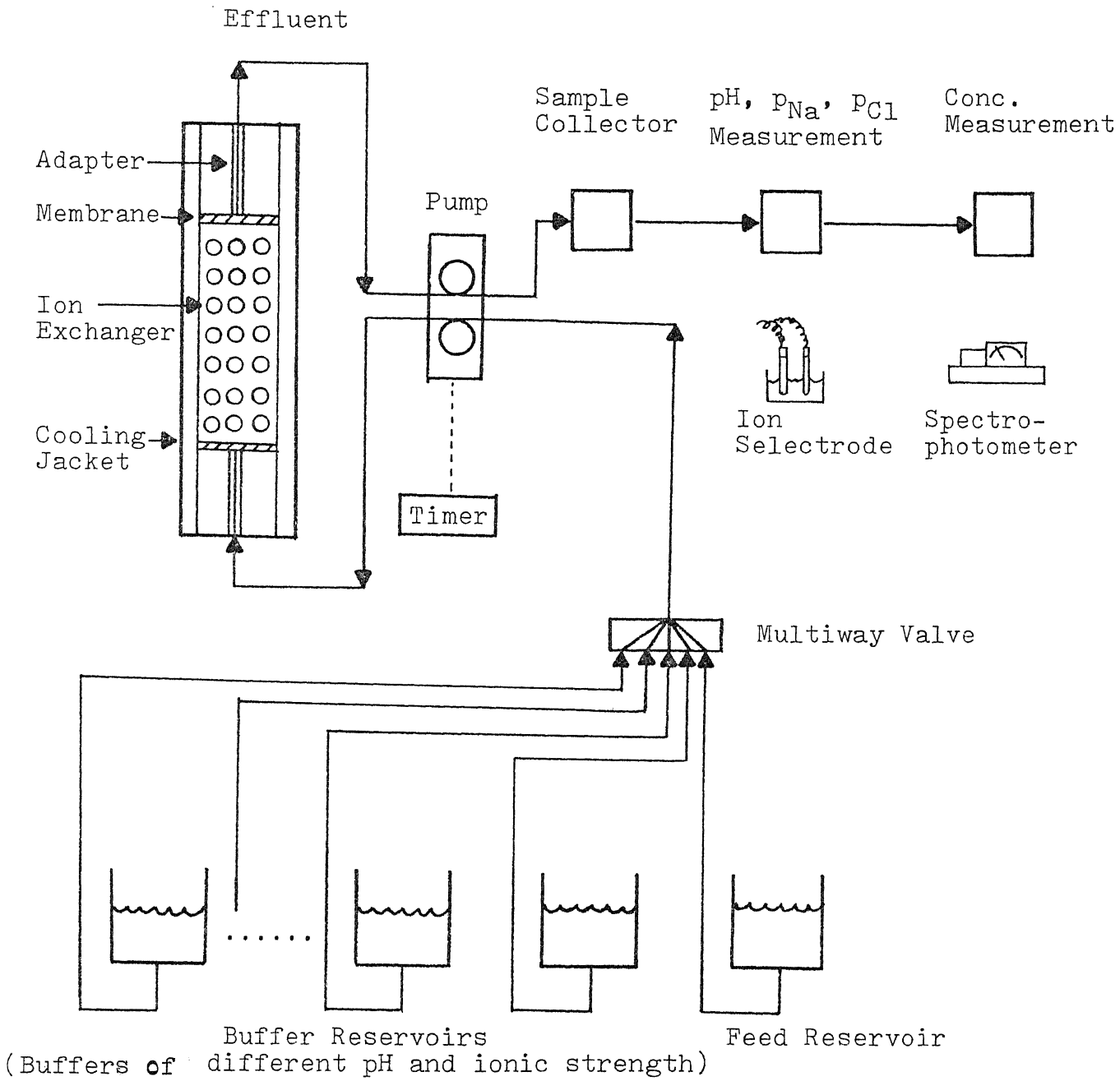

Fig. 36 Experimental Apparatus for Cyclic Zone Adsorption

results for the separation of two enzyme will be discussed in Ch.5.

The column assemblies were maintained at 278 K using a refrigeration unit with circulation of cooling water through the the column jackets or the jackets of the Uniphor buffer chamber. The external buffer reserviors (2 liter volume) was kept at 288 K. Reciprocating flow through the system was achieved by using a reversible peristalic pump manufactured by Pharmacia. The feed pump was connected to a timer for precise measurement of the sample volume. Multiway valves were installed on each inlet channel in order to introduce the reservior liquids, feed and buffer at different pH and/or ionic strength. Each sample stream was collected in a clean test tube at equal time intervals. The pH and pNa/pCL and protein concentration was measured for each sample collected.

The pHM61 laboratory pH meter was used for pH measurement. The concentration of sodium ion and chloride ion were denoted as pNa and pCL, respectively. The pNa were measured by K401 Calomel electrode as reference electrode and G502 Na sodium selectrode. The pCL was measured by F1012CL chloride selectrode with a K701 Calomel electrode as reference electrode. All of these ion selectrodes were purchased from Radiometer Instrument Co.

Each sample concentration was determined by using a Bausch

and Lomb-710 spectrometer. Hemoglobin was determined by absorbance at a wavelength of 403 μm, and the hemoglobin absorbance reading were corrected for pH as explained in Appendix A. Total protein was determined by absorbance at a wavelength of 595 μm by using Bio-Rad protein assay. Albumin concentrations were then determined by difference. The details of the measurement and method are given in Appendix A-1. The enzyme activity of alkaline phosphatase was determined by measuring the increament of absorbance, at the wavelength of 405 μm within a constant time interval, resulting from the hydrolysis of p-nitrophenylphosphate (Worthington, 1977). The measured activity for each sample was then divided by the activity of the feed and denoted as r_{405}. The Bio-Rad protein assay was used to determine the total protein concentration by measuring absorbance at wavelength of 595 μm. With a treatment similar to the enzyme activity, the total concentration was denoted as r_{595}. The details of concentration measurements are given in Appendix A-2.

3-3 Ion exchange and buffer systems

The pH and ionic strength dependence of ion exchangers have been discussed in Sec.1-4-1. Sepharose ion exchangers are based on Sepharose CL-6B. The two resins can be differentiated as:

1. Anion exchanger, Diethylaminoethyl (DEAE), R^{+}

   The counter ion for DEAE Sepharose is Cl^{-}.

2. Cation exchanger, Carboxymethyl (CM), R^-

The counter ion for CM Sepharose is Na^+.

The counter ions Na^+ and Cl^- reveal the necessity for the measurement of pNa and pCl. Because the sites at which Na^+ or Cl^- attached to the ion exchanger may very well be the active sites for protein molecule to attach on. If there is vigorous competition between ions, the protein molecules may be desorpted from the ion exchanger. The desorption/adsorption phenomenon illustrates the basic separation principle and thus the physical meaning of equilibrium constant, m (discussed in Sec.2-1).

The choice of buffer system is actually an optimization between that adsorbed proteins and ion exchangers. In general, the procedures are tedious but straight forward. First of all, we may start from the choice of ion exchanger matrix. The general procedures have been discussed in Sec. 1-4-1 of pH dependence. As with the choice of ion exchanger, there are a number of variables which have to be considered. These include:

<u>The choice of buffer substance</u>

If the buffering ions carry a charge opposite to that of the functional groups of the ion exchanger, they will take part in the ion exchange process and cause local disturbance in pH.

Therefore, it is preferable to use;

a. Cationic buffer (positive) with anion exchanger (R^+).

b. Anion buffer (negative) with cation exchangers (R^-).

For example, Tris, ammonium, and alkylamines are cationic buffers associate with anion exchanger (R^+) at the starting pH of 1pH unit above pI for the protein of interest. Acetate, phosphate, and glycine are anionic buffers and associated with cation exchanger (R^-) at the starting pH of 1pH unit below pI of the protein.

Based on the criteria discussed above, the buffer systems were chosen. Three buffer systems were used for cation exchange to separate the model protein system as discussed in Ch.4. These buffer systems are:

1. phosphate, Na_2HPO_4 + NaH_2PO_4
2. Tris-Maleate + NaOH +NaCl
3. Acetate, Na Ac + HAc +NaCl

Note that the buffer systems are all anionic buffers and have Na^+ as the counter ion. The cation buffer system- Tris +HCl was used for anion exchanger (R^+) as presented in Ch. 5. The Cl^- ion will be the index of ionic strength for the elution of the enzyme in a real system. The pCl is an important index in the method development for separation. Appendix A-3 will give the detail preparation of four buffer systems.

The choice of buffer pH and ionic strength

Buffer pH should be chosen so that substances of interest have a net charge opposite to that of the ion exchange resin. The starting pH should be about 1 pH unit above the pI of the substances of interest for anion exchange and 1 pH unit below the pI for cation exchange. Substances can be dissociated from the ion exchangers by pH cyclic zone or by concentration cyclic zone. The details have been discussed in Sec. 1-4-1 and 1-4-2. According to the prior method development in cyclic zone, the procedures are set up for for the separation of protein mixtures.

pH cyclic zone

Refer to Fig. 6a in Ch.1 (P.29), different levels of buffer pH for adsorption and desorption are set up as following.

Adsorption stage: At a pH of 4.4 , both Hm and Ab carry a positive charge because their pI's are pH 6.7 and 4.7 respectively. Thus, both can be adsorbed by the resins.

Desorption stage: At a pH of 5.7 , the impurity Ab will carry a negative charge and elute first. Hm still carries a positive charge and is retained. At a pH of 8.5 , Hm becomes negatively charged and elutes.

All buffer solutions have an ionic strength of 0.1M so that that the pH is the control parameter. The pH is changed from one level to another level as the step input.

Concentration cyclic zone

It is critical and necessary to locate the optimal isoionic concentrations for a specific buffer system in order to develope the purification strategy. Generally speaking, we need to find the isoionic concentration that will elute the first impurity components from the solid phase but retain the component of interest and other impurities. A second isoionic concentration is picked so as to elute the component of interest from solid phase but retain any other impurities. Finally, a third isoionic concentration is used to elute all retaining impurities and refresh the resin for the next cycle.

The separation of the enzyme was performed on an anion exchanger R^+ with Tris-HCl buffer. Obviously, the counter ion is chloride and pCl will be used as the index of isoionic concentration. The buffer solution is prepared by mixing of same molarity of Tris and HCl solutions at different volume ratios to obtain a specific pH (as discussed in Appendix A). Thus, both the pH level and molarity of acid and base will affect the counter ion concentration, Cl^-.

Figure 37 demonstrates the result that pCl is a function of molar concentration and pH level. At one pH level, one ionic strength will have only one pCl value. At the high pH (8.5), it

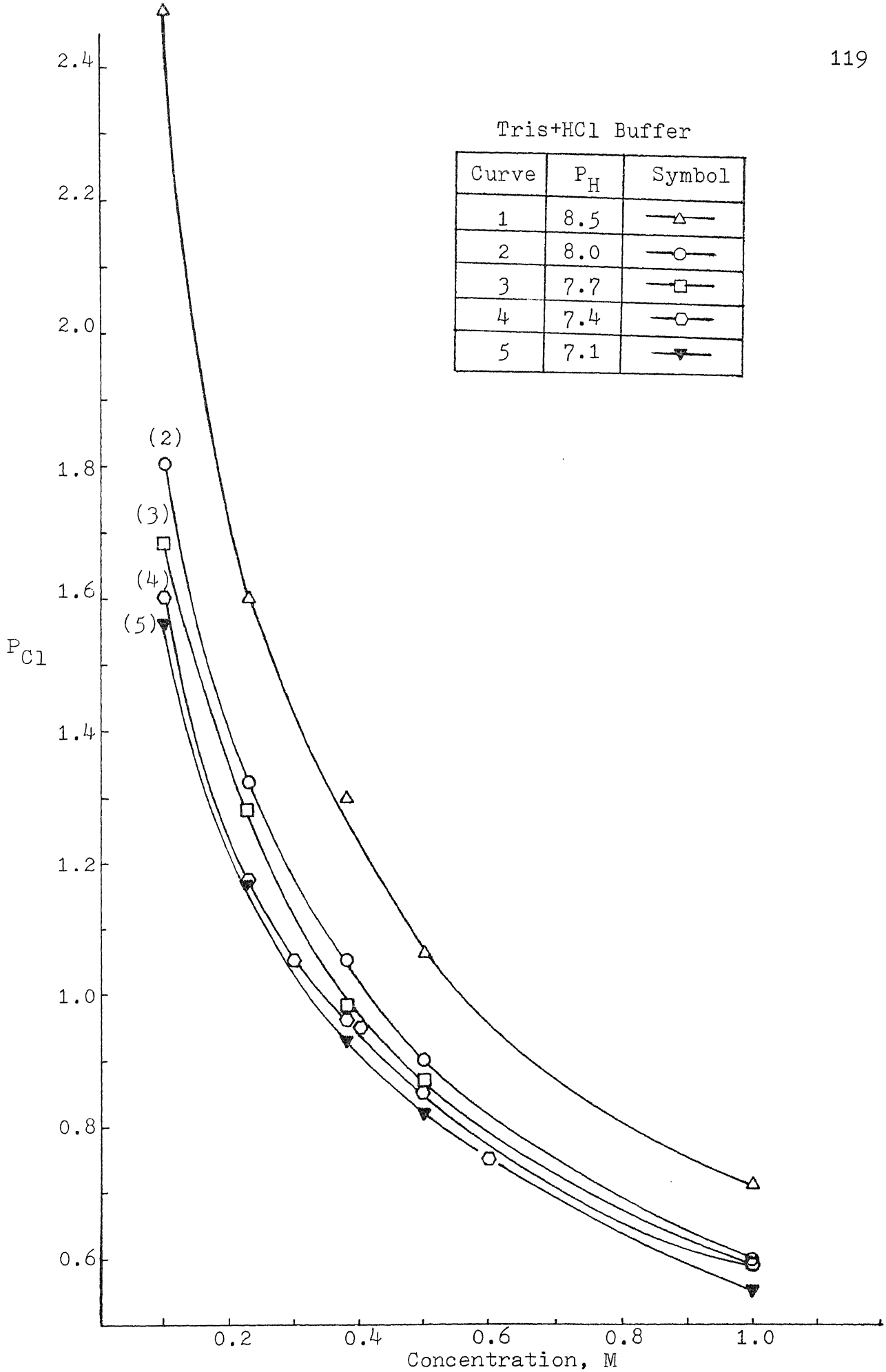

Fig. 37 P_{Cl} v.s. Ionic Strength as Function of pH for Tris-HCl Buffer

requires higher molar concentration in order to obtain the same pCl value as compared with low pH level. This is a result of the fact that mixing ratio of HCl at low pH level is much less than the high pH level. In Ch. 5, we choose pH of 7.4 for all the experiments which were run, because the mixing ratio of Tris/HCl is close to one that can minimize the local pH disturbance during the ion exchange stage. The enzyme will carry a negative charge in this pH environment and be adsorbed by the solid phase.

In Fig.38, we have summarized three isoionic points and ionic concentrations for enzyme and impurity groups respectively. Point A is the ionic strength that the first impurity group starts to elute at 0.17M or pCl = 1.28 , i.e., point A is the lowest ionic strength which effects the elution of enzyme. Below the pCl=1.28, the enzyme will start to elute at 0.18M or pCl=1.22. Again, point B is the lowest concentration which elutes the second impurity group. Between the narrow concentration range of 0.18M to 0.325M, the enzyme theoretically can be eluted with no impurity interferences. Point C is the minimum ionic strength required to elute the rest of the impurities from the ion exchanger and refresh the resin.

We will demonstrate the method of locating the three isoionic points experimentally in Ch.5 in order to optimize separation. From the above arguments, we are ready to set up the procedures as shown in Fig.6b (P.29) for concentration cyclic

P_H7.4 Tris+HCl Buffer

	Isoionic Point	Isoionic Conc.	1st. Peak	2nd. Peak
r_{595}	1.28	0.17M	A	-
r_{405}	1.22	0.18M	B	-
r_{595}	1.03	0.325M	-	C

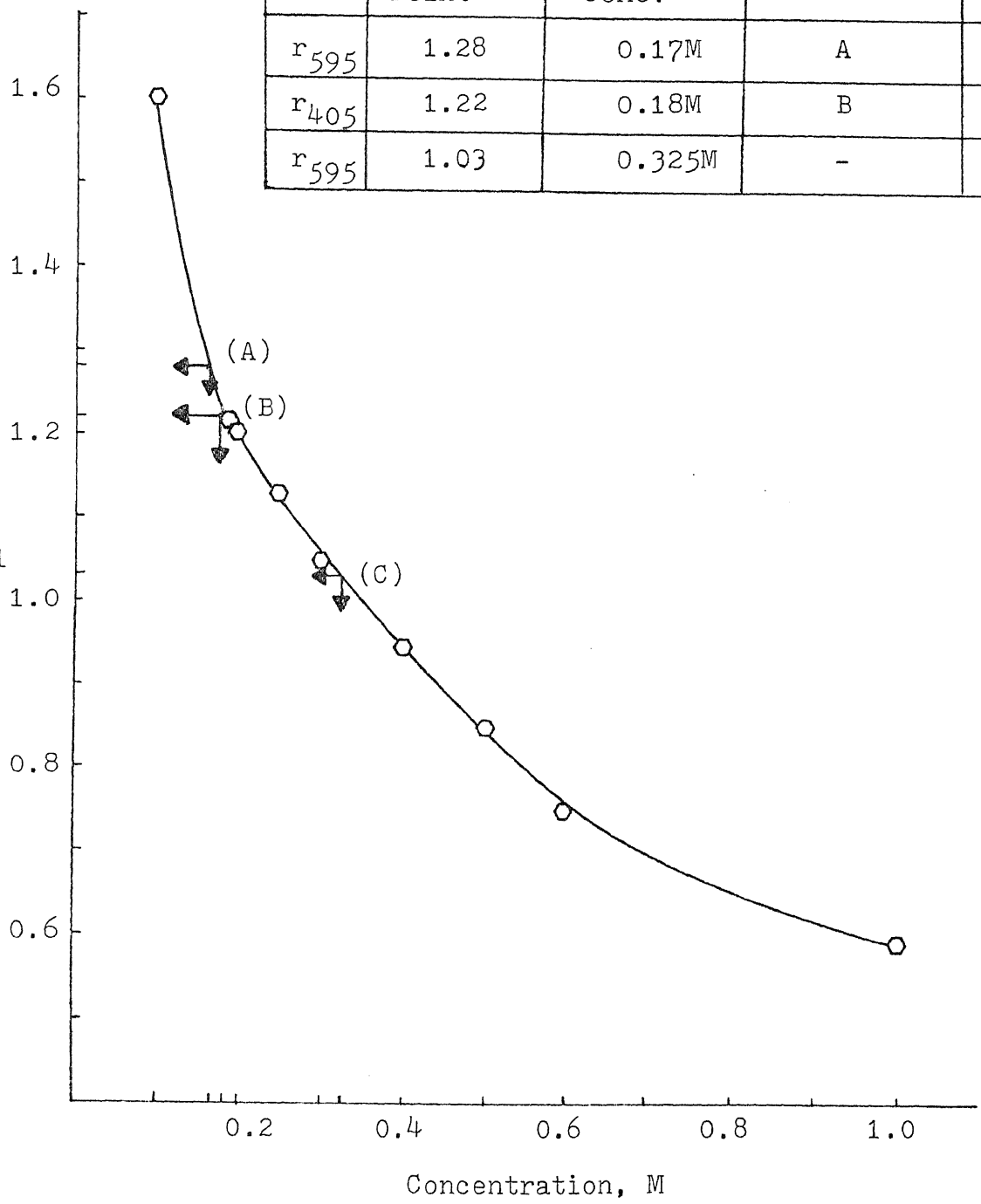

Fig. 38 Ionic Points of Enzyme Alkaline Phosphatase as Function of Buffer Concentration

zone. The procedures are similar to those for pH cyclic zone in that the adsorption stage and two or three sub-desorption stages are applied for the whole process. The number of sub-desorption stage depends on whether the first impurity group is adsorbed or not. For the system discussed in Ch.5 , three sub-desorption stages are chosen.

Adsorption: At a pH of 7.4, both enzyme and impurities will carry negative charge because the pIs are near pH = 4.7. The feed components are all adsorbed by the anion exchanger.

Desorption:

Stage 1: The incoming buffer ionic strength is adjusted to be between the first and second isoionic points so that only the first impurity group will elutes and the other components will be retained.

Stage 2: The incoming buffer ionic strength is adjusted to be between the second and third isoionic points so that only the enzyme will elutes.

Stage 3: The incoming ionic strength should be higher than the third isoionic point in order to completely elute the impurity group as a recycle stream or waste.

If the adsorption feed ionic strength is adjusted between the first and second isoionic concentrations so that the first group of impurities will not be bound on the resin; therefore,

the sub-desorption stage 1 can be omitted.

Note that the change of one ionic strength to another level is performed as step change input. The experimentally observed transient behavior will be discussed in Ch.4 and Ch.5 . However, as far as the resolution is concerned, the sub-desorption stage 2 should be designed in order to have the maximum elution of enzyme and a minimum elution of the second impurity group. Technically, this can be done by adjusting the elution ionic strength to be closer to the first isoionic point which will prolong the amount of time required to change from low to high ionic strength. Alternatively, this can also be done by dividing the interval between the initial and final ionic strength into several sub-intervals and make small discrete increments in the ionic strength. We call this the continuous step change. Therefore, the slope of concentration profile is decreased. The continuous step change in concentration will improve the resolution. The experimental results demonstrate the idea of transient behavior of the continuous step change and their effect on the purity and the yield of enzyme product (see Chapter 5).

3-4 Mode of operation for protein desorption

As discussed previously, the pH and ionic strength will govern the solute distribution between the mobile and solid phase. Figure 6 shows both the step change of pH for pH cyclic zone and

the step change in concentration for concentration cyclic zone. In the discussion of model development for ion exchange chromatography, it was assumed that the adsorption/desorption process is instantaneous. In fact, from the experimental observation confirms this to be valid as assumption. For both the model protein and real system, the adsorption stage only used up a very small amount of resin. The proteins are trapped at the top of the column as a narrow and sharp band. The length of resin bound with proteins is negligible in comparison to the total column length (approximately of 1mm length). When the desorption buffer is applied to the column, there is a transient change in profile of pH or ionic strength. The desorption will occur only if the transient profile has passed below the isoelectric point in pH cyclic zone or isoionic point in concentration cyclic zone. It is reasonable to assume that the desorption band can be approximated as an impulse input of very concentrated feed at the top of the column at time of zero where the isoelectric point or isoionic point are reached. As the peak travels through the column it broadens due to the combined effects of axial and internal diffusion, equilibrium distribution of solute between mobile and solid phase, and mass transfer resistance.

From the discussion above, we may conclude that:

1. The pH and ionic strength are the control parameters in

method development. Good separation results are expected as long as these parameters are optimized.

2. The step feed input will generate a transient in either pH or concentration profile within the column.

3. Each component will be desorbed only the transient curve pass below their isoelectric point or isoionic point. Thus, Hm will start to elute after pH 6.7 from R^- resin because above this pH value the Hm will carry negative charge. Enzyme alkaline phosphatase will start to elute at above its isoionic point (pCl = 1.22).

4. The elution of protein can be approximated as an impulse input at the top of column due to step change in operating conditions (such as pH or ionic strength of buffer).

5. From the argument 4 that it is obvious to define the desorption phase lag as the difference in elution volume between the starting pH or ionic strength, i.e., the running condition of step change, corresponding to their isoelectric point or isoionic point on the transient profiles. It is necessary that the elution volume consumed has to be added up to the elution volume predicted from the surface adsorption model.

6. The tube volume used for the experimental runs also has to be considered. The prediction of elution volume in Ch.4 and Ch.5 are calculated based on the summation of phase lag, tube volume, and the predicted volume.

4. Chromatographic separation of binary model system

The separation of protein mixtures of Hm and Ab were performed on a chromatographic column packed with CM-Sepharose (R^-) ion exchanger. The Ab was treated as the impurity and Hm was treated as the component of interest. The experimental results obtained from pH cyclic zone are interpreted and predicted by the surface adsorption model.

Results from the separation of Hm and Ab are shown in Figures 39 and 40. In both figures 39a and 40a pH and pNa are plotted as functions of elution volume, while Figures 39b and 40b show $\left[Y_p/Y_o\right]_{Hm}$ and $\left[Y_p/Y_o\right]_{Ab}$ as function of retention volume. Experimental and predicted elution profile are compared in Figures 39b and 40b for the surface adsorption model. Initially, Hm and Ab were equally weighed and mixed with buffer to form 0.02wt% solutions of various pH. At the time zero, 60 cc of pH 4.4 feed was pumped into the column. Both proteins carried positive charge and were adsorbed at the top of the column. A dark brown band was observed during the experimental run. After the adsorption was done, the first subdesorption stage was performed by pumping 60 cc of pH 5.7 solution into the column in order to elute the impurity. The pH value within the column was shifted from pH 4.4 to 5.7 and the sodium ion was recorded and denoted as pNa. The Ab was eluted right after its isoelectric point of pH=4.7 . Because Ab will be negatively charged only when

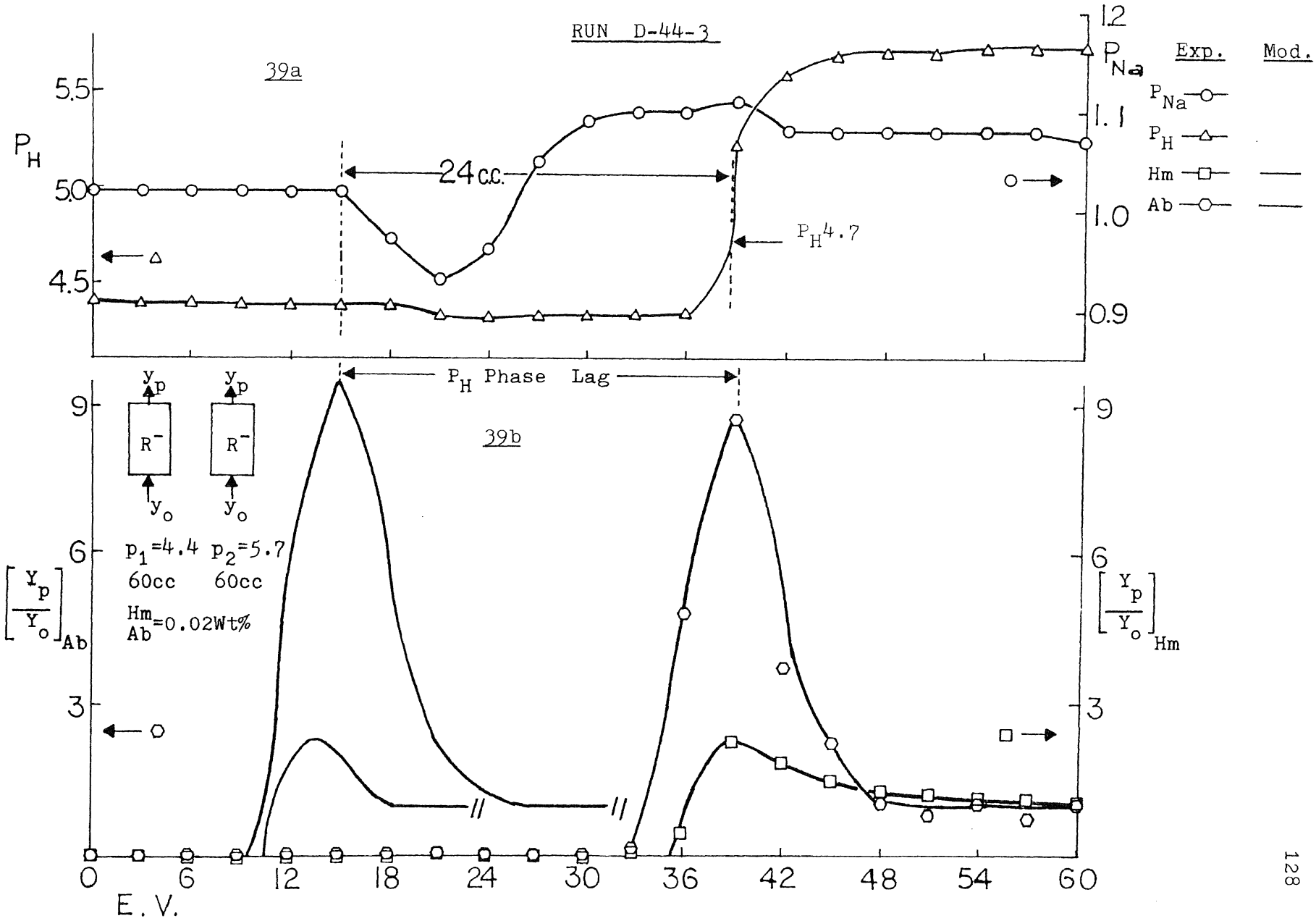

Fig. 39 Separation of Protein Model System Hm and Ab, Desorption of Ab

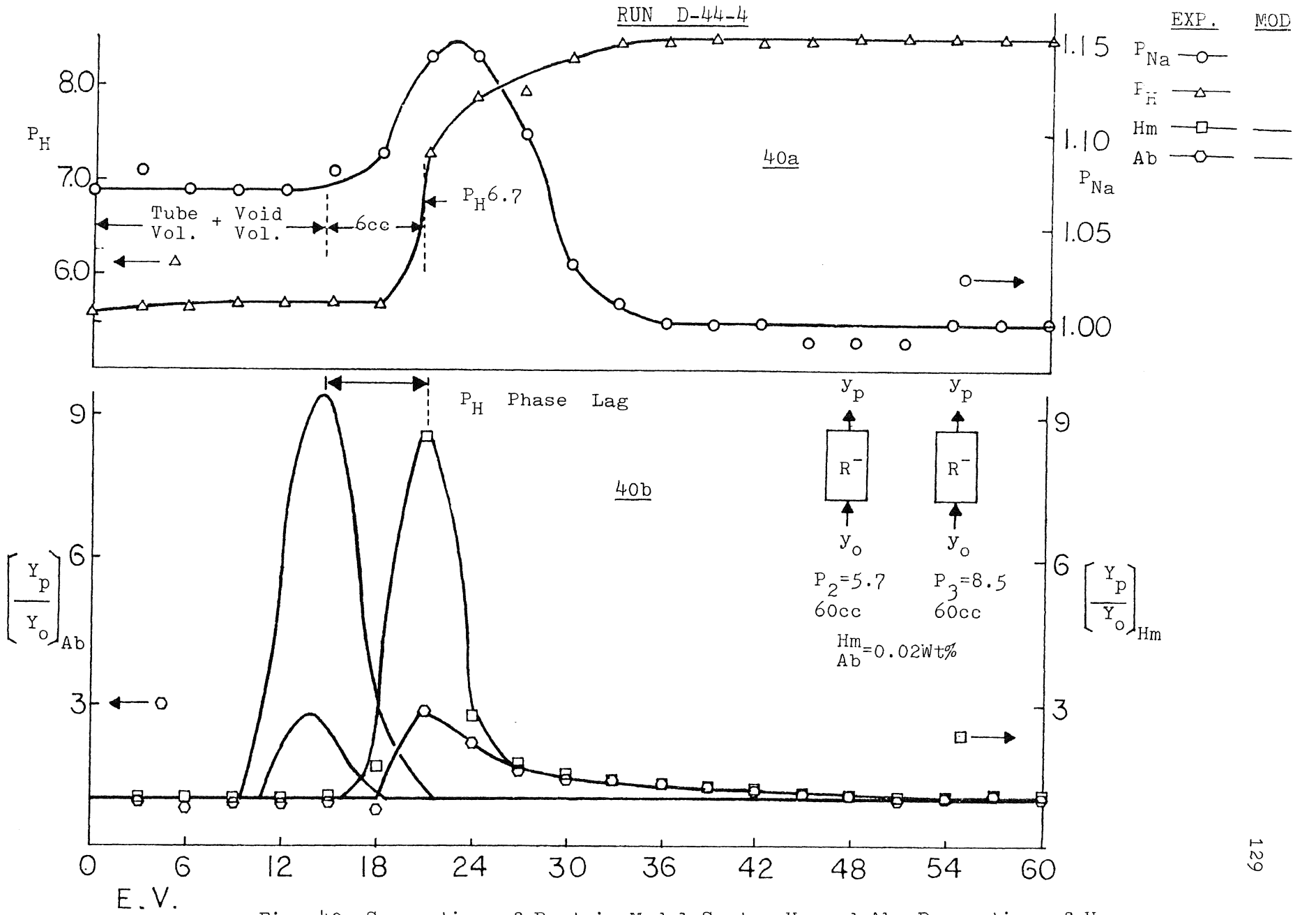

Fig. 40 Separation of Protein Model System Hm and Ab, Desorption of Hm

the pH of the surrounding buffer is above 4.7. Figure 39a shows that pH 4.7 was reached after an the elution volume of 39 cc. This elution volume was greater than one bed volume plus the tube volume (15 cc). This results from the local pH disturbance of the two different buffer systems (NaAc + HAc buffer and Tris-Ma + NaOH). The HAc and NaOH was neutralized at the interface of the two buffer solutions and the consumption of NaOH and HAc was achieved between elution of 15 cc and 39 cc. Within this range, the pH value dropped from 4.4 to 4.2 and then increased to 4.7 . Note that Ab will start to elute only if the surrounding pH is greater than its isoelectric point, pH=4.7 . This results from the fact that Ab will carry same negative charge as the solid phase. The phase lag was defined as the difference between the elution volume of 15 cc and the point where pH4.7 was reached. This is the point where the impurity Ab starts to elute. The experimental elution curves indicated the highest peak for Ab and Hm were started right after pH 4.7 . Small amounts of Hm were eluted with the major Ab peak suggesting interaction between the two proteins. It should be noted that the rise in pH from 4.2 to 5.7, the elution of Ab, and the pNa curve rise all occur simultaneously. This demonstrates the fact that in order to elute the protein from the solid phase, the pH must be over its isoelectric point. In addition, the sodium ions in solution must be returned to the solid phase to exchange with the protein molecule. The ion exchange process is proceeds instantaneously only if the above mentioned requirements are satisfied.

The curves calculated using the surface adsorption model for Hm and Ab are shown in Fig.39b. Note that the model is not involved in the prediction of the phase lag and tube volume. Both were measured experimentally. The calculated elution curves have been adjusted 3 cc ahead as the tube volume. The calculated peak maximum for the Hm and Ab curves occur at an elution volume of 15 cc. The difference between calculated and experimental elution volumes for Hm and Ab is 24 cc. This is equal to the previously defined phase lag. This shows that the phase lag is mainly caused by the transient behavior of pH step change. In addition, the desorption of Ab can be approximately as impulse input. It should be noted that the experimental and predicted area and shape are fairly similar.

Figure 40a illustrates the desorption of Hm in terms of pH and pNa curves. The pH value within the column was changed from 5.7 to 8.5 using the same Tris-Ma +NaOH buffer system. Because this is the same buffer system, no pH disturbance is observed as with that shown in Figure 39a. The Hm will carry a negative charge when the pH value is above its isoelectric point (pH=6.7). The pH starts to change at elution volume 15 cc. This is equal to the sum of one bed volume plus the tube volume. The phase lag was then measured from 15 cc to 21 cc. This is pH 6.7 occurs. Again, the pH shift, the pNa rise, and the protein desorption all occur simultaneously. The calculated elution curves for Hm and Ab show reasonable similar elution area and peak shape. The phase

lag predicted by the model is equal to 6 cc, which agrees with the experimentally measured value.

The Hm was studied alone for the effect of flow rate on elution profile. The experiment was performed on a semi-preparative column which has been discussed in Sec. 3-2. The pH within the column is cycled from pH 6 to pH 8. Adsorption of Hm occurs at pH 6, while desorption occurs at pH 8 on the cation exchanger. Figures 41 and 42 shows pH and $\left[Y_p / Y_o \right]$ v.s. elution volume. At time zero, 67.5 cc (one bed volume) of pH 6 feed was introduced into the bottom of the column displacing the pH 8 buffer. Changing from pH 8 to 6 will enhance the adsorption of Hm since at this pH it carries an opposite charge to that of the resin. We, then, add 67.5 cc of pH 8 buffer which displacies the solution. Changing from pH 6 to 8 will elute the Hm into mobile phase since it now carries the same charge as the solid phase. This completes one cycle of adsorption and desorption.

The phase lag was measured as the difference in elution volume between a pH of 6 and Hm's isoelectric point which occurs at a pH of 6.7. This is equal to 8 cc. Hm will carry a negative charge and start to elute from the solid phase when the pH is higher than 6.7. Again, the observed phase lag is same as the predicted value. Also note that there is no interactions between

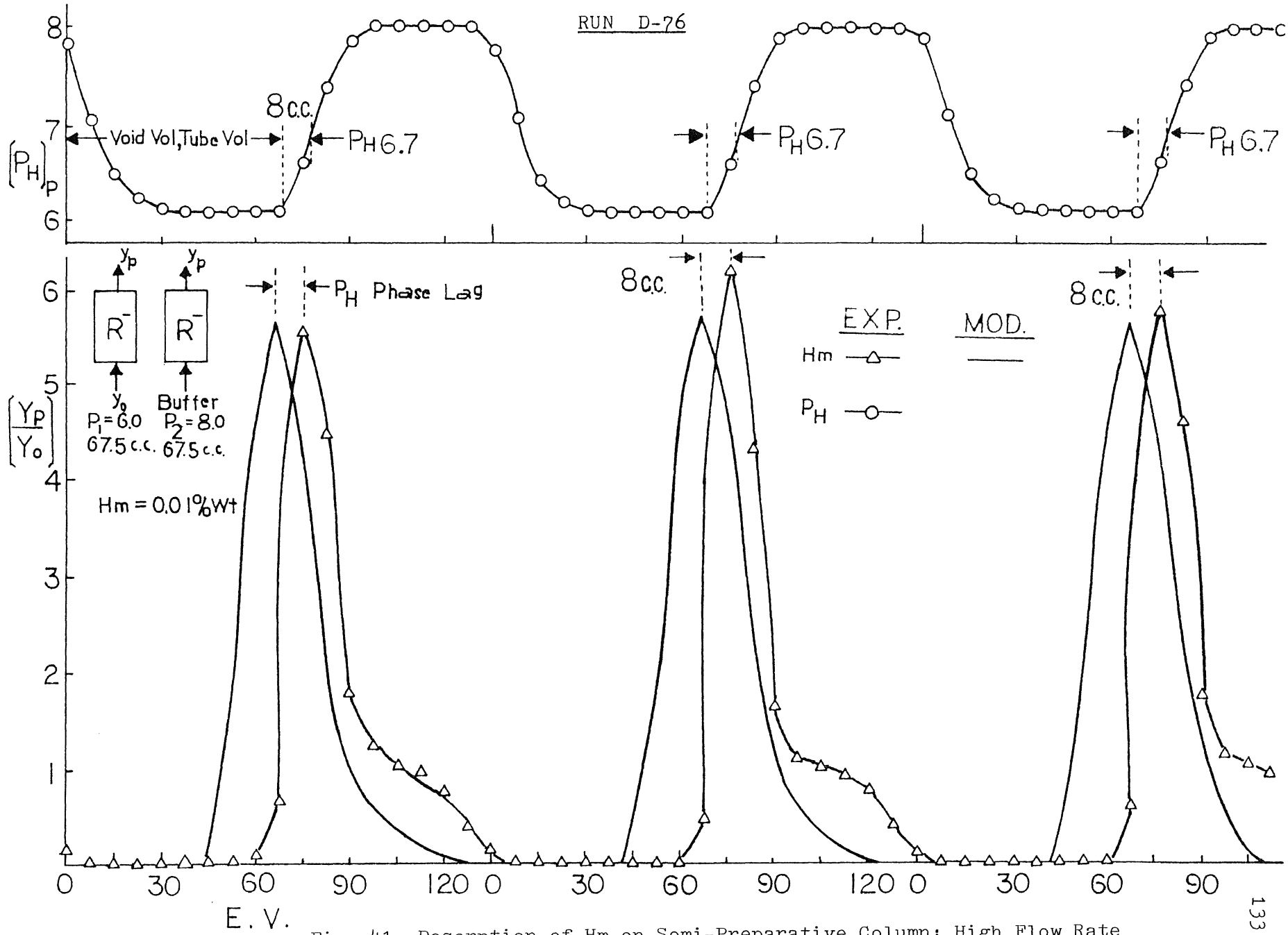

Fig. 41 Desorption of Hm on Semi-Preparative Column: High Flow Rate

two pH levels because of same buffer system. The calculated elution profile also verified the similarity of elution area and shapes. The difference between Figure 41 and Figure 42 is flow rate. The high flow rate tends to introduce large mixing effects at the interface of the two pH solutions. The transient profile for low flow rate shown in Figure 42 has a sharp pH shifting as compared with that shown in Figure 41. The different magnitude of mixing effect generates different amounts of phase lag and peak shape. The small phase lag shown in Figure 42 produces a sharp peak, while the larger phase lag shown in Figure 43 results in peak broadening. Again, Figure 42 shows that the calculated and the observed curves have similar phase lag, elution area, and peak shape.

Figure 43 illustrates the effects of flow rate on the pH transient profile. This figure shows the results from three different flow rates based upon the same pH step change. This illustrates the fact that the higher flow rate will result in peak broadening and tailing due to the larger phase lag. Low flow rate will result in a sharp peak and better resolution since the magnitude of mixing effect is relatively small.

Figure 44 concludes the effects of the flow rate on the magnitude of phase lag. For the extremely high or low flow rate,

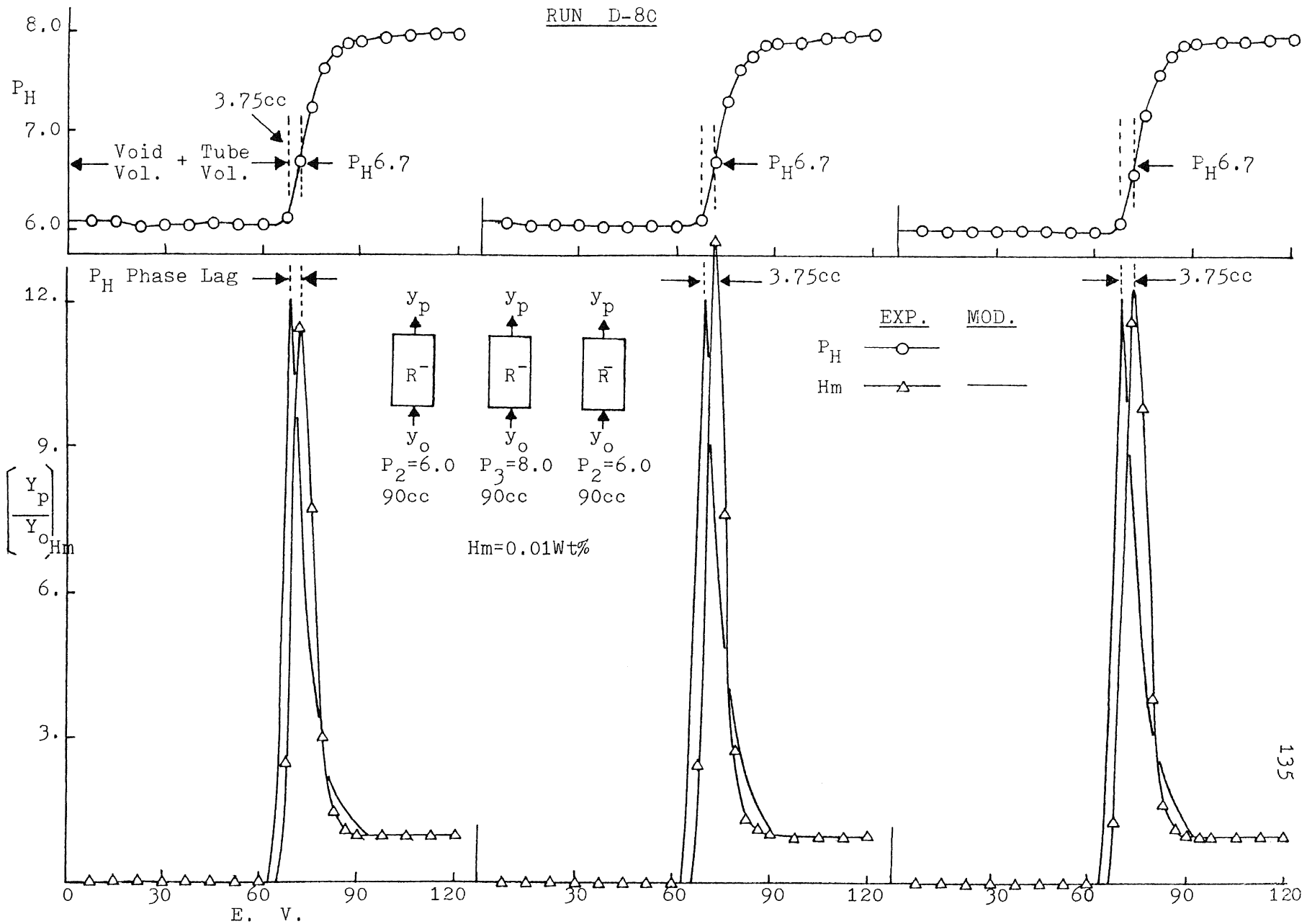

Fig. 42 Desorption of Hm on Semi-Preparative Column: Low Flow Rate

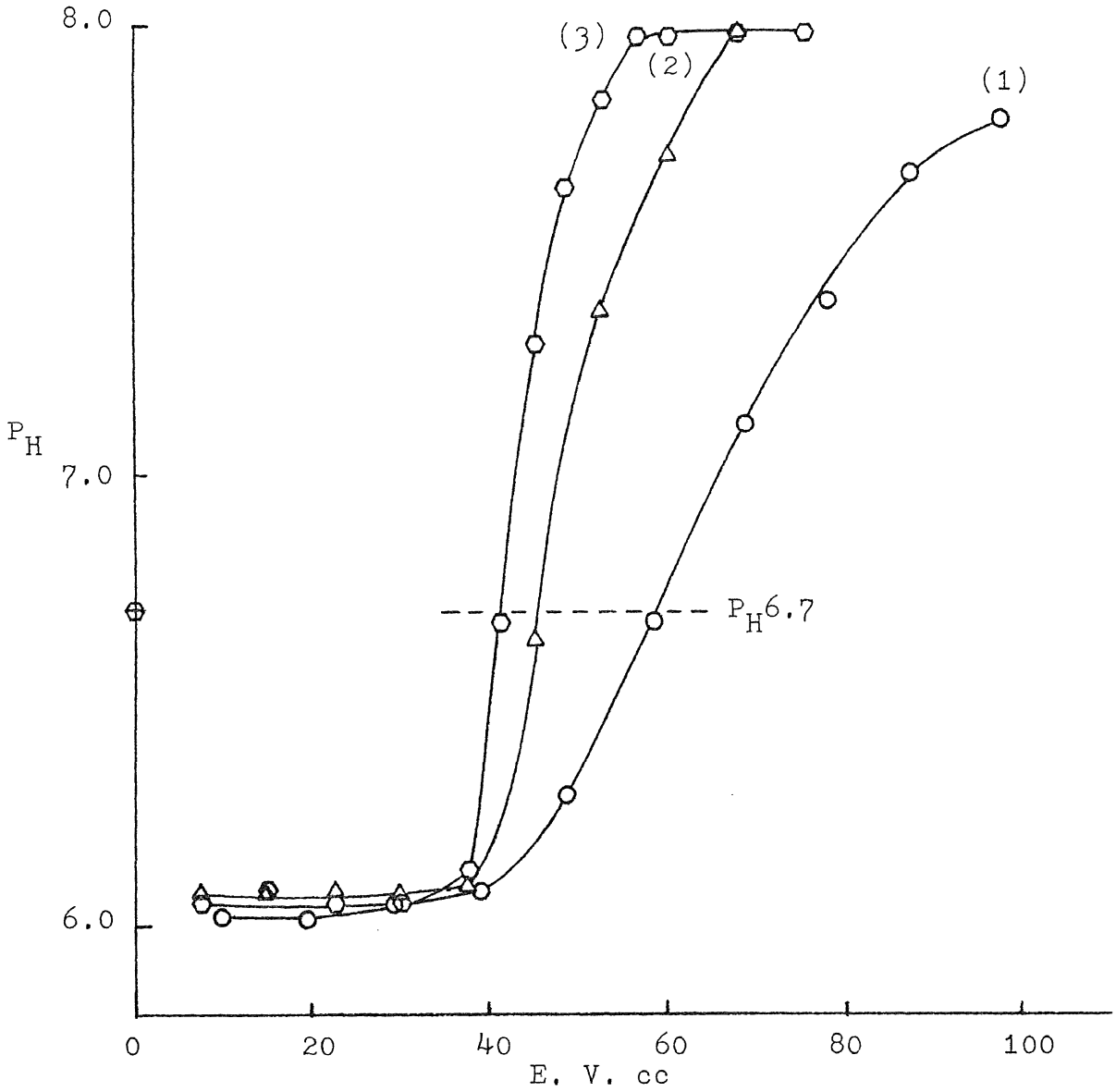

CURVE	Q, cm^3/min	LAG, cc
1	3.25	20.0
2	2.50	8.0
3	1.00	3.75

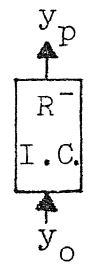

P_3=8.0

I.C. in the column: P_2=6.0

Buffer: 0.1M NaH_2PO_4 + Na_2HPO_4

S : 5 cm^2

L : 15cm

Fig. 43 Effect of Flow Rate on pH Wave and Phase Lag

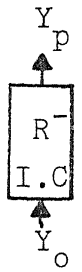

P_3=8.0

I.C. in the column: P_2=6.0

Buffer: 0.1M NaH_2PO_4+ Na_2HPO_4

S : 5.0cm^2

L : 15cm

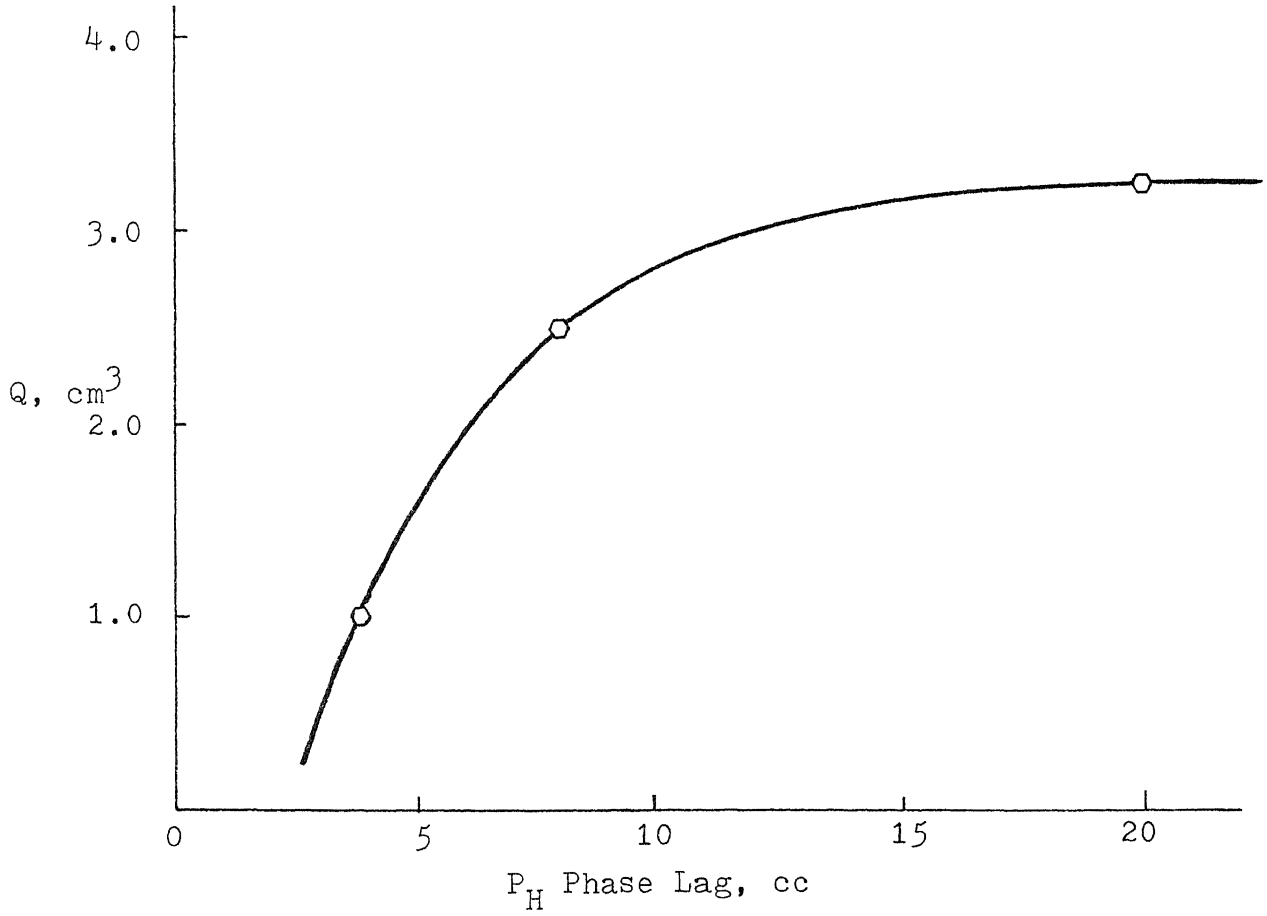

Fig. 44 Phase Lag as Function of Flow Rate

the amounts of phase lag shown in Figure 44 seem to approach to a limiting value. This implies that the resolution of the ion exchange chromatographic column on pH cyclic zone is regulated by the pH and the flow rate. The flow rate will only affect the broadness of the peak. If both production rate and resolution are of interest, the optimal flow rate will result in a trade off between the production rate and resolution. However, if the resolution is not of concern, the high flow rate can be applied in order to provide a larger production rate.

Table 1 lists the buffer system, protein feed concentration, operating conditions and tube volume used for each experiment. Table 2 lists the peak height and the retention volume for the purpose of comparing experimental and calculated results. In addition, the parameters used for the model calculation summarized on the right hand side of this table. The elution volume is located at the peak apex for the calculated profiles. The calculated retention volume shown in Table 2 is the summation of elution volume, the experimentally measured phase lag, and the tube volume. Both calculated peak height and retention volume are in the good agreement with experimental observations.

Table 1 Experimental Parameters for Hm and Ab

RUN	Buffer	Feed	Condition
D-76	0.1M Na_2HPO_4 + 0.1M NaH_2PO_4	0.01Wt% Hm in 0.1M Buffer	Q: 2.5cm^3/min S: 5cm^2 L: 15cm Tube Vol.: 13.6cc 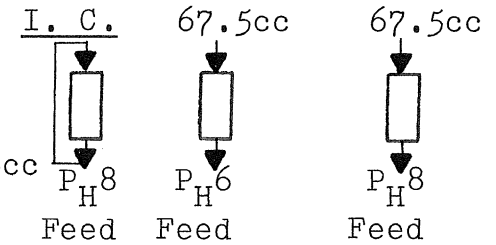
D-80	"	"	Q: 1.0cm^3/min S: 5cm^2 L: 15cm Tube Vol.: 13.6cc 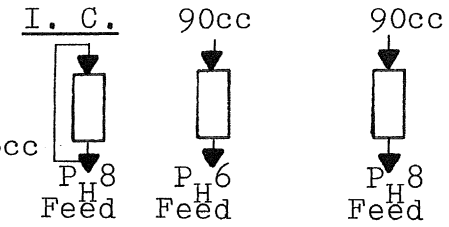
D-44-3	P_H5.7 0.1M Tris-Ma + 0.1M NaOH + 0.1M NaCl P_H4.4 0.1M NaAc + 0.1M HAc + 0.1M NaCl	Hm: 0.02 Wt% in Ab P_H5.7 and 4.4 Buffer	Q: 1.0cm^3/min S: 2 cm^2 L: 8.0cm Tube Vol.: 2.75cc 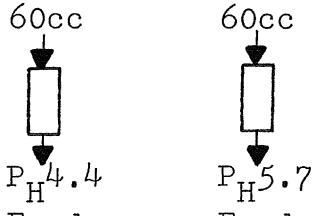
D-44-4	P_H5.7 0.1M Tris-Ma + 0.1M NaOH + 0.1M NaCl P_H8.5 0.1M Tris-Ma + 0.1M NaOH + 0.1M NaCl	"	Q: 1.0cm^3/min S: 2cm^2 L: 8.0cm Tube Vol.: 2.75cc 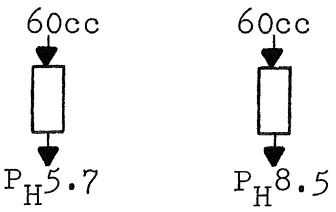

Table 2 Relations of Model Parameters and Experimental Run for Hm and Ab

Run	$C_{I_{Hm}}$	$C_{I_{Ab}}$	Peak Height		Phase Lag,cc	Retention Vol.		m	Model Parameters						
			Exp.	Mod.		Exp.	Mod.		E_d	k_f	a	ϵ	Q	S	L
D-76	67.5	-	5.87	5.71	8.00	75.00	74.10	$1x10^5$	0.25	$1x10^{-3}$	150	0.75	2.5	5	15
D-80	90.0	-	12.15	12.20	3.75	71.25	72.35	$1x10^4$	0.028	$1x10^{-4}$	150	0.75	1.0	5	15
D-44-3	-	60.0	8.73	9.67	24.00	39.00	38.75	$1x10^6$	0.14	$5.5x10^{-7}$	"	0.78	1.0	2	8
D-44-3	60.0	-	2.26	2.27	24.00	39.00	37.75	0.1	0.15	$6.7x10^{-4}$	"	"	1.0	2	8
D-44-4	60.0	-	8.45	9.38	6.00	21.00	19.75	$1x10^6$	0.15	$1.0x10^{-7}$	"	"	1.0	2	8
D-44-4	-	60.0	2.88	2.84	6.00	21.00	19.75	0.1	0.14	$4.6x10^{-4}$	"	"	1.0	2	8

* Tube volume is shown in Table 1.

5. Chromatographic separation of multicomponent real system

The isolation of the enzyme, alkaline phosphatase, was performed on a chromatographic column packed with DEAE-Sepharose (R^+) ion exchanger. The buffer solution used to elute this enzyme was Tris +HCl. The relationship between the resin and buffer solution has been discussed in Sec.3-3 . The isolation of the enzyme was achieved by the concentration cyclic zone. The content of this chapter will emphasize the separation method development and the interpretation of experimental results using the surface adsorption model.

5-1 Enzyme isolation and location of three isoionic points

The purpose of the experimental runs described in this section is to locate the three isoionic points. These are the lowest buffer ionic strength required to elute the enzyme and two impurty groups. Once these points are determined, we can examine the relationship of the elution profile to the ionic strength in order to optimize the operating condition and achieve a high purity enzyme product.

Figures 45a and 45b show the enzyme and total protein elution profiles which results from increasing the buffer ionic strength of the pH 7.4 buffer. The experimental results are

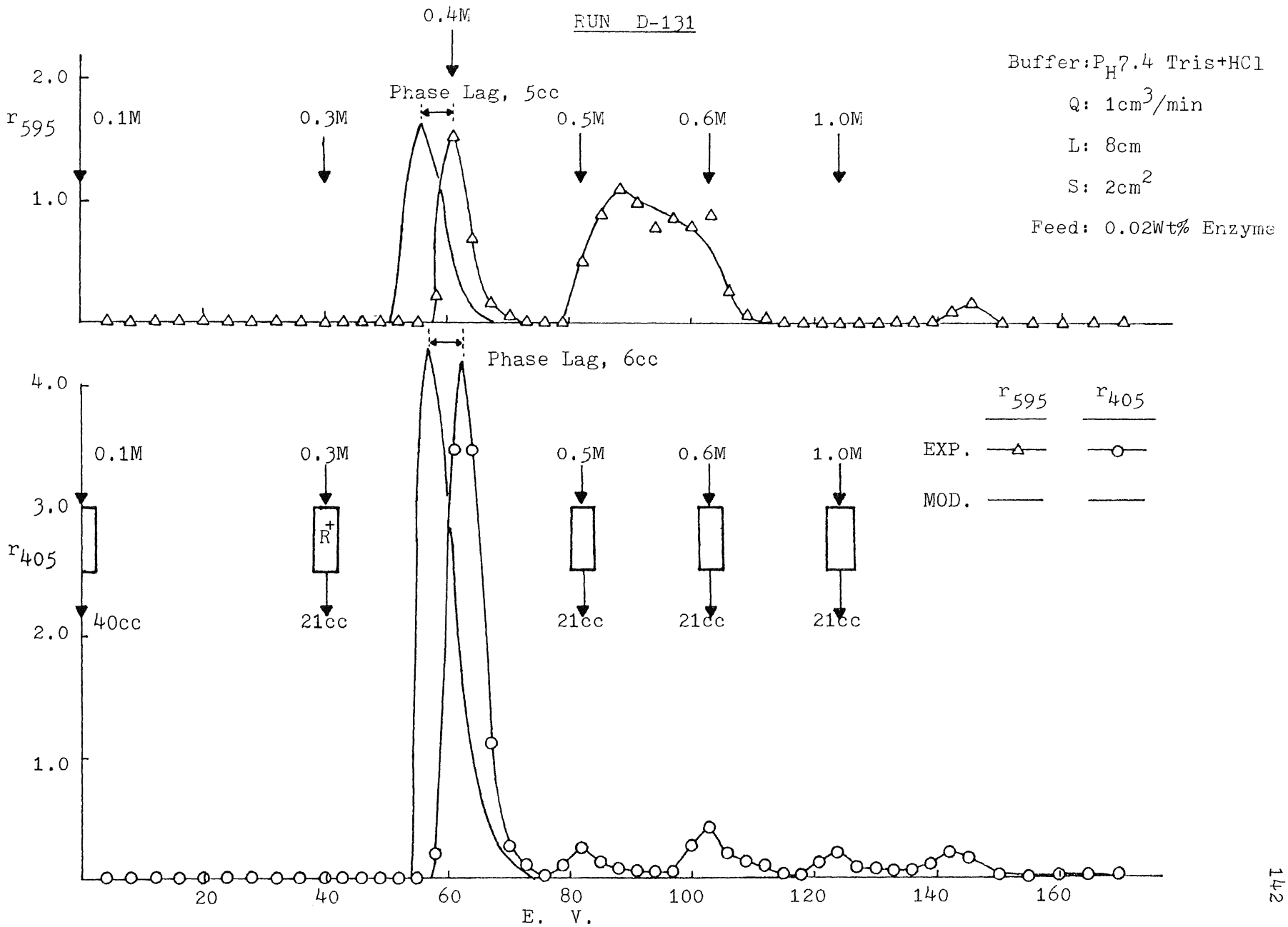
RUN D-131
0.4M
Phase Lag, 5cc
Phase Lag, 6cc
0.1M
0.3M
0.5M
0.6M
1.0M
r_{595}
r_{405}
2.0
1.0
4.0
3.0
40cc
21cc
R^+
Buffer: P_H 7.4 Tris+HCl
Q: 1cm^3/min
L: 8cm
S: 2cm^2
Feed: 0.02Wt% Enzyme
EXP.
MOD.
20
40
60
80
100
120
140
160
E. V.

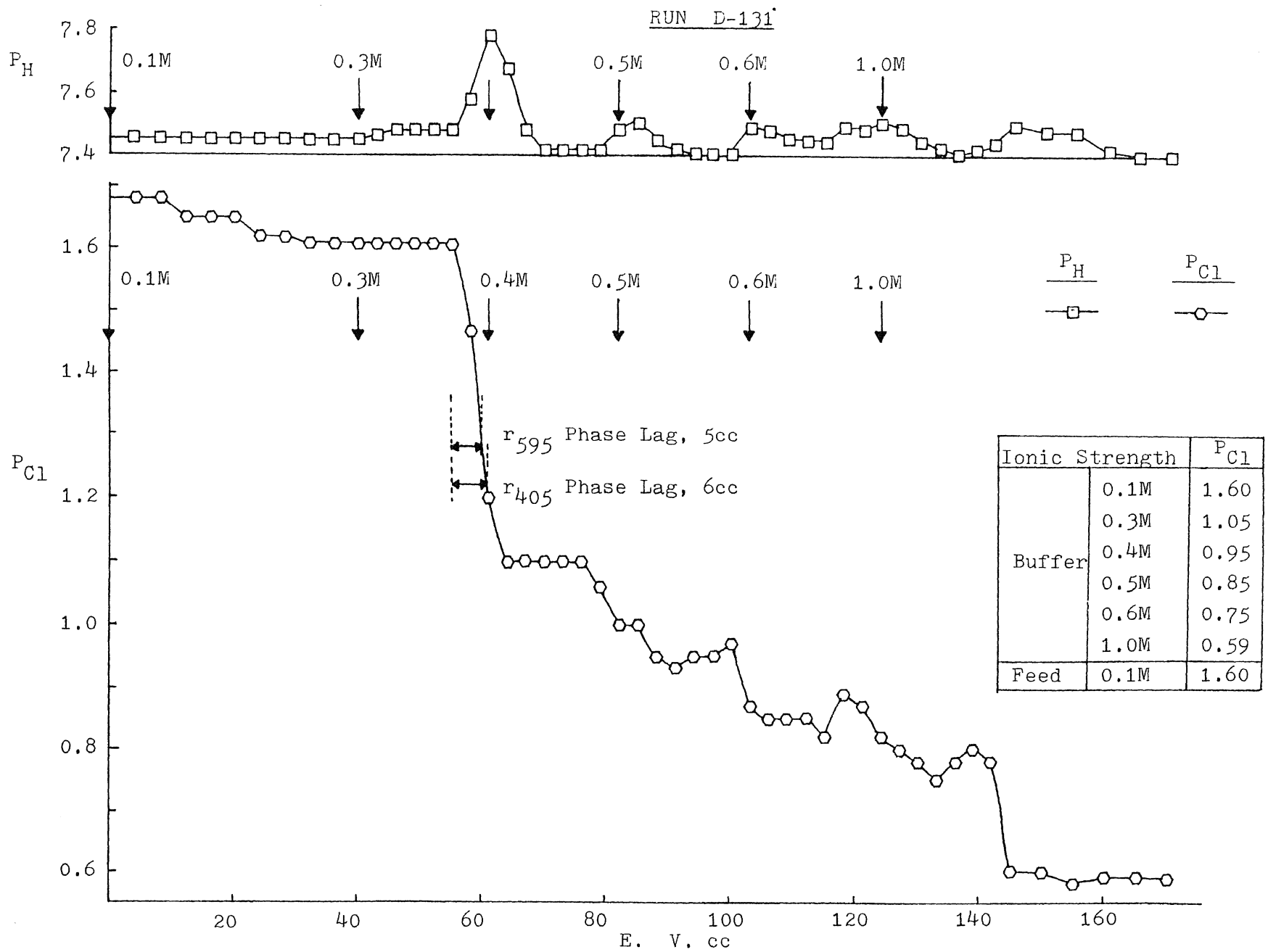

Ionic Strength		P_{Cl}
Buffer	0.1M	1.60
	0.3M	1.05
	0.4M	0.95
	0.5M	0.85
	0.6M	0.75
	1.0M	0.59
Feed	0.1M	1.60

Fig. 45b pH Wave and P_{Cl} Wave for Fig. 45a

plotted as curves of total protein (r_{595}), enzyme (r_{405}), pH and pCl with respect to elution volume. Note that the elution of proteins, the pH wave, and transient pCl curve shift occur simultaneously. The occurrence of local pH disturbance is due to ion exchange between adsorbed protein molecules and counter ions, Cl^-. The transit profile of the incoming buffer solution will provide the counter ions required to exchange the adsorbed protein molecules from the solid phase. This implies that both the total protein and the enzyme will be eluted at a specific ionic strength, called the isoionic point. From Figure 45a, we can roughly estimate that the enzyme will be eluted before 0.3M and the first and second impurities will be eluted before and after 0.3M.

Using the information from Figure 45, we can obtain adequate separation of the component of interest with ionic strength of 0.3 and 1.0M. From these two ionic strength, the transient pCl curve dropped from 1.60 to 1.05 and then from 1.05 to 0.59 when buffer ionic strength was changed from 0.3 to 1.0M. The pH disturbance also resulted from each step change. The ionic strength 0.3M will simultaneouly elute 80% of the enzyme and 30.5% of the total protein while 1.0M will elute the rest of the enzyme and total proteins.

Figure 47 shows the elution of enzyme and total proteins using buffers of 0.25M and 0.6 M ionic strength. The peaks

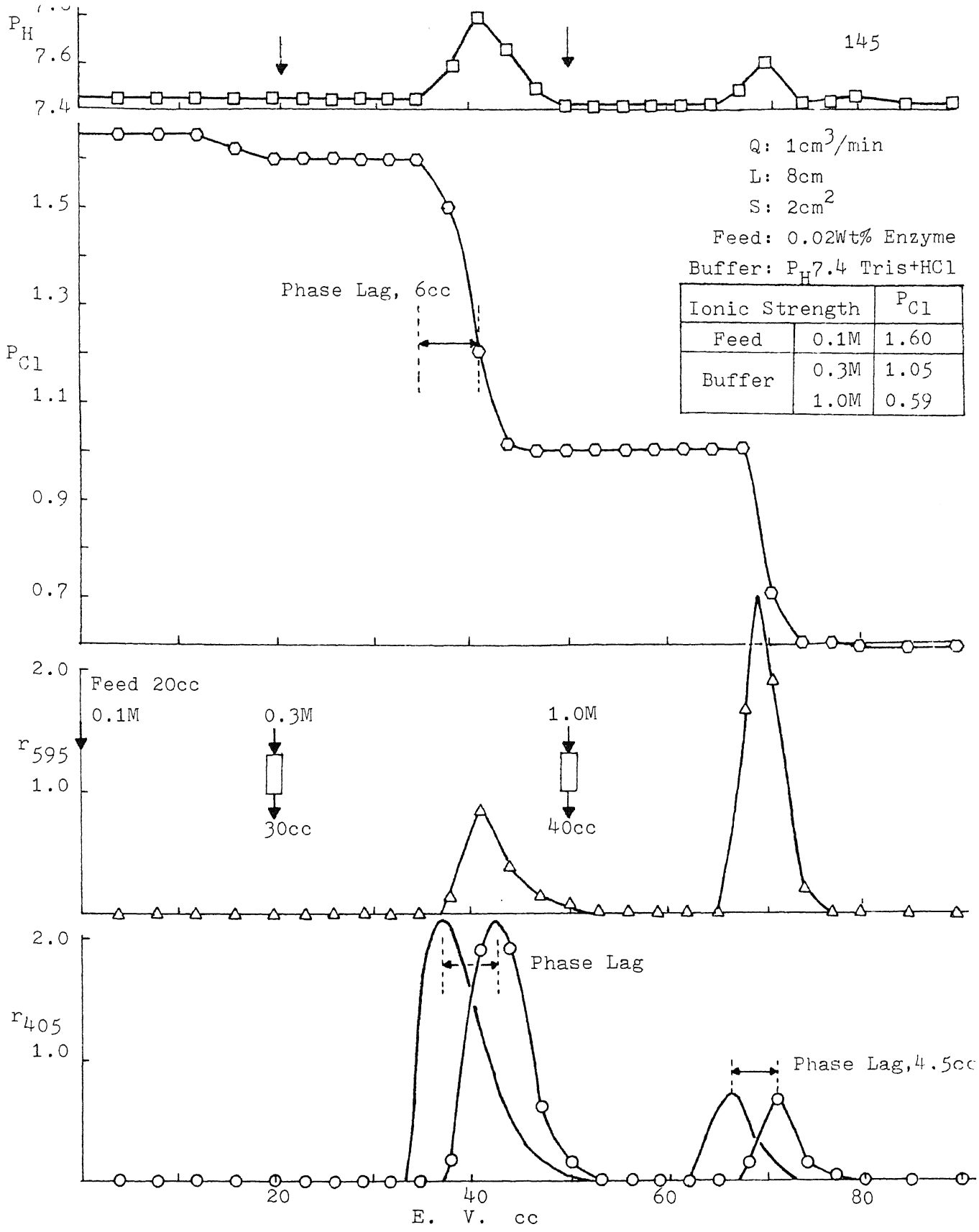

Fig. 46 Elution of Total Protein and Enzyme at 0.3 and 1.0M (RUN D-132)

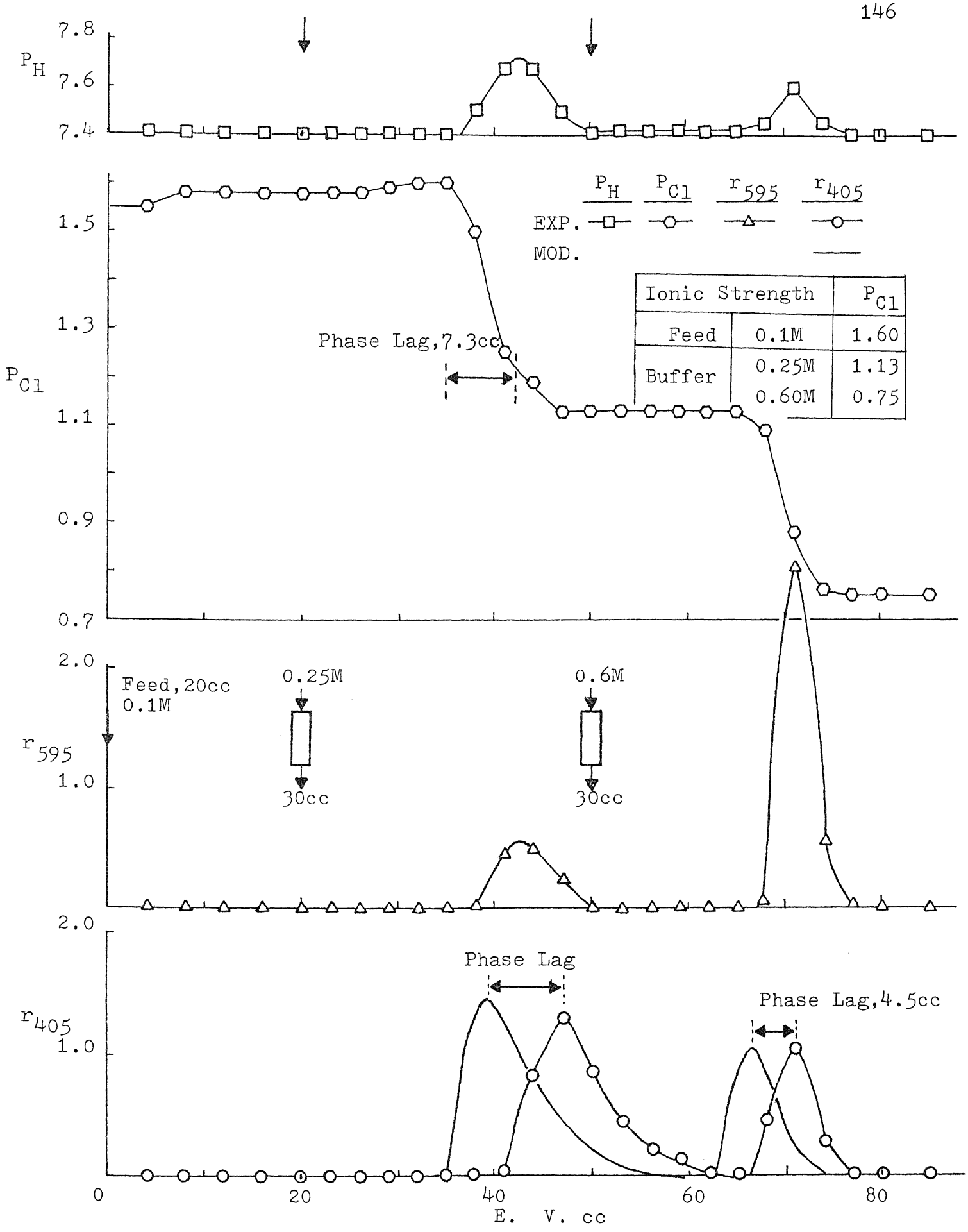

Fig. 47 Elution of Total Protein and Enzyme at 0.25 and 0.6M

eluted by 0.25M are relatively small and broad when compared with those eluted with the 0.3M buffer (see Figure 46). Buffer solution of 0.25M desorbs less protein than 0.3M, while 0.6M desorbs all proteins. The transient pCl drops from 1.60 to 1.13 (0.25M) and then from 1.13 to 0.75 (0.6M) that elute the enzyme and total proteins into two separated peaks. Again, the rise of pH wave appeared simultaneously with the transient pCl wave.

Figure 48 demonstrates the elution at ionic strength of 0.23M and 0.38M and 0.6M. A low ionic strength of 0.23M results in shorter and broader peaks with long tails. The eluted peaks tend to overlap with each other (low resolution); this is not observed in the previous runs. Also note that the first peak of enzyme and total proteins eluted by 0.23M are split into two peaks with the total protein eluting first. This implies that the the first impurity group has a lower isoionic point than that of enzyme; however, both are quite close to each other.

Figure 49 shows the elution profiles at an ionic strength of 0.21M and 0.35M and 0.6M. Again, the low ionic strength causes the transient pCl wave to become flat; and the eluted protein peaks becomes flatter and smaller as compared with those shown in Figure 48. The peaks for the enzyme and the first impurity group are well resolved due to late appearance of the isoionic point for enzyme.

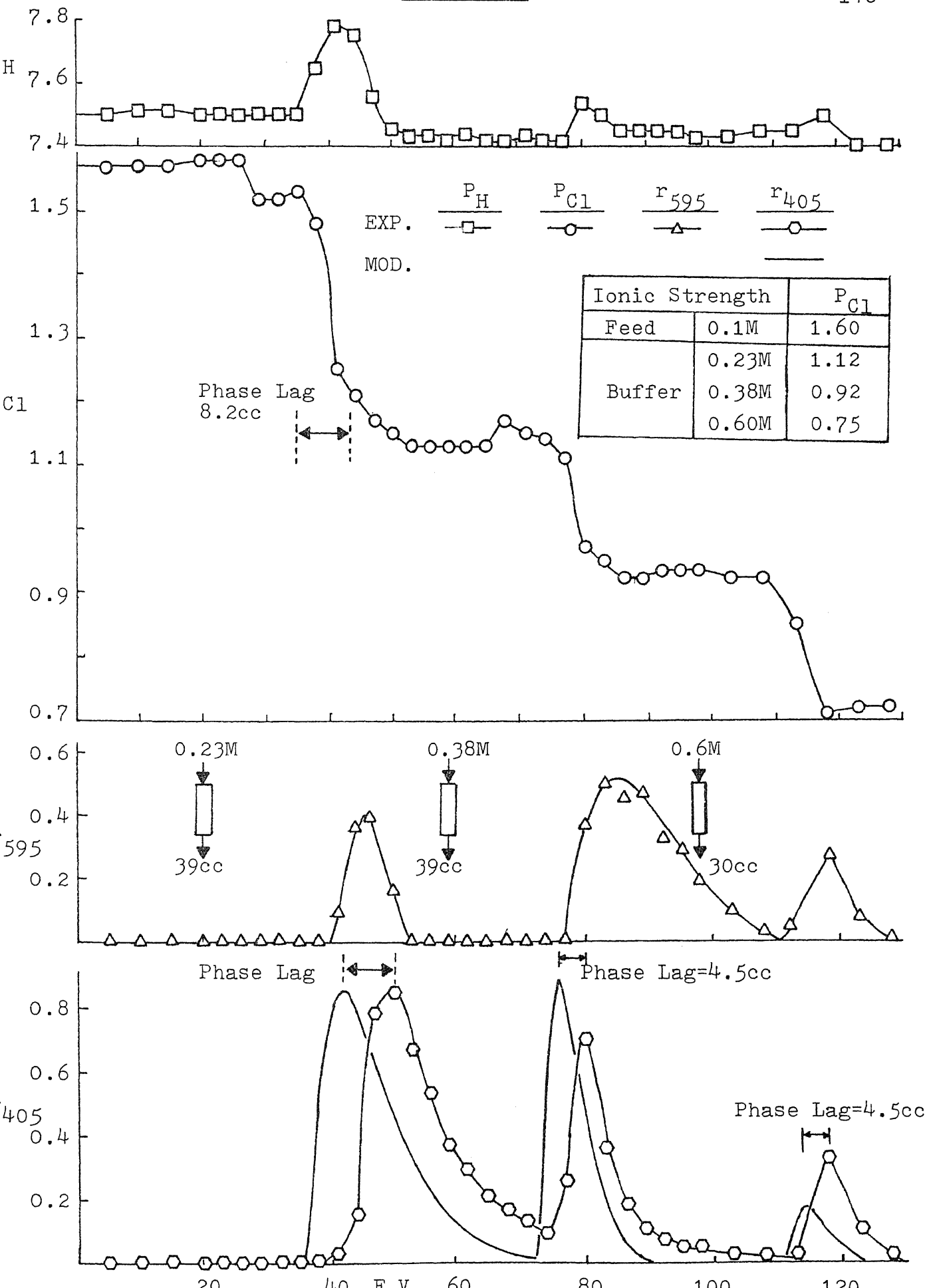

Ionic Strength		P_{Cl}
Feed	0.1M	1.60
Buffer	0.23M	1.12
	0.38M	0.92
	0.60M	0.75

Fig. 48 Elution of Total Protein and Enzyme at 0.23, 0.38 and 0.6M

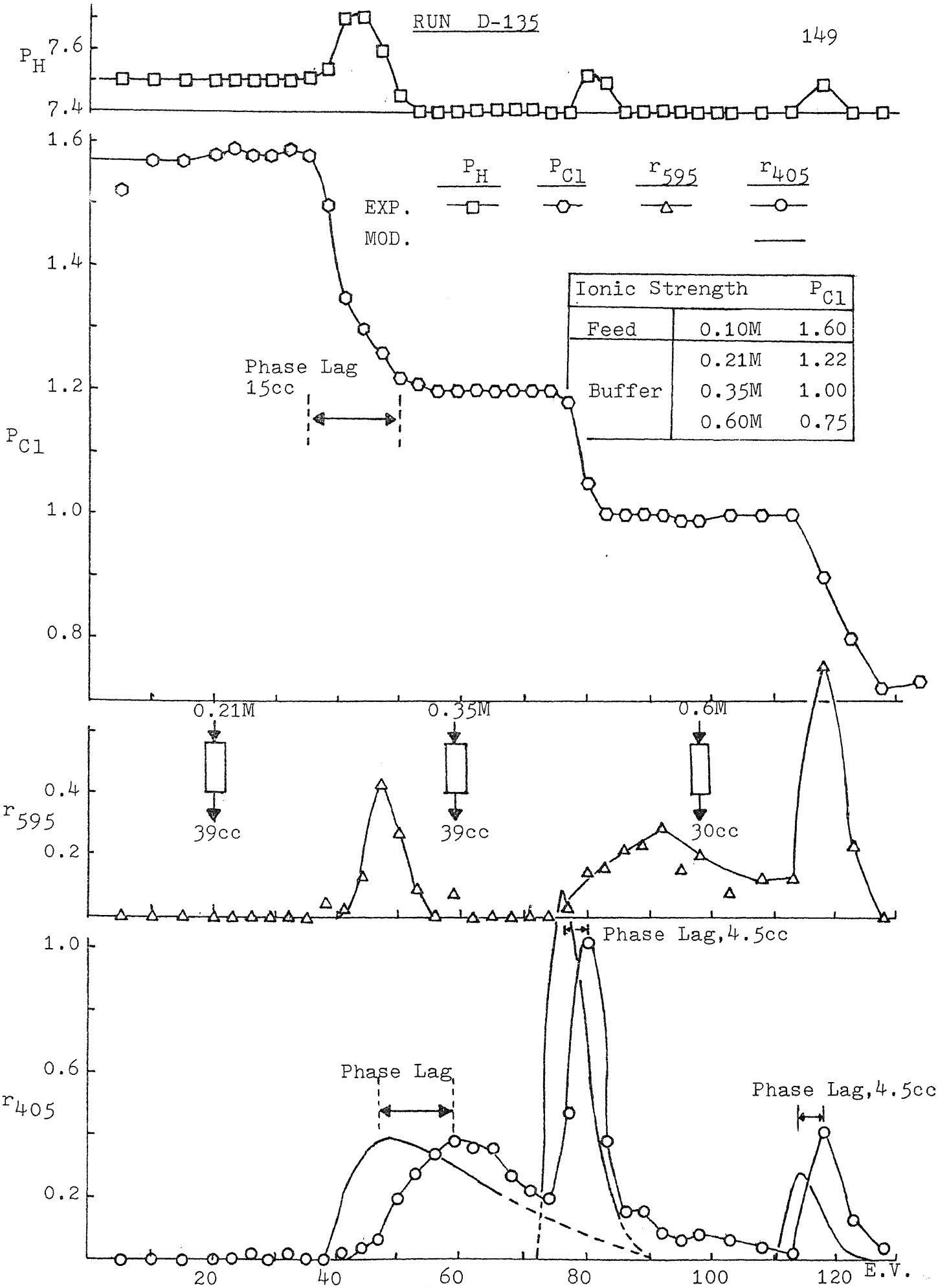

Fig. 49 Elution of Total Protein and Enzyme at 0.21, 0.35 and 0.6M

We have shown that the first impurity group can be eluted further appart from the first peak of enzyme by lowering the ionic strength from 0.3M to 0.21M. We also observe that the effect of lowering the ionic strength is to delay the pCl fall resulting in the elution of less proteins. Therefore, if we graduately reduce the ionic strength, we will eventually reach a point that will start to elute the component of interest (enzyme and two parts of impurity).

Figures 50 and 51 show the elution profiles for the enzyme and total protein for buffer ionic strength of 0.4M and 0.35M respectively. Both of the ionic strength are actually higher than the first and second isoionic points for the impurity. This causes a co-elution of two total impurity peaks. Figure 51 demonstrates the co-elution of the first and second peaks for r_{595}. One can infer that the sharp rise was contributed to by the first isoionic point and flat tail was contributed to by the second isoionic point. The tails of the first and second peaks overlap. Figure 51 (0.35M buffer) shows the overlap effect more clearly than that shown in Figure 50 (0.4M buffer). Because the 0.35M buffer elutes the second part of impurity peak late in elution time and less in elution area as compared with that for the 0.4M buffer. Figure 52 shows that no significant enzyme is eluted when a low buffer (0.2M) is used. The first impurity will elute much earlier than the enzyme. The incoming ionic strength of 0.2M causes r_{595} to have a small flat peak, while r_{405} is not

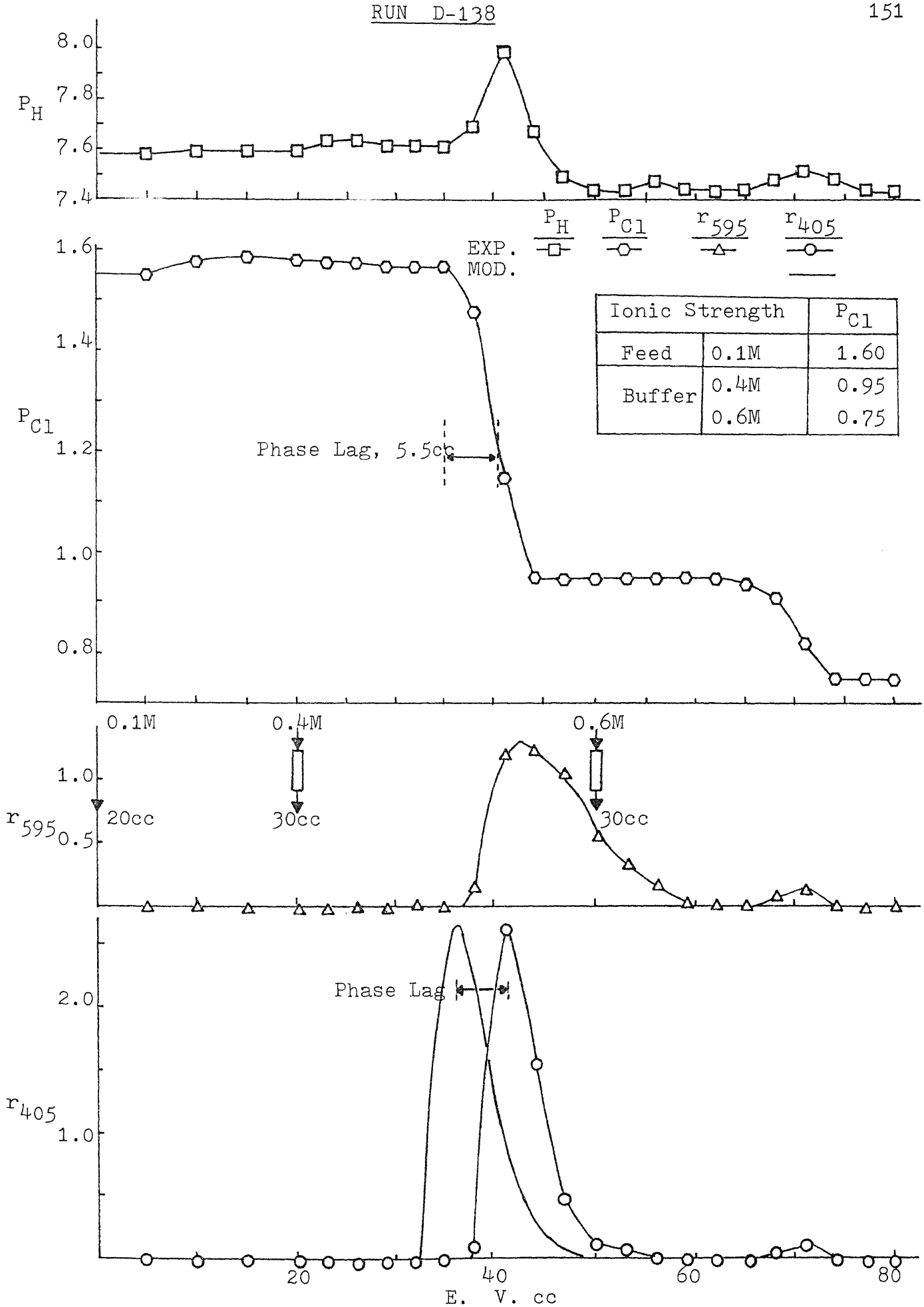

Fig. 50 Elution of Total Protein and Enzyme at 0.4 and 0.6M

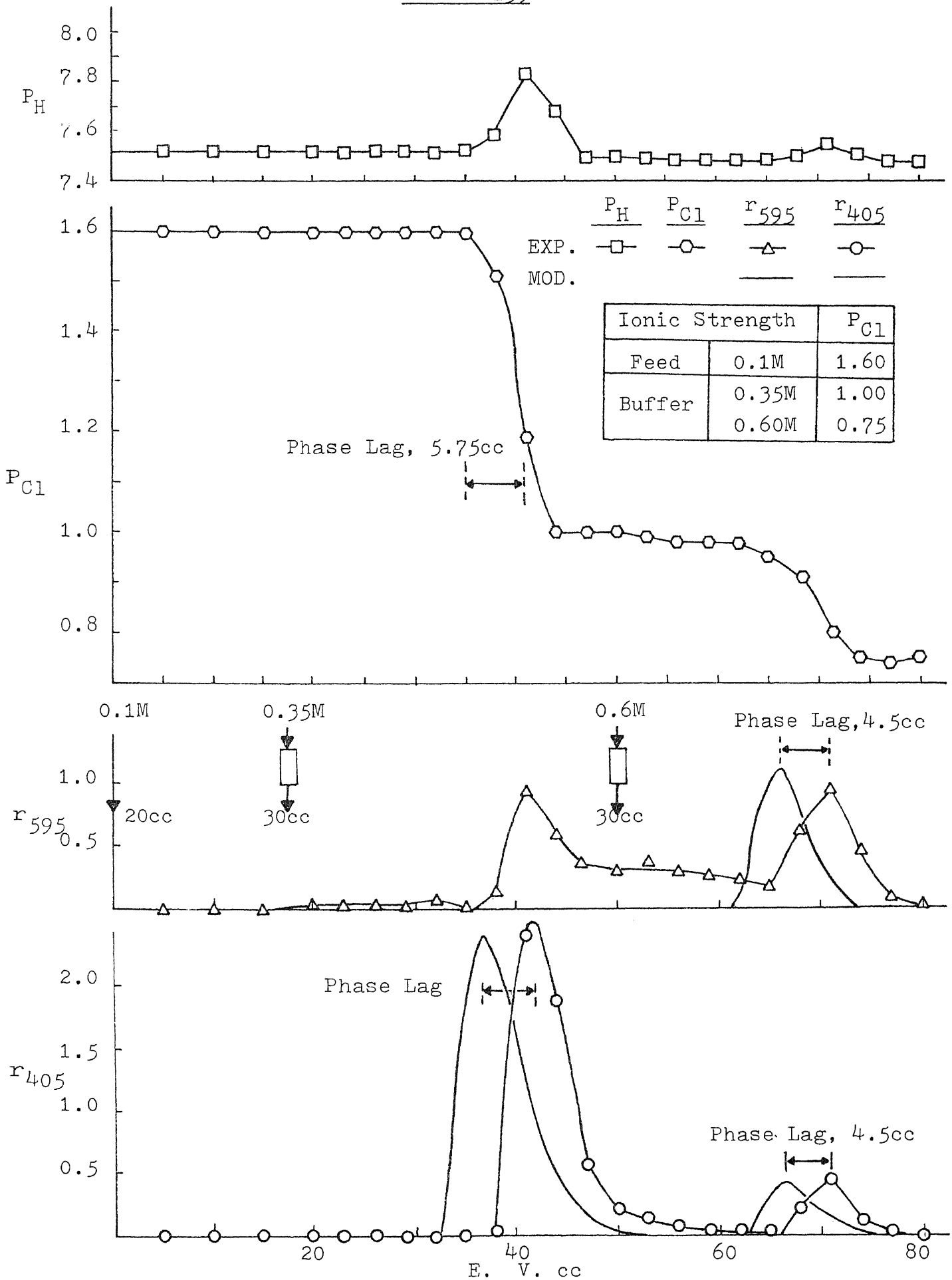

Fig. 51 Elution of Total Protein and Enzyme at 0.35 and 0.6M

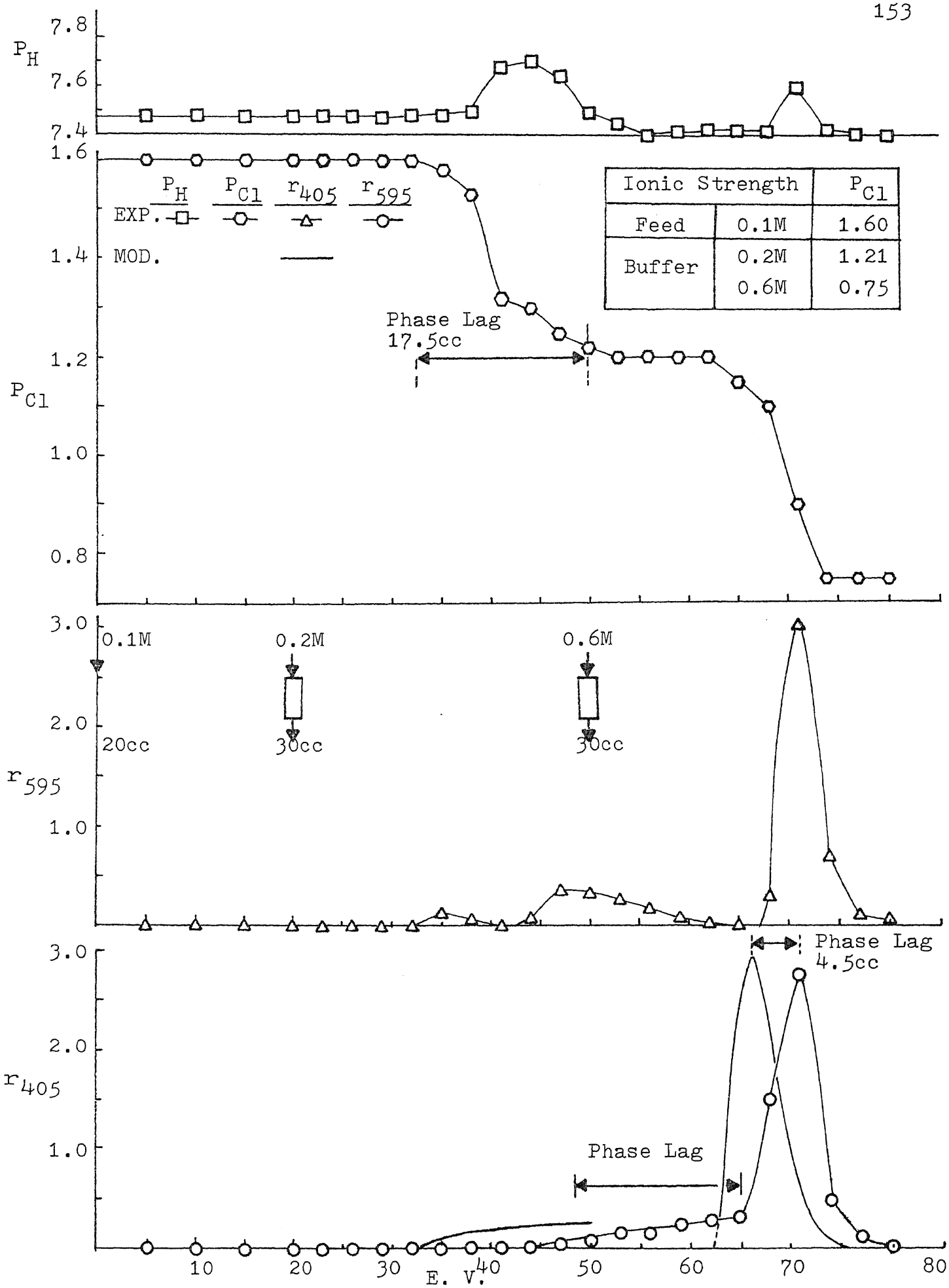

Fig. 52 Elution of Total Protein and Enzyme at 0.2 and 0.6M

eluted. Figure 53 shows that protein profiles are eluted at 0.19M and 0.3M and 0.6M. The first incoming 0.19M ionic strength eluted a small peak of r_{595} and no significant enzyme r_{405}. Also, the r_{595} first peak has a tremendous delay due to a relatively small change in pCl profiles. The ionic strength of 0.3M then elutes the rest of the r_{595} peak. Note that the r_{405} has a sharp peak. The pCl drop from 1.60 to 1.22 (0.19M) to 1.05 (0.3M) to 0.75 (0.6M) to generate three peaks for r_{595} and two peaks for r_{405}. We can therefore estimate three isoionic points 0.17M and 0.18M and 0.325M respectively (see in Figure 38). Buffer ionic strength of 0.18M is used instead of 0.19M to insure no enzyme is eluted with the first impurity.

Figures 54a and 54b show the extreme case of elution with an buffer ionic strength of 0.6M and 1.0M respectively. The incoming 0.6M buffer ionic strength will elute everything including enzyme and impurities. This also demonstrates the case of no separation. The ionic strength 0.6M will cover three isoionic points and strong enough to elute all the adsorbed proteins simultaneously. Figure 54b shows the pCl drop from 1.60 to 0.75 which covers all the pCl values for all three isoionic points, and finally become 0.59 (1.0M).

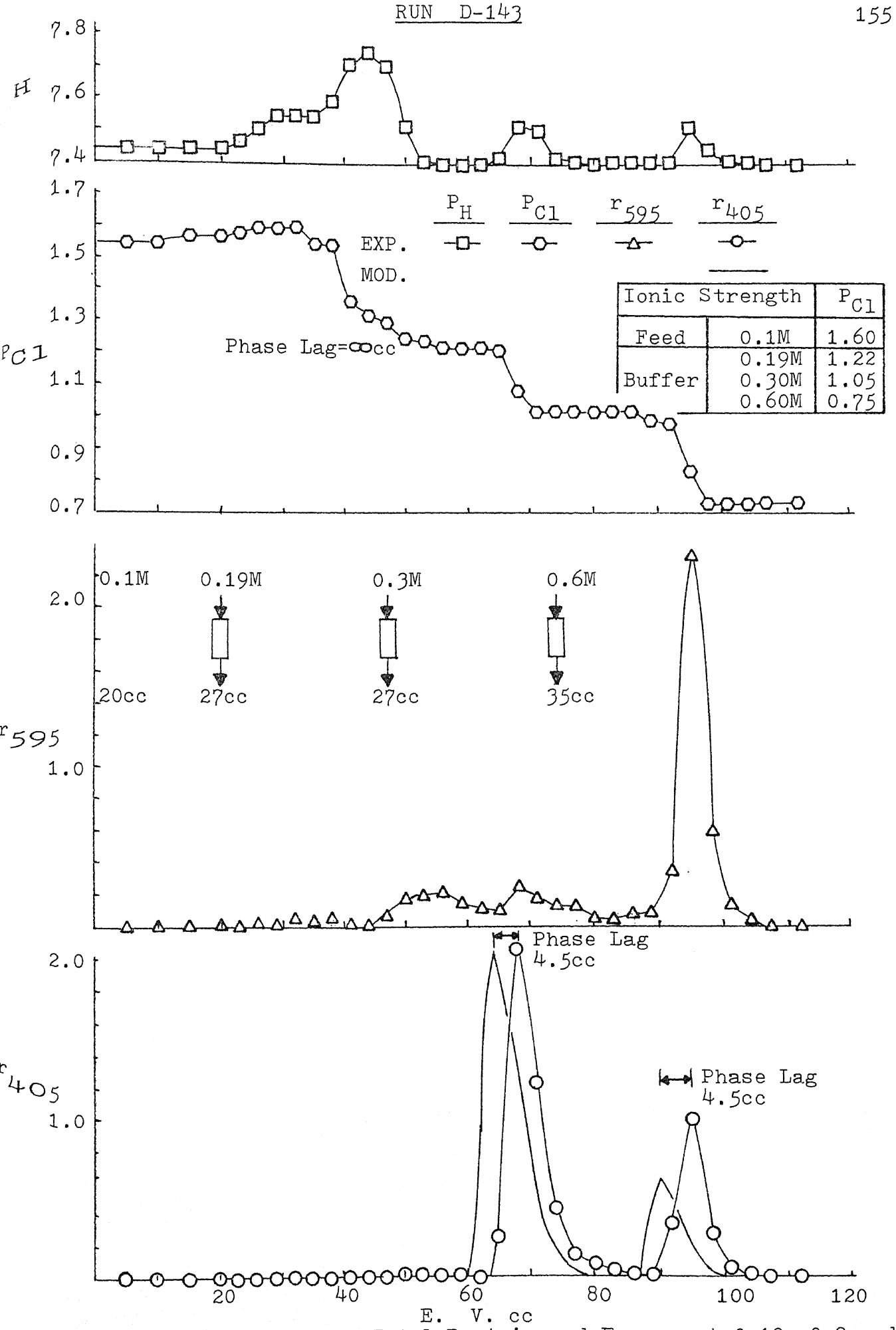

Fig. 53 Elution of Total Protein and Enzyme at 0.19, 0.3 and 0.6M

RUN D-145

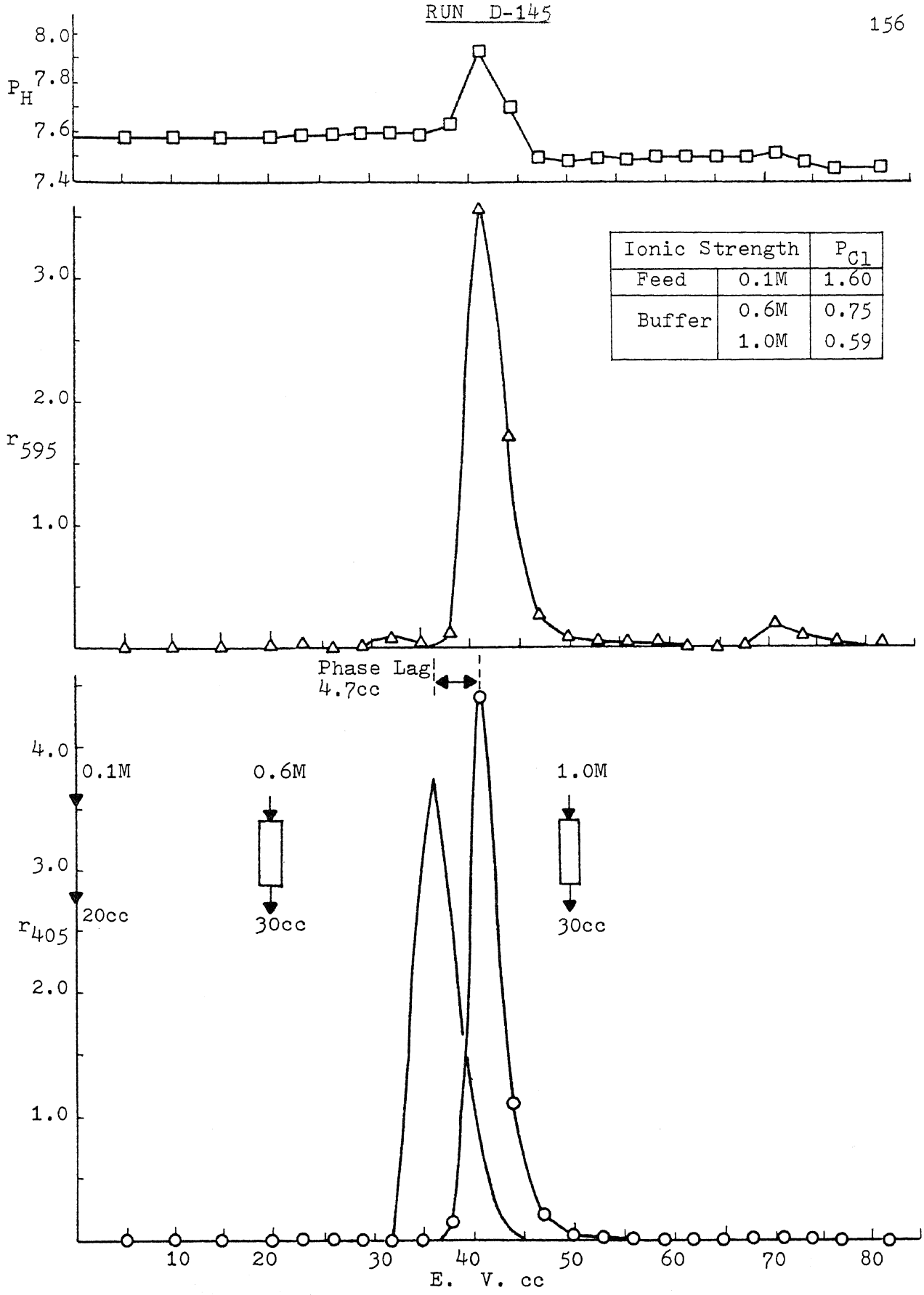

Fig. 54a Elution of Total Protein and Enzyme at 0.6 and 1.0M

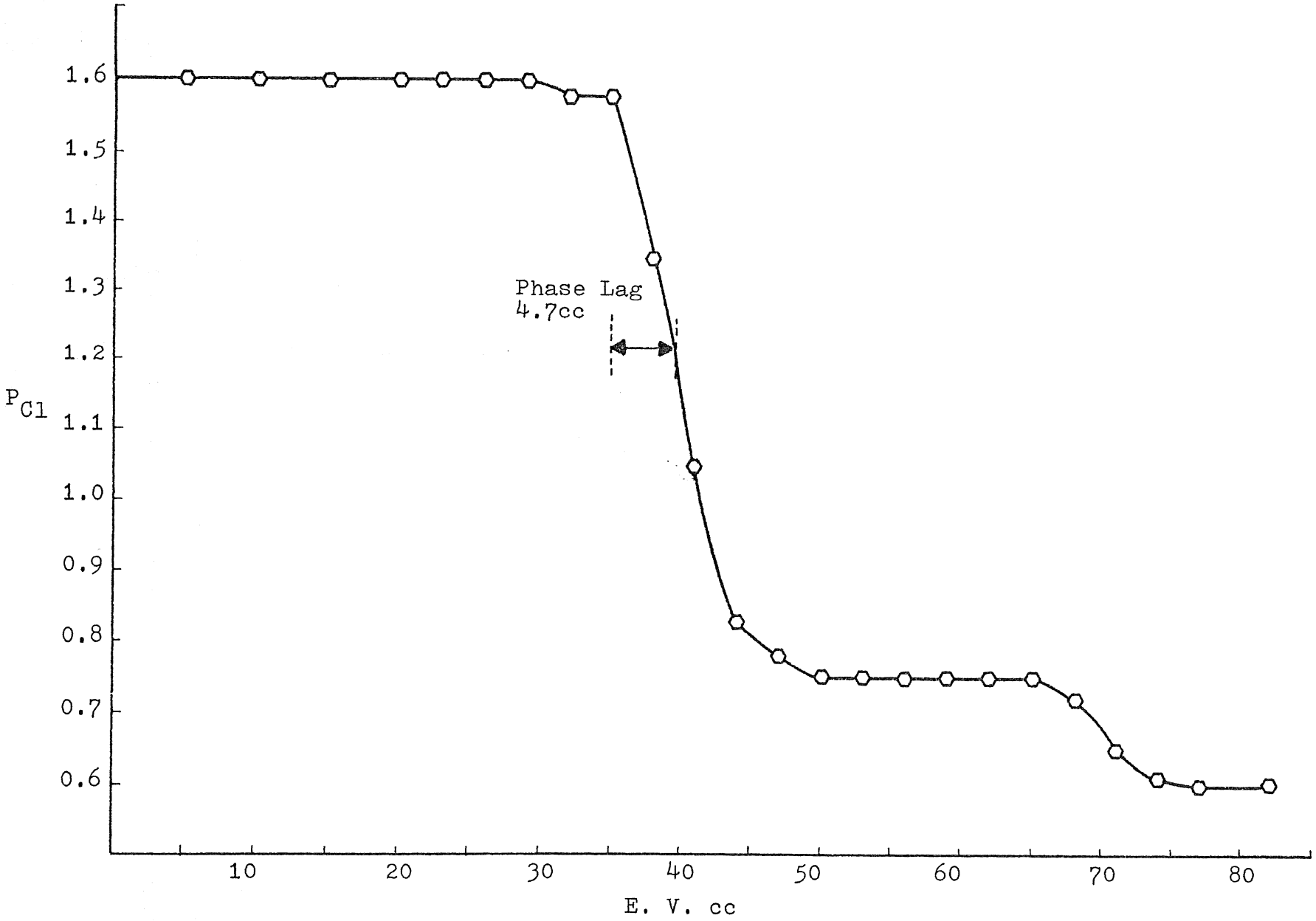

Fig. 54b pH Wave and P_{Cl} Wave for Fig. 54a

RUN D-145

Separation optimization

Figures 45 to 54 show single step change in the input buffer ionic strength. Generally, the transient pCl profile for a single step change is sharp and has a significant change in pCl. It will only elute a limited amount of proteins. However, if a multiple step changes are performed, the pCl transient is prolonged and the protein separation efficiency will be increased. Base upon this phenomenon, an optimization of separation was achieved using a multiple step changes to maximize the purity and recovery of enzyme product.

Figure 55 illustrates the effect of multiple step changes. The initial input buffer ranges from 0.21M to 0.25M to have 65.3% recovery of the enzyme and co-elute 22.8% of impurities. The impurity peak elute earlier than the enzyme peak. The 0.6M buffer elutes the rest of proteins. Figure 56 shows another method for multiple step changes in buffer ionic strength. The initial buffer concentration ranges from 0.21M to 0.29M to obtain a 85.9% recovery of the enzyme; but more impurity was co-eluted (33.7%) as compared with that in Figure 55. Figure 57 shows the initial elution for buffer ionic strength ranging from 0.21M to 0.25M. The amount of enzyme eluted shown in Figure 57 (74.7%) lies in between that of Figures 55 (65.3%) and 56 (85.9%). The amount of impurity (36.3%) which is rather constant as compared with that in Figure 56 (33.7%).

RUN D-136

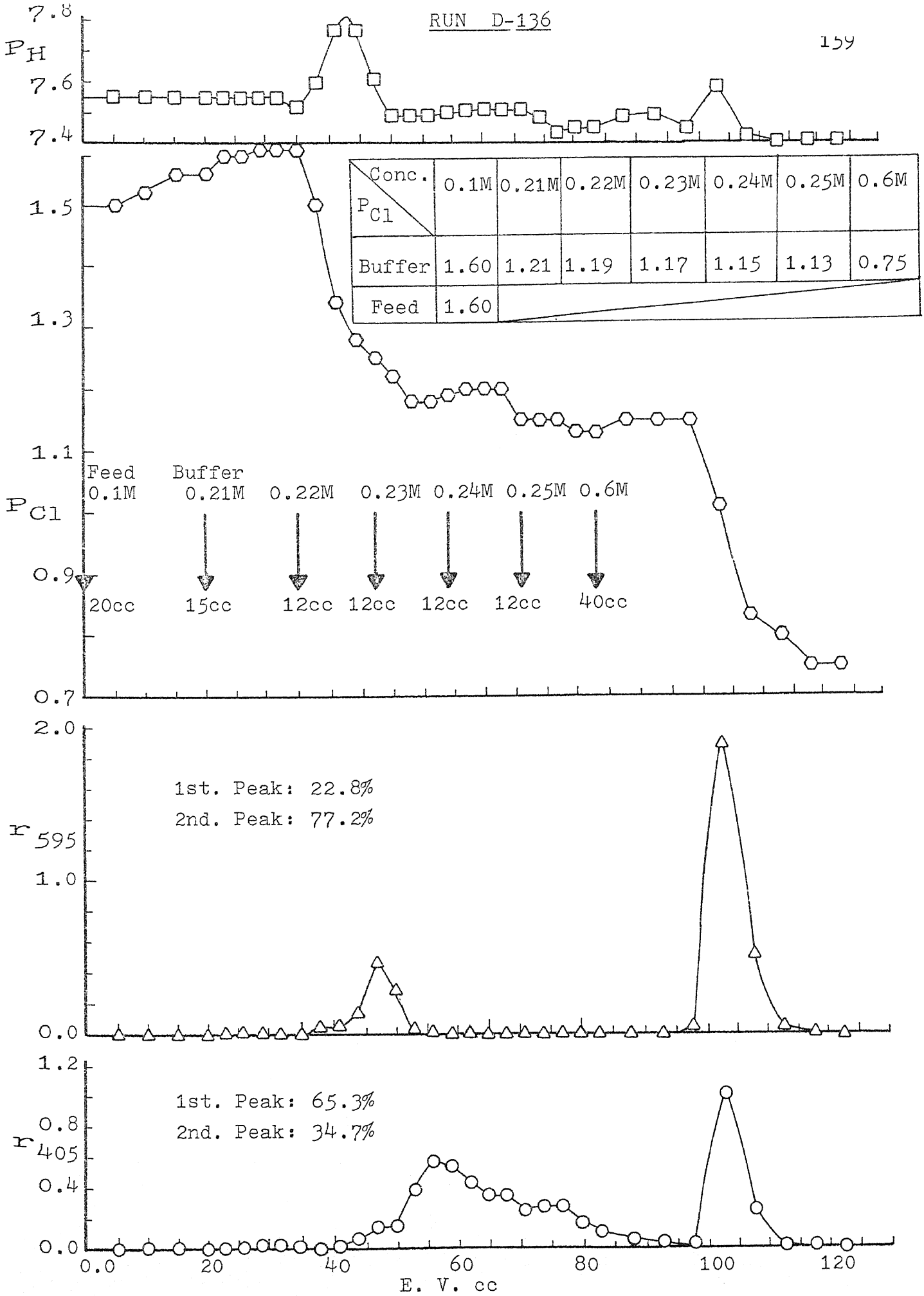

Conc. / P_{Cl}	0.1M	0.21M	0.22M	0.23M	0.24M	0.25M	0.6M
Buffer	1.60	1.21	1.19	1.17	1.15	1.13	0.75
Feed	1.60						

Fig. 55 Optimization of Isolation of Enzyme, Option 1

RUN D-137

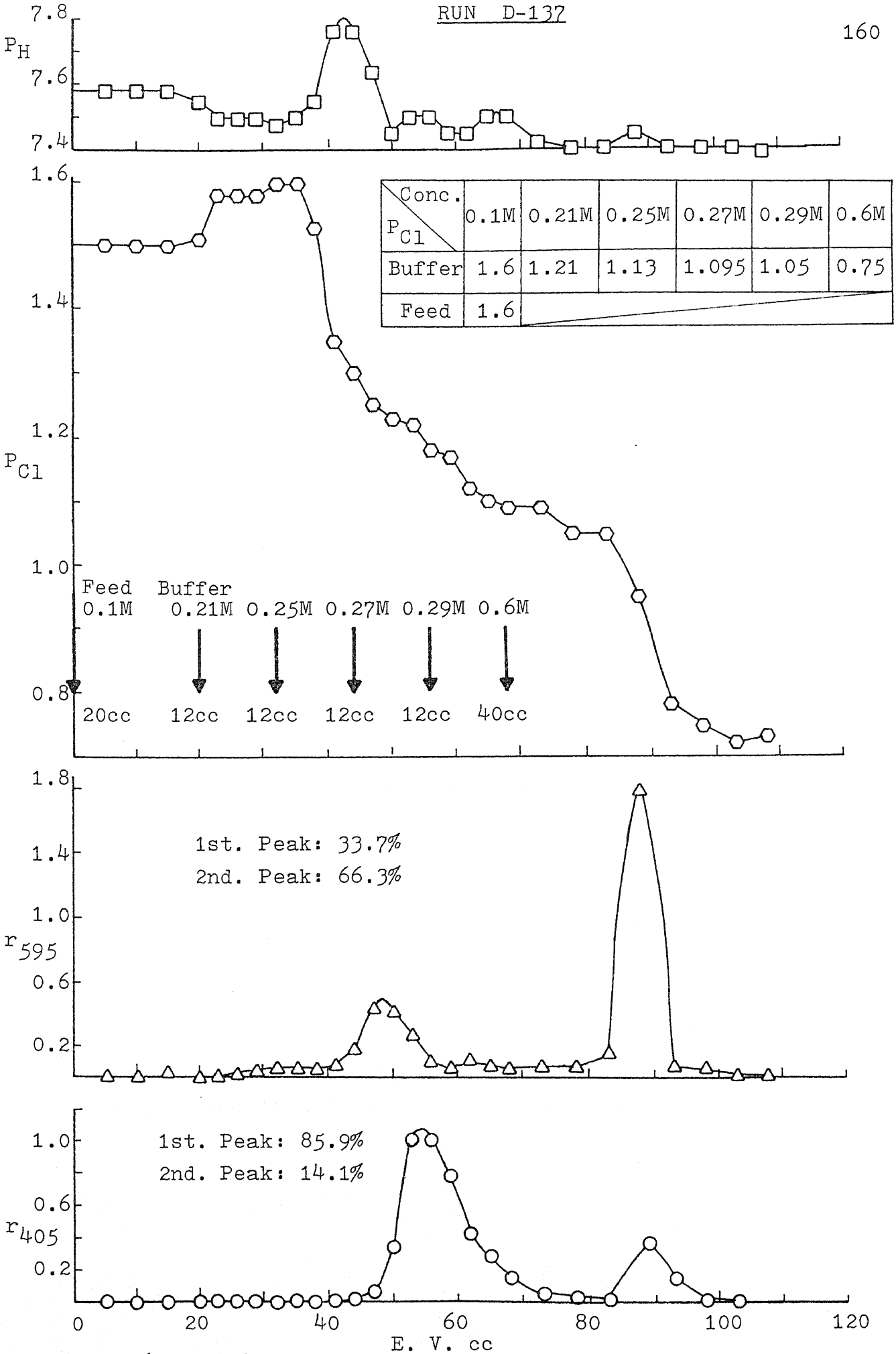

Conc. / P_{Cl}	0.1M	0.21M	0.25M	0.27M	0.29M	0.6M
Buffer	1.6	1.21	1.13	1.095	1.05	0.75
Feed	1.6					

Fig. 56 Optimization of Isolation of Enzyme, Option 2

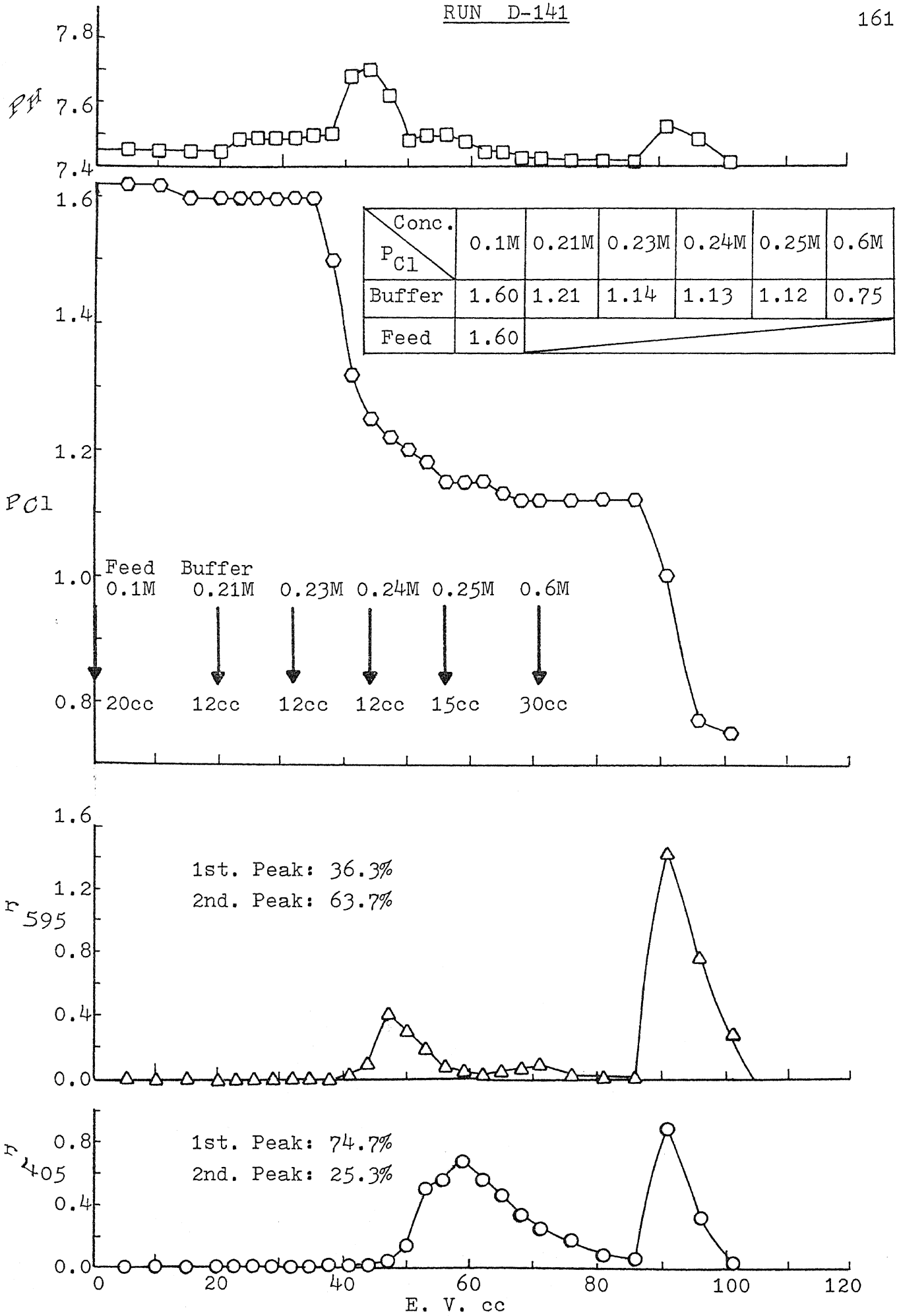

Conc. / P_{Cl}	0.1M	0.21M	0.23M	0.24M	0.25M	0.6M
Buffer	1.60	1.21	1.14	1.13	1.12	0.75
Feed	1.60					

Fig. 57 Optimization of Isolation of Enzyme, Option 3

Figure 58 shows the method to concentrate the recoveryed enzyme. The sample is collected from the elution volume of 57cc to 86cc as shown in Figure 57. It was diluted with water to a final volume of 62cc (pCl=1.60). The diluted solution was then reintroduced into the column, the enzyme was adsorbed again by the resin. Then, a 0.6M buffer was applied to elute the enzyme in a small elution volume to concentrate the enzyme.

Figure 59a and Figure 59b concludes the optimization of enzyme isolation. Enzyme was isolated between two buffer ionic strengths (0.19M and 0.6M). The initial elution buffer for the enzyme ranged from 0.22M to 0.25M. This concentration lies between the two isoionic points. As a result, the enzyme eluted in a nearly pure form. The multiple step changes can elute only the enzyme, because the 0.19M buffer can elute a maximum amount of the first impurity group. The resin bed is flushed again with 0.21 to 0.25M buffer in order to recover any remaining enzyme, however, no significant additional enzyme is eluted. This results from the fact that the liquid and solid phase reach equilibrium after the first cycle. Rising the buffer ionic strength will elute more enzyme, but the second part of impurity will start to elute and lower the enzyme purity. Table 3 lists all the experimental parameters for isolating the enzyme. Each experimental run corresponds to the figures which have been discussed in this chapter.

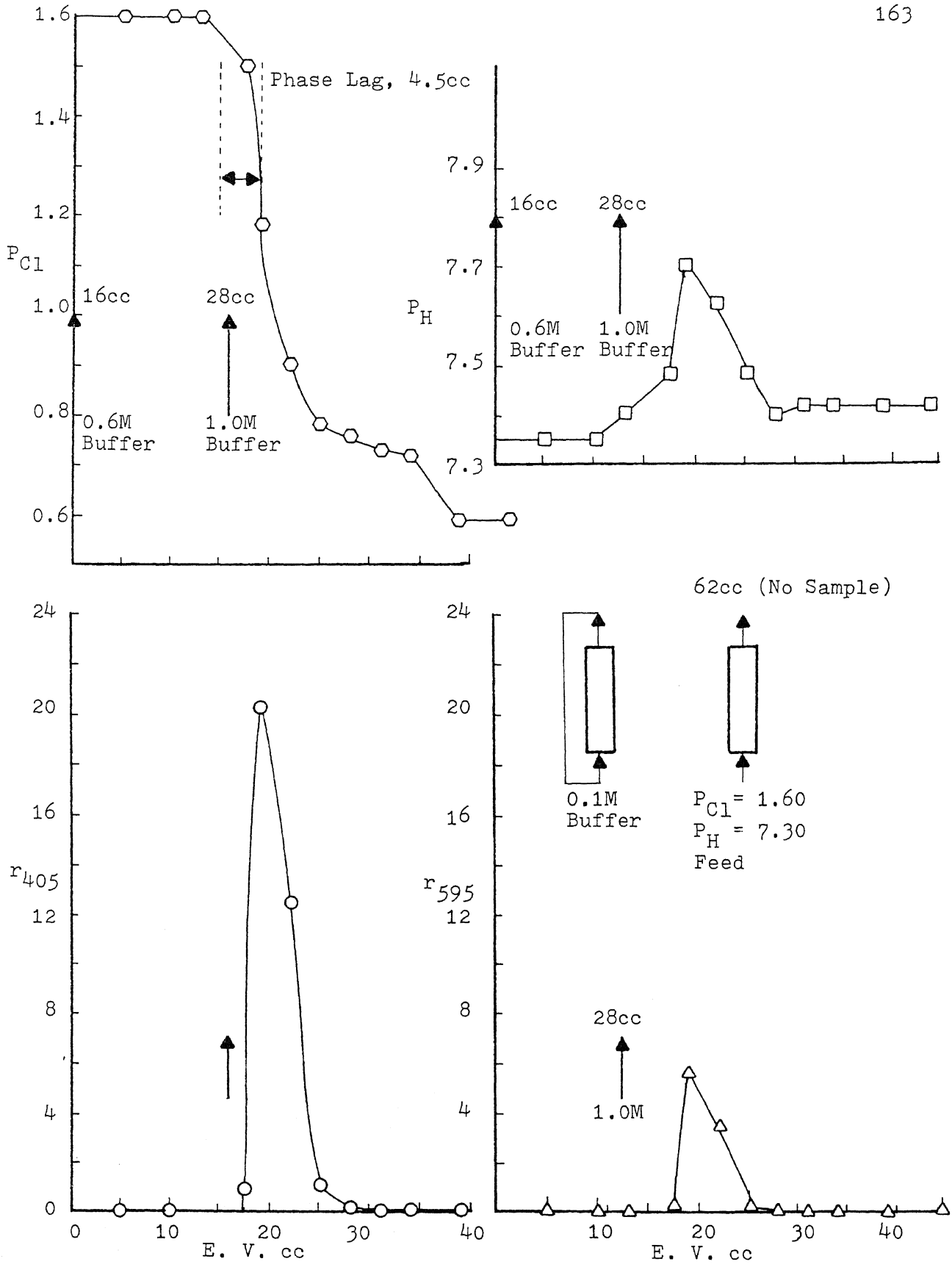

Fig. 58 Method of High Concentration Enzyme Recovery

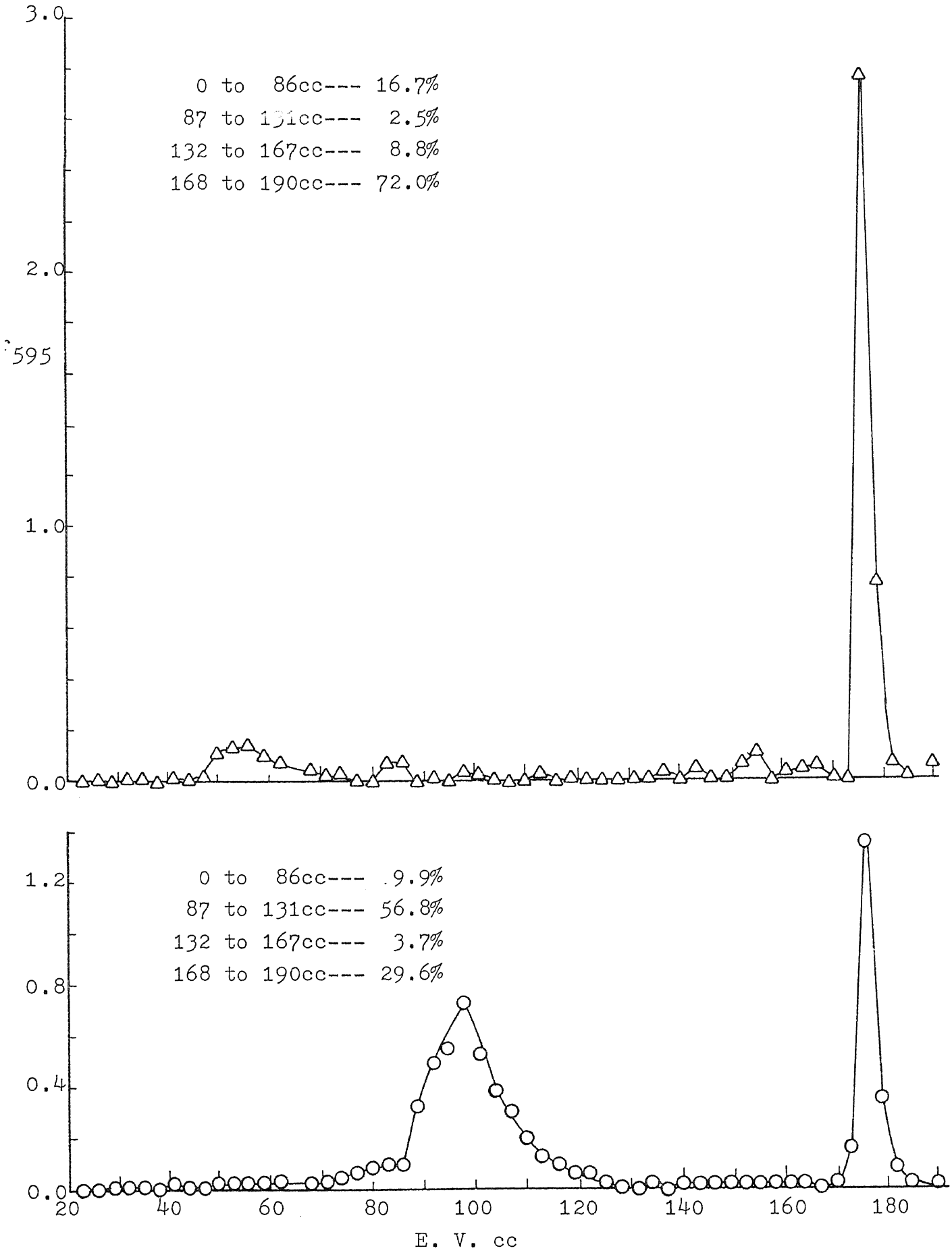

Fig. 59a Optimization of Isolation of Enzyme, Option 4

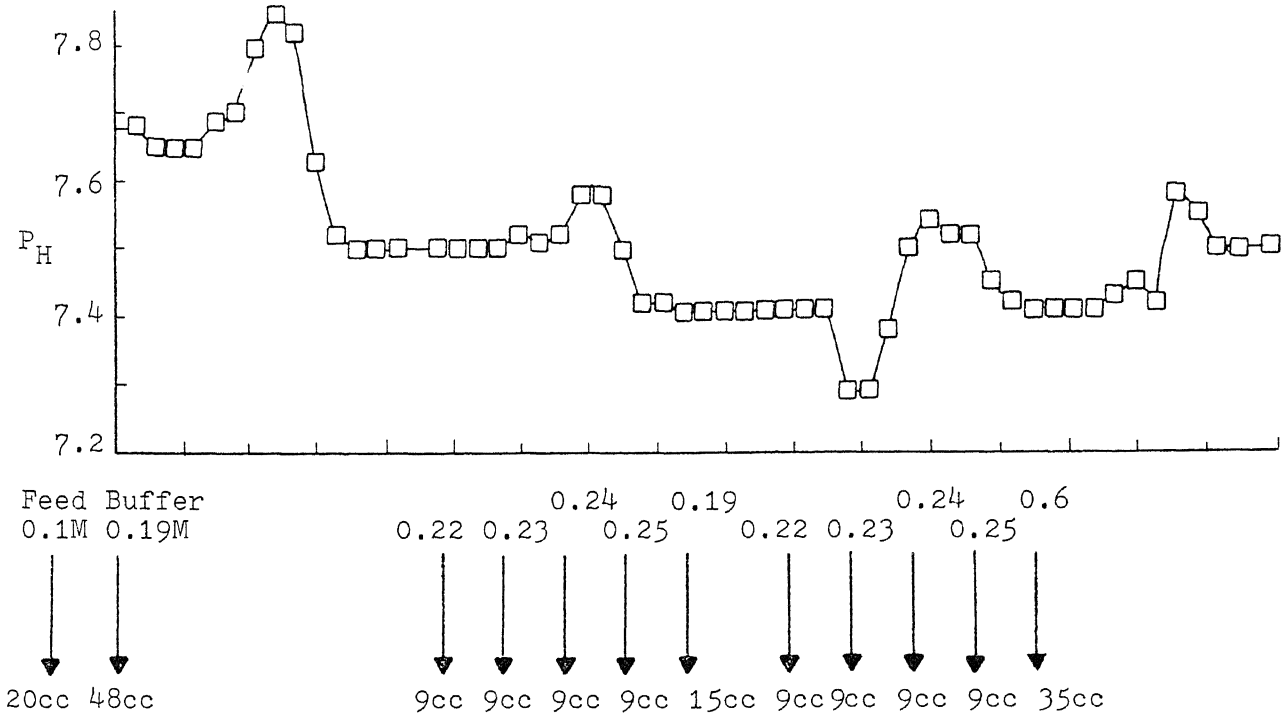

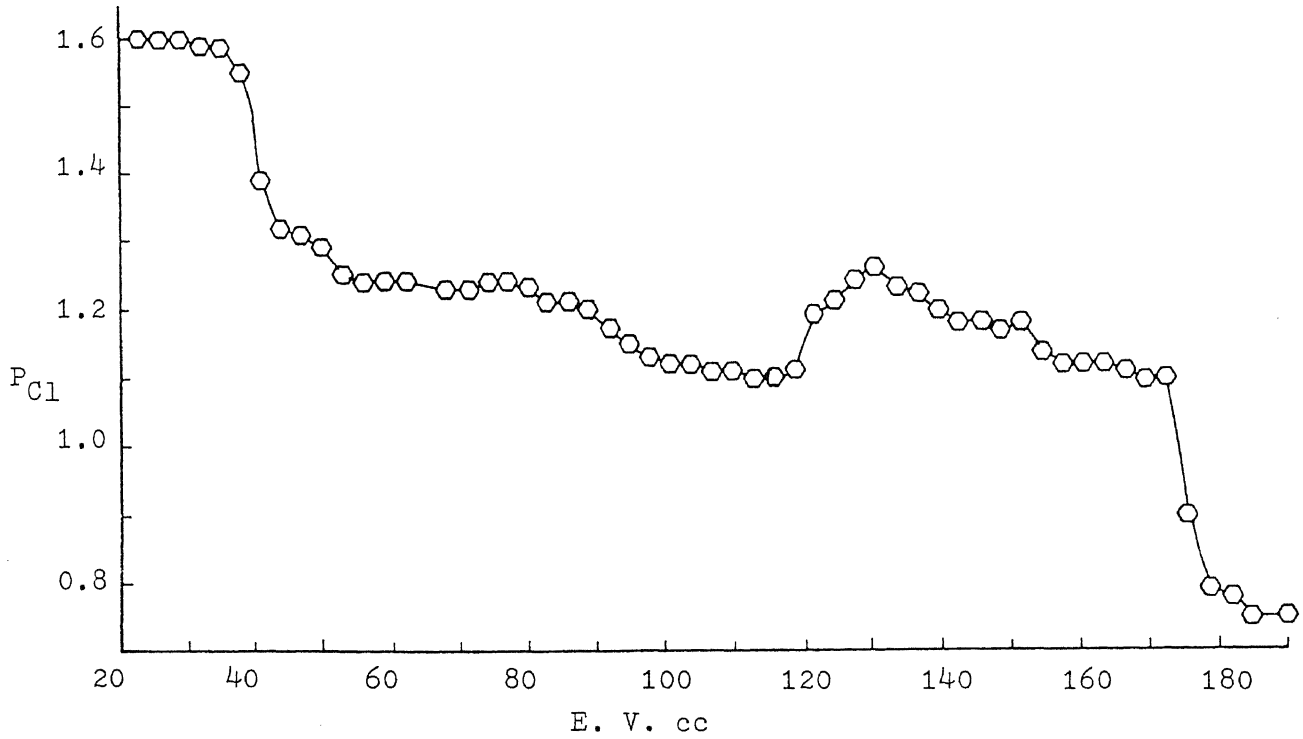

Fig. 59b pH Wave and P_{Cl} Wave for Fig. 59a

Table 3 Experimental Parameters

Initial Condition

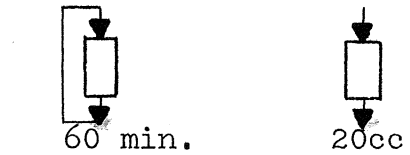

Buffer: pH 7.4 Tris + HCl (0.1M to 1.0M)

Feed : 0.02Wt% alkaline phosphatase in pH 7.4 Buffer

Resin : R^+ Anion Exchanger, DEAE-Sepharose CL-6B

Q: 1.0cm^3/min

S: 2.0cm^2

L: 8.0cm

Tube Vol.: 4 c.c.

RUN	Condition	RUN	Condition
D-131	0.1M Feed → 40cc; 0.3M Buffer → 21cc; 0.4M " → 21cc; 0.5M " → 21cc; 0.6M " → 21cc; 1.0M " → 46cc	D-132	0.3M Buffer → 30cc; 1.0M " → 40cc
D-133	0.25M Buffer → 30cc; 0.6M " → 30cc	D-134	0.23M Buffer → 39cc; 0.38M " → 39cc; 0.6M " → 30cc
D-135	0.21M Buffer → 39cc; 0.35M " → 39cc; 0.6M " → 30cc	D-138	0.4M Buffer → 30cc; 0.6M " → 30cc

RUN	Condition	RUN	Condition
D-139	0.35M Buffer → 30cc; 0.6M " → 30cc	D-140	0.2M Buffer → 30cc; 0.6M " → 30cc
D-142	0.1M Feed → 62cc; 0.6M Buffer → 16cc; 1.0M " → 28cc	D-143	0.19M Buffer → 27cc; 0.3M " → 27cc; 0.6M " → 35cc
D-145	0.6M Buffer → 30cc; 1.0M " → 30cc	D-136	0.21M Buffer → 15cc; 0.22M " → 12cc; 0.23M " → 12cc; 0.24M " → 12cc; 0.25M " → 12cc; 0.6M " → 40cc
D-137	0.21M Buffer → 12cc; 0.25M " → 12cc; 0.27M " → 12cc; 0.29M " → 12cc; 0.6M " → 40cc	D-141	0.21M Buffer → 12cc; 0.23M " → 12cc; 0.24M " → 12cc; 0.25M " → 15cc; 0.6M " → 30cc
D-144	0.19M Buffer → 48cc; 0.22M " → 9cc; 0.23M " → 9cc; 0.24M " → 9cc; 0.25M " → 9cc	D-144	0.19M " → 15cc; 0.22M " → 9cc; 0.23M " → 9cc; 0.24M " → 9cc; 0.25M " → 9cc; 0.6M " → 35cc

5-2 Model prediction of enzyme

In order to scale up and optimize the chromatographic column operation from the bench scale to production scale, Sufficient data is required from bench scale test. Scale up may not be economically feasible, however, based upon purely experimental work with no the coordination of theoretical aspects. This is true since most biologically active materials are rare and expensive. As a result, model prediction of elution profile and optimization procedures can be more efficiently set up to determine the operating condition and dimensions of column for large scale production.

Because of the large size of protein molecules, the surface adsorption without pore diffusion model can be applied for accurate elution prediction. We have previously discussed the relationship between the mass transfer coefficient k_f and the equilibrium constant m (Sec.2-1-1). Figure 60 shows the calculated peak height v.s. equilibrium constant for different mass transfer coefficients k_f. As previously discussed, a small value of k_f means high mass transfer resistance. A high equilibrium constant (m) means the solute molecules tend to stay in the mobile phase. Different combinations of k_f and m might may give the same peak height. The calculated profile, however, may have a distinct shape and elution retention time.

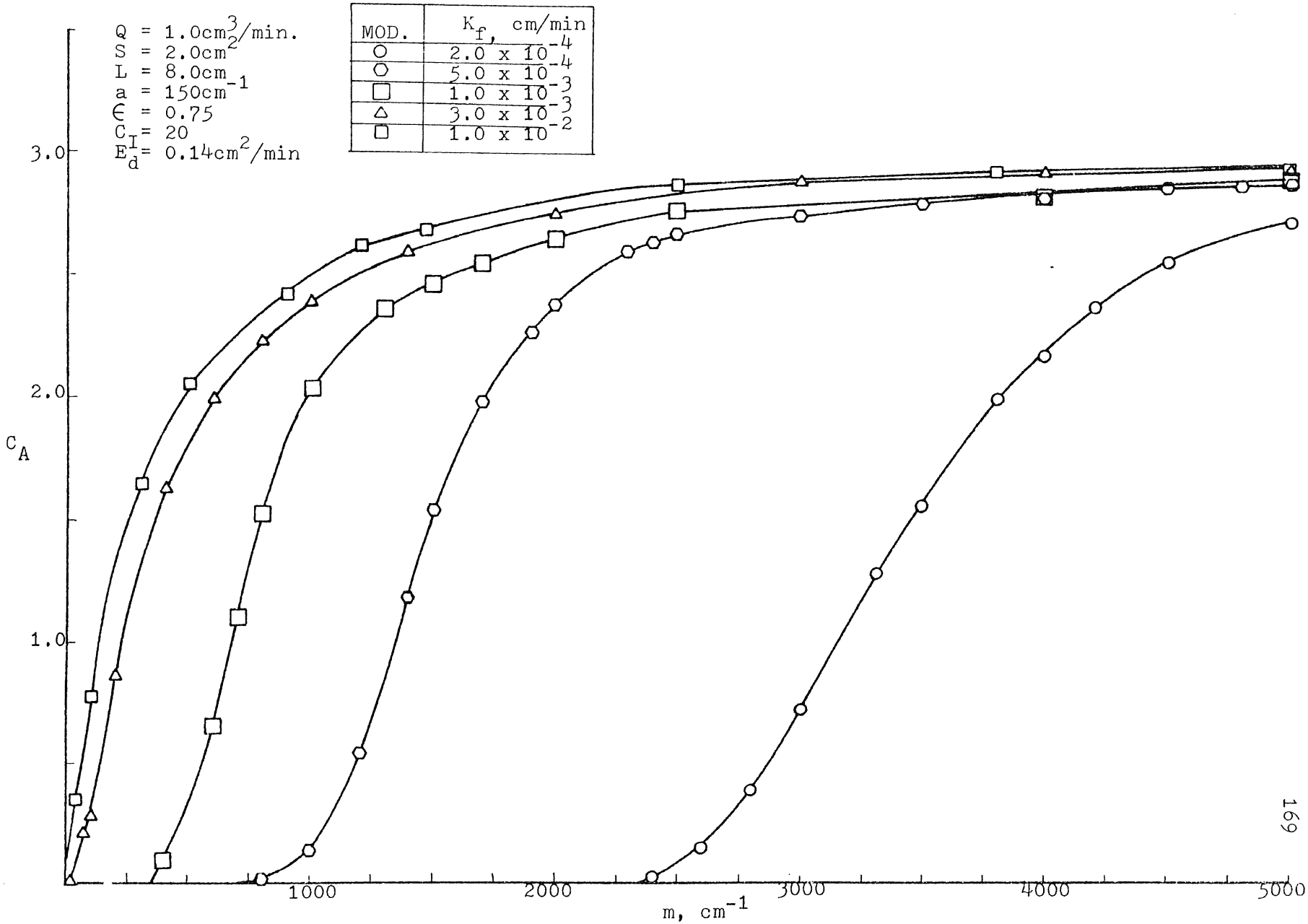

Fig. 60 Calculation Peak Height v.s. Equilibrium Constant m with Variation of Mass Transfer Coefficient k_f

Figure 61 shows the calculated percent recovered for elution profile with different equilibrium constants as a function of the mass transfer coefficient. A small mass transfer coefficient ($k_f = 5x10^{-4}$) requires a larger equilibrium constant in order to give the same percent recovery. We may conclude from Figures 60 and 61 that the different combinations of k_f and m may give the same percent recovery and peak height. The physical meaning of the operating condition, however, is completely different.

Figures 62 to 66 show the calculated elution profile v.s. time for different combinations of k_f and m. Different combinations show different peak shape and retention time, but they may have similar peak heights and percent recovery. Figures 62 and 63 demonstrate that a high mass transfer resistance ($k_f = 2x10^{-4}$) will give a group of small and sharp peaks for different values of m, this is similar to the results shown in Figures 60 and 61. Figure 64 shows that a low mass transfer resistance ($k_f = 1x10^{-3}$) will give a group of larger and broader peaks. Thus, if the mass transfer resistance is smaller, (as shown in Figure 65 and Figure 66) the calculated peak will become even taller and broader. In addition, the peak shape and retention time are quite different when compared with previous figures.

So far, we have discussed how the model parameters will

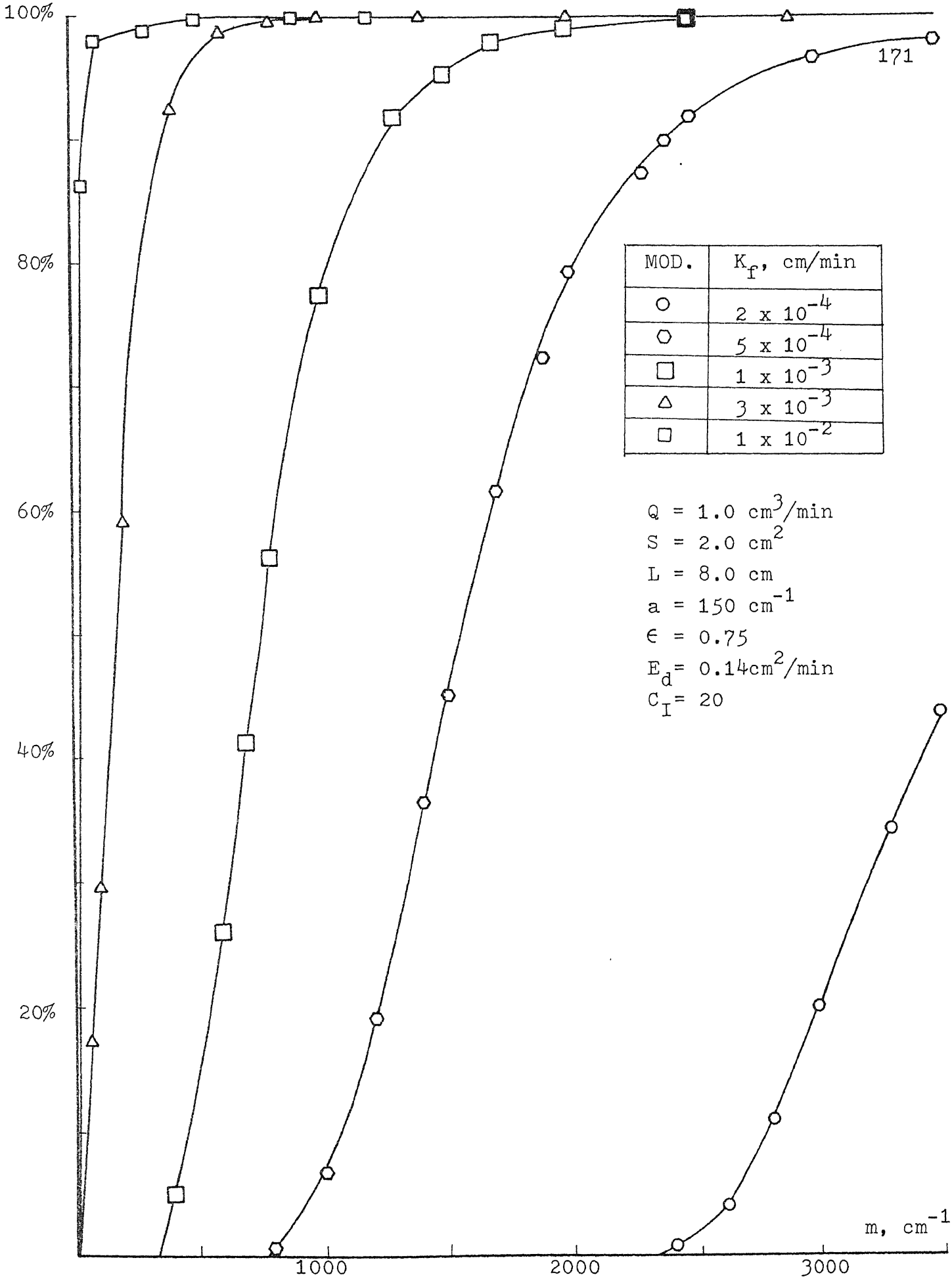

Fig. 61 Calculated Elution Recovery v.s. Equilibrium Constant m with Variation of k_f

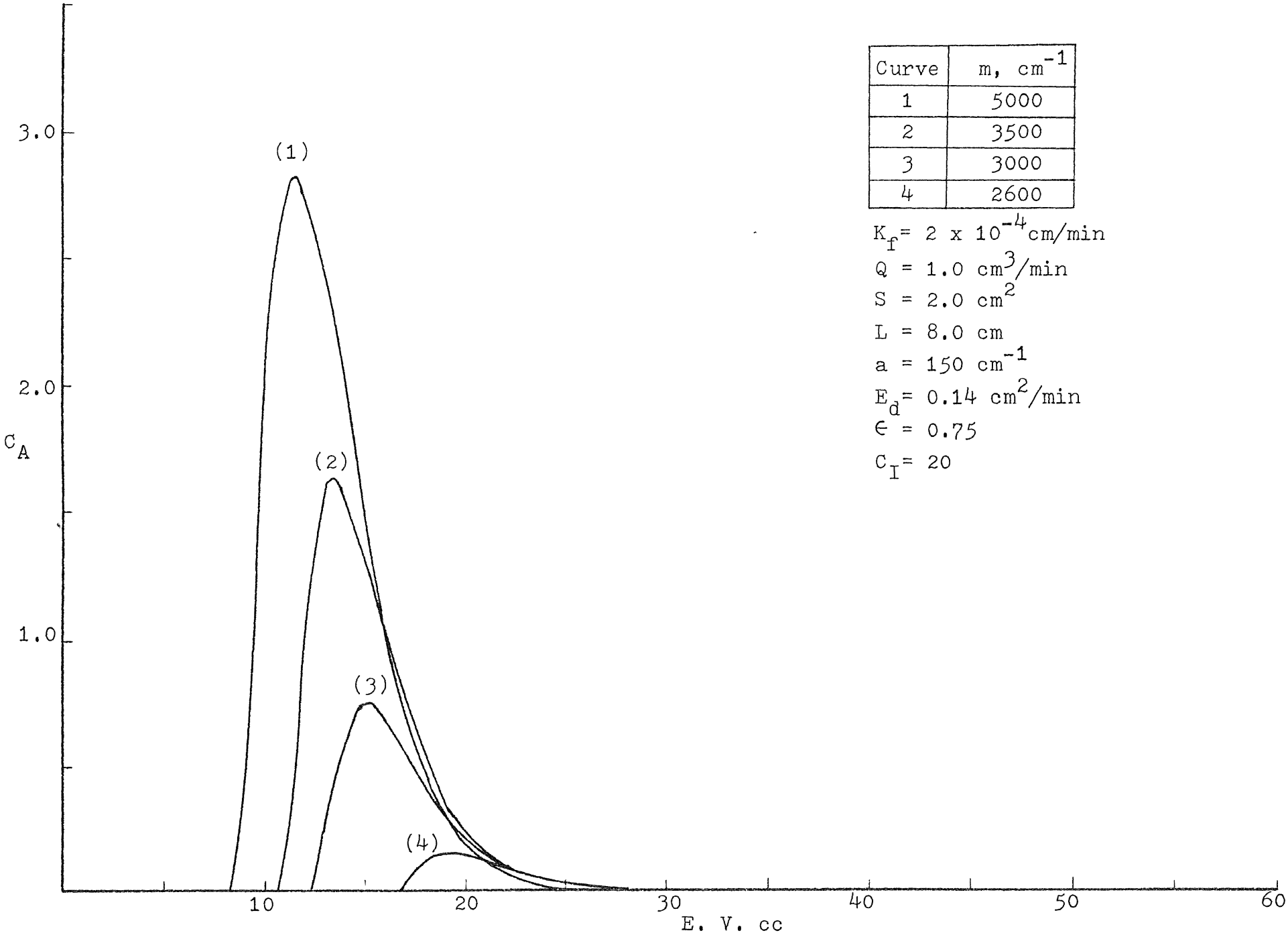

Curve	m, cm^{-1}
1	5000
2	3500
3	3000
4	2600

$K_f = 2 \times 10^{-4}$ cm/min
$Q = 1.0$ cm^3/min
$S = 2.0$ cm^2
$L = 8.0$ cm
$a = 150$ cm^{-1}
$E_d = 0.14$ cm^2/min
$\epsilon = 0.75$
$C_I = 20$

Fig. 62 Effect of Equilibrium Constant m for $k_f = 2 \times 10^{-4}$

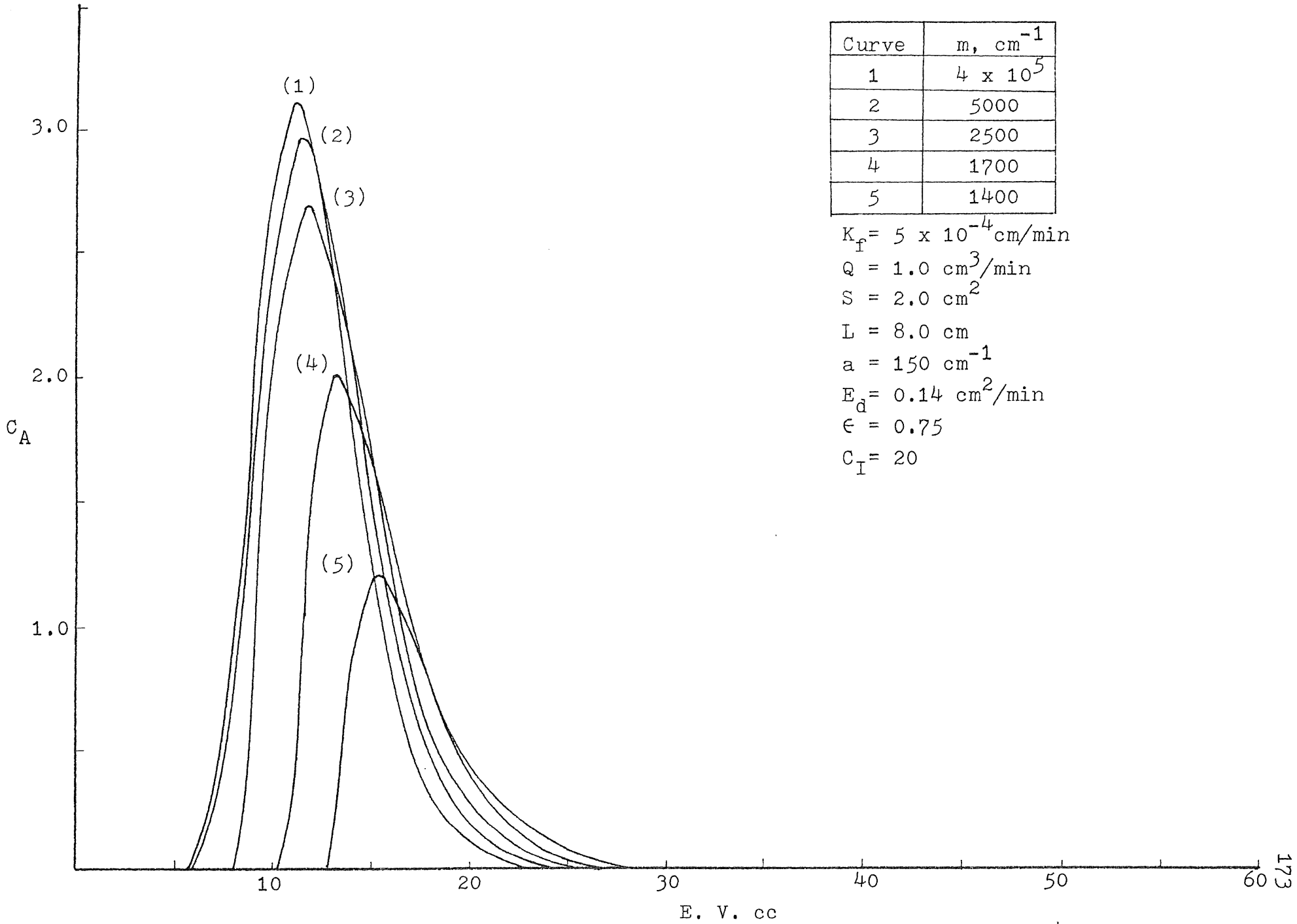

Curve	m, cm^{-1}
1	4×10^5
2	5000
3	2500
4	1700
5	1400

$K_f = 5 \times 10^{-4}$ cm/min
$Q = 1.0\ cm^3/min$
$S = 2.0\ cm^2$
$L = 8.0$ cm
$a = 150\ cm^{-1}$
$E_d = 0.14\ cm^2/min$
$\epsilon = 0.75$
$C_I = 20$

Fig. 63 Effect of Equilibrium Constant m for $k_f = 5 \times 10^{-4}$

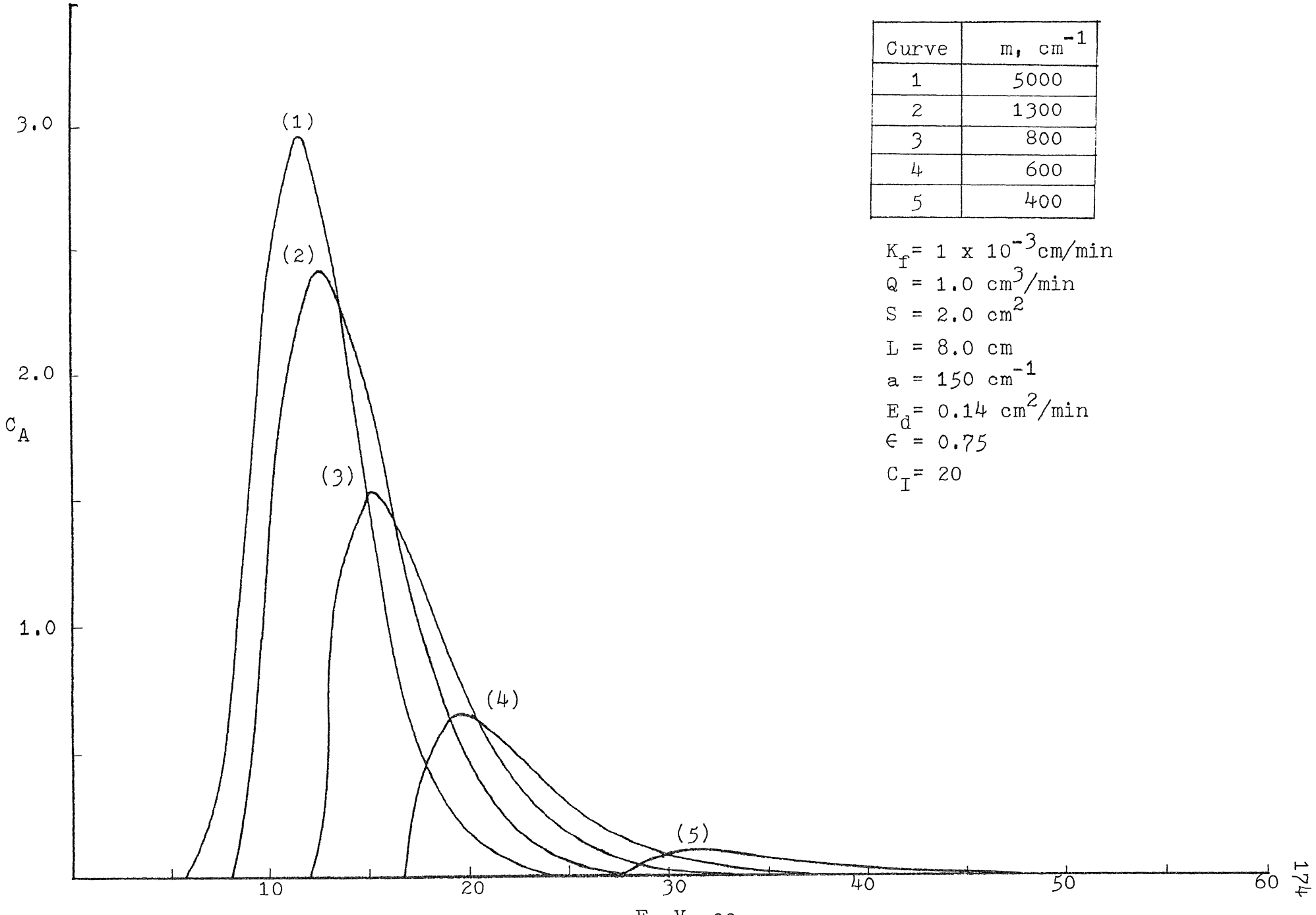

Curve	m, cm^{-1}
1	5000
2	1300
3	800
4	600
5	400

$K_f = 1 \times 10^{-3}$ cm/min
$Q = 1.0$ cm^3/min
$S = 2.0$ cm^2
$L = 8.0$ cm
$a = 150$ cm^{-1}
$E_d = 0.14$ cm^2/min
$\epsilon = 0.75$
$C_I = 20$

Fig. 64 Effect of m for $k_f = 1 \times 10^{-3}$

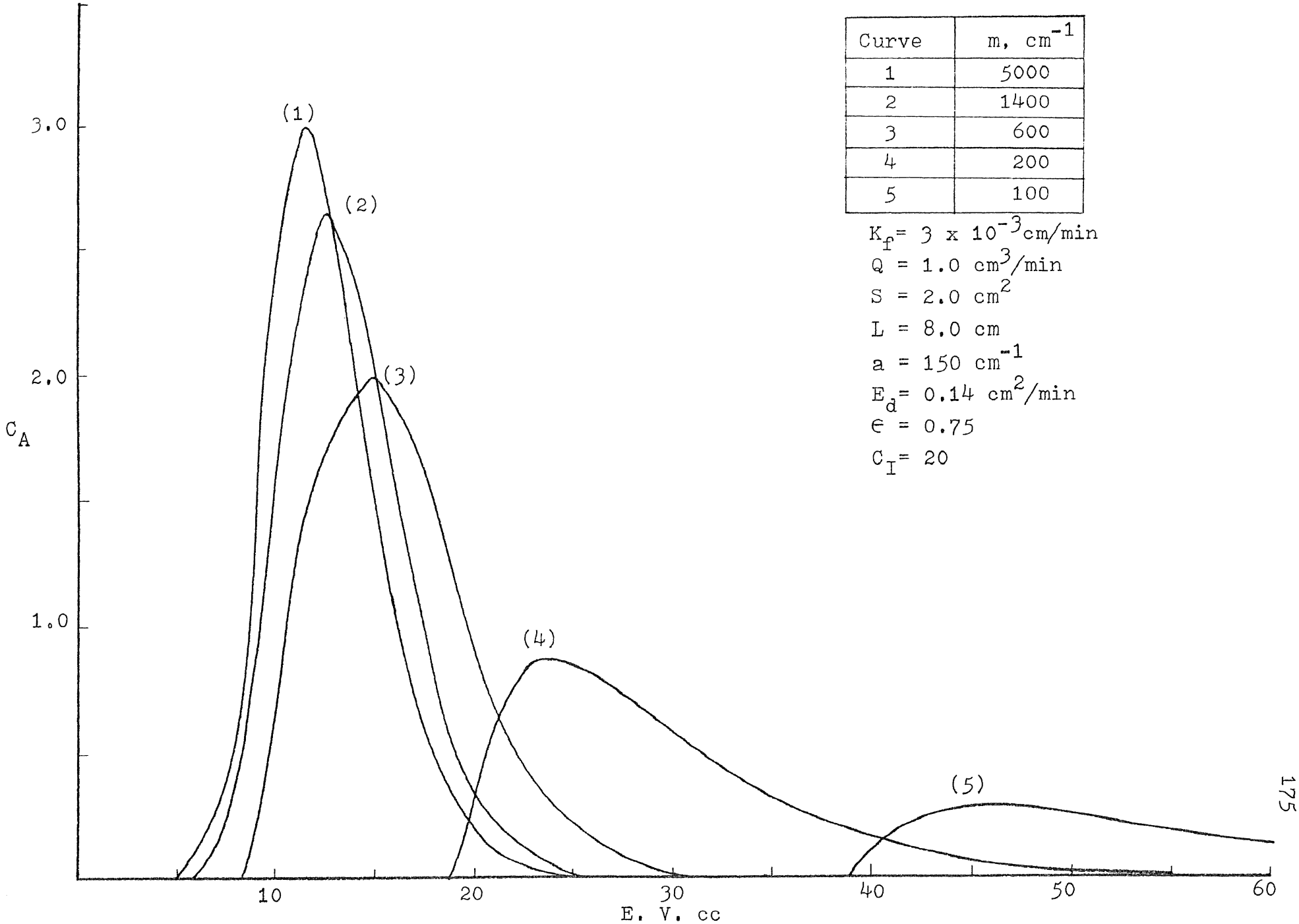

Curve	m, cm^{-1}
1	5000
2	1400
3	600
4	200
5	100

$K_f = 3 \times 10^{-3}$ cm/min
$Q = 1.0$ cm^3/min
$S = 2.0$ cm^2
$L = 8.0$ cm
$a = 150$ cm^{-1}
$E_d = 0.14$ cm^2/min
$\epsilon = 0.75$
$C_I = 20$

Fig. 65 Effect of m for $k_f = 3 \times 10^{-3}$

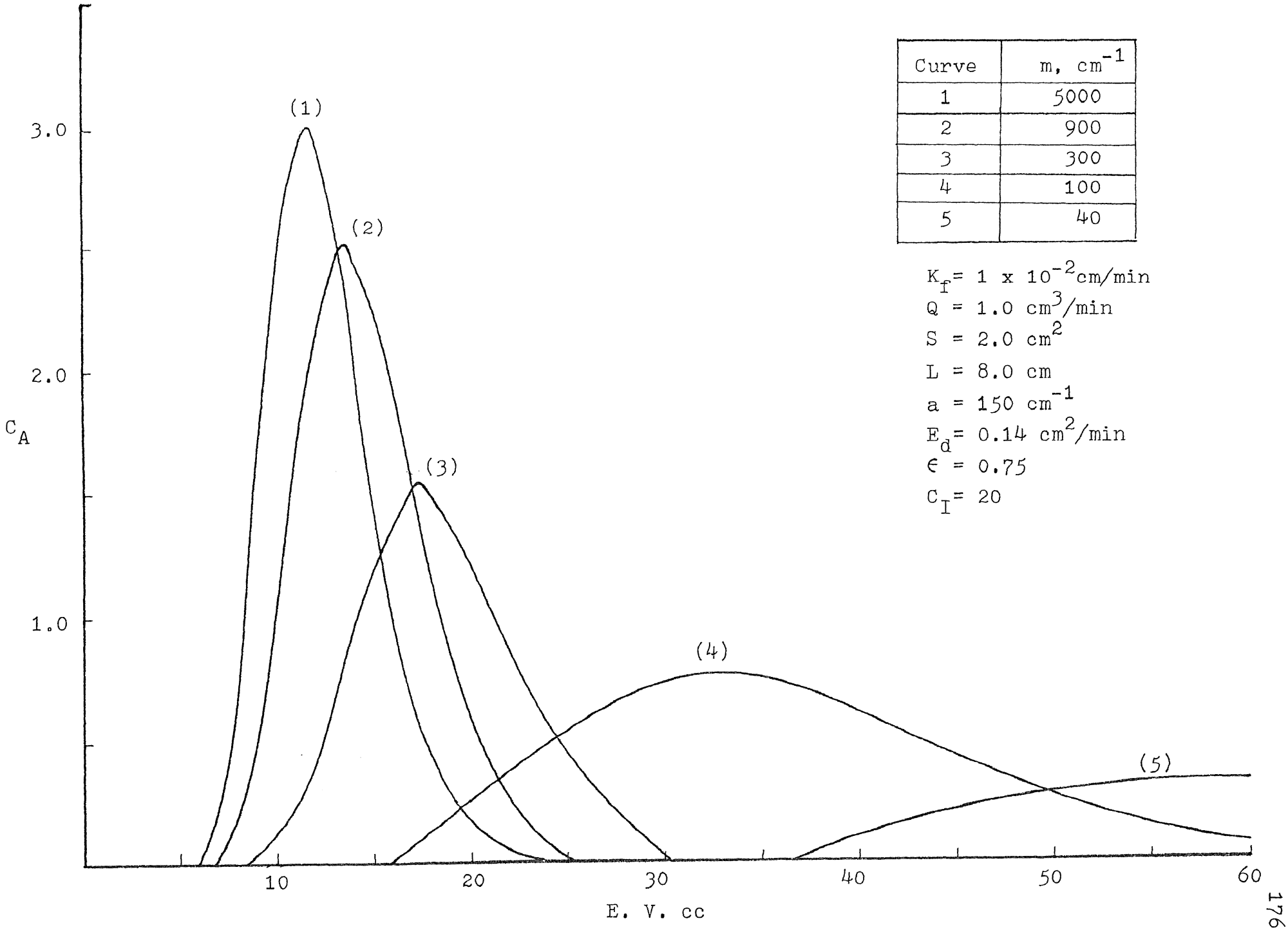

Curve	m, cm^{-1}
1	5000
2	900
3	300
4	100
5	40

K_f = 1 x 10^{-2} cm/min
Q = 1.0 cm^3/min
S = 2.0 cm^2
L = 8.0 cm
a = 150 cm^{-1}
E_d = 0.14 cm^2/min
ϵ = 0.75
C_I = 20

Fig. 66 Effect of m for $k_f = 1x10^{-2}$

affect the calculated elution profile, peak area, shape and retention time. We have also shown that the retention time for an ion exchange column results from the combined effects of column void volume and transient phase lag. Figure 67 shows the phase lag for the initial buffer concentration of 0.1M (pCl = 1.60) as a function of buffer ionic strength. The phase lag is defined as the difference in elution volume between the initial buffer condition 0.1M and the isoionic concentration of eluted protein. Figure 67 shows that a low ionic strength of incoming buffer will cause a large phase lag. A high buffer ionic strength will give a sharp transient step change resulting in a small phase lag. Table 4 list the phase lag for single step change with various buffer ionic strength. The phase lags are plotted against the buffer concentration and corresponding $|\Delta p_{Cl}|$ as shown in Figure 68. The phase lag is related to only the buffer ionic strength. Thus, the phase lag for intermediate buffer concentration can be extrapolated directly from figure 68. After having discussed the surface adsorption model for calculated elution profiles and the corresponding phase lag, we are now ready to predict the elution peaks for alkaline phosphatase (r_{405}). The calculated elution profiles (solid lines) are plotted in the previously discussed figures. The results are shown in Figures 46 to 54. Here the experimental r_{405} elution profiles (dotted lines) are plotted against the calculated ones (solid lines). The difference in elution volume between the dotted lines and the solid lines is the predicted

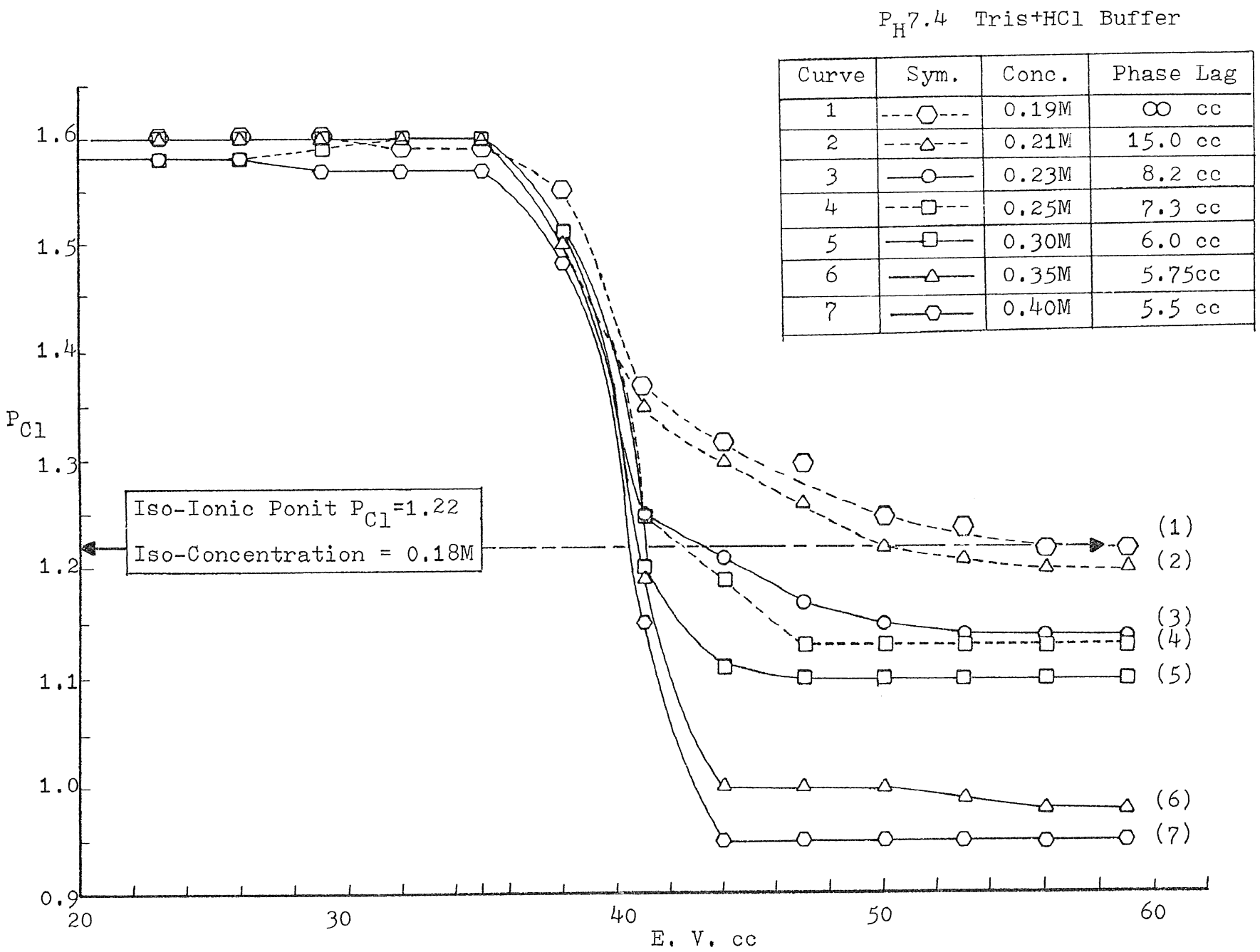

Fig. 67 Effect of Buffer Concentration on Phase Lag

Table 4 Phase Lag of Enzyme 1st. Peak

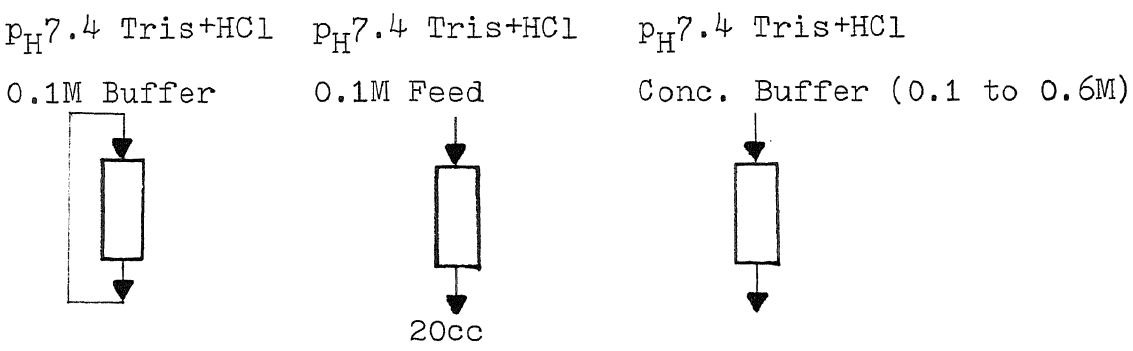

Run	Conc. Buffer, M	$\lvert\Delta$Conc.$\rvert$, M	$\lvert\Delta P_{Cl}\rvert$	Phase Lag, c.c.
D-143	0.19	0.01	0.37	∞
D-140	0.20	0.02	0.395	17.5
D-135	0.21	0.03	0.41	15
D-134	0.23	0.05	0.44	8.2
D-133	0.25	0.07	0.47	7.3
D-132	0.30	0.12	0.55	6.0
D-139	0.35	0.17	0.60	5.75
D-138	0.40	0.22	0.65	5.5
D-145	0.60	0.42	0.85	4.7

* Iso-Concentration= 0.18M

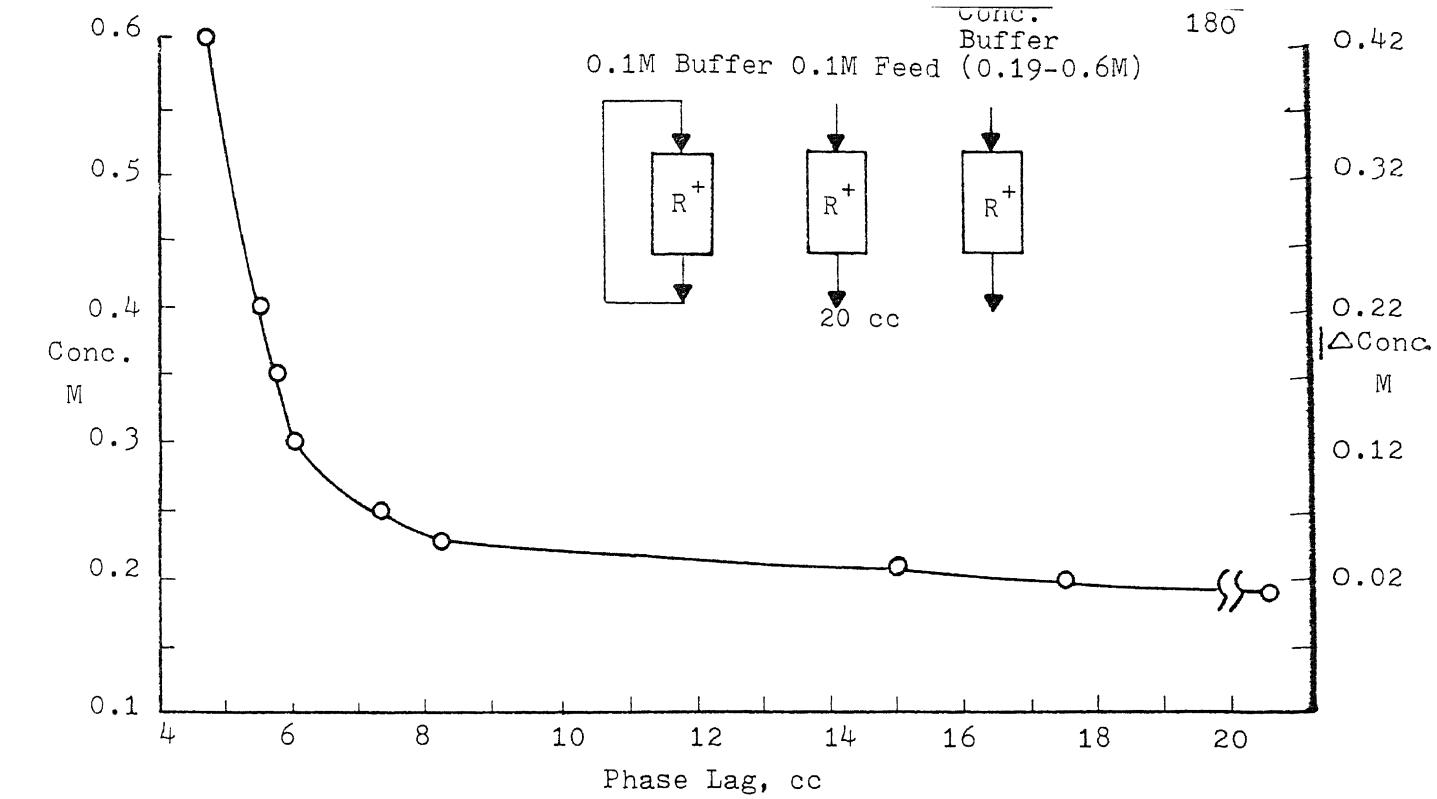

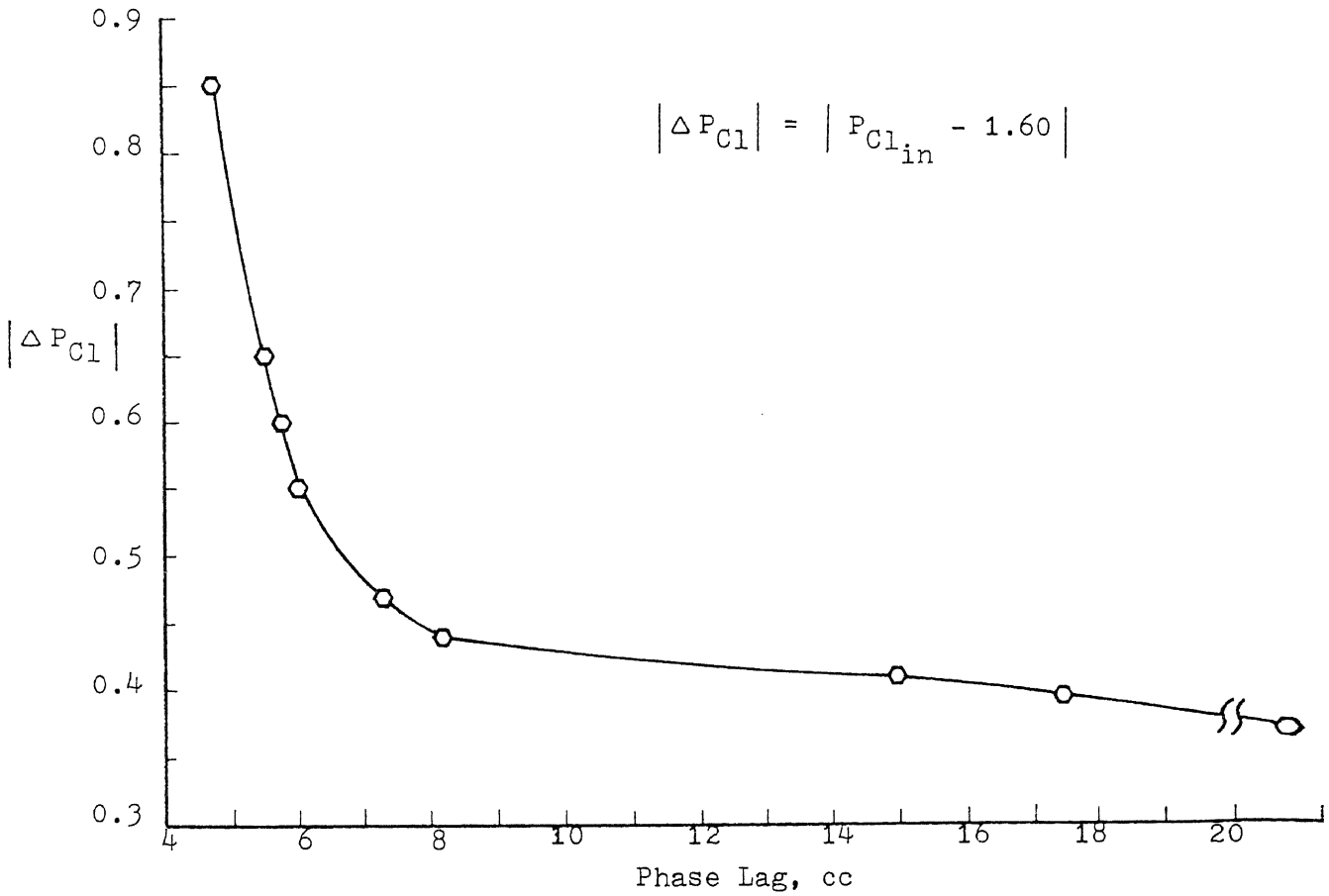

Fig. 68 r_{405} 1st. Peak Phase Lag v.s. Buffer Concentration in term of |△Conc.| and |△pCl|

phase lag for each case. Note that the phase lag is defined experimentally from the pCl curve. The first peaks of r_{405} enzyme are calculated based on the appropriate value of model parameters. Thus, those model parameters can be directly related to the experimental operating conditions (buffer ionic strength).

The second peaks of enzyme (r_{405}) are calculated based on the information of model parameters for first peaks. The $|\Delta \text{conc.}|$ or $|\Delta \text{pCl}|$ are obtained as the difference between initial and final buffer ionic strength. The corresponding model parameters are extroplolated from the figures. Those figures will be discussed later.

The bottom of Figure 46 (p.145) compares calculated r_{405} (solid line) and experimental r_{405} (dotted line) elution profiles for a buffer concentration of 0.3M. The difference in elution volume between the solid and the dotted lines is 6cc which agrees with the experimental measurement based on the pCl curve shown at the top of Figure 46. Figures 47 to 54, the first peaks of enzyme r_{405} with calculated results are compared for several buffer concentrations (0.25M, 0.23M, 0.21M, 0.4M, 0.35M, 0.2M, 0.19M, 0.6M). The experimental and calculated r_{405} (solid lines) are agree in shapes, peak height, elution area, and retention time. The experimental data and the calculated curves are in good agreement.

The model parameters used in the prediction of the first peaks of enzyme are listed in Table 5 for easy comparison. Figure 69 shows the relationship between the axial dispersion E_d and the buffer concentration, while Figure 70 shows the relationship between the equilibrium constant m and the buffer concentration. For both figures, the $|\Delta \text{conc.}|$ axis are also shown on the right hand side of the figure. The $|\Delta \text{conc.}|$ is defined as the difference between the incoming buffer concentration and iso-ionic strength of the enzyme (0.18M).

The prediction of the second peak enzyme r_{405} is facilitated by finding $|\Delta \text{conc.}|$ and extraploating the model parameters directly from Figures 69 and 70. The phase lag for each case will be 4.5cc because the buffer concentration was higher than the iso-concentration of the enzyme. Again, the calculated and experimental r_{405} (solid line) curves are compared in Figures 46 to 54. Table 6 compares the predicted and experimental results for the second peak of r_{405}. The $|\Delta \text{conc.}|$ is taken as the difference between the initial concentration within the column and that of the new buffer which is introduced. The material balance on the enzyme was performed by substracting the enzyme eluted in the first peak from the total feed into the column. The elution profile is then calculated based on the value of E_d and m which were extrapolated from Figures 69 and 70. These

Table 5 Relations of Model Parameters and Experimental Run for Enzyme 1st. Peak

Run	Initial Buffer	Conc. Buffer	$\sum r_{405}$% Exp.	$\sum r_{405}$% Mod.	Retention Vol. Exp.	Retention Vol. Mod.	Peak Height Exp.	Peak Height Mod.	m, cm^{-1}	E_d, cm^2/min	k_f, cm/min
D-145	0.1M	0.6M	98.5	97.2	41.0	41.2	4.41	3.56	3200	0.082	1×10^{-3}
D-138	"	0.4M	93.6	90.6	41.0	41.5	2.63	2.67	1600	0.120	1×10^{-3}
D-139	"	0.35M	84.6	85.0	41.0	41.75	2.39	2.42	1300	0.129	1×10^{-3}
D-132	"	0.3M	80.0	80.0	42.5	43.0	2.17	2.16	1050	0.140	1×10^{-3}
D-133	"	0.25M	67.6	67.2	47.0	46.8	1.35	1.44	630	0.161	1×10^{-3}
D-134	"	0.23M	60.8	60.7	50.0	50.2	0.846	0.848	340	0.189	1×10^{-3}
D-135	"	0.21M	43.4	43.2	59.0	62.0	0.386	0.392	160	0.210	1×10^{-3}
D-140	"	0.20M	12.0	14.2	65.0	66.0	0.207	0.248	90	0.230	1×10^{-3}

1. Model Parameters: C_I= 20, Q= 1.0cm^3/min, S= 2.0cm^2, L= 8.0cm, a= 150 cm^{-1}, ϵ = 0.75
2. Phase Lag is shown on Table 4, Tube Volume= 4.0cc

Table 6 Prediction with Model Parameters and Experimental Run for Enzyme 2nd. Peak

Run	Initial Buffer	Conc. Buffer	ΔM, M	C_I	$\sum r_{405}$% Exp.	$\sum r_{405}$% Mod.	Peak Height Exp.	Peak Height Mod.	Rentention Vol. Exp.	Rentention Vol. Mod.	m, cm^{-1}	E_d, cm^2/min	k_f, cm/min
D-132	0.30	1.0	0.70	3.97	20.0	19.6	0.67	0.72	71.0	70.5	3700	0.08	1×10^{-3}
D-133	0.25	0.6	0.35	6.56	32.4	31.6	1.18	1.06	71.0	70.5	2600	0.094	"
D-134	0.23	0.38	0.15	7.57	27.5	31.3	0.69	0.88	80.0	80.5	1200	0.133	"
D-135	0.21	0.35	0.14	11.37	40.4	46.7	1.02	1.29	80.0	80.5	1150	0.1355	"
D-138	0.40	0.60	0.20	1.99	6.4	8.7	0.121	0.254	71.0	71.5	1470	0.123	"
D-139	0.35	0.60	0.25	3.01	15.45	13.68	0.45	0.425	71.0	71.0	1800	0.1133	"
D-140	0.20	0.60	0.40	17.15	88.0	83.4	2.75	2.96	71.0	70.5	3000	0.0855	"
D-143	0.19	0.30	0.11	19.40	68.3	77.3	2.06	2.00	68.0	68.5	980	0.144	"

* Model Parameters: Q=1.0 cm^3/min, S= 2 cm^2, L= 8 cm, a= 150 cm^{-1}, ϵ= 0.75

Phase Lag is 4.5cc for all Conc. Buffer; Tube Volume is 4cc.

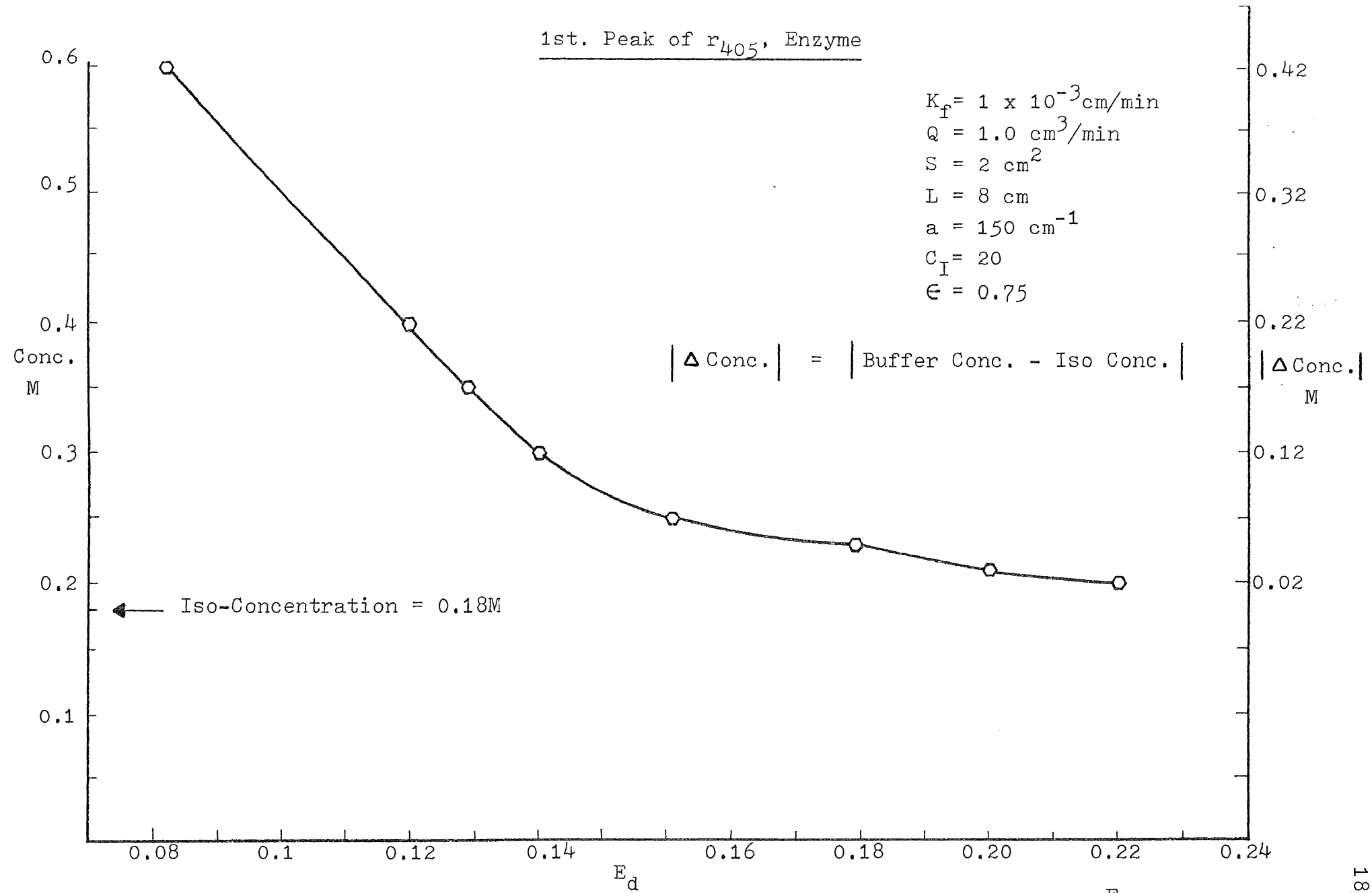

Fig. 69 r_{405} 1st. Peak, Correlation of Axial Dispersion E_d on Buffer Concentration and |Δ Conc.|

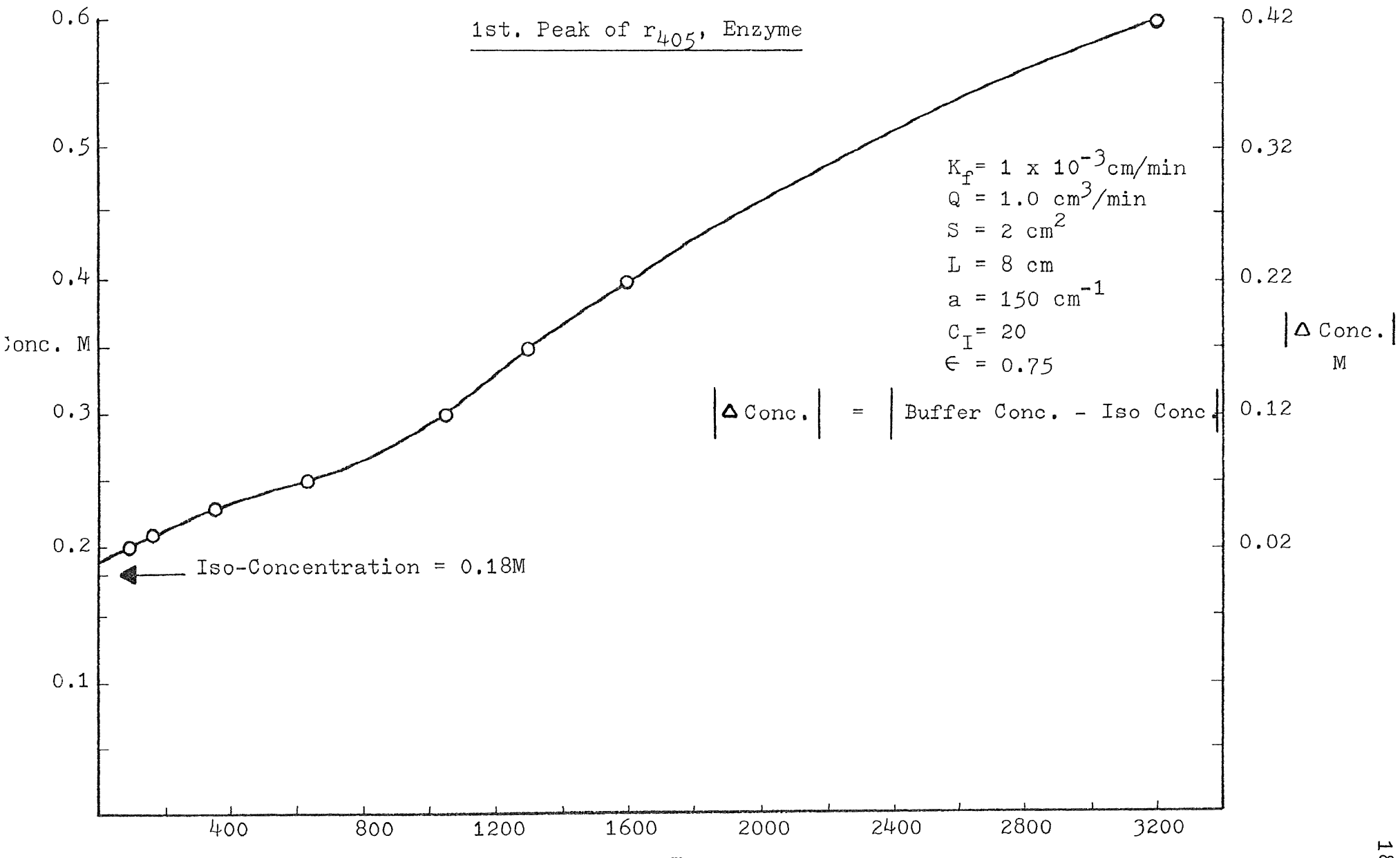

Fig. 70 r_{405} 1st. Peak, Correlated of Equilibrium Constant m on Buffer Concentration and |Δ Conc.|

parameters are tabulated on the right side of Table 6. The predicted and experimental enzyme recovery, peak height, and retension volume are compared and found to be in good agreement.

5-3 Model prediction of total protein

The predicted elution profile for the total protein applies similar procedures as that for the enzyme. We need to obtain a set of optimal model parameters which are directly related to the buffer concentration. With the aid of phase lag, we are able to predict the retention time, peak area, and peak shapes. The only difference between the enzyme and total protein is that the total protein has two peaks - first and second peak of r_{595}. Despite the difference, the procedure is almost the same as we have discussed in Section 5-2 .

Figure 71 shows the experimental elution profile for the first peak of r_{595} by 0.19M buffer. The phase lag indicated by the difference between 0.10M and 0.19M is 16cc. The calculated curve is plotted as solid line and the phase lag is taken as the difference in elution volume between the experimental and calculated curves.

RUN D-144

r_{595} 1st. peak

Iso-Ionic Point, P_{Cl} = 1.28

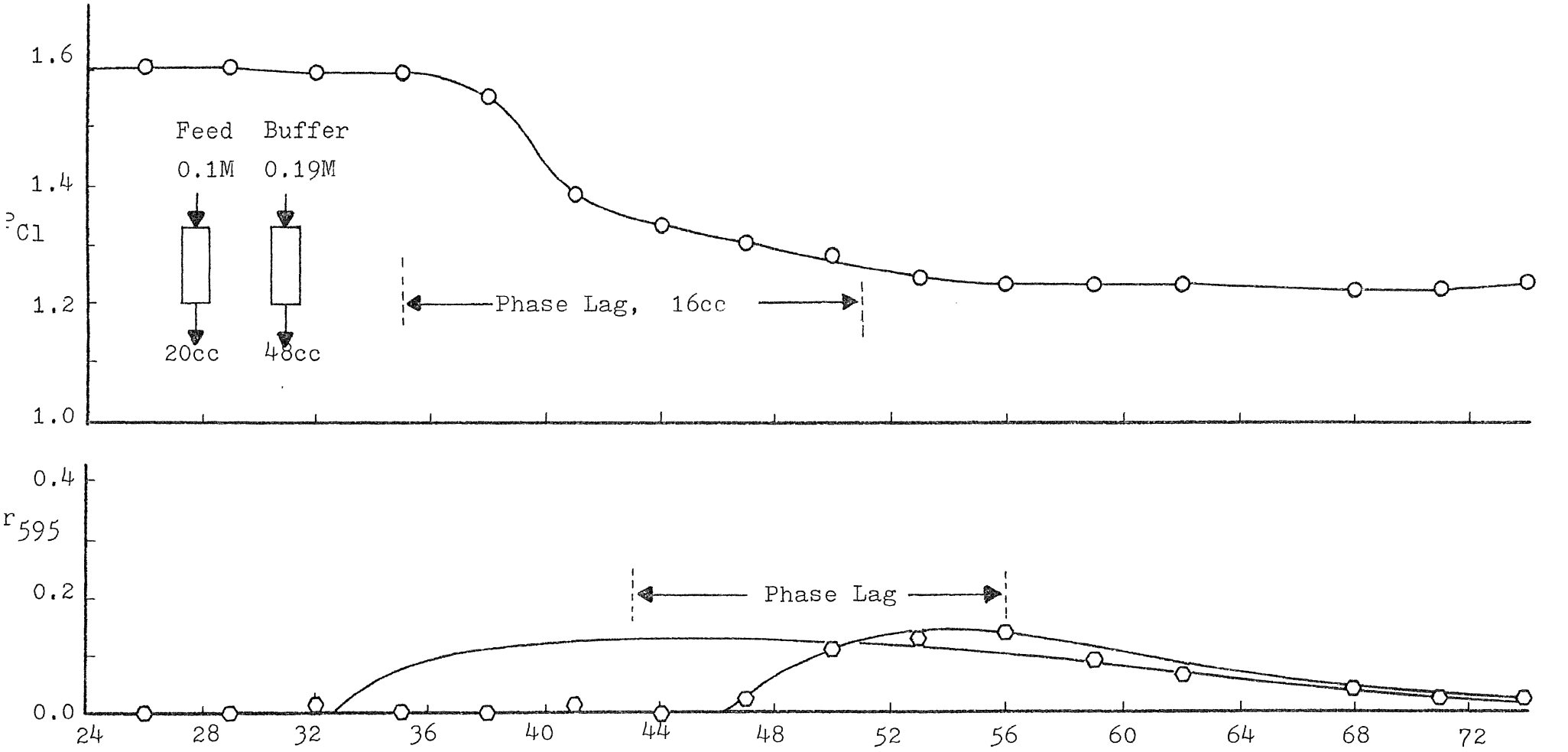

Fig. 71 r_{595} 1st. Peak and Elution Prediction for 0.19 M

Figure 72 shows the calculated and experimental elution profile for a 0.20M buffer. When the ionic strength of the incoming buffer is increased, the eluted area of the first peak of r_{595} will be increased. The phase lag indicated by the pCl curve is 11cc. Figures 73 to 76 show the first peak of r_{595} eluted by the buffer concentrations of 0.21M, 0.23M, 0.25M, and 0.3M. Again, an increase in buffer concentration will result in an increase in the first peak of r_{595}. The peak maximum occurs at a buffer concentration of 0.3M. If the buffer ionic strength is higher than 0.3M, the second peak of r_{595} will start to elute, This will be discussed in more detail later.

The phase lag will decrease as the incoming buffer ionic strength is increased. Table 7 list the phase lag for buffer concentration ranging from 0.19M to 0.30M. The experimental measurement of phase lag is also plotted with the buffer concentration, and $|\Delta M|$, and $|\Delta pCl|$. The definition of $|\Delta M|$ and $|\Delta pCl|$ are shown in Figure 77. Note that the iso-concentration of first peak of r_{595} is 0.17M.

The experimental results shown in Figures 71 to 76 and the corresponding model parameters applied to the calculation of elution profiles are listed in Table 8. The experimental results are compared with the model prediction for percent recovery, peak

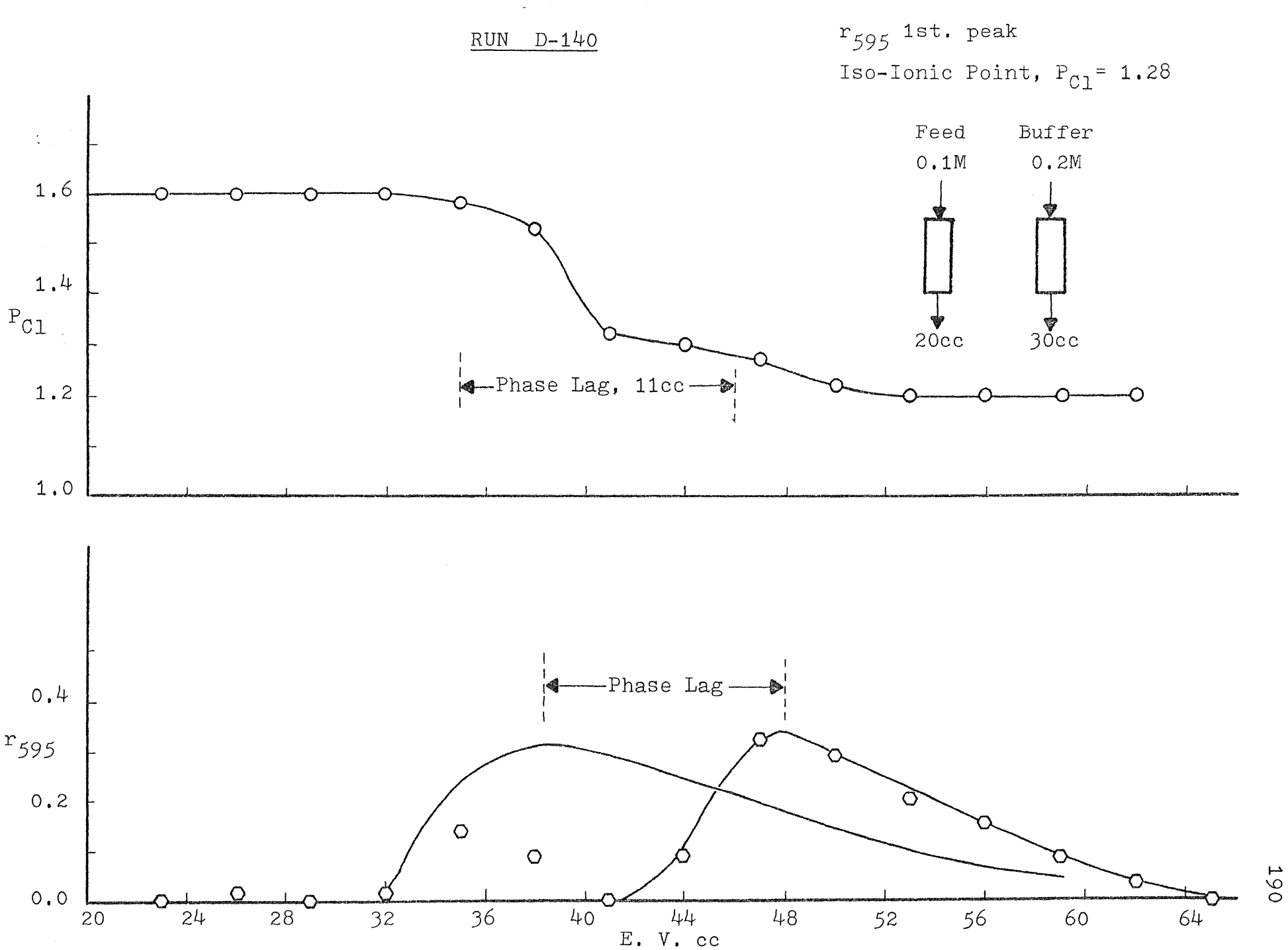

Fig. 72 r_{595} 1st. Peak and Elution Prediction for 0.20 M

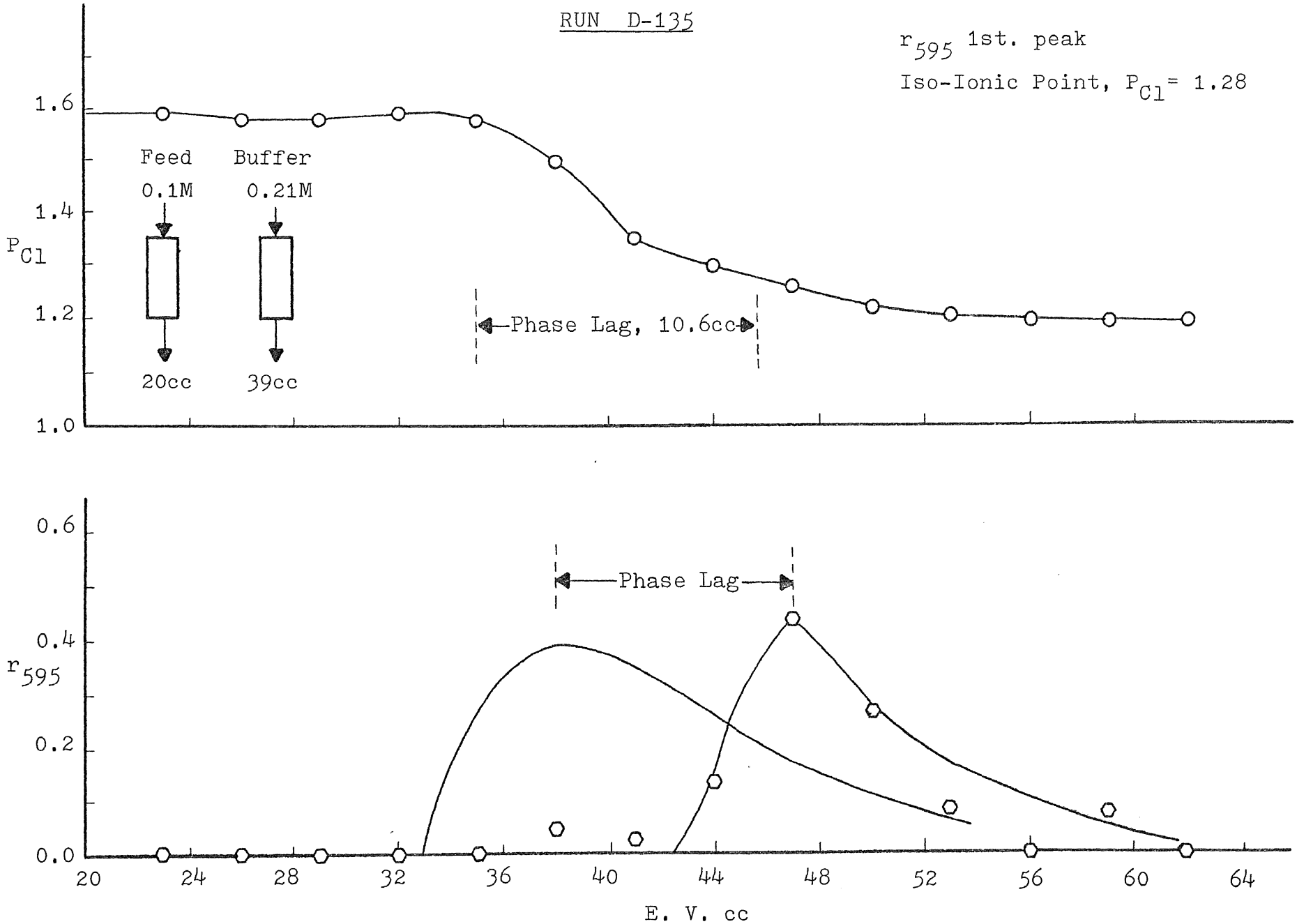

Fig. 73 r_{595} 1st. Peak and Elution Prediction for 0.21 M

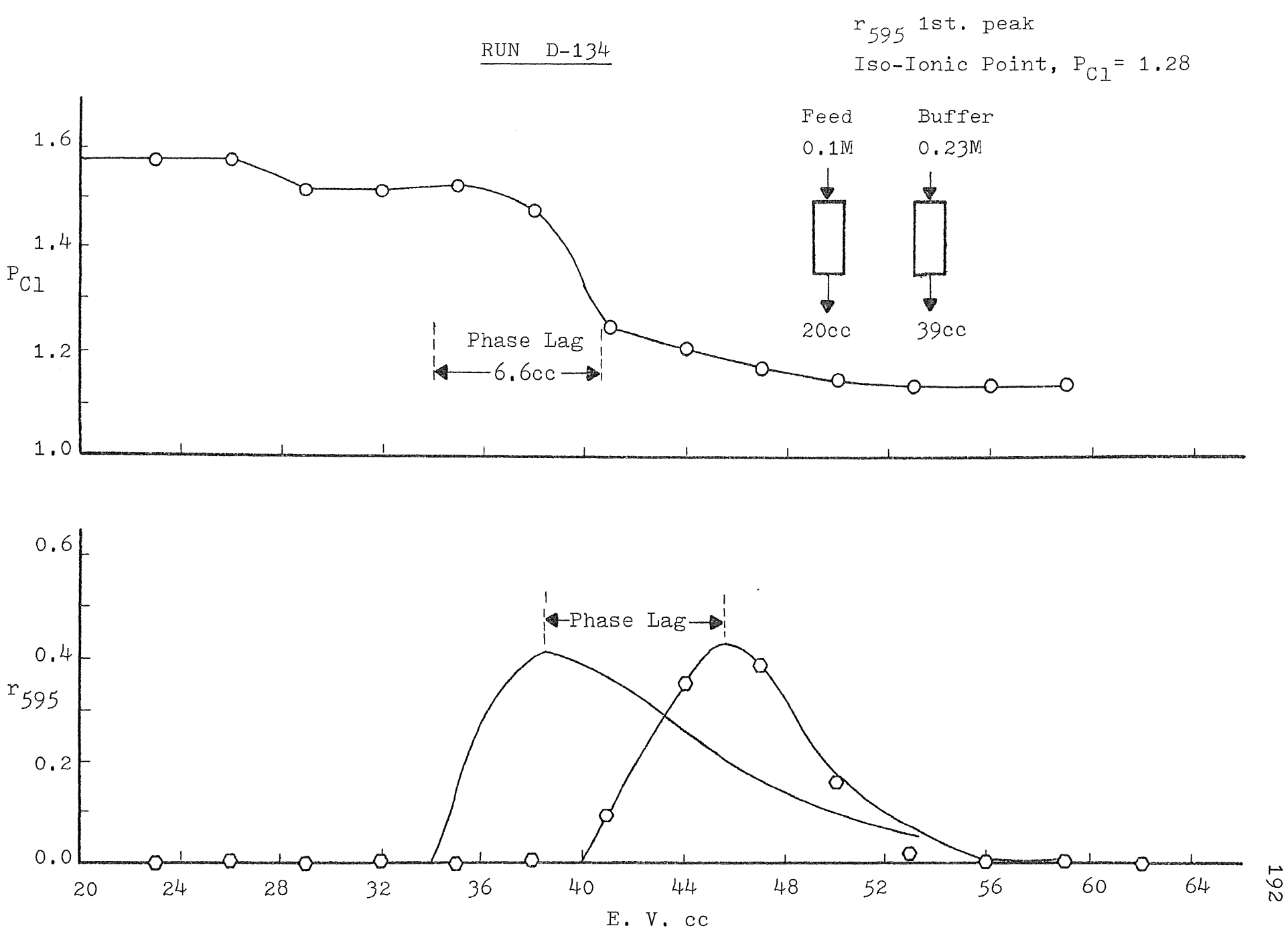

Fig. 74 r_{595} 1st. Peak and Elution Prediction for 0.23 M

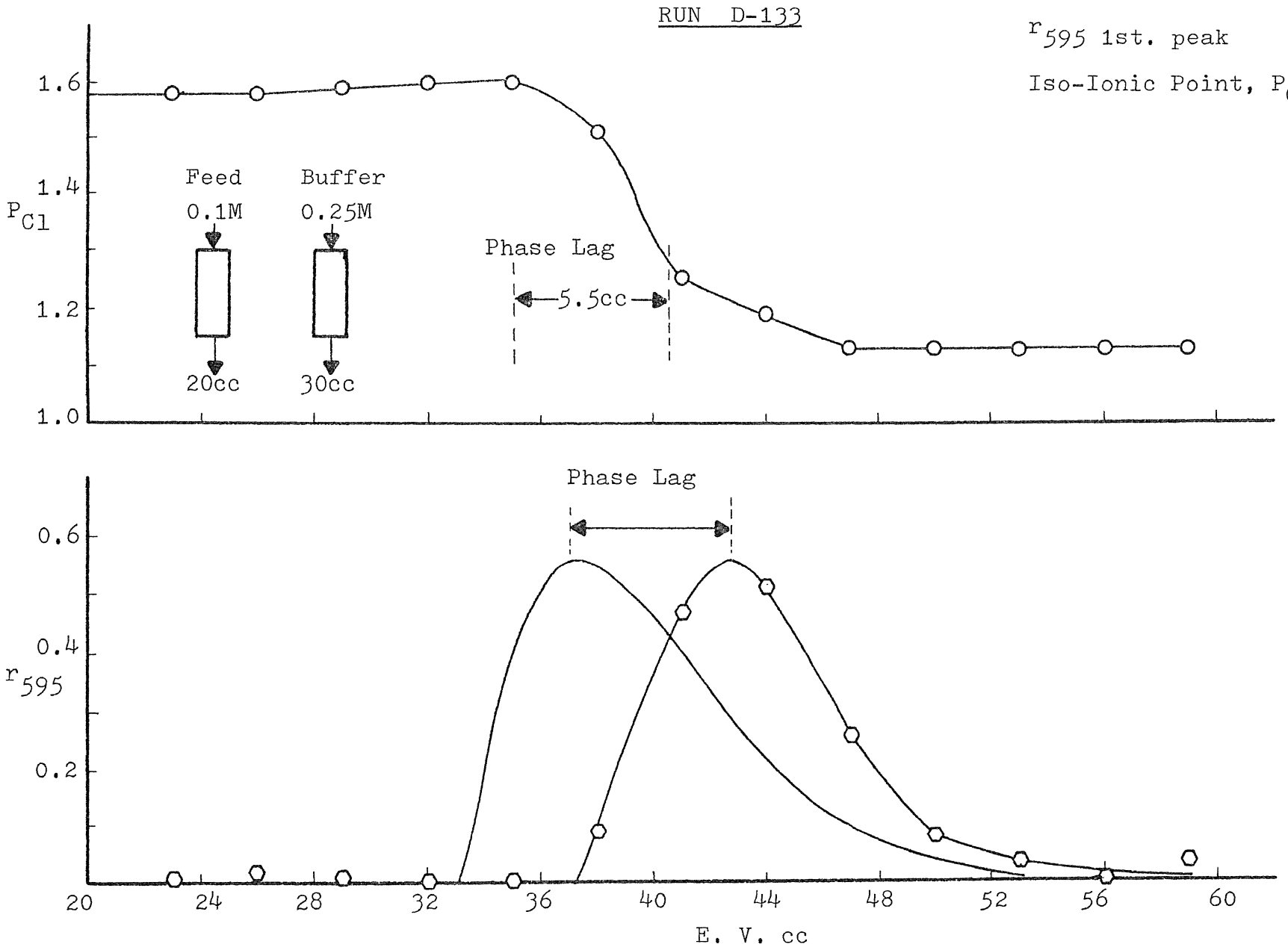

Fig. 75 r_{595} 1st. Peak and Elution Prediction for 0.25 M

RUN D-132

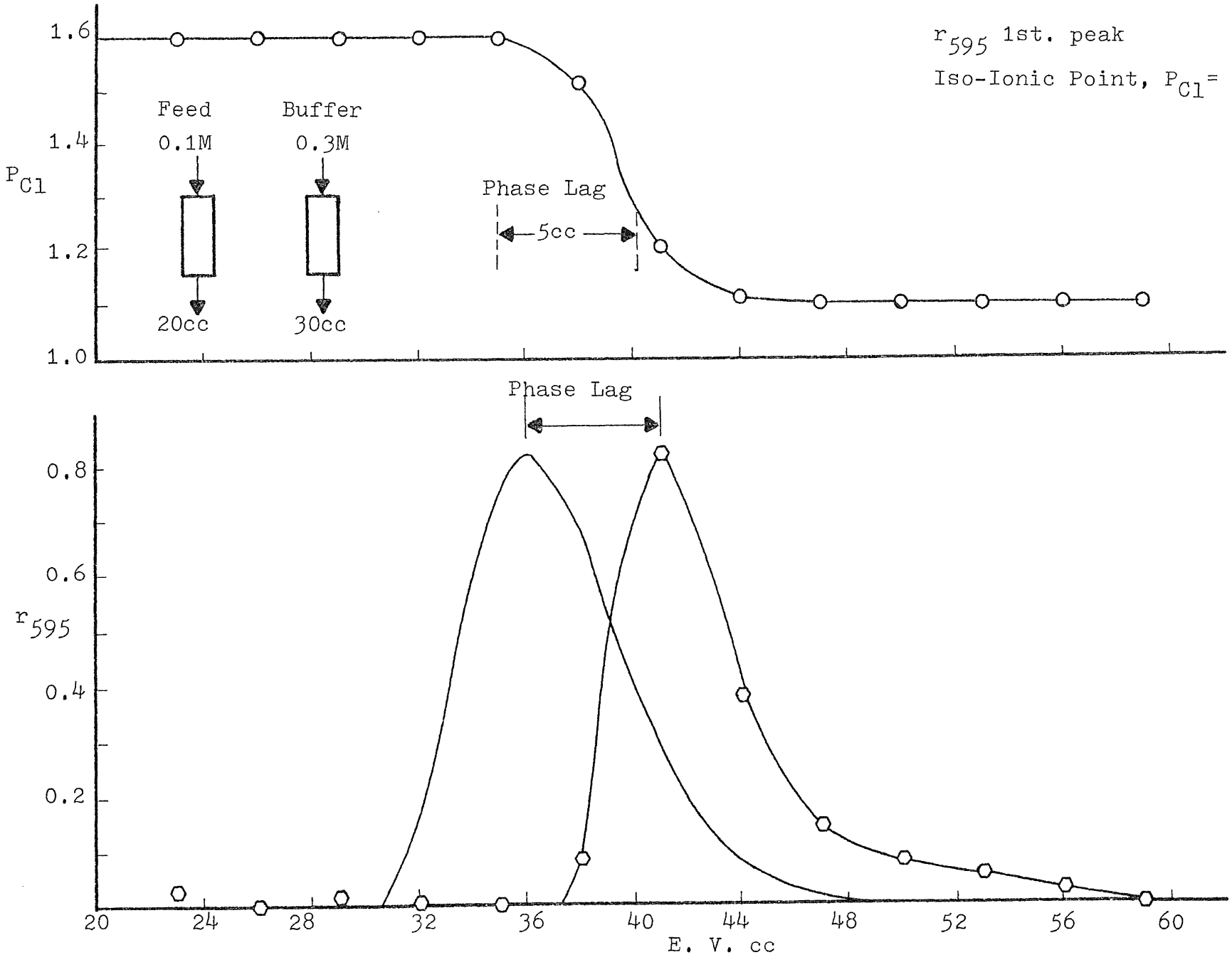

Fig. 76 r_{595} 1st. Peak and Elution Prediction for 0.30 M

Table 7 Phase Lag of Total Protein 1st. Peak

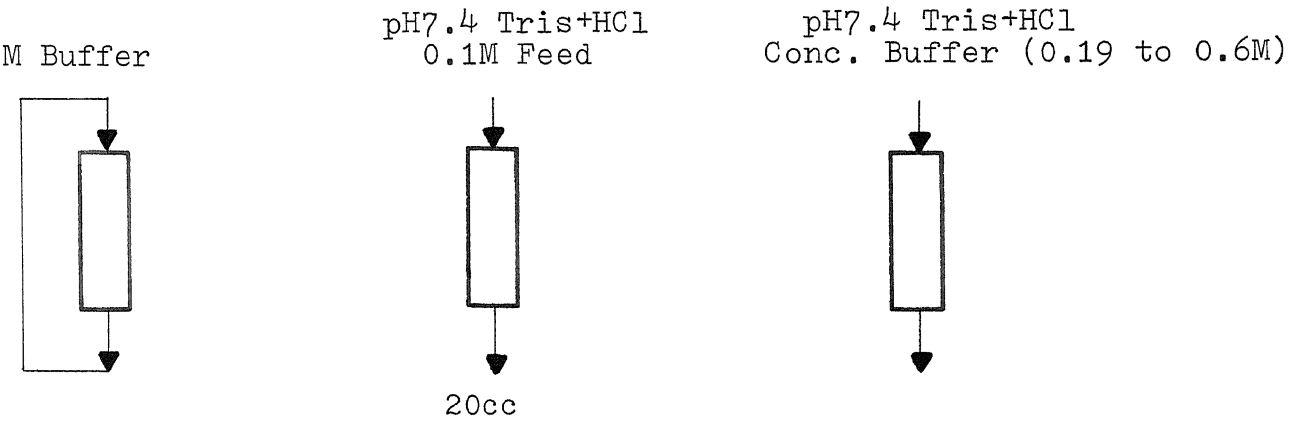

Run	Conc. Buffer, M	$\lvert\Delta$Conc.$\rvert$, M	$\lvert\Delta P_{Cl}\rvert$	Phase Lag, c.c.
D-144	0.19	0.02	0.37	16.0
D-140	0.20	0.03	0.395	11.0
D-135	0.21	0.04	0.41	10.6
D-134	0.23	0.06	0.44	6.6
D-133	0.25	0.08	0.47	5.5
D-132	0.30	0.13	0.55	5.0
D-139	0.35	0.18	0.60	5.0
D-138	0.40	0.23	0.65	4.3
D-145	0.60	0.43	0.85	3.7

* Iso-Concentration Of r_{595} 1st. peak is 0.17M

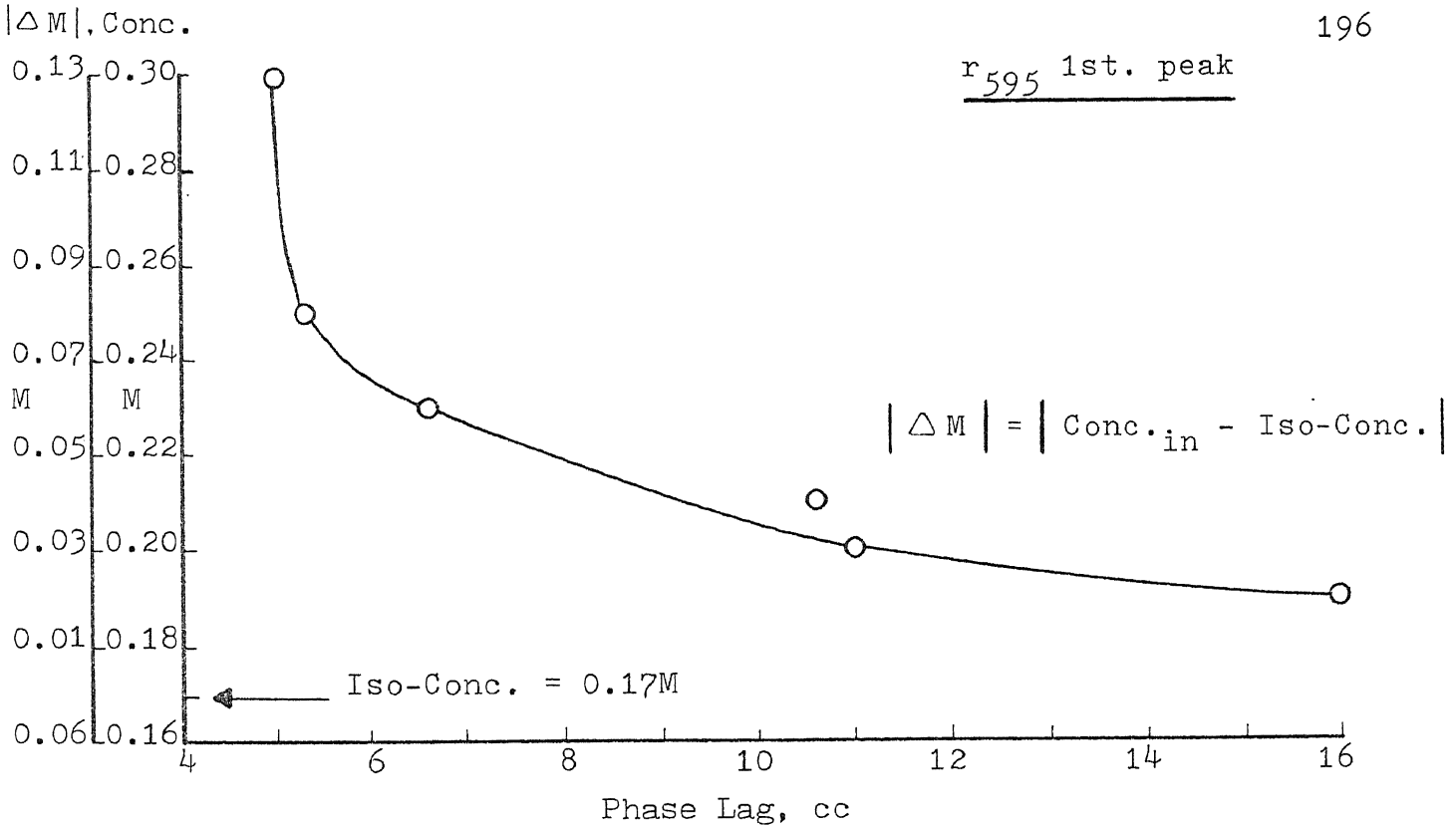

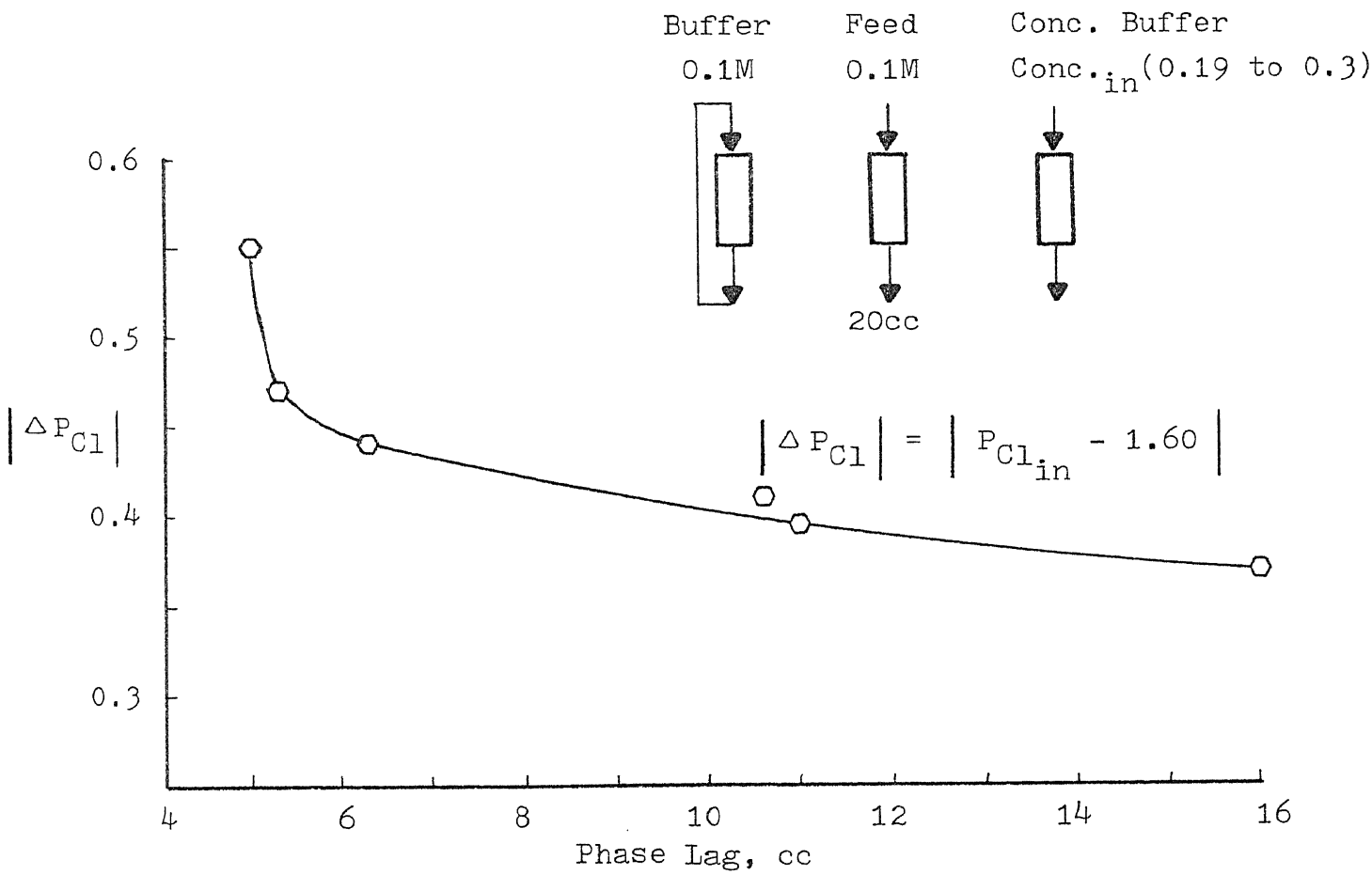

Fig. 77 Phase Lag v.s. Buffer Concentration in term of $|\Delta M|$ and $|\Delta pCl|$

Table 8 Relations of Model Parameters and Experimental Run for Total Protein 1st. Peak

Run	Initial Buffer, M	Conc. Buffer, M	C_I	$\Sigma r_{405}\%$ Exp.	$\Sigma r_{405}\%$ Mod.	Peak Height Exp.	Peak Height Mod.	Rention Vol. Exp.	Rention Vol. Mod.	Model Parameters m, cm^{-1}	Model Parameters E_d, cm^2/min	Model Parameters k_f, cm/min^2
D-132	0.10	0.30	6	30.5	29.8	0.825	0.823	41.0	41.0	2200	0.135	1×10^{-3}
D-133	"	0.25	6	27.7	24.7	0.560	0.557	42.0	42.5	800	0.165	1×10^{-3}
D-134	"	0.23	6	23.6	22.8	0.430	0.410	46.0	45.1	520	0.180	1×10^{-3}
D-135	"	0.21	6	21.97	22.35	0.438	0.390	47.0	49.1	450	0.200	1×10^{-3}
D-140	"	0.20	6	20.17	23.58	0.340	0.313	48.0	49.5	330	0.220	1×10^{-3}
D-144	"	0.19	6	13.80	16.70	0.139	0.139	56.0	59.0	135	0.240	1×10^{-3}

* Model Parameters: Q= 1.0cm^3/min, S= 2.0cm^2, L= 8.0cm, a= 150cm^{-1}, $\in$ = 0.75

Phase Lag is shown on Table 7; Tube volume is 4cc.

area, peak height, and retention volume. The model parameters are tabulated on the right side of Table 8. The model parameters are also plotted in Figure 78 to demonstrate the relationship between the axial dispersion E_d and equilibrium constant m for different ionic strength and $|\Delta M|$.

We have now completed the discussion of the relationship between the buffer ionic strength, phase lag, and model parameters for the first peak of r_{595}. We will now discuss the prediction of the second peaks of r_{595} which are eluted under the same experimental conditions as the first peak of r_{595}. The second peak of r_{595} was eluted after increasing the buffer concentration from 0.35M to 1.0M as shown in Figures 79 to 82. High buffer concentration will elute a sharp peak with no tailing. The phase lags for each buffer concentration are listed in Table 9. Again, the phase lag for a 1.0M buffer ionic strength has the smallest value (3.7cc). The comparison between model parameters and experimental results is given in Table 10. This table shows the peak area, peak height, retention time, material balance, and the corresponding model parameters applied to the elution prediction. Using the information from Table 10, we generate Figure 83. This shows the model parameters E_d and m plotted as a function of buffer concentration and $|\Delta M|$. Note that the iso-concentration of second peak of r_{595} is 0.325M.

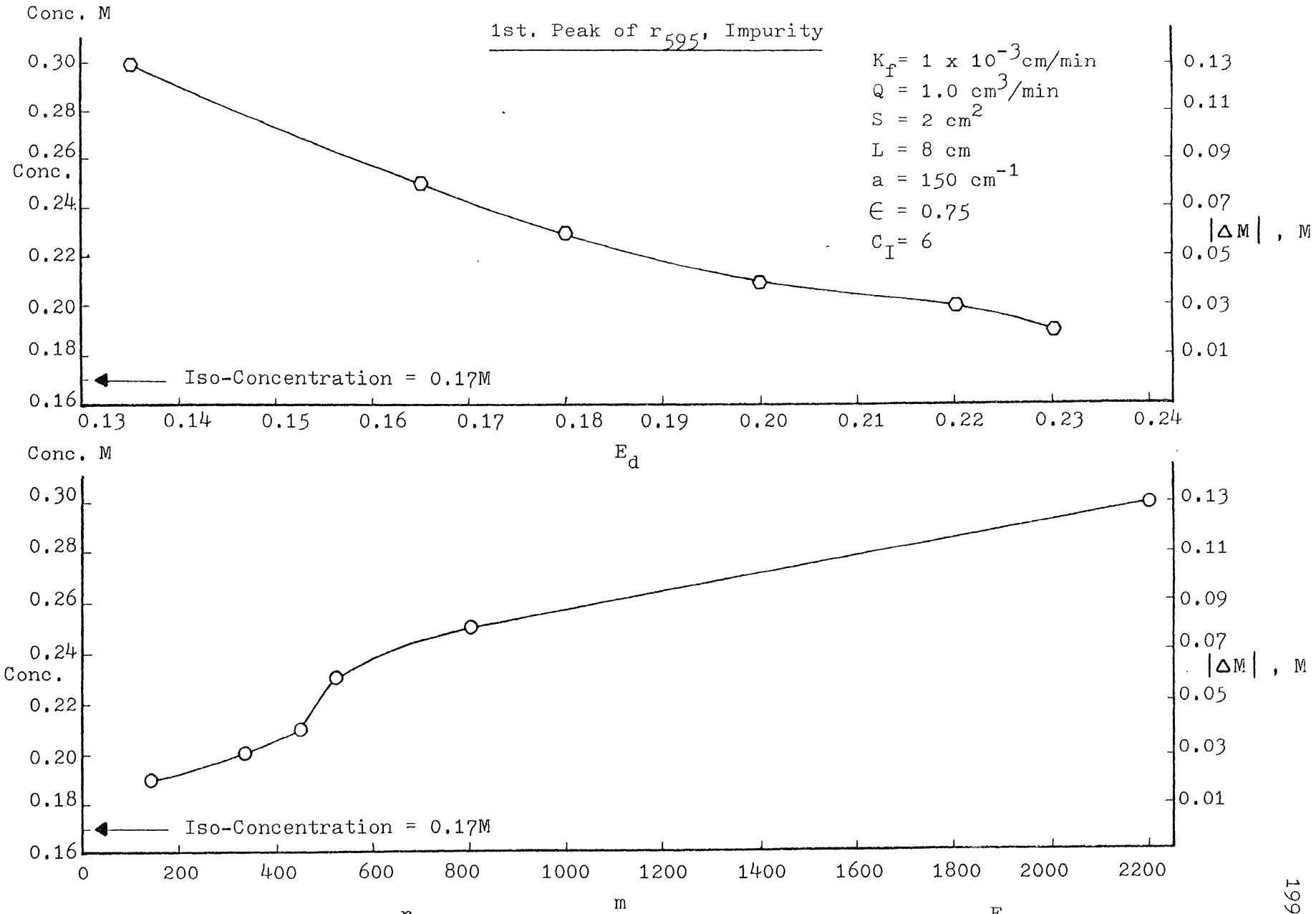

Fig. 78 r_{595} 1st. Peak, Correlation of Axial Dispersion E_d and Equilibrium Constant m on Buffer Concentration and $|\Delta M|$

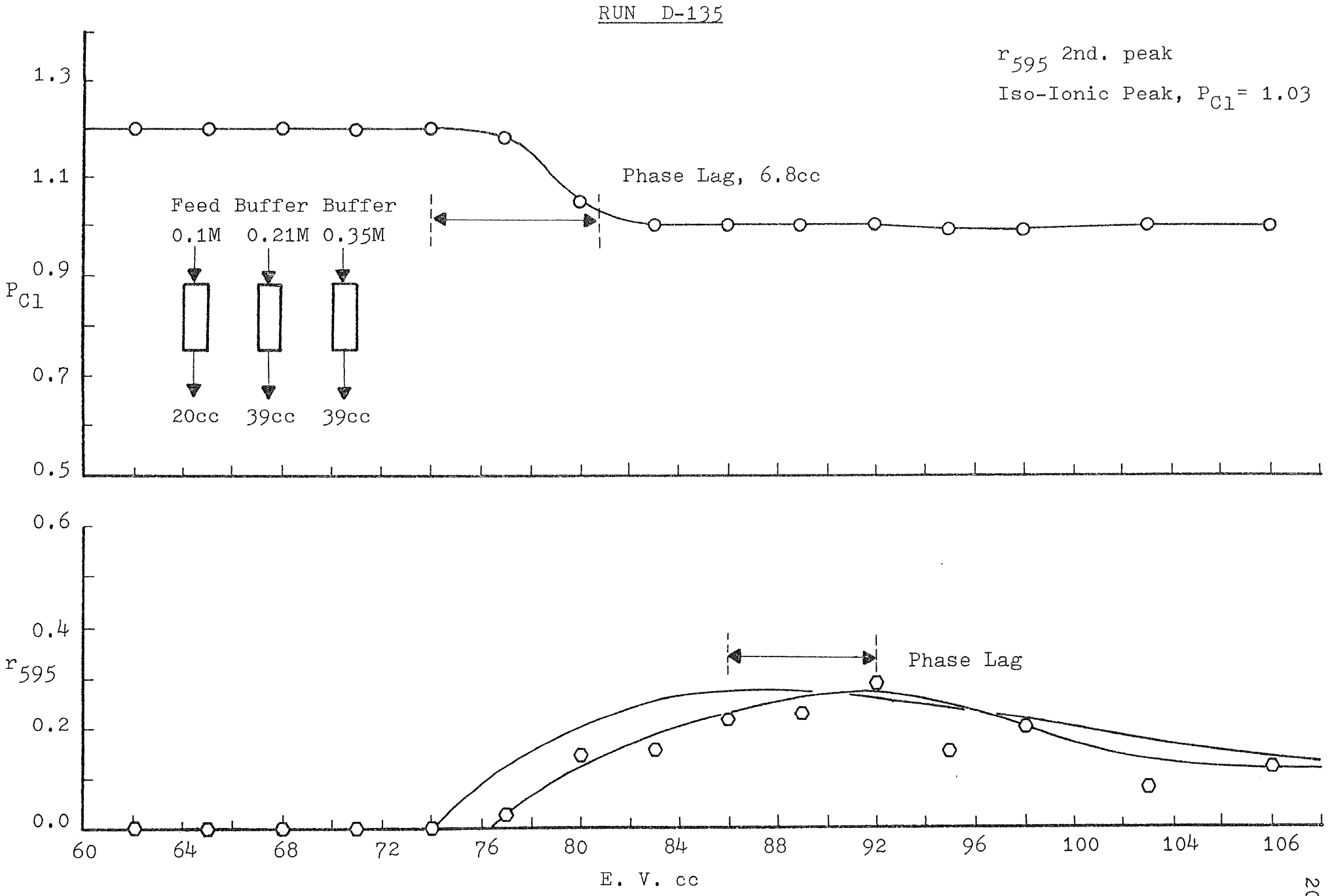

Fig. 79 r_{595} 2nd. Peak and Elution Prediction for 0.35 M

RUN D-134

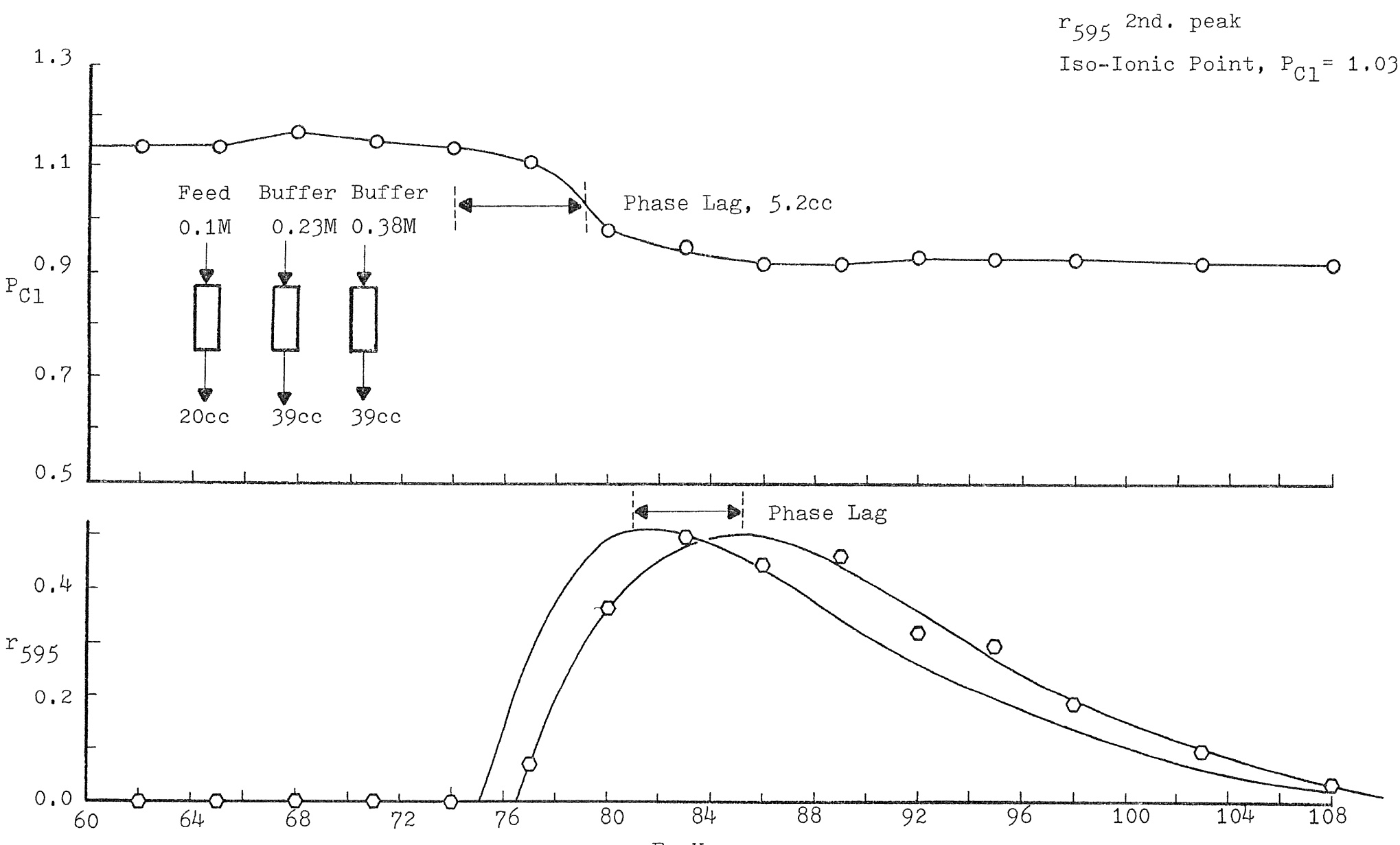

Fig. 80 r_{595} 2nd. Peak and Elution Prediction for 0.38 M

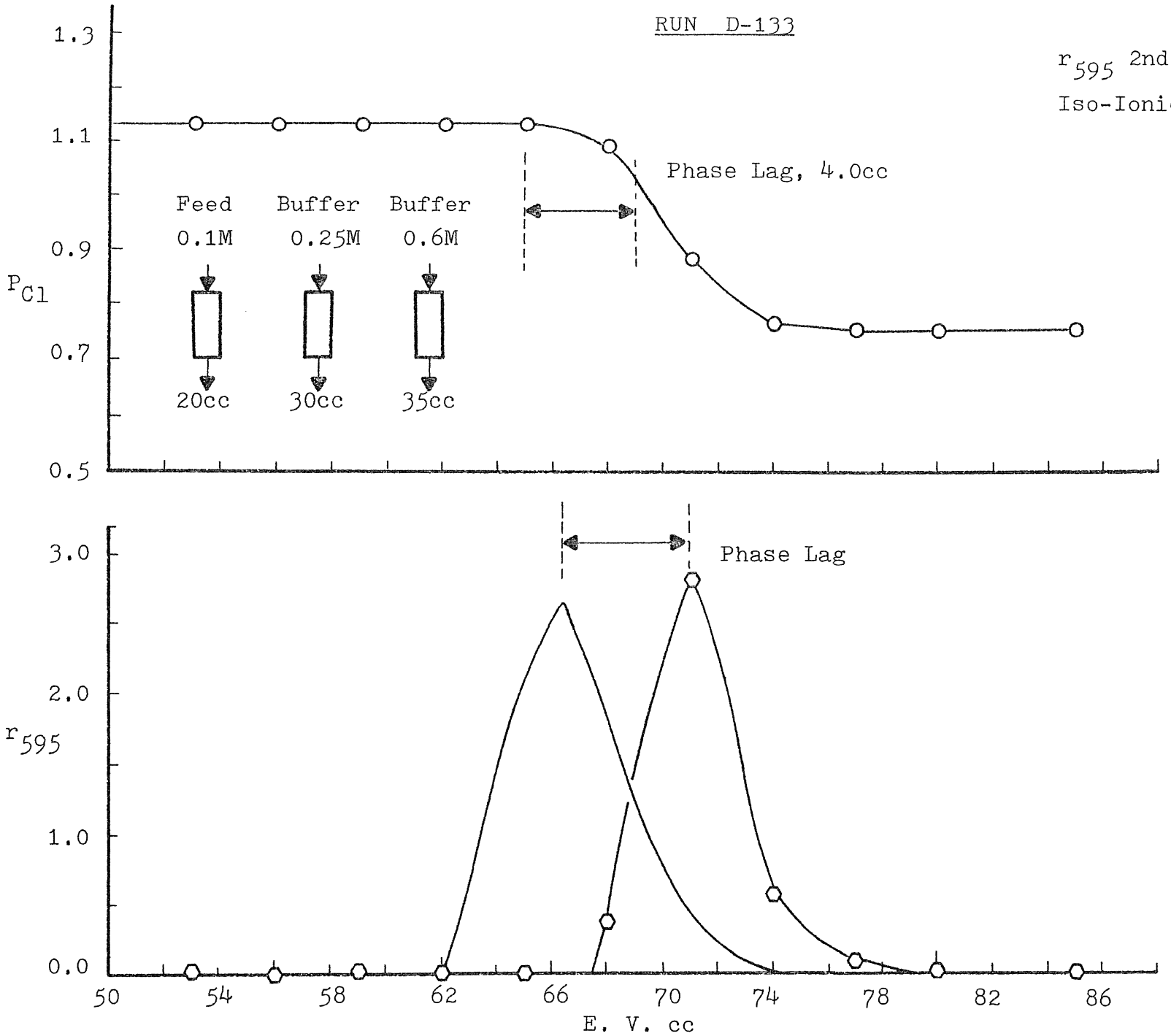

Fig. 81 r_{595} 2nd. Peak and Elution Prediction for 0.60 M

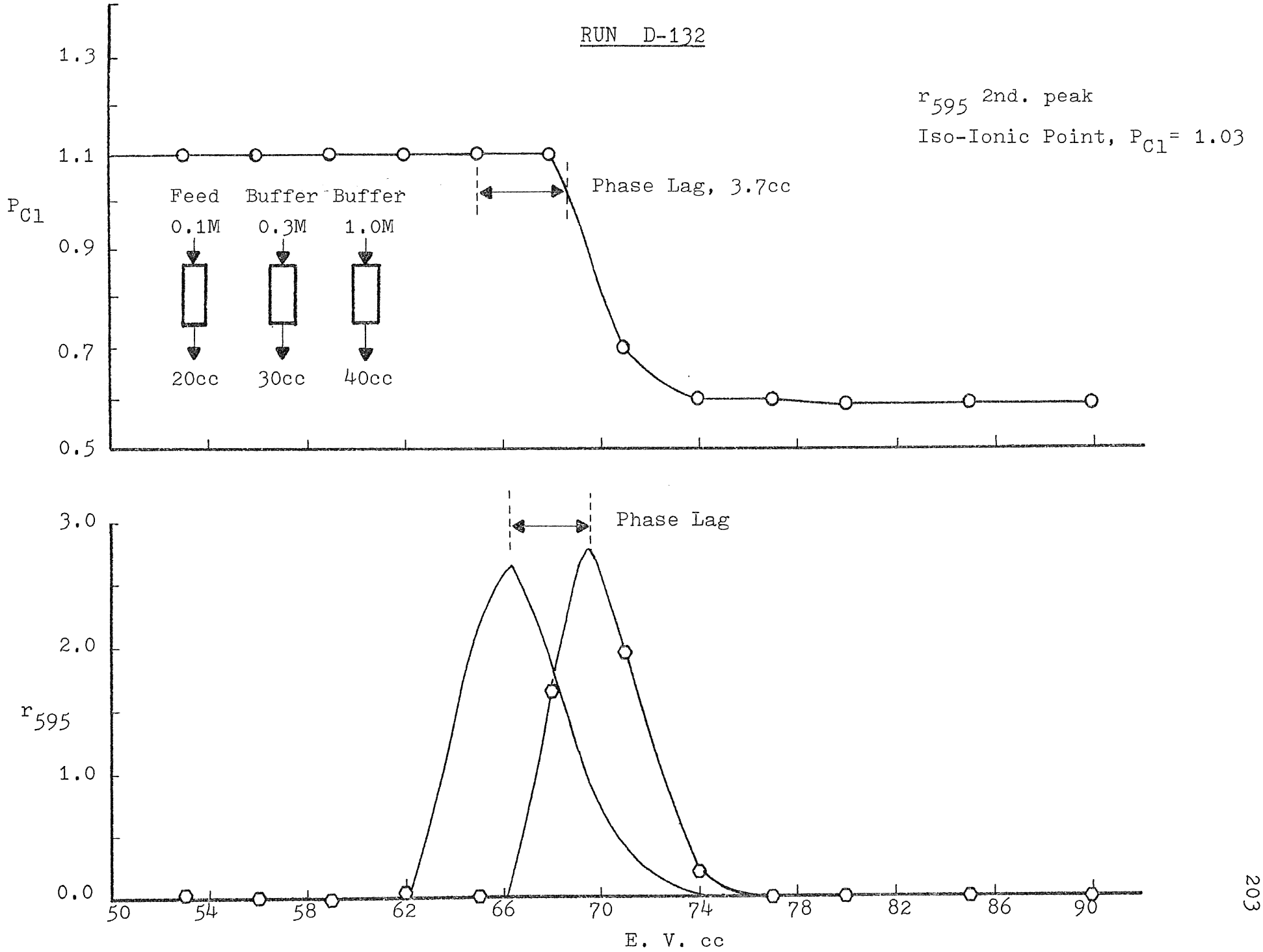

Fig. 82 r_{595} 2nd. Peak and Elution Prediction for 1.00 M

Table 9 Phase Lag of Total Protein 2nd. Peak

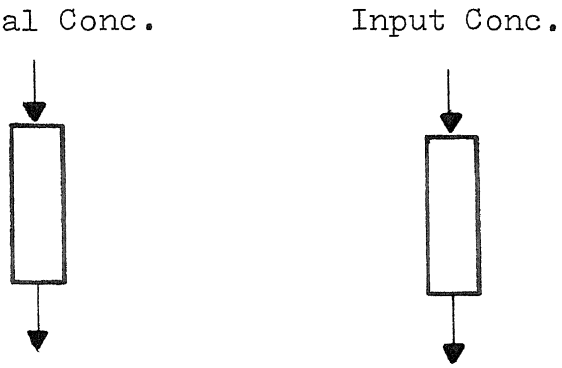

Run	Initial Concentration, M	Input Concentration, M	Phase Lag, c.c.
D-132	0.30	1.0	3.7
D-133	0.25	0.6	4.0
D-134	0.23	0.38	5.2
D-135	0.21	0.35	6.8

* Iso-Concentration of r_{595} 2nd. peak is 0.325M

Table 10 Relations of Model Parameters and Experimental Run for Total Protein 2nd. Peak

Run	Initial Buffer, M	Conc. Buffer, M	C_I	$\sum r_{595}$%		Peak Height		Retention Vol.		Model Parameter		
				Exp.	Mod.	Exp.	Mod.	Exp.	Mod.	m, cm^{-1}	E_d, cm^2/min	k_f, cm/min
D-132	0.30	1.00	14	69.5	69.9	2.80	2.60	69.5	69.7	3700	0.077	1×10^{-3}
D-133	0.25	0.60	14	72.3	68.8	2.83	2.50	71.0	70.0	3400	0.082	1×10^{-3}
D-134	0.23	0.38	14	61.1	42.7	0.50	0.51	84.0	86.7	290	0.195	1×10^{-3}
D-135	0.21	0.35	14	32.2	33.98	0.286	0.273	92.0	93.8	140	0.220	1×10^{-3}

* Model Parameters: Q= 1.0cm^3/min, S= 2.0cm^2, L= 8.0cm, a= 150cm^{-1}, ϵ= 0.75

Phase Lag is shown in Table 9; Tube Volume is 4cc.

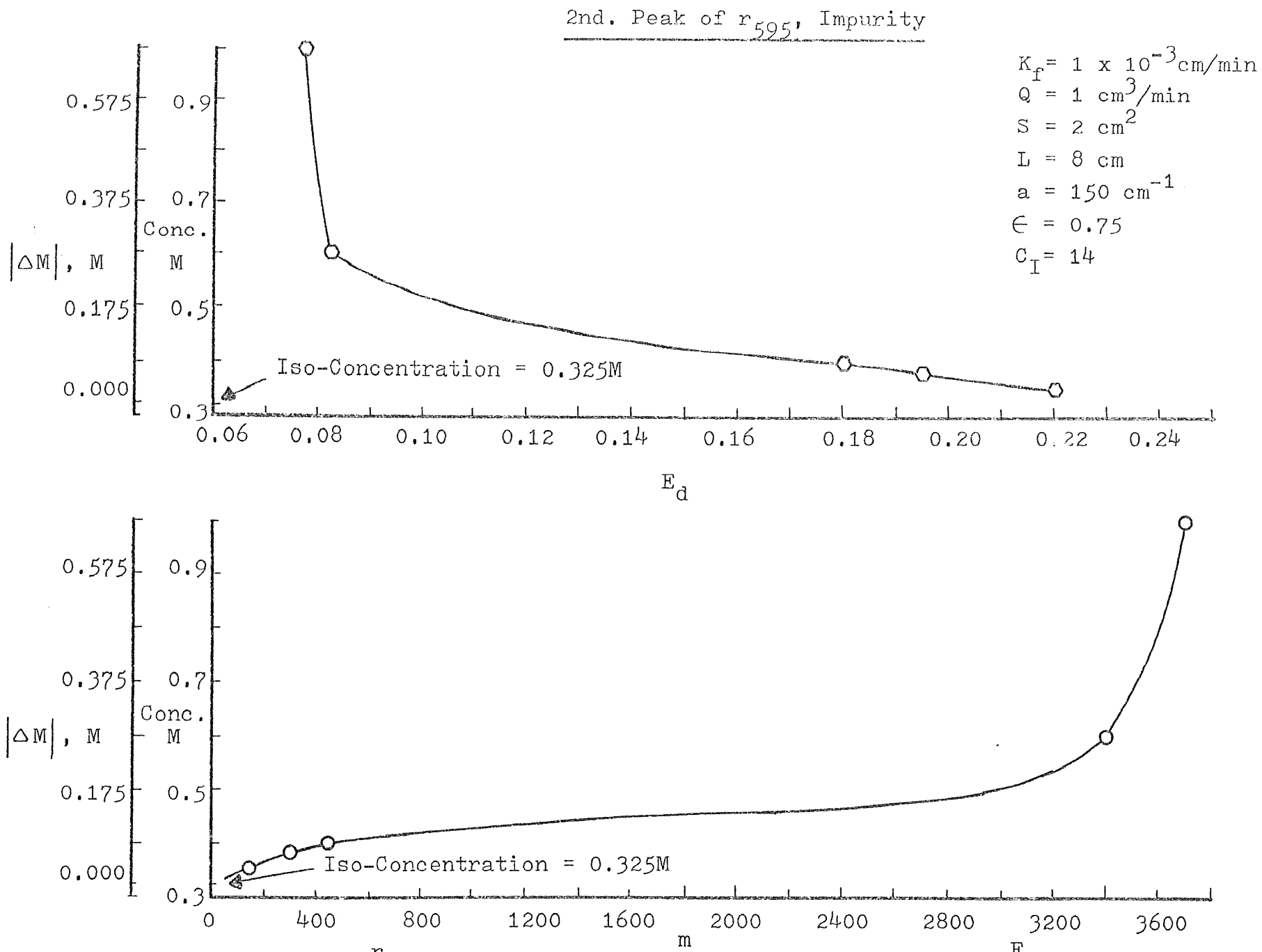

Fig. 83 r_{595} 2nd. Peak, Correlation of Axial Dispersion E_d and Equilibrium Constant m on Buffer Concentration and $|\Delta M|$

We have discussed the relation between phase lag and model parameters for the first and second peaks of r_{595}. The first and second iso-concentrations are 0.17M and 0.325M respectively. We will now discuss the co-elution of the impurity group of two r_{595} peaks. If an ionic strength for the incoming buffer is greater than the ionic strength of second isoconcentration. Total protein r_{595} will elute as a single peak with siginificant tail. In fact that this peak results from the co-elution of two impurity groups. These two peaks are eluted one right after the other and superimposed as a single peak.

Figures 84 to 86 show the elution profiles for buffer concentrations of 0.35M, 0.40M and 0.60M. The phase lag in each case is taken from the first peak of r_{595}. The elution profile shown in Figure 84 is composed of two parts which are the first peak of r_{595} and second peak of r_{595}. The dotted lines are the calculated curves for each case. The summation of the two dotted curves completes the prediction of total proteins elution with 0.35M buffer. The calculated and experimental results are in good agreement. The experimentally measured phase lag agrees with the model prediction. The elution profile shown in Figure 85 also results from the superimposition of the first and second peaks of r_{595}. The experimental results do not tell the relative area of superimposition; however, the two calculated curves demonstrate the magnitude of the contributed peaks. Figure 86

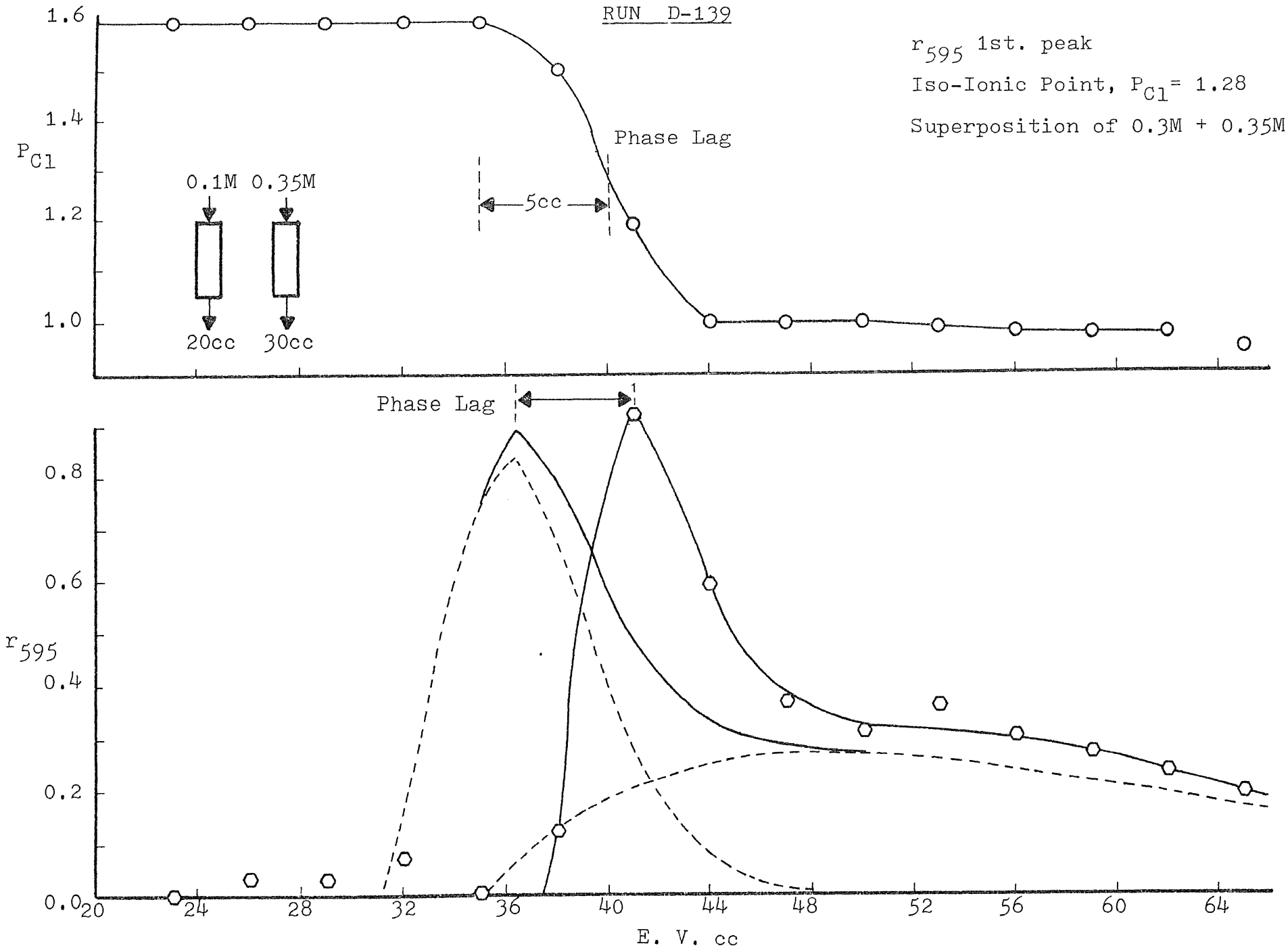

Fig. 84 r_{595} 1st. Peak and Elution Prediction by Superposition for 0.35M

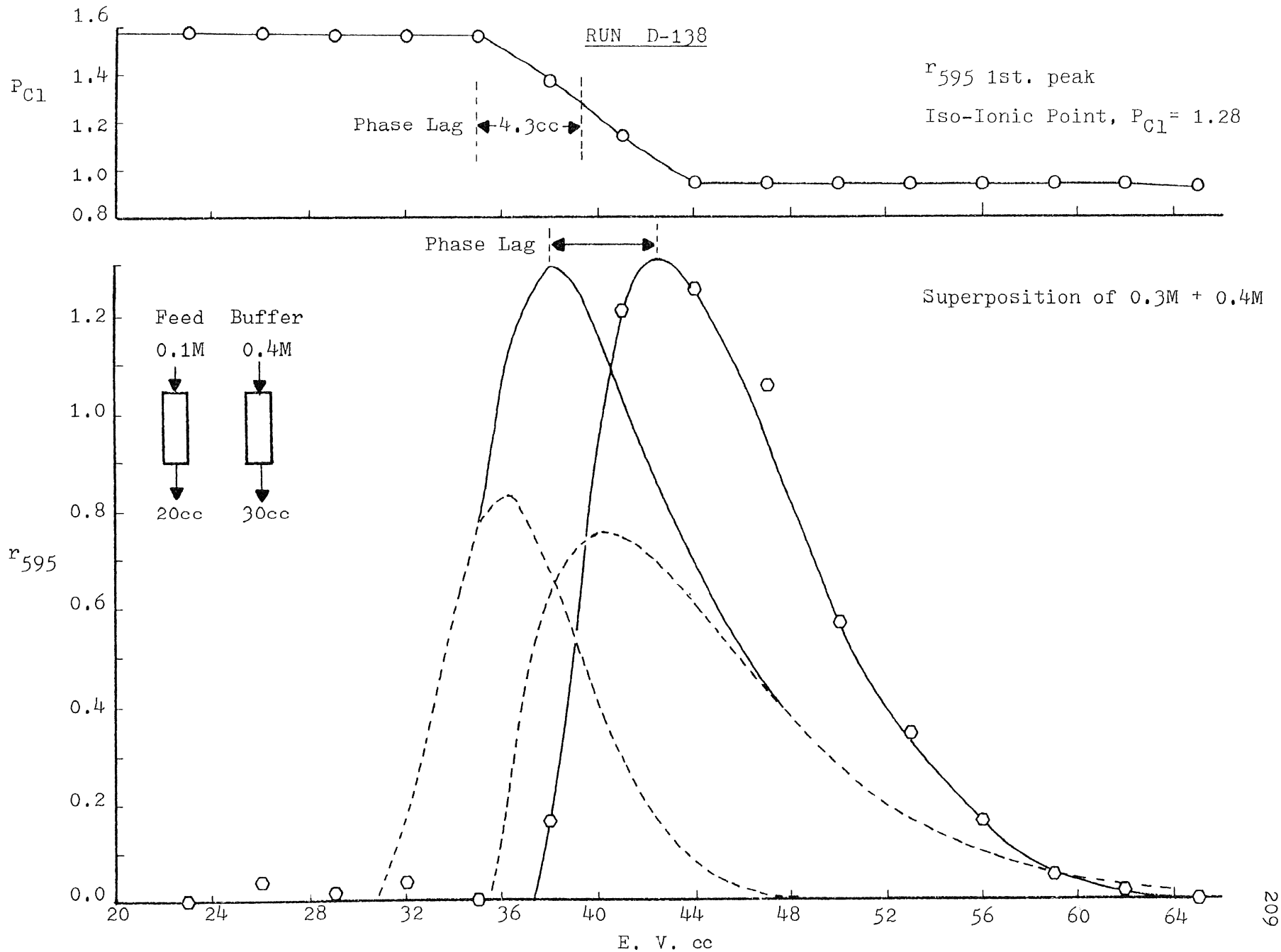

Fig. 85 r_{595} 1st. Peak and Elution Prediction by Superposition for 0.40 M

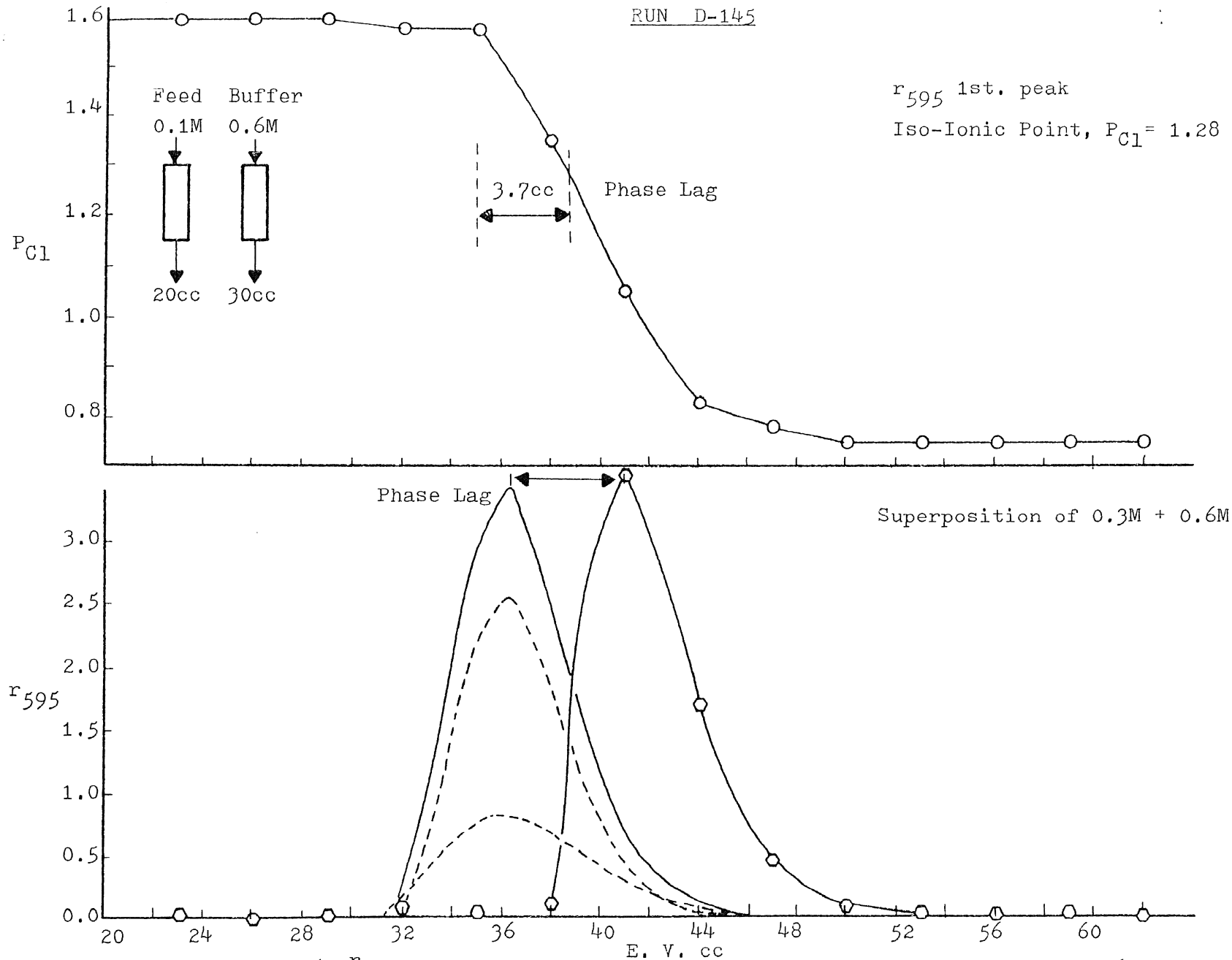

Fig. 86 r_{595} 1st. Peak and Elution Prediction by Superposition for 0.60 M

demonstrates that the calculated and experimental results for 0.3M and 0.6M buffer agree quite well. Note that the phase lag is measured based on the co-elution of the first peak of r_{595}. Because the first peak of r_{595} starts earlier and the second peak superimposes with the first peak. Based on this argument, we can generate the phase lag ranging from 0.18M to 0.6M. The results are shown in Figure 87. Again, the phase lag is plotted by buffer concentration and $|\Delta M|$.

The model parameters used for predicting co-elution and the corresponding experimental results are shown in Table 11. This table shows the good agreement between predicted and experimental peak areas, retension times, and peak heights. Figure 88 demonstrates the peak height of each curve eluted by different buffer concentration for the first peak of enzyme r_{405} and total protein of r_{595}. These are compared with the calculated peak height and shows a good agreement. The same curve shown on the lower part of the figure is repoltted with a dotted line on the upper part of the figure. This allows one to easily tell the range of buffer concentration at which the enzyme and its impurity can be separated. This concentration lies between 0.22M and 0.30M.

Figure 89 demonstrates a similar idea as Figure 88 from different viewpoint. The separation factor (S.F.) is defined as

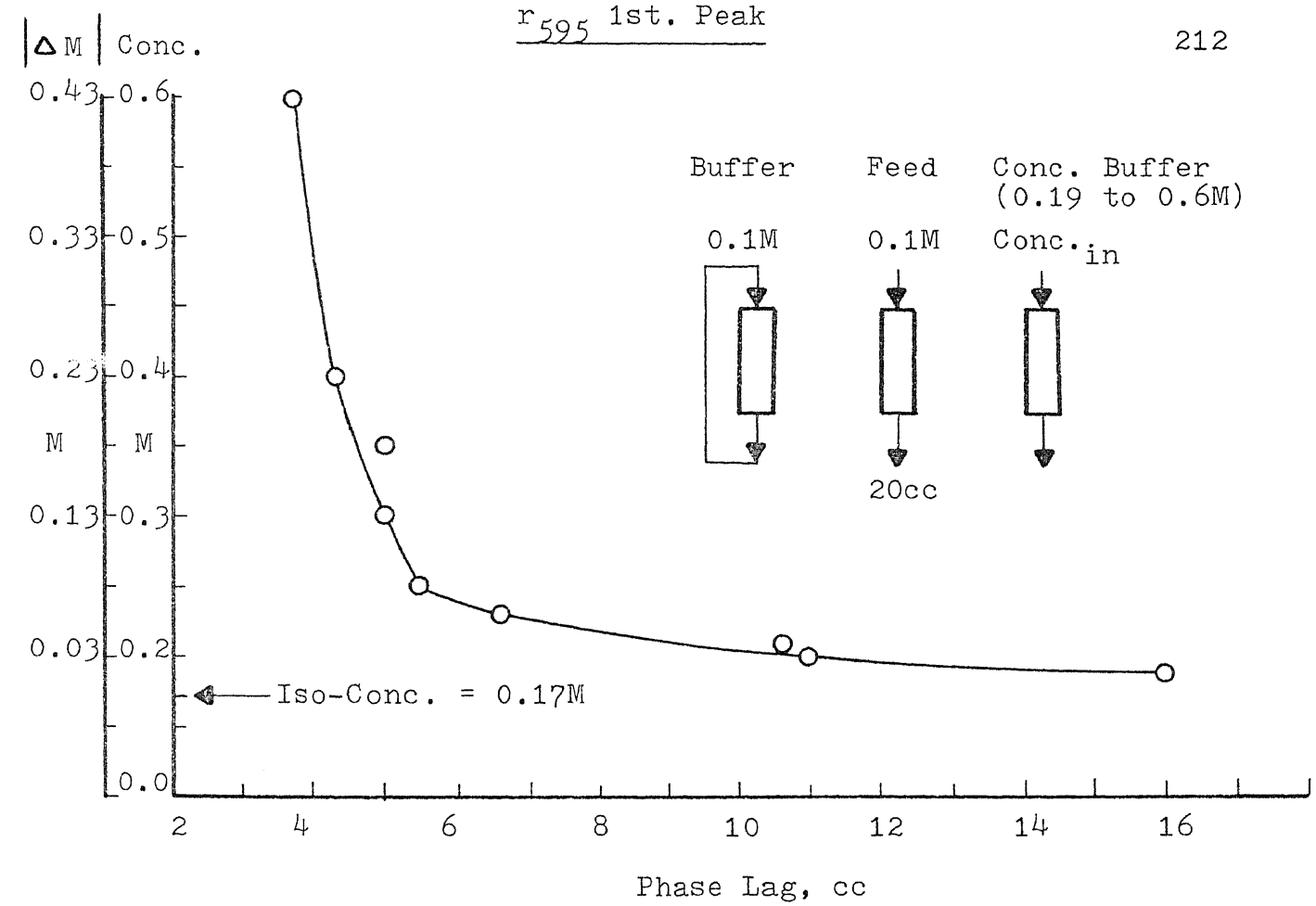

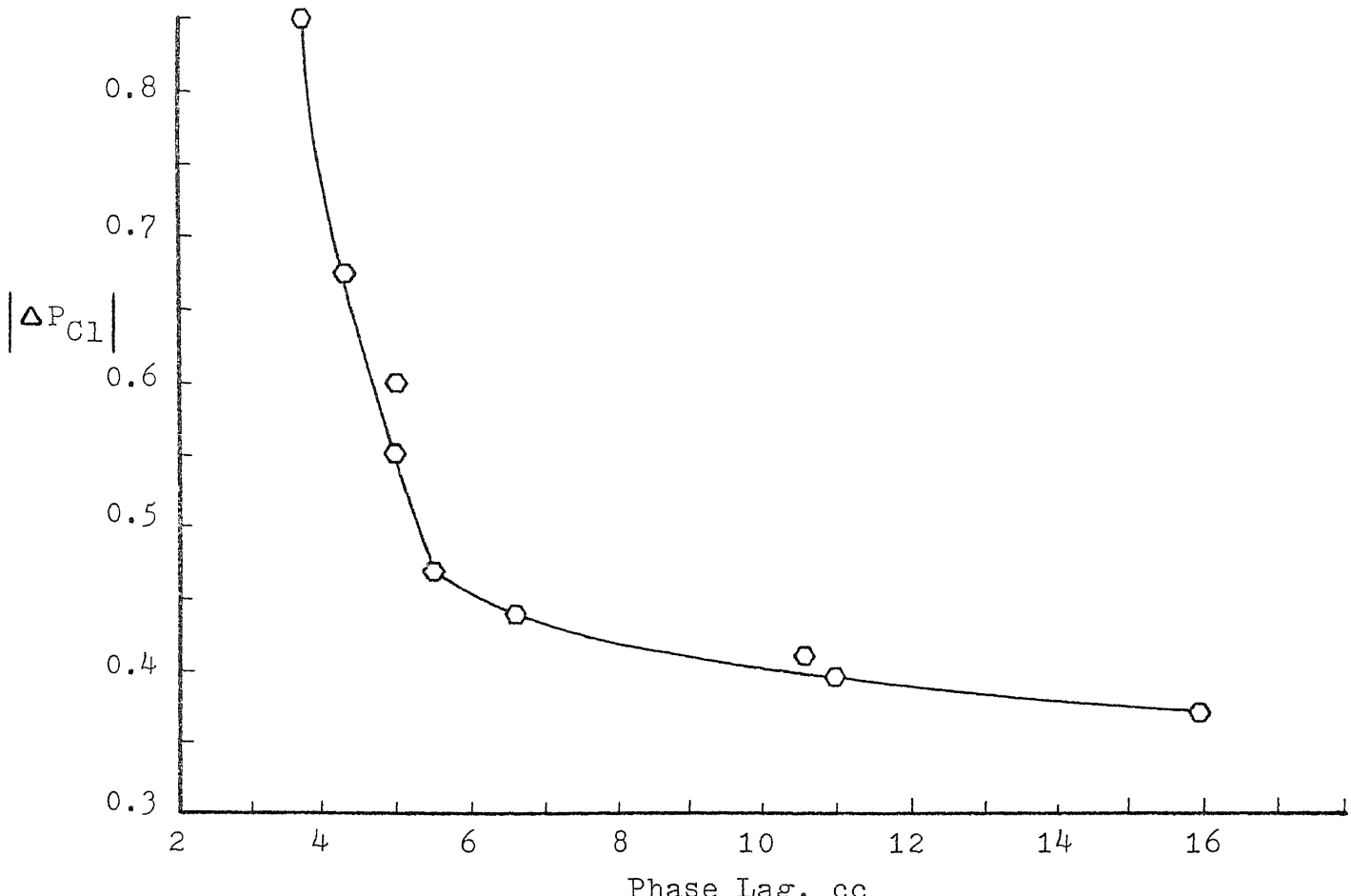

Fig. 87 r_{595} 1st. Peak, Phase Lag v.s. Buffer Concentration in Term of $|\Delta M|$ and $|\Delta P_{Cl}|$

Table 11

Prediction with Model Parameters and Experimental Run for Total Protein 1st. Peak by Superposition

Run	Initial Conc. M	Conc. Buffer, M	C_I	Σr_{595}% Exp.	Σr_{595}% Mod.	Peak Height Exp.	Peak Height Mod.	Retention Vol. Exp.	Retention Vol. Mod.	Model Parameter m, cm^{-1}	Model Parameter E_d, cm^2/min	Model Parameter k_f, cm/min^2
D-139	0.10	0.35	14	61.2	67.6	0.926	0.877	41.0	42.0	140	0.220	1×10^{-3}
D-138	"	0.40	14	95.9	76.1	1.310	1.307	42.5	42.3	435	0.180	1×10^{-3}
D-145	"	0.60	14	98.5	98.6	3.555	3.330	41.0	39.7	3400	0.082	1×10^{-3}

1. Model parameter of 0.3M buffer used for superposition are from Table 8; m= 2200, C_I= 6, E_d= 0.135 and k_f= 1×10^{-3}.
2. Model parameter of m and E_d and k_f for 0.35 and 0.6M are from Table 10; and 0.4M is from Fig.83 and with Q= $1.0 cm^3/min$, S= $2.0 cm^2$, L= 8.0cm, a= $150 cm^{-1}$ and $\in$ = 0.75.
3. Phase lag is based on conc. buffer input as shown in Table 7 and tube volume is 4cc.

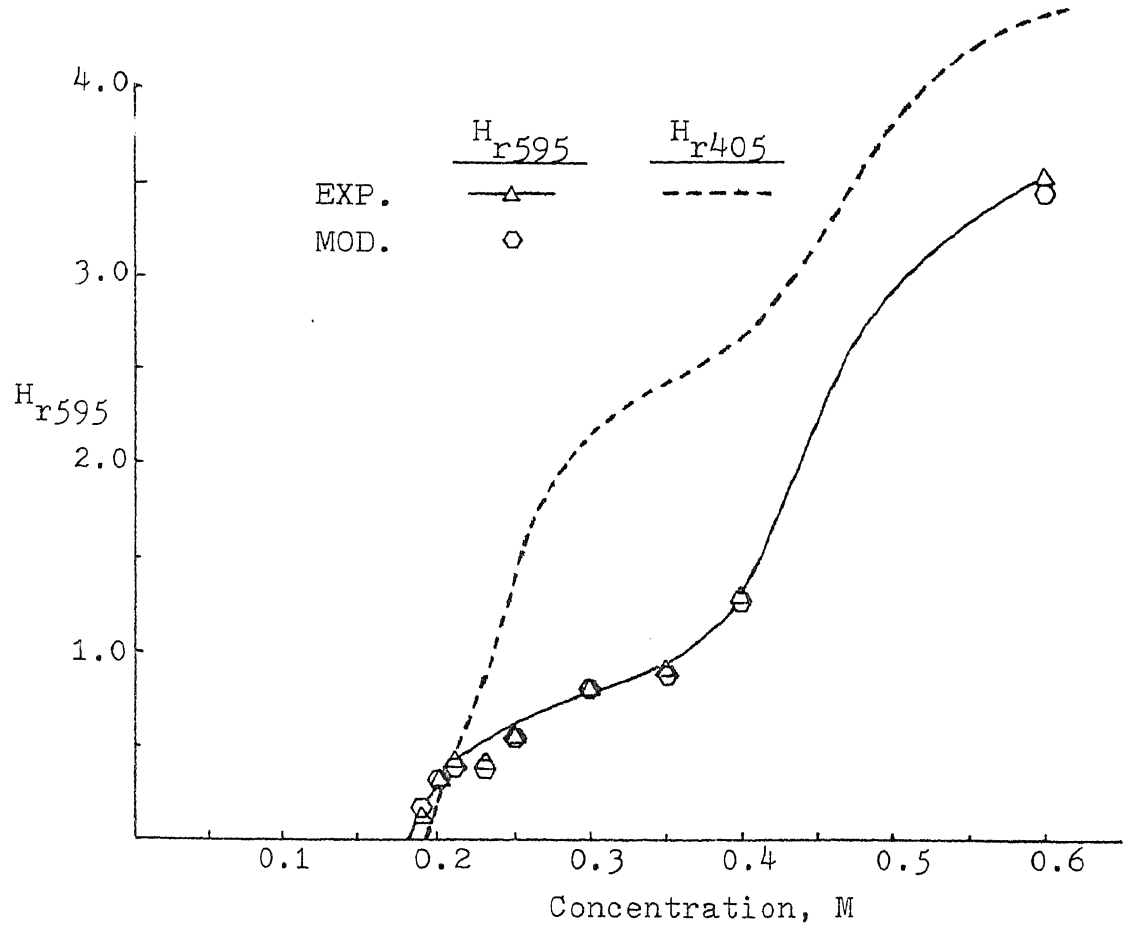

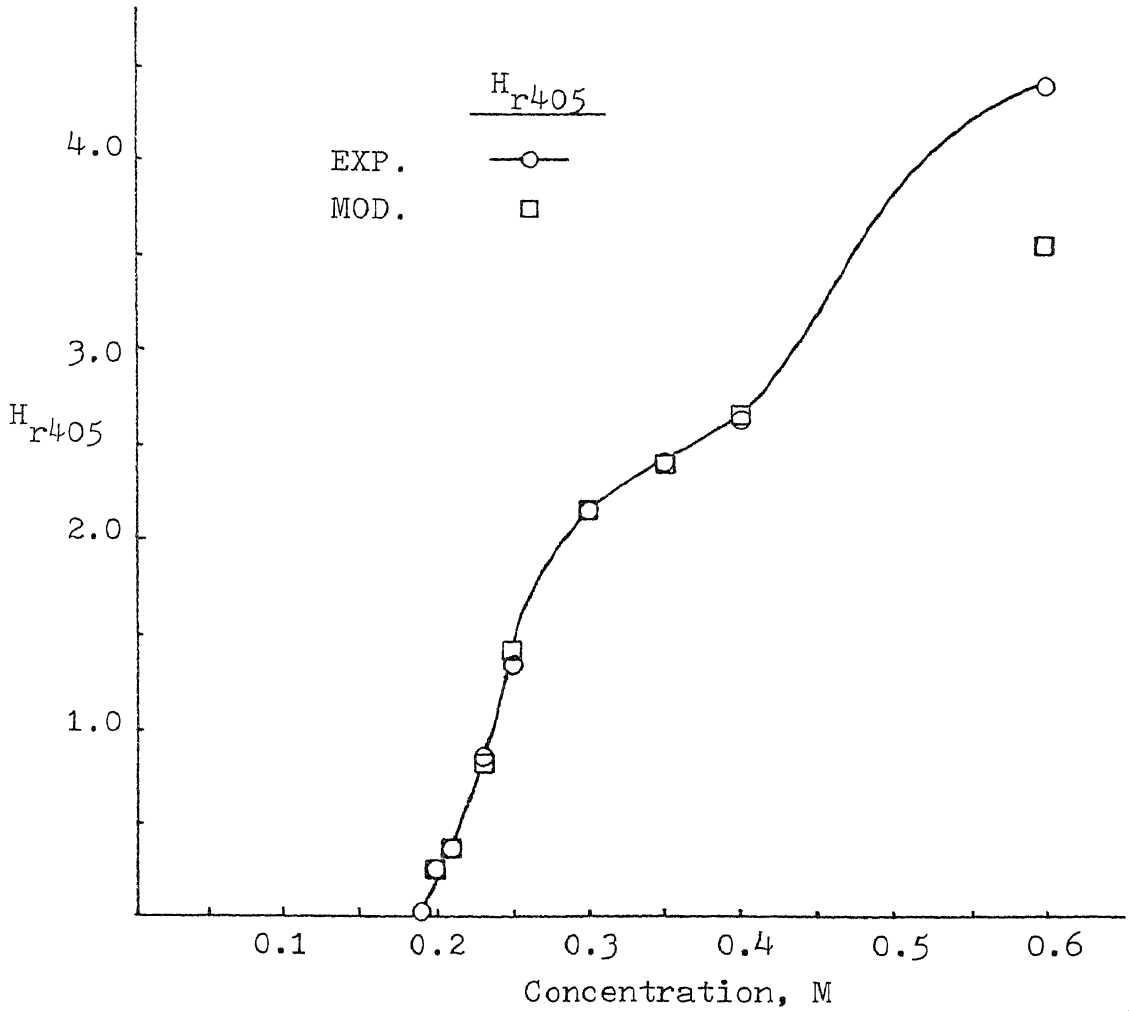

Fig. 88 Elution Peak Height H_{r595} and H_{r405} v.s. Buffer Concentration

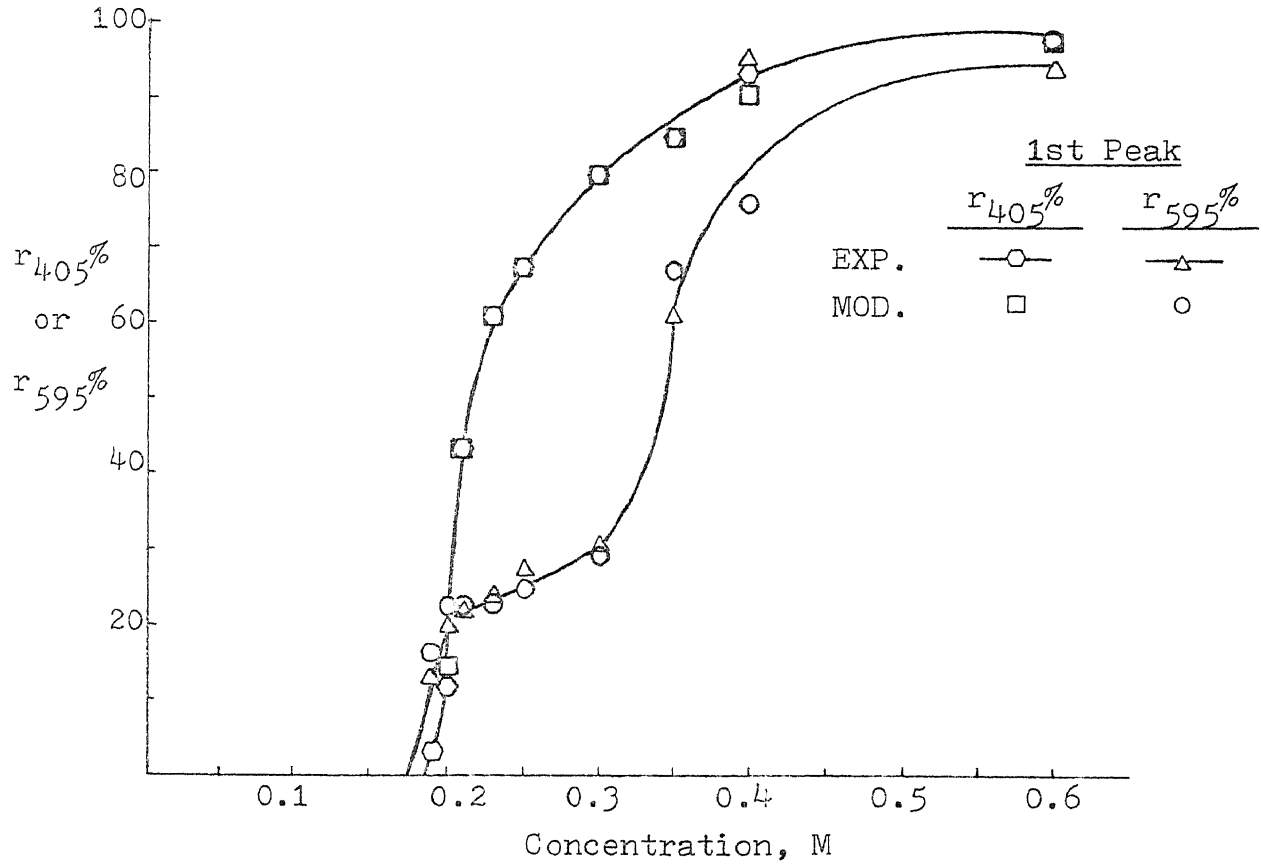

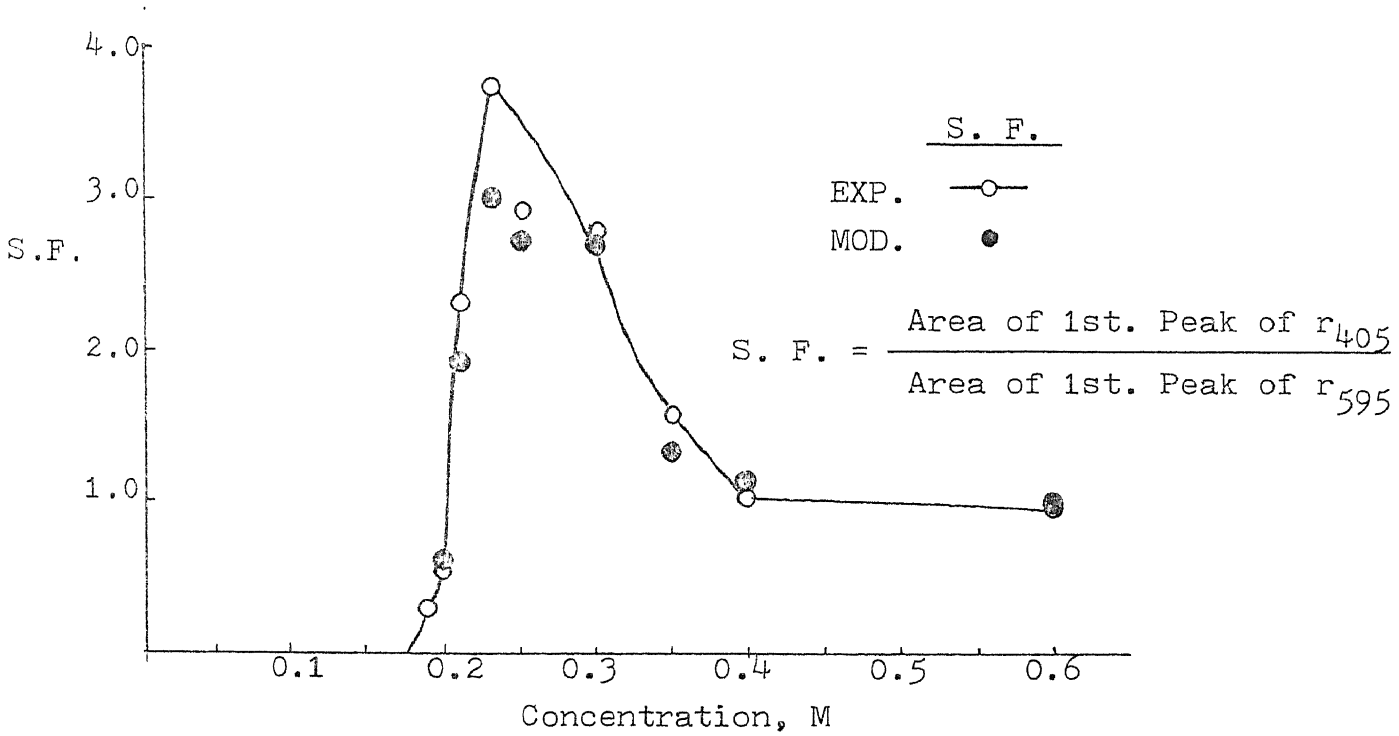

Fig. 89 Recovery Area of $r_{405}\%$ and $r_{595}\%$ v.s. Buffer Concentration and Separation Factor v.s. Buffer Concentration

the area of first peak of r_{405} divided by the area of first peak of r_{595}. Obviously, our goal is to maximize the S.F. i.e., maximizing the area of r_{405} while minimizing the area of r_{595}. At the top of the figure 89, a comparison between the percent recovery for r_{405} and r_{595} is shown. Again, the experimental results and model prediction agree quite well. The high concentration of 0.6M eluted almost 100% of the enzyme and the impurities. In the moderate concentration range between 0.22M and 0.30M, the separation can be performed. The lower part of the Figure 89 shows the S.F. as a function of the buffer concentration for enzyme-alkaline phosphatase. A maximum separation factor that could be obtained by single step change is roughly between 3 and 4 for a buffer concentration of 0.23M. However, we have experimentally demonstrated in Sec.5-1 that a better separation can be achieved by multiple step changes.

Table 12 demonstrates how the experimental results between a single step change and a multiple step changes for different buffer concentration to affect the S.F. and the enzyme percent recovered. For a single step change, the separation factor shows a highest value of 3.73 for 0.23M buffer and a lowest peak area (60.8%). Multiple step changes can give a better separation than a single step change.

Table 12

S.F. of Single Step Change in Buffer Concentration

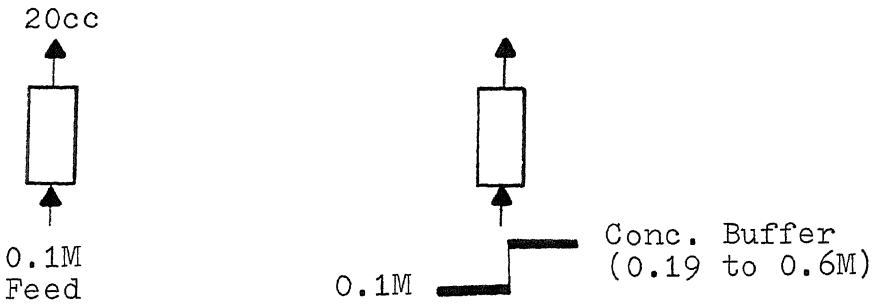

Run	Buffer Concentration, M	S. F.	Enzyme%
D-140	0.1 → 0.20	0.53	12.0
D-135	0.1 → 0.21	2.68	43.4
D-134	0.1 → 0.23	3.73	60.8
D-133	0.1 → 0.25	2.93	67.6
D-132	0.1 → 0.30	2.80	80.0
D-139	0.1 → 0.35	1.59	84.6
D-138	0.1 → 0.40	1.03	93.6
D-145	0.1 → 0.60	0.95	98.5

S.F. of Multiple Step Changes in Buffer Concentration

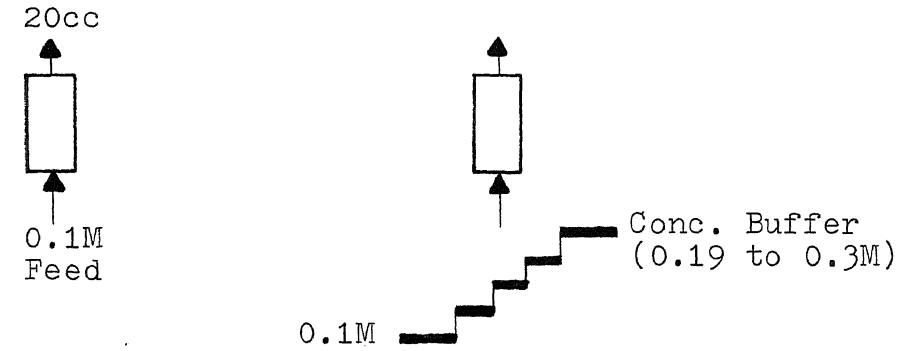

Run	Buffer Concentration	S. F.	Enzyme%
D-136	0.1→0.21→0.22→0.23→0.24→0.25	15.8	65.3
D-137	0.1→0.21→0.25→0.27→0.29→	6.5	85.9
D-141	0.1→0.21→0.23→0.24→0.25→	5.9	74.7
D-143	0.1 → 0.19 → 0.30	5.0	68.3
D-144	0.1→0.19→0.21→0.22→0.23→0.24→0.25	29.1	59.3

$$\text{S.F.} = \frac{\text{Purified Enzyme Area}}{\text{Total Protein Area}} \quad ; \quad \text{Enzyme\%} = \frac{\text{Purified Enzyme area}}{\text{Total Enzyme Area}} 100$$

Obviously, the experimental method for multiple step changes is tedious, but, the purity and the recovery of the enzyme are high and justify the effort. Note that the data shown for Run D-144 have an enzyme recovery of 59.3% and an S.F. of 29.1. This demonstrates that the purity and recovery for multiple step changes are far superior to single step change.

6. Chromatographic column behavior evaluation and model application

Chromatography involves the separation of a mixture of components by virtue of differences in the equilibrium constant between the solute molecules and solid phase. Due to the complex interactions of the parameters, the operation record for a chromatographic column will provide a chromatographer with a better understanding of the machine operation and mobile phase selection. Aside from the variation in construction of column packings and column dimensions, other important parameters need to be considered. The main concerns of separation feasibility evaluation are based on the composition of the mobile phase, the effects of the mobile phase on the solute molecules, and the relationship between the solute molecules and the solid phase. Also, the flow rate of the mobile phase will affect the transient profiles within the chromatographic column such as buffer pH and buffer ionic strength. The overall effects of the parameters can create a very large difference in chromatographic column performance.

In chapter 4 and chapter 5, we have discussed how the buffer pH and buffer concentration will affect the adsorption/desorption behavior on a protein system. The prediction of elution profile by the surface adsorption model was also discussed. In this

chapter, we will compare the rate theory and the plate theory, which have been discussed in Section 1-3.

The following equations are the mostly used for the purpose of chromatographic column evaluation.

1. Adjusted retention time, t'_R

$$t'_R = t_R - t_M \qquad \text{(D-1)}$$

where t_R is the retention time of a solute, t_M is the retention time of an unretained solute such as buffer.

2. Retention volume, V_R

$$V_R = Q * t_R \qquad \text{(D-2)}$$

where Q is volume flow rate for the column.

3. Capacity ratio, $K = \dfrac{t_R - t_M}{t_M} = \dfrac{t'_R}{t_M}$ (D-3)

where t'_R is the adjusted retention time, t_M is the retention time of unretained solute.

4. Number of theoretical plates, N

$$N = 16\,(t_R/W_b)^2 \quad \text{or,} \quad N = 5.545\,(t_R/W_h)^2 \qquad \text{(D-4)}$$

where t_R is the retention time of solute, W_b is the peak width at base, W_n is the peak width at 1/2 peak height.

5. Number of effective theoretical plates, N_{eff}

$$N_{eff} = 5.545 \left(\frac{t_R'}{W_h}\right)^2 \qquad \text{(D-5)}$$

where t_R' is the adjusted retention time of solute, W_h is the peak width at one-half peak height.

6. The "Height Equivalent to Theoretical Plate", HETP,

$$HETP = h = L/N \qquad \text{(D-6)}$$

where L is the column length, N is the number of theoretical plates.

7. Coating efficiency, CE

$$CE = \left(\frac{h_{theor}}{h_{exp}}\right)_{min} \qquad \text{(D-7)}$$

where

$$h_{theor} = r\sqrt{\frac{11K^2+6K+1}{3(1+K)^2}}$$

$$h_{exp} = \frac{L}{N} \qquad \text{(D-8)}$$

r = column radius

8. Separation number, Trennzahl (TZ)

$$TZ = \frac{t_{R(c_{n+1})} - t_{R(c_n)}}{W_{0.5(c_n)} + W_{0.5(c_{n+1})}} - 1 \qquad \text{(D-9)}$$

where c_{n+1} and c_n are members of a homologous series, t_R is the retention time, $W_{0.5}$ is the peak width at one-half peak height.

9. Asymmetry or tailing factor, TF

$$TF = (b/a) 100 \qquad \text{(D-10)}$$

where "b" is area of the rear half of a tailing peak and "a" is area ofthe front half of a tailing peak. Note that both halves are measured at 10% of the peak height above the baseline.

The key parameters in the above equations are t_R, t_M, W_b, and W_h. The t_R is the time measured from zero to the point where the peak maximum emerges, and t_M is measured the same way as t_R for an unretained solute, such as the buffer.

6-1 Ion exchange chromatography column evaluation

In chapter 5, we have applied Eq.A-42 in the prediction of enzyme elution profiles on the ion exchange resin. Also, we have discussed the operation of an ion exchange column in an on/off adsorption and desorption system. The protein molecules will be adsorpted by carrying opposite charge to that of the resin, and eluted from the resin when the protein molecules carry the same charge. However, Eq.A-42 and B-49 are derived based on the plug flow assumption; i.e., the change within the column is strictly

a step change. There is no transient behavior from one pH to another pH, or one buffer concentration to another buffer concentration. The experimental results of pH and pCl profiles have demonstrated these transients do exist. The modification of Eq.A-42 and B-49 is necessary in order to correctly predict the retention time, t_R. Therefore, the dimensionless term of will be changed to τ_R,

$$R = \frac{E_d\, t}{L^2} + \frac{E_d\, t_{phase}}{L^2} = (\, t + t_{phase}) \frac{E_d}{L^2} = t_R \frac{E_d}{L^2}$$

The Eq. A-42 becomes,

$$C_A(\tau_R,1) = \sum_{m=1}^{2} \sum_{n=1}^{\infty} e^{(\frac{A}{2} + p_{mn}\tau_R)} \frac{\beta_n^{\,2}}{(1+\frac{B\alpha r}{(p_{mn}+\alpha r)^2})(U*\sin\frac{\beta_n}{2} - V*\cos\frac{\beta_n}{2})} \frac{E_d^{\,2}}{L^4} \quad \text{(A-43)}$$

where $U = \dfrac{\beta_n^{\,2}(A+1)+A^2}{A\,\beta_n}$, $V = (A^2 - \beta_n^{\,2}) / 2A$

The Eq. B-49 becomes,

$$C_A(\tau_R,1) = \sum_{n=1}^{\infty} \sum_{m=1}^{\infty} e^{(\frac{A}{2} + p_{mn}\tau_R)} \frac{\beta_n^{\,2}}{(\frac{dF}{dp})*(\, U*\sin\frac{\beta_n}{2} - V*\cos\frac{\beta_n}{2}\,)} \frac{E_d^{\,2}}{L^4} \quad \text{(B-50)}$$

where $\dfrac{dF}{dp} = -\dfrac{dF}{dS_{mn}}$ = Eq. B-45, $U = \dfrac{\beta_n^{\,2}(A+1)+A^2}{A\,\beta_n}$, $V = \dfrac{A^2 - \beta_n^{\,2}}{2A}$

Actually, the average linear velocity v defined in Sec.2-1 is equal to $v = L/t_M$ where L is the column length and t_M is the retention time of unretained solute such as buffer. Thus, $t_M = L/v$ is substituted into Eq.D-1 to have the solute retention time t_R equal to the buffer retention time t_M plus adjusted retention time t_R'. Therefore, we can conclude that the adjusted retention time is actually equivalent to the phase lag we defined. There is aphase lag for ion exchange, affinity, and any other adsorption/desorption column system. In chapter 5, we have optimized the model parameters with respect to the elution profiles that are controlled by the buffer concentration. The phase lag for the different buffer concentration can be related to model parameters. Therefore, we will be able to predict the retention time t_R, peak height, peak shape, and elution time. Obviously, if we can predict the retention time, we can easily calculate the retention volume V_R from Eq. D-2 . Thus the plate theory relates the equations used for chromatograpgy column efficiency evaluation. These can now be expressed in terms of rate theory. This is valid because the Eqns. A-43 and B-50 can be used for the prediction of peak area, shape, height, and retention time. The characteristic parameters for calculated peaks (such as $W_{0.5}$ and t_R') are easily determined. Once we have the information needed for Eq. D-1 to Eq. D-10, we can perform chromatographic column evaluation and use the predicted

model parameters from the ion exchange model to predict other operating conditions. The column efficiency evaluation parameters developed by the plate theory (such as "Number of theoretical plates" and "Number of effective theoretical plates" and "HETP") can now be directly related to the operating conditions and ion exchange model parameters (such as equilibrium constant, mass transfer coefficient, and axial dispersion coefficient).

6-2 Gel permeation chromatographic column evaluation

Gel permeation chromatography (GPC) permits solute mixtures to be separated by their effective molecular weight and shape. Elution is performed on a rigid, porous, non-ionic support, and pores are similar in size to those of the sample molecules. Small molecules can enter freely into the pores of the stationary phase and thus have a long retention time. Large molecules are excluded from all pores and have a short retention time. Molecules are, therefore, eluted in the order of decreasing of molecular size.

The difference between the GPC and the ion exchange chromatographic column is the inertness of the solid phase.

There is no phase lag for GPC. The retention time is mainly governed by the axial dispersion, mass transfer resistance, and the effective molecular diffusivity. Thus, the calculated elution profile will represent the actual experimental elution profile. The expression of equations for GPC column evaluation is straight forward, i.e., the calculated retention time t_R is the experimental retention time.

$$C_A(\tau,1) = \sum_{m=1}^{\infty}\sum_{n=1}^{\infty} e^{(\frac{A}{2}+p_{mn}\tau)} \frac{\beta_n^2}{(\frac{dF}{dp})*(U*\sin\frac{\beta_n}{2} - V*\cos\frac{\beta_n}{2})} \frac{E_d^2}{L^4} \qquad (C\text{-}27)$$

$$U = \frac{\beta_n^2(A+1)+A^2}{A\beta_n}, \qquad V = \frac{A^2-\beta_n^2}{2A}$$

where dF/dp = Eq. C-25 and $\tau = t_R*Ed/L^2$

The Eq. C-27 will be used to calculate the elution profile. The corresponding peak characteristics are measured from the calculated results directly in order to apply Equations D-1 to D-10 to GPC column evaluation.

7. Conclusion

Three mathematical models have been derived to simulate the transient behavior for an impulse input in a chromatographic column. Two of the models are developed for the ion exchange column and characterized as the surface adsorption model and the surface adsorption with pore diffusion model. In both models the effects of axial dispersion, mass transfer resistance, and equilibrium relationships. The distinction between two models is the significance of pore diffusion for solute molecules. Third model for gel permeation chromatography (GPC) emphasizes the role of internal diffusion within the solid matrix in additional to the combined effects of axial dispersion and mass transfer resistance.

The models are solved analytically with two of novel and realistic boundary conditions. One is specified as the solute mass conservation of back mixing at the column inlet due to the axial dispersion, and the second consider the total material balance of solute molecules throughout the whole column. We have discussed all the system parameters to examine how they will affect the elution profile for chromatographic operation. The conclusions are listed as follows:

1. The mass transfer mechanisms are considered as a series of combined parameters. These are the axial dispersion, mass transfer resistance, equilibrium relationship, and the internal diffusion. The equilibrium relationship is not considered for the GPC column and the internal diffusion is not considered for the elution with large molecules.

2. The magnitude of axial dispersion will become significant for a short column with wide crossectional area. The effect of axial dispersion is only significant when the superficial velocity is low.

3. The elution profile of an ion exchange column is governed by the combined effects of mass transfer resistance and the equilibrium relationship. A high mass transfer coefficient means low transfer resistance and the equilibrium relationship will be the major factor. On the other hand, the solute will be more likely to stay in the liquid phase when the mass transfer resistance is high.

4. Large cross sectional area and long column lengths will give broad peaks. Generally speaking, the long duration of solute in the column will cause more mixing, axial dispersion, and decrease in column efficiency.

5. The high contact surface area will diminish the mass transfer resistance. For a high mass transfer resistance and low equilibrium constant, high contact surface area will increase the mass transfer rate.

The experimental investigation for the separation of proteins was performed on an ion exchange column. The model protein system, hemoglobin and albumin, was separated on a CM-Sepharose cation exchanger by pH cyclic zone. The elution peaks were verified and agreed well with the surface adsorption model predictions. The real protein system, enzyme alkaline phosphatase (Human Placenta) HPAP, was separated on DEAE-Sepharose by concentration cyclic zone. The elution profiles were fitted well with the surface adsorption model. An optimization and purification method was also developed for enzyme isolation. The optimal ionic strength for enzyme desorption is 0.23M of Tris-HCl buffer, such that only enzyme will be eluted. The highest separation factor achieved by multiple step changes in buffer ionic strength is 29.1, with 59.3% recovery of high purity enzyme product.

For both pH and concentration cyclic zone, the elution phase lag was defined as the difference of elution volume from the initial column condition (such as pH 6) to protein isoelectronic

point (such as pH 6.7) or isoionic point (such as 0.17M). With the aid of phase lag, the experimental results can be well explained by the surface adsorption model. This can also become the basis of efficiency evaluation for the ion exchange and GPC column. Thus, the basic empirical equations used for the efficiency evaluation by the Plate Theory, can now be predicted and expressed by the Rate Theory, i.e., the models derived in this work.

Nomenclature

A : dimensionless parameter, $QL/S\epsilon E_d$

a : effective contact area per unit bed volume, $a = 3(1-\epsilon)/r_o$
cm^2/cm^3

B : dimensionless parameter, $ak_f L^2/E_d \epsilon$

Bi : Biot number, $Bi = k_f r_o/D_s$, dimensionless

c : dimensionless group, $r_o^2 E_d/L^2 D_s$

c_A : solute concentration in fluid phase, g-mole/cc

c_A^* : equilibrium concentration of solute at solid-fluid interface, g-mole/cc

c_{AS} : solute concentration on solid phase, $g\text{-mole}/cm^2$

C_I : impulse strength, g-mole/cc-min

C_m : solute concentration in mobile phase, g-mole/cc

C_s : solute concentration in the stationary phase, g-mole/cc

C_A : dimensionless solute concentration in fluid phase, $(c_A - c_{A,to}) E_d/C_I L^2$

C_A^* : dimensionless equilibrium solute concentration at fluid-solid interface, $(c_A - c_{A,to})E_d/C_I L^2$

C_{AS} : dimensionless solute concentration on solute phase, $(c_{AS} - c_{AS,to})E_d/C_I L^2$

CE : coating efficiency

E_d : solute axial dispersion coefficient in fluid phase, cc^2/min

E.T. : elution time, min

E.V. : elution volume, cc

F : function of p, F(p)

H.E.P.T. : height equivalent to a theoretical plate

k_F : calibration constant with respect to feed

k_{pH} : calibration constant with respect to sample

k_f : mass transfer coefficient of solute in fluid phase, cm/min

K : capacity ratio

L : column length, cm

m : area based equilibrium constant, cm^2/cm^3, or cm^{-1}

m_v : volume based equilibrium constant, dimensionless

M : buffer concentration, molarity, g-mole/liter

N : number of theoretical plates

N_{AZ} : axial dispersion mass flux, g-mole/cm^2-min

N_{eff} : number of effective theoretical plates

p : dummy variable of Laplace transform, dimensionless

pCl : active chloride ion concentration in buffer, $-\log(Cl^-)$

pH : the measure index of acidity, $-\log(H^+)$

pI : isoelectric point for proteins

pNa : active sodium ion concentration in buffer, $-\log(Na^+)$

Q : volume flow rate, cc/min

R : dimensionless radial distance, r/r_o

r_o : radius of solid particle, cm

R_B : buffer absorbance reading at wavelength 595 μm

R_f : feed absorbance reading at wavelength of 403, 405, or 595 μm

R_S : sample absorbance reading at wavelength of 403,405 or 595 μm

r_{595} : ratio of sample to feed concentration

r_{405} : ration of enzyme activity of sample to feed

S : cross sectional area of packed column, cm^2

t : time, min

t_M : retention time of unretained solute, min

t_o : time instant, $t_o = 0$

t_R' : adjusted retention time for solute, min

t_R : retention time of solute, min

TF : asymmetry or tailing factor

TZ : separation number

V_m : volume of mobile phase

V_s : volume of stationary phase

v : superficial velocity of fluid phase, cm/min

$W_{0.5}$: peak width at one-half peak height

Y_o : feed concentration, measured by light adsorbance from spectrophotometer

Y_p : sample concentration, measured by light adsorbance from spectrophotometer

Z : axial direction, flow direction, cm

Greek letters

$\delta(t)$: impulse function, min

ϵ : void fraction of the packed bed

π : constant, 3.14159

τ : dimensionless time. $E_d t/L^2$

τ_R : dimensionless elution time, $E_d t_R/L^2$

η : dimensionless distance in axial direction, Z/L

γ : dimensionless distribution ratio, $m\epsilon/a$

$\alpha\gamma$: dimensionless parameter, $mk_f L^2/E_d$

β_n : eigenvalues of eigenfunction $\tan(\beta_n/2) = -2A\beta_n/(A^2-\beta_n^2)$

φ : dimensionless parameter, $(A^2+\beta_n^2)/4$

ξ : dimensionless parameter, $(A^2+\beta_n^2)/4$

ω : dimensionless parameter, $ak_f L^2/E_d\epsilon$

Literature cited

Ahmed, Z.M., "Parametric Pumping with pH and Ionic Strength Enzyme Purification", Dr. Eng. Sc. Dissertation, NJIT, 1981

Bird, R.B., W.E. Stewart, and E.N. Lightfoot, Transport Phenomena, Hohn Wiley & Sons Inc., NY, 702, 1960

Burkee Barker, III, Robert L. Pigford, "Cycling Zone Adsoprtion: Quantitative Theory and Experimental Results," I&EC Fundamentals, 10, 2, 1971, p.283

Busbice, M.E., and Wankat, P.C., "pH Cycling Zone Separation of Sugars," Journal of Chromatography, 114, 1975, p. 369

Chao, R. and H.E. Hoelscher, "Simultaneous Axial Dispersion and Adsorption in a Packed Bed," AIChE. J., 12 (2), 1966, p.271

Chen, H.T. Rastogi, A.K.,. Kim, C.Y. and Rak, J.L., "Nonequilibrium Parametric Pumps," Separation Science, 11, 1976, p.335-346

Chen H. T., Hsien, T.K., Lee, H.C. and Hill, F.B., "Separation of Proteins via Semicontinuous pH Parametric Pumping," AIChE Journal, 23, 1977, p. 695-701

Chen, H.T. Wong, Y.W., and Wu, S., "Continuous Fractionation of Protein Mixtures by pH Parametric Pumping," AIChE Journal, 25, 1979a, p.320-327

Chen, H.T., Yang, W.T., Pancharoen, U and Parisi, R., "Separation of Proteins via Multicolumn pH Parametric Pumping," AIChE Journal, 26, 1980a, p.839-849

Chen, H.T., Pancharoen, U., Yang. W.T., Kerobo, C.O. and Parisi, R.J., "Separation of Proteins via pH Parametric Pumping," Separation Science and Technology, 15, 1980b, p. 1377-1391

Chen, H.T., Yang, W.T., Wu, C.M., Kerobo, C.O. and Jajalla, V. "Semicontinuous pH Parametric Pumping: Process Characteristics and Protein Separations," Separation Science and Technology, 10, 1981a, p.43-61

Chen, H.T., Ahmed, Z.M. and Rollan, V., "Parametric Pumping with pH and Ionic Strength: Enzyme purification", I&EC Fundamentals, 20, 1981b, p.171-174

Colowick and Kaplan, "Methods in Enzymology", Vol. 1, 1955
Deisler Jr. P>E> and R.H. Wilhelm, "Diffusion in Beds of Porous Solids, "Ind. Eng. Chem., 45(6), 1219, 1953

Dore, J.C., and P.C. Wankat, "Multicomponent Cycling Zone Adsorption," Chem. Engr. Sci., 32, 1976, p.921

Gluechauf,E., Trans. Faraday Soc. 51, 34, 1955

Gregory, R.A. "Comparison of Parametric Pumping with Conventional Adsorption," AIChE Journal, 20, 1974, p.294-300

Grushka, E., Snyder, L.R., and Knox, J.H., "Advances in Brand Spreading Theories", J. Chromat. Sci., 13, 1975, p.25

Gupta, R., and N.H. Sweed, "Equilibrium Theory of Cycling Zone Adsorption," I&EC Foundamentals, 10, 1971, p.280

Helen, C. Hollein, Hsien-Chih Ma, Ching-Rong Huang, and Chen, H.T., "Parametric Pumping with pH and Electric Field: Protein Separation," I&EC Foundamentals, 21, 1982, p. 205-214

Hamilton, P.B., Bogue, D.C., and Anderson, R.A., "Ion Exchange Chromatography of Amino Acids Analysis of Diffusion (Mass Transfer) Mechanism", 32, 13, 1960, p.1783

Hill, F.B., Wong, Y.W. and Chan, Y.N.I., "A Temperature Swing Process for Hydrogen Isotope Separation," AIChE Journal, 28, 1982, p.1-6

Hougen, O.A. and W.R. Marshall," Adsorption from a Fluid Stream Flowing through a Stationary Branular Bed," Chem. Engr. Prog., 43, (4), 1947, p.197

James, A.T. and Martin, A.T.P., Biochem. J. 50, 679, 1950

Kasten, P.R., L. Lapidus, and N.R. Amundson, "Mathematics of Adsorption in Bed. v.s. Effect of Intraparticle Diffusion in Flow System in Fixed Bed," J. Phy. Chem., 56, 1952, p.683

Kazuhiro Nakanishi, et. al. "Ion Exchange Chromatography of Proteins prediction of Elution Curves and Operating Conditions. I, Theoretical Considerations," Biotechnology and Bioengineering, Vol. XXV, 1465, 1983

Kazuhiro Nakanishi, et. al. "Ion Exchange Chromatography of Proteins Prediction of Elution Curves and Operating Conditions, II. Experimental Verification," Biotechnology and Bioengineering. Vol. XXV, 1373, 1983

Kenlemans, A.I.M., "Gas Chromatography," Reinhold Pub. Co., New York, 1959

Knox, J.H., and M. Saleem, "Mobile and Stationary Phase Contributions to Peak Dispersion in Gas Chromatography", J. Chromatog. Sci., 10, 1972, p.80

Knox, J.H., "Partical Aspects of LC Theory", J. Chromatog. Sci., 15, 1977, p.352

Latty, J.A., "The use of Thermally Sensitive Ion Exchange Resin or Electrically Sensitive Liquid Crystals as Adsorbent," Ph.D. Dissertation, University of California, Berkeley, 1974

Lipidus, L. and N.R. Amundson, "Mathematics of Adsorption in Beds, VI. The Effect of Longitudinal Diffusion in Ion Exchange and Chromatographic Column," J. Phy. Chem., 56, 1952, p.984

Ma, Hsien-Chih., "Parametric Pumping with pH and Electric Field: Protein Separations," M.S. Thesis, 1981, NJIT

Martin, A.J.P. and Synge, R.L.M., Biochem. J. 35, 1358, 1941

Pigford, R.L., B. Baker and D.E. Blum, "Cycling Zone Adsorption, A New Separation Process," I&EC Fundamentlas, 8, 1969, p.848

R.J. Hamilton and P.A. Sewell "Introduction to high performance liquid chromatography" 2nd. edition., Chapman and Hall Ltd. London, 1982

Raghavan, N.S. and D.M. Ruthven, "Numerical Simulation of a Fixed Bed Adsorption Column by the Method of Orthogonal Collocation," AIChE J., 29(6), 922, 1983

Rasmuson, A., and I. Neretnieks, "Exact Solution of a Model for Diffusion in Particles and Longitudinal Dispersion in Packed Beds," AIChE J., 26(4), 686, 1980

Rasmuson, A., "Exact Solution of a Model for Diffusion and Transient Adsorption in Particles and Longitudinal Dispersion in Packed Beds, "AIChE J., 27(6), 1032, 1981

Rice, R.G. and Foo, S.C., "Continuous Desalination Using Cyclic Mass Transfer on Bifunctional Resins," I&EC Fundamentals, 20, 1981, p.150-155

Rolke, R.W., and Wilhelm, R.H., "Recuperative Parametric Pumping: Model Development and Experimental Evaluation," I&EC Fundamentals, 8,1969, p.235-246

Rolle, R.W. and Wilhelm, R.H., "Recuperative Parametric Pumping: Model Development and Experimental Evaluation," I&EC Fundamentals, 8, 1969, p.235-246

Rosen, J.B., "Kinetics of a Fixed Bed System for Solid Diffusion into Spherical Particles," J. Chem. Phy., 20(3), 387, 1952

Rosen, J.B., "General Numerical Solution for Solid Diffusion in Fixed Beds, "Ind. Eng. Chem., 48(6), 1590, 1954

Snyder, L.R., Anal. Chem. 39, 1967, p.698

Snyder, L.R., J. Chromatog. Sci., 7, 1969, p.352

Snyder, L.R., "A Rapid Approach to Selective the Best Experimental Conditions for High Speed Column Chromatography, Part ii," J. Chromatog. Sci., 10, 1972, p.369

Stokes, J.D. and Chen, H.T. "Design and Scale Up of A Continuous Parsametric Pumping System", I&EC Process design and development, 18, 1979, p.147-154

Stewart, H.N.M., Amos, R., and Perry, S.G., J. Chromatog. 38, 1968, p.209

Stokes, J.D. "Separastion of Muiticomponent Mixtures via Thermal Parametric Pumping", Dr. Eng. Sc. Disseration, NJIT, 1976

Stryer, "Biochemistry" 2nd. edition, W.H. Freeman and company, NY

Sweed, N.H. and Rigaudeau, J.M. "Equilibrium Theory and Scale Up of Parametric Pumping," AIChE Symposium Series, 71, No.152, 1975, p.1-5

Van Deemter, J.J., Zuiderweg, F.J., Klinkenberg, A>< "Logitudinal Diffusion and Resistance to Mass Transfer as Causes of Nonideality in Chromatography. Chem. Engr. Sci., 5, 271, 1956

Van Der Vlist, E., "Oxygen and Nitrogen Enrichment in Air By Cycling Zone Adsorption," Separation Science & Tech., 6, 1971, p.727

Wankat, P.C., "Thermal Wave Cycling Zone Adsorption," Journal of Chromatography, 88, 1974, p.211

Wankat, P.C., "Cyclic Separation Technologies," Nato Portugee Meeting, 1978

Wankat, P.C., "Continuous Recuperative Mode Parametric Pumping," Chemical Engineering Science, 33, 1978b, p.723-733

Weaver, K. and Hamrin, C.E., "Separation of Isotopes by Heatless Adsorption," Chemical Engineering Science, 29, 1974, p.1873-1882

Wilhelm, R.H., Rice, A.W. Rolke, R.W. and Sweed, N.H., "Parametric Pumping : A Dynamic Principle for Separating Fluid Mixtures," I&EC Fundamentals, 7, 1968, p.337-349

Wilhelm, R.H. and Sweed, N.H., "Parametric Pumping: Separation of Mixture of Toluene and n-Heptane", Science, 159, 1968, p.522-524

Wong, Y.W. and Hill, F.B., "Equilibrium and Kinetics Studies of Hydrogen Isotope Exchange on Vanadium Hydride," AIChE Journal, 25, 1979, p.592-599

Wong, Y.W., Hill, F.B. and Chan, Y.N.I., "Studies of the Separation of Hydrogen Isotopes by a Presure Swing Adsorption Process," Separation Science and Techonology, 15, 1980, p.423

Worthington Biochemical Corp. "Enzyme Manual", 1977

Zwiebel, I. and R.L. Gariepy, "Adsorption of Binary Mixtures in Fixed Beds," AIChE Symp. Series, 67 (117), 17, 1971

Zwiebel, I., R.L. Gariepy, and J>J> Schnitzer, "Fixed Bed Desorption Behavior of Gases with Nonlinear Equilibrium Part I. Dilute, One Component, Isothermal System," AIChE J., 18(6), 1139, 1972

Zwiebel, I., C>M> Kralik, and J>J> Schnitzer, "Fixed Bed Desorption Behavior of Gases with Nonlinear Equilibrium: Part II. Dilute, Multicomponent, Isothermal System," AIChe J., 20(5), 915, 1974

Appendix A

Experimental Calculations and Buffer Solution System

A-1 Concentration Measurements for Hemoglobin and Albumin

Hemoglobin

The absorbance of hemoglobin (403 μm) is strongly dependent on pH level of the protein solution. Fig.90 shows the relative absorbance reading from Bausch and Lomb spectrophotometer. The pH level of solution is ranged from 4.0 to 8.5 whereas the maximum absorbance equalsto unity at pH=6.0 . It is recommended that the absorbance reading should be corrected with the pH value correspondent to sample and feed, i.e.,

$$r_H = Y_p / Y_o = R_s / R_f * k_F / k_{pH} \quad \text{(A-1)}$$

Thus, we will obtain the r_H value which is independent of pH level. Eq. A-1 can be even simplified as

$$r_H = Y_p / Y_o = R_s / k_{pH} * \text{constant} \quad \text{(A-2)}$$

where constant = k_F / R_f because pH level of feed is fixed.

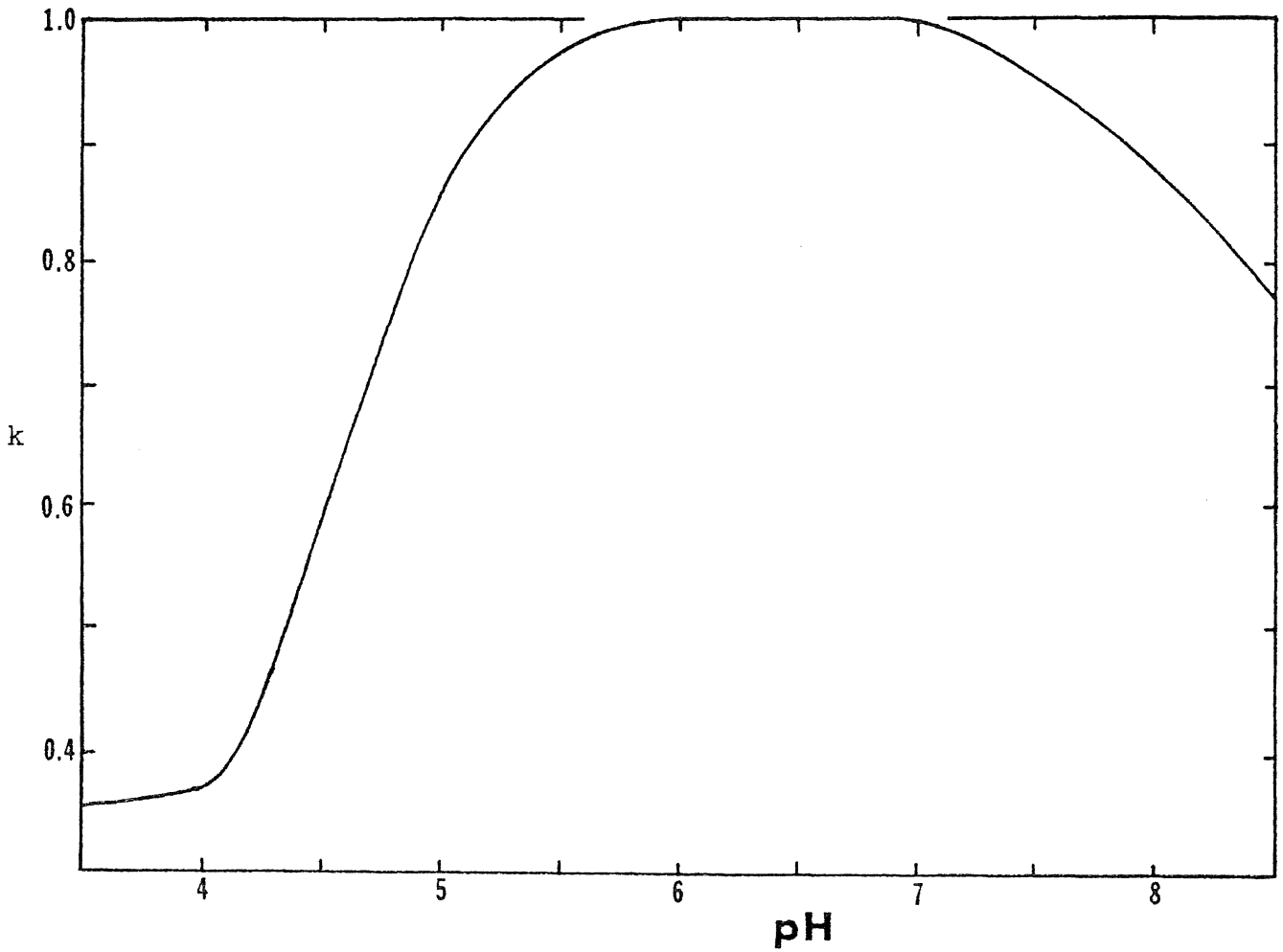

Fig. 90 pH Correlation Curve for Hemoglobin Concentration

Albumin

Total protein concentration was measured at 595 μm using Bio-Rad protein assay. The commercial dye was diluted according to the manufacture's instructions. Three to five cc of dye were used to analyze 0.1 cc sample. The buffer was also measured at both pH's and the absorbance reading at 595μm were corrected by substracting the appropriate buffer readings.

The albumin concentration is then calculated by the difference between total protein (595 μm) and hemoglobin concentration.

$$r_A = (R_s - R_B)/(R_f - R_B) * 2 - r_H \quad \text{(A-3)}$$

or $$r_A = (R_s - R_B) * \text{constant} - r_H \quad \text{(A-4)}$$

where constant= $2/(R_f - R_B)$, because pH level of feed and buffer are fixed.

Dye preparation

In stead of purchasing Bio-Rad protein assay, the dye can be prepared from stock chemicals and gives equivalent results to the Bio-Rad reagent The procedures are for 500cc dye preparation.

1. Dissolve 0.1 g Brilliant Blue G in 25ml ethyl alcohol in a 500ml beaker. Dilute to 275ml with 250ml of distilled water.

2. Drop 50ml H_3PO_4 into the former solution and dilute to 500ml with 175ml distilled water.

3. The solution is then filtrated through No.4 filter paper twice.

A-2 Concentration measurements for alkaline phosphatase

The reagent used to measure the concentration of the enzyme by detecting its activity at 405μm and 30^{o}C was that suggested by Worthington, and it consists of two parts. The preparation procedures are listed as following.

Part A

1. Weighted 8.512 gram of 2-amino-2 methyl-1 propanol (Eastman Kodak,USA) and mixed with 70ml of distilled water, then, solution was adjusted to pH=10.0 by using concentrated HCl (2-5M).

2. The former solution was diluted to 90ml by adding distilled water. Then, 0.372 gram of NaCl was dropped and pH was adjusted 10.2 .

3. The mixture was then completed to 100ml by adding distilled water, filtrated with No.4 filter paper and kept in refrigerator.

Part B

1. Measure 0.1841 gram of p-Nitrophenol Phosphate Disodium salt (J.T. Baker Chemical) and mixed completely with 18ml distilled water.

2. 0.0023 gram of Mg Acetate was dropped and the solution pH was adjusted to 7.0 by using dilute HCl. Because the pH change is sensitive to the HCl concentrated.The mixture was diluted to 20ml by using distilled water and kept in refrigerator.

The reagent was prepared by mixing A and B in the ratio of 13 to 3, respectively. The mixing of two parts solution should be done not earlier one hour before the measurement. Discard the rest of the reagent if it is unused. For analysis, 0.1ml of the sample was added to 3ml to 5ml of the reagent. The mixture was completely mixed by vibrator and allowed to react for 2-3 minutes at 30 ^{o}C; then a reading was obtained as soon as possible at wavelength of 405 μm within a fixed time range by measuring the reaction rate. Then, r_{405} is calculated;

$$r_{405} = R_s / R_f \qquad (A\text{-}5)$$

Total protein

The Bio-Rad reagent and dye preparation are discussed in Appendix A-1. The absorbance reading was obtained at 595 μm and at 30 ^{o}C. The similar procedures are followed according to albumin discussed in Appendix A-1. Thus, the r_{595} are calculated as;

$$r_{595} = (R_s - R_B) / (R_f - R_B) \qquad (A\text{-}6)$$

or $r_{595} = (R_s - R_B) * \text{constant}$

where constant= $1/(R_F - R_B)$, these two readings are fixed for feed and buffer.

A-3 Buffer solution systems

Table 33 Phosphate Buffer

The phosphate buffer was made up by mixing equal molar solutions of monobasic sodium phosphate, NaH_2PO_4, and dibasic sodium phosphate, Na_2HPO_4, until the desired pH was obtained. The correct properties may be estimated from the data below.

NaH_2PO_4, ml	Na_2HPO_4, ml	pH	NaH_2PO_4, ml	Na_2HPO_4	pH
93.5	6.5	5.7	33.0	67.0	7.1
92.0	8.0	5.8	28.0	72.0	7.2
90.0	10.0	5.9	23.0	77.0	7.3
87.7	12.3	6.0	19.0	81.0	7.4
85.0	15.0	6.1	16.0	84.0	7.5
81.5	15.0	6.2	13.0	87.0	7.6
77.5	22.5	6.3	10.5	90.5	7.7
73.5	26.5	6.4	8.5	91.5	7.8
68.5	31.5	6.5	7.0	93.0	7.9
62.5	37.5	6.6	5.3	94.7	8.0
56.5	43.5	6.7			
51.0	49.0	6.8			
45.0	55.0	6.9			
39.0	61.0	7.0			

Table 34 Tris-Maleate buffer

The Tris-maleate/NaOH buffer was made up by mixing equal molar solutions of Tris-maleate and sodium hydroxide, until the desired pH was obtained. The Tris-maleate was made up by dissolving equal mole of Tris(hydroxymethyl) aminomethane and maleic acid in one liter of distilled water. The mixing proportions for the buffer may be estimated from the data below.

Tris-maleate, ml	NaOH,ml	pH	Tris-ma, ml	NaOH, ml	pH
50	7.0	5.2	50	51	7.2
50	10.8	5.4	50	54	7.4
50	15.5	5.6	50	58	7.6
50	20.5	5.8	50	63.5	7.8
50	26.0	6.0	50	69	8.0
50	31.5	6.2	50	75	8.2
50	37.0	6.4	50	81	8.4
50	42.5	6.6	50	86.5	8.6
50	45.0	6.8			
50	48.0	7.0			

Ref: Colowich and Kaplan, Methods in Enzymology Vol.1 1955

Table 35 Acetate Buffer

The preparation of Acetate buffer was made up by mixing equal molar solutions of sodium acetate, NaAc, and Acetic acid, HAc, until the desired pH was obtained. The mixing proportions for specific pH can be estimated as follows.

HAc, ml	NaAc, ml	pH	HAc, ml	NaAc, ml	pH
46.3	3.7	3.6	20.0	30.0	4.8
44.0	6.0	3.8	14.8	35.2	5.0
41.0	9.0	4.0	10.5	39.5	5.2
36.8	13.2	4.2	8.8	41.2	5.4
30.5	19.5	4.4	4.8	45.2	5.6
25.5	24.5	4.6			

Table 36 Tris Buffer

The preparation of Tris buffer was made up by mixing equal molar solutions of Tris(hydroxymethyl) aminomethane and HCl until the desired pH was obtained. The mixing proportions for specific pH can be estimated as follows.

Tris, ml	HCl, ml	pH
50	5.0	9.0
50	8.1	8.8
50	12.2	8.6
50	16.5	8.4
50	21.9	8.2
50	26.8	8.0
50	32.5	7.8
50	38.4	7.6
50	41.4	7.4
50	44.2	7.2

Appendix B

DATA TABULATION

Table 13

Run D-76

	pH	403μ
Feed	6.05	0.450
	8.02	0.379

Note: 1. 7.5cc/sample

2. Calculation of r_H, refer to Section .

$$r_H = \frac{R_s}{k_{pH}} \times 2.308$$

No.	pH	403μ	r_H	No.	pH	403μ	r_H
1	7.83	0.058	0.147	28	6.08	0.222	0.493
2	7.03	0.017	0.040	29	6.58	0.926*	6.213
3	6.48	0.008	0.018	30	7.43	0.674*	4.313
4	6.21	0.008	0.018	31	7.90	0.638	1.645
5	6.11	0.007	0.016	32	8.02	0.421	1.111
6	6.08	0.008	0.018	33	8.02	0.383	1.010
7	6.08	0.009	0.020	34	8.03	0.359	0.948
8	6.08	0.010	0.022	35	8.03	0.286	0.755
9	6.07	0.045	0.100	36	8.03	0.156	0.412
10	6.09	0.306	0.680	37	7.90	0.056	0.144
11	6.62	0.838*	5.587	38	7.11	0.015	0.035
12	7.39	0.672*	4.480	39	6.48	0.007	0.016
13	7.86	0.696	1.777	40	6.22	0.007	0.016
14	8.01	0.427	1.124	41	6.12	0.010	0.022
15	8.02	0.382	1.008	42	6.10	0.008	0.018
16	8.02	0.364	0.960	43	6.10	0.015	0.033
17	8.02	0.290	0.765	44	6.08	0.017	0.038
18	8.02	0.152	0.401	45	6.09	0.023	0.051
19	7.78	0.064	0.161	46	6.11	0.276	0.613
20	7.08	0.018	0.037	47	6.62	0.873*	5.820
21	6.42	0.008	0.018	48	7.43	0.690*	4.600
22	6.18	0.008	0.018	49	7.92	0.682	1.745
23	6.10	0.008	0.018	50	8.02	0.431	1.137
24	6.08	0.010	0.022	51	8.04	0.394	1.043
25	6.08	0.011	0.024	52	8.04	0.365	0.965
26	6.08	0.014	0.031	53	8.03	0.286	0.755
27	6.08	0.021	0.047	54	8.03	0.157	0.414

* Sample concentration was diluted to 1/3 by adding pH 6 buffer.

Table 14

Run D-80

	pH	403μ
Feed	6.02	0.439
	8.00	0.396

Note: 1. 7.5cc/sample

2. For sample 10-15, 37-42, 64-69 are 3.75cc/sample.

3. Calculation of r_H, refer to Section . $r_H = \frac{R_s}{k_{pH}} \times 2.217$

No.	pH	403μ	r_H	No.	pH	403μ	r_H
1	6.08	0.006	0.014	28	6.08	0.008	0.018
2	6.08	0.011	0.026	29	6.05	0.007	0.016
3	6.03	0.011	0.026	30	6.05	0.012	0.027
4	6.05	0.014	0.032	31	6.05	0.013	0.030
5	6.05	0.015	0.034	32	6.05	0.016	0.036
6	6.08	0.017	0.039	33	6.05	0.018	0.041
7	6.05	0.018	0.041	34	6.05	0.021	0.048
8	6.05	0.025	0.057	35	6.05	0.026	0.059
9	6.13	1.064	2.423	36	6.12	1.088	2.478
10	6.69	1.008**	11.481	37	6.72	1.168**	13.30
11	7.25	1.130*	7.722	38	7.32	1.118*	7.640
12	7.65	1.284	3.041	39	7.64	1.131	2.676
13	7.82	0.622	1.515	40	7.82	0.594	1.319
14	7.90	0.458	1.133	41	7.88	0.462	1.138
15	7.92	0.419	1.041	42	7.90	0.421	1.042
16	7.95	0.411	1.027	43	7.92	0.376	0.931
17	7.98	0.404	1.017	44	7.98	0.407	1.025
18	8.00	0.399	1.008	45	7.98	0.405	1.020
19	8.00	0.399	1.008	46	8.00	0.402	1.015

** Sample concentration was diluted to 1/5 by adding pH 6 buffer.

* Sample concentration was diluted to 1/3 by adding pH 6 buffer.

No.	pH	403	r_H
55	6.03	0.010	0.023
56	6.03	0.010	0.023
57	6.03	0.012	0.027
58	6.03	0.013	0.030
59	6.03	0.015	0.034
60	6.03	0.016	0.036
61	6.02	0.017	0.039
62	6.02	0.021	0.048
63	6.10	0.058	1.321
64	6.60	1.024**	11.633
65	7.20	1.411*	9.868
66	7.59	1.705	3.883
67	7.80	0.692	1.680
68	7.92	0.467	1.157
69	7.92	0.418	1.035
70	7.95	0.415	1.038
71	7.95	0.408	1.021
72	7.98	0.407	1.028
73	7.98	0.398	1.003

** Sample concentration was diluted to 1/5 by adding pH 6 buffer.

* Sample concentration was diluted to 1/3 by adding pH 6 buffer.

Table 15

Run D-44-3

	pNa	pH	403μ	595μ		595μ
Feed	1.00	4.43	0.520	0.822	Buffer	0.440
	1.05	5.65	0.851	0.851		0.451

Note: 1. 3.0cc/sample

2. Calculation of r_H and r_A refer to Section

pH 4.4 to 5.05

$$r_H = \frac{R_s}{k_{pH}} \times 1.013$$

$$r_A = (R_s - 0.446) \times 5.319 - r_H$$

pH 5.05 to 7.1

$$r_H = \frac{R_s}{k_{pH}} \times 1.166$$

$$r_A = (R_s - 0.451) \times 5.00 - r_H$$

No.	pNa	pH	403μ	595μ	r_H	r_A	No.	pNa	pH	403μ	595μ	r_H	r_A
1	1.02	4.42	0.000	0.455	0.00	0.05	11	1.10	4.35	0.007	0.475	0.014	0.14
2	1.02	4.42	0.000	0.452	0.00	0.05	12	1.10	4.38	0.247	1.444	0.475	4.83
3	1.02	4.40	0.000	0.446	0.00	0.04	13	1.11	5.20	1.793	1.550*	2.260	8.73
4	1.02	4.40	0.001	0.460	0.00	0.07	14	1.08	5.55	1.513	1.599	1.800	3.74
5	1.02	4.42	0.002	0.452	0.00	0.03	15	1.08	5.65	1.226	1.187	1.447	2.23
6	0.97	4.40	0.002	0.46	0.00	0.12	16	1.08	5.70	1.102	0.911	1.295	1.00
7	0.93	4.35	0.004	0.461	0.01	0.07	17	1.08	5.68	1.050	0.862	1.233	0.82
8	0.96	4.32	0.006	0.463	0.01	0.08	18	1.08	5.70	1.008	0.890	1.184	1.04
9	1.05	4.35	0.006	0.462	0.01	0.07	19	1.08	5.70	0.985	0.836	1.157	0.77
10	1.09	4.35	0.005	0.465	0.01	0.09	20	1.07	5.70	0.925	0.867	1.087	0.99

* Sample concentration was diluted to 1/2 by adding pH 5.7 buffer.

Table 16

Run D-44-4

	pNa	pH	403μ	595μ		595μ
Feed	1.05	5.65	0.851	0.851	Buffer	0.451
	1.02	8.50	0.816	0.867		0.443

Note: 1. 3.0cc/sample

2. Calculation of r_H and r_A refer to Section

pH 5.05 to 7.1

$$r_H = \frac{R_s}{k_{pH}} \times 1.166$$

$$r_A = (R_s - 0.451) \times 5.0 - r_H$$

pH 7.1 to 8.5

$$r_H = \frac{R_s}{k_{pH}} \times 0.943$$

$$r_A = (R_s - 0.443) \times 4.72 - r_H$$

No.	pNa	pH	403μ	595μ	r_H	r_A	No.	pNa	pH	403μ	595μ	r_H	r_A
1	1.08	5.65	0.923	0.845	1.086	0.89	11	1.01	8.45	1.174	0.945	1.412	0.96
2	1.07	5.68	0.907	0.824	1.066	0.80	12	1.00	8.45	1.096	0.913	1.322	0.90
3	1.07	5.70	0.908	0.852	1.067	0.94	13	1.00	8.50	1.052	0.902	1.289	0.88
4	1.07	5.70	0.887	0.829	1.042	0.85	14	1.00	8.45	1.010	0.942	1.218	1.13
5	1.08	5.70	0.878	0.851	1.032	0.97	15	0.99	8.48	0.983	0.892	1.205	0.914
6	1.09	5.70	1.395	0.926	1.639	0.74	16	0.99	8.50	0.973	0.874	1.192	0.84
7	1.14	7.30	1.799	0.923**	8.452	2.88	17	0.99	8.50	0.956	0.873	1.172	0.857
8	1.14	7.88	0.919	0.727*	2.831	1.19	18	1.00	8.50	0.936	0.892	1.147	0.972
9	1.10	7.95	1.629	1.044	1.736	1.10	19	1.00	8.50	0.920	0.891	1.127	0.988
10	1.03	8.28	1.341	0.979	1.542	0.99	20	1.00	8.50	0.921	0.893	1.128	0.996

** Sample was diluted to 1/5 by adding pH 5.7 buffer.

* Sample was diluted to 1/3 by adding pH 5.7 buffer.

Table 17

Run D-131

	Conc.	p_{Cl}	pH	405μ	595μ
Buffer	1.0M	0.59	7.4	-	0.409
	0.6M	0.75	7.4	-	0.409
	0.5M	0.85	7.4	-	0.409
	0.4M	0.945	7.4	-	0.409
	0.3M	1.05	7.4	-	0.409
Feed	0.1M	1.60	7.4	0.0447	0.5115

Note: 1. 3.0cc/sample

2. Calculation of r_{405} and r_{595}, refer to Section

$$r_{405} = \frac{R_s}{R_f} \quad , \quad r_{595} = (R_s - 0.409) \times 9.756$$

No.	E.V.	pH	405μ	595μ	r_{405}	r_{595}	p_{Cl}
1	4cc	7.45	-	-	-	-	1.68
2	8	7.45	-	-	-	-	1.68
3	12	7.45	0	0.406	0.00	0.00	1.65
4	16	7.45	0	-	0.00	-	1.65
5	20	7.45	0	-	0.00	-	1.65
6	24	7.45	0	0.396	0.00	0.00	1.62
7	28	7.45	-	-	-	-	1.62
8	32	7.45	0	-	0.00	-	1.61
9	36	7.45	0	0.400	0.00	0.00	1.61
10	40	7.45	0	0.401	0.00	0.00	1.61
11	43	7.46	0	0.406	0.00	0.00	1.61
12	46	7.48	0	0.399	0.00	0.00	1.61
13	49	7.48	0	0.401	0.00	0.00	1.61
14	52	7.48	0	0.399	0.00	0.00	1.61
15	55	7.48	0	0.399	0.00	0.00	1.61

No.	E.V.	pH	405μ	595μ	r_{405}	r_{595}	p_{Cl}
16	58	7.58	0.009	0.433	0.20	0.234	1.47
17	61	7.78	0.155	0.565	3.47	1.52	1.20
18	64	7.68	0.155	0.478	3.47	0.673	1.10
19	67	7.48	0.050	0.425	1.118	0.156	1.10
20	70	7.42	0.012	0.416	0.268	0.068	1.10
21	73	7.42	0.005	0.407	0.112	0.00	1.10
22	76	7.42	0.00	0.409	0.00	0.00	1.10
23	79	7.42	0.005	0.408	0.112	0.00	1.06
24	82	7.48	0.011	0.461	0.246	0.510	1.00
25	85	7.50	0.006	0.500	0.134	0.890	1.00
26	88	7.45	0.004	0.521	0.089	1.090	0.95
27	91	7.42	0.003	0.510	0.067	0.990	0.93
28	94	7.41	0.003	0.489	0.067	0.780	0.95
29	97	7.41	0.003	0.497	0.067	0.860	0.95
30	100	7.41	0.011	0.491	0.246	0.800	0.97
31	103	7.49	0.019	0.500	0.425	0.887	0.87
32	106	7.48	0.009	0.435	0.200	0.253	0.85
33	109	7.45	0.006	0.417	0.134	0.078	0.85
34	112	7.45	0.005	0.415	0.112	0.058	0.85
35	115	7.45	0.002	0.411	0.045	0.019	0.82
36	118	7.49	0.002	0.407	0.045	0.00	0.90
37	121	7.49	0.006	0.416	0.134	0.068	0.87
38	124	7.50	0.007	0.416	0.157	0.068	0.82
39	127	7.49	0.004	0.409	0.089	0.00	0.80
40	130	7.45	0.004	0.403	0.089	0.00	0.78
41	133	7.43	0.003	0.401	0.067	0.00	0.75
42	136	7.41	0.003	0.399	0.067	0.00	0.78

No.	E.V.	pH	405μ	595μ	r_{405}	r_{595}	p_{Cl}
43	139	7.42	0.005	0.396	0.112	0.00	0.80
44	142	7.45	0.009	0.420	0.200	0.107	0.78
45	145	7.50	0.007	0.428	0.157	0.185	0.60
46	150	7.48	0.001	0.406	0.022	0.00	0.60
47	155	7.48	0.001	0.406	0.022	0.00	0.58
48	160	7.42	0.002	0.399	0.045	0.00	0.59
49	165	7.40	0.001	0.401	0.022	0.00	0.59
50	170	7.40	0.002	0.413	0.045	0.038	0.59

Table 18

Run D-132

	Conc.	p_{Cl}	pH	405μ	595μ
Buffer	0.1M	1.60	7.4	-	0.404
	0.3M	1.05	7.4	-	0.403
	1.0M	0.59	7.4	-	0.404
Feed	0.1M	1.60	7.4	0.046	0.5145

Note: 1. 3.0cc/sample

2. Calculation of r_{405} and r_{595}, refer to Section

$$r_{405} = \frac{R_s}{0.046} \quad , \quad r_{595} = (R_s - 0.404) \times 9.050$$

No.	E.V.	pH	p_{Cl}	405μ	595μ	r_{405}	r_{595}
1	4cc	7.45	1.65	0	-	0.00	-
2	8	7.45	1.65	0	0.403	0.00	0.00
3	12	7.45	1.65	0	-	0.00	-
4	16	7.45	1.62	0	0.407	0.00	0.027
5	20	7.45	1.60	0	-	0.00	-
6	23	7.45	1.60	0	0.407	0.00	0.027
7	26	7.45	1.60	0	0.404	0.00	0.00
8	29	7.45	1.60	0	0.406	0.00	0.018
9	32	7.45	1.60	0	0.405	0.00	0.009
10	35	7.45	1.60	0	-	0.00	-
11	38	7.58	1.51	0.004	0.419	0.087	0.136
12	41	7.78	1.20	0.087	0.495	1.890	0.823
13	44	7.65	1.11	0.086	0.446	1.870	0.380
14	47	7.48	1.10	0.028	0.420	0.609	0.145

No.	E.V.	pH	p_{Cl}	405μ	595μ	r_{405}	r_{595}
15	50	7.42	1.10	0.007	0.413	0.152	0.081
16	53	7.42	1.10	0.004	0.410	0.087	0.054
17	56	7.42	1.10	0.002	0.407	0.043	0.027
18	59	7.41	1.10	0.001	0.404	0.021	0.00
19	62	7.42	1.10	0.001	0.409	0.021	0.045
20	65	7.42	1.10	0.001	0.407	0.021	0.027
21	68	7.48	1.10	0.007	0.587	0.152	1.656
22	71	7.60	0.70	0.031	0.619	0.674	1.946
23	74	7.42	0.60	0.007	0.426	0.152	0.200
24	77	7.43	0.60	0.003	0.404	0.065	0.00
25	80	7.45	0.59	0.002	0.398	0.043	0.00
26	85	7.42	0.59	0.001	0.400	0.021	0.00
27	90	7.42	0.59	0.001	0.397	0.021	0.00

Table 19

Run D-133

	Conc.	p_{Cl}	pH	405μ	595μ
Buffer	0.10M	1.59	7.4	-	0.406
	0.25M	1.13	7.4	-	0.406
	0.60M	0.75	7.4	-	-
Feed	0.10M	1.59	7.4	0.0827	0.5195

Note: 1. 3.0cc/sample

2. Calculation of r_{405} and r_{595}, refer to Section

$$r_{405} = \frac{R_s}{0.0827} \quad , \quad r_{595} = (R_s - 0.406) \times 8.81$$

No.	E.V.	pH	p_{Cl}	405μ	595μ	r_{405}	r_{595}
1	4cc	7.42	1.55	0	-	0.00	-
2	8	7.42	1.58	0.001	0.400	0.00	0.00
3	12	7.42	1.58	-	-	-	-
4	16	7.42	1.58	0	0.406	-	0.00
5	20	7.42	1.58	-	-	-	-
6	23	7.42	1.58	0.002	0.407	0.024	0.008
7	26	7.42	1.58	0.001	0.409	0.012	0.0176
8	29	7.41	1.59	0.001	0.407	0.012	0.008
9	32	7.40	1.60	0	0	0.00	0.00
10	35	7.40	1.60	0.001	0.403	0.012	0.00
11	38	7.50	1.51	0.001	0.416	0.012	0.088
12	41	7.68	1.25	0.013	0.459	0.157	0.467
13	44	7.67	1.19	0.070	0.464	0.846	0.510
14	47	7.50	1.13	0.112	0.435	1.354	0.255

No.	E.V.	pH	p_{Cl}	405μ	595μ	r_{405}	r_{595}
15	50	7.42	1.13	0.073	0.415	0.883	0.079
16	53	7.42	1.13	0.040	0.410	0.484	0.035
17	56	7.42	1.13	0.022	0.407	0.267	0.008
18	59	7.42	1.13	0.013	0.410	0.157	0.035
19	62	7.42	1.13	0.008	0.408	0.097	0.0176
20	65	7.42	1.13	0.005	0.405	0.060	0.00
21	68	7.45	1.09	0.039	0.449	0.470	0.379
22	71	7.60	0.88	0.098	0.727	1.185	2.828
23	74	7.45	0.76	0.024	0.471	0.290	0.573
24	77	7.40	0.75	0.007	0.417	0.0846	0.097
25	80	7.40	0.75	0.003	0.408	0.036	0.0176
26	85	7.40	0.75	0.003	0.407	0.036	0.008

Table 20

Run D-133.5

pH 8.5 buffer

Conc. M	0.10	0.23	0.38	0.50	1.00
p_{Cl}	2.43	1.60	1.29	1.06	0.71

pH 8.0 buffer

Conc. M	0.10	0.23	0.38	0.50	1.00
p_{Cl}	1.80	1.32	1.05	0.90	0.60

pH 7.7 buffer

Conc. M	0.10	0.23	0.38	0.50	1.00
p_{Cl}	1.68	1.23	0.98	0.87	0.58

pH 7.4 buffer

Conc. M	0.10	0.19	0.20	0.25	0.30	0.40	0.50	0.60	1.0(
P_{Cl}	1.60	1.22	1.20	1.13	1.05	0.945	0.85	0.75	0.5(

pH 7.1 buffer

Conc. M	0.10	0.23	0.38	0.50	1.00
p_{Cl}	1.56	1.18	0.93	0.82	0.55

* Buffer: Tris + HCl

Table 21

Run D-134

	Conc.	p_{Cl}	pH	405μ	595μ
Buffer	0.23M	1.12	7.4	-	0.404
	0.38M	0.92	7.4	-	0.404
	0.60M	0.75	7.4	-	0.404
Feed	0.10M	1.59	7.4	0.078	0.5165

Note: 1. 3.0cc/sample

2. Calculation of r_{405} and r_{595}, refer to Section

$$r_{405} = \frac{R_s}{0.078} \quad , \quad r_{595} = (R_s - 0.404) \times 8.889$$

No.	E.V.	pH	p_{Cl}	405μ	595μ	r_{405}	r_{595}
1	5cc	7.50	1.57	-	-	-	-
2	10	7.51	1.57	0.00	0.405	0.00	0.009
3	15	7.51	1.57	-	-	-	-
4	20	7.50	1.58	0.00	0.408	0.00	0.035
5	23	7.50	1.58	0.00	-	0.00	-
6	26	7.50	1.58	0.001	0.045	0.0128	0.009
7	29	7.51	1.52	0.00	-	0.00	-
8	32	7.51	1.52	0.001	0.405	0.0128	0.009
9	35	7.51	1.53	0.001	0.403	0.0128	0.00
10	38	7.65	1.48	0.001	0.405	0.0128	0.009
11	41	7.79	1.25	0.002	0.415	0.0256	0.098
12	44	7.75	1.21	0.012	0.444	0.1538	0.356
13	47	7.56	1.17	0.061	0.448	0.782	0.391
14	50	7.43	1.15	0.066	0.422	0.846	0.160
15	53	7.42	1.14	0.052	0.406	0.6667	0.018

No.	E.V.	pH	p_{Cl}	405μ	595μ	r_{405}	r_{595}
16	56	7.42	1.14	0.041	0.405	0.5256	0.009
17	59	7.41	1.14	0.029	0.405	0.3718	0.009
18	62	7.42	1.14	0.023	0.404	0.2948	0.00
19	65	7.41	1.14	0.016	0.403	0.2051	0.00
20	68	7.41	1.17	0.013	0.405	0.1667	0.009
21	71	7.42	1.15	0.010	0.405	0.1282	0.009
22	74	7.41	1.14	0.007	0.403	0.0897	0.00
23	77	7.41	1.11	0.02	0.412	0.2564	0.071
24	80	7.54	0.97	0.054	0.445	0.6923	0.364
25	83	7.50	0.95	0.028	0.460	0.3589	0.498
26	86	7.45	0.92	0.014	0.454	0.1790	0.444
27	89	7.45	0.92	0.008	0.456	0.1026	0.462
28	92	7.45	0.93	0.006	0.440	0.0769	0.320
29	95	7.45	0.93	0.004	0.437	0.0510	0.293
30	98	7.45	0.93	0.004	0.425	0.0510	0.187
31	103	7.43	0.92	0.002	0.415	0.0256	0.098
32	108	7.45	0.92	0.002	0.408	0.0256	0.036
33	113	7.45	0.85	0.002	0.409	0.0258	0.044
34	118	7.50	0.71	0.026	0.434	0.3330	0.267
35	123	7.40	0.72	0.008	0.412	0.1025	0.071
36	128	7.40	0.72	0.002	0.403	0.0256	0.00

Table 22

Run D-135

	Conc.	p_{Cl}	pH	405μ	595μ
Buffer	0.21M	1.22	7.4	-	0.405
	0.35M	1.00	7.4	-	0.405
	0.60M	0.75	7.4	-	0.405
Feed	0.10M	1.59	7.4	0.044	0.510

Note: 1. 3.0cc/sample

2. Calculation of r_{405} and r_{595}, refer to Section

$$r_{405} = \frac{R_s}{0.044} \quad , \quad r_{595} = (R_s - 0.405) \times 9.5238$$

No.	E.V.	pH	p_{Cl}	405μ	595μ	r_{405}	r_{595}
1	5cc	7.50	1.52	-	-	-	-
2	10	7.50	1.57	0	-	0	-
3	15	7.50	1.57	-	-	0	-
4	20	7.50	1.58	0.001	-	0.0227	-
5	23	7.50	1.59	-	-	0	-
6	26	7.50	1.58	0.001	-	0.0227	-
7	29	7.50	1.58	0	-	0	-
8	32	7.50	1.59	0.001	0.401	0.0227	0
9	35	7.51	1.58	0	0.402	0	0
10	38	7.54	1.50	0	0.410	0	0.0476
11	41	7.70	1.35	0.001	0.408	0.0227	0.0286
12	44	7.71	1.30	0.002	0.419	0.0455	0.1333
13	47	7.60	1.26	0.003	0.451	0.0682	0.4380
14	50	7.45	1.22	0.009	0.433	0.2045	0.2667
15	53	7.40	1.21	0.012	0.414	0.2727	0.0857

No.	E.V.	pH	p_{Cl}	405μ	595μ	r_{405}	r_{595}
16	56cc	7.40	1.20	0.015	0.404	0.3410	0
17	59	7.40	1.20	0.017	0.413	0.3860	0.0760
18	62	7.41	1.20	0.016	0.405	0.3640	0
19	65	7.40	1.20	0.016	0.404	0.3640	0
20	68	7.40	1.20	0.012	0.401	0.2727	0
21	71	7.40	1.20	0.010	0.403	0.2270	0
22	74	7.40	1.20	0.009	0.402	0.2045	0
23	77	7.40	1.18	0.021	0.407	0.4770	0.0286
24	80	7.52	1.09	0.045	0.420	1.0230	0.1429
25	83	7.47	1.00	0.017	0.421	0.3860	0.1523
26	86	7.40	1.00	0.007	0.428	0.1590	0.2190
27	89	7.40	1.00	0.007	0.429	0.1590	0.2286
28	92	7.40	1.00	0.004	0.435	0.0900	0.2857
29	95	7.40	0.99	0.003	0.421	0.0682	0.1524
30	98	7.40	0.99	0.004	0.426	0.0900	0.2000
31	103	7.40	1.00	0.003	0.413	0.0682	0.0762
32	108	7.40	1.00	0.002	0.418	0.0455	0.1238
33	113	7.40	1.00	0.001	0.418	0.0227	0.1238
34	118	7.49	0.90	0.018	0.491	0.4090	0.8190
35	123	7.39	0.80	0.006	0.429	0.1360	0.2286
36	128	7.35	0.72	0.002	0.405	0.0455	0
37	133	7.35	0.74	0.000	0.406	0	0
38	138	7.35	0.74	0.001	0.406	0.0227	0

Table 23

Run D-136

	Conc.	p_{Cl}	pH	405μ	595μ
Buffer	0.21M	1.21	7.4	-	0.4125
	0.22M	1.19	7.4	-	0.4125
	0.23M	1.17	7.4	-	0.4125
	0.24M	1.15	7.4	-	0.4125
	0.25M	1.13	7.4	-	0.4125
	0.60M	0.75	7.4	-	0.4125
Feed	0.10M	1.60	7.4	0.0535	0.511

Note: 1. 3.0cc/sample

2. Calculation of r_{405} and r_{595}, refer to Section

$r_{405} = \frac{R_s}{0.0535}$, $r_{595} = (R_s - 0.4125) \times 10.152$

No.	E.V.	pH	p_{Cl}	405μ	595μ	r_{405}	r_{595}
1	5cc	7.55	1.50	-	-	-	-
2	10	7.55	1.52	0	0	0	0
3	15	7.55	1.55	-	-	-	-
4	20	7.55	1.55	0	0.414	0	0.0150
5	23	7.55	1.58	-	-	-	-
6	26	7.55	1.58	0.002	0	0.037	0
7	29	7.55	1.59	0.001	-	0.019	-
8	32	7.55	1.59	0.001	0.413	0.019	0.0100
9	35	7.52	1.59	0.001	0.414	0.019	0.0150
10	38	7.60	1.50	0	0.417	-	0.0457
11	41	7.75	1.34	0.002	0.417	0.037	0.0457
12	44	7.75	1.28	0.004	0.426	0.074	0.1370

No.	E.V.	pH	p_{Cl}	405μ	595μ	r_{405}	r_{595}
13	47cc	7.61	1.25	0.007	0.458	0.1308	0.4620
14	50	7.49	1.22	0.008	0.440	0.1495	0.2790
15	53	7.49	1.18	0.021	0.422	0.3925	0.0960
16	56	7.49	1.18	0.031	0.419	0.5790	0.0660
17	59	7.50	1.19	0.029	0.411	0.5420	0
18	62	7.51	1.20	0.023	0.416	0.4300	0.0200
19	65	7.51	1.20	0.019	0.414	0.3550	0.0150
20	68	7.51	1.20	0.019	0.408	0.3550	0
21	71	7.51	1.15	0.014	0.414	0.2620	0.0150
22	74	7.48	1.15	0.015	0.414	0.2800	0.0150
23	77	7.43	1.15	0.015	0.411	0.2800	0
24	80	7.45	1.13	0.010	0.413	0.1870	0.0100
25	83	7.45	1.13	0.006	0.411	0.1120	0
26	88	7.48	1.13	0.004	0.413	0.0750	0.0100
27	93	7.49	1.15	0.003	0.408	0.0560	0
28	98	7.45	1.15	0.002	0.418	0.0374	0.0560
29	103	7.58	1.01	0.034	0.599	1.0090	1.8930
30	108	7.42	0.83	0.014	0.467	0.2620	0.5530
31	113	7.40	0.80	0.002	0.417	0.0370	0.0457
32	118	7.41	0.75	0.001	0.411	0.0190	0
33	123	7.40	0.75	0.002	0.407	0.0370	0

Table 24

Run D-137

	Conc.	p_{Cl}	pH	405μ	595μ
Buffer	0.21M	1.21	7.4	-	0.426
	0.25M	1.13	7.4	-	0.426
	0.27M	1.095	7.4	-	0.426
	0.29M	1.05	7.4	-	0.426
	0.60M	0.75	7.4	-	0.426
Feed	0.10M	1.60	7.4	0.104	0.5235

Note: 1. 3.0cc/sample

2. Calculation of r_{405} and r_{595}, refer to Section

$$r_{405} = \frac{R_s}{0.104} \quad , \quad r_{595} = (R_s - 0.426) \times 10.256$$

No.	E.V.	pH	p_{Cl}	405μ	595μ	r_{405}	r_{595}
1	5cc	7.58	1.50	-	-	-	-
2	10	7.58	1.50	0	0.427	0	0.0100
3	15	7.58	1.50	-	-	-	-
4	20	7.55	1.51	0	0.430	0	0.0410
5	23	7.50	1.58	-	-	-	-
6	26	7.50	1.58	0	0.428	0	0.0205
7	29	7.50	1.58	0	0.430	0	0.0410
8	32	7.48	1.60	0.001	0.429	0.0096	0.0300
9	35	7.50	1.60	0.003	0.430	0.0288	0.0410
10	38	7.55	1.53	0.001	0.430	0.0096	0.0410
11	41	7.71	1.35	0.002	0.433	0.0192	0.0718
12	44	7.71	1.30	0.004	0.443	0.0385	0.1740
13	47	7.64	1.25	0.008	0.468	0.0769	0.4307

No.	E.V.	pH	p_{Cl}	405μ	595μ	r_{405}	r_{595}
14	50cc	7.45	1.23	0.036	0.466	0.3460	0.4100
15	53	7.50	1.22	0.120	0.451	1.1540	0.2560
16	56	7.50	1.18	0.117	0.436	1.1250	0.1025
17	59	7.45	1.17	0.081	0.431	0.7790	0.0510
18	62	7.45	1.12	0.044	0.435	0.4230	0.0920
19	65	7.50	1.10	0.030	0.432	0.2880	0.0610
20	68	7.50	1.09	0.016	0.430	0.1540	0.0410
21	73	7.42	1.09	0.006	0.432	0.0577	0.0615
22	78	7.40	1.05	0.003	0.431	0.0288	0.0513
23	83	7.40	1.05	0.003	0.433	0.0288	0.0720
24	88	7.45	0.95	0.038	0.600	0.3650	1.7850
25	93	7.40	0.78	0.008	0.480	0.0769	0.5540
26	98	7.40	0.75	0.001	0.431	0.0096	0.0510
27	103	7.40	0.72	0.001	0.427	0.0096	0.0100
28	108	7.39	0.73	0.001	0.427	0.0096	0.0100

Table 25

Run D-138

	Conc.	p_{Cl}	pH	405μ	595μ
Buffer	0.40M	0.95	7.4	-	0.428
	0.60M	0.75	7.4	-	0.428
Feed	0.10M	1.60	7.4	0.1075	0.527

Note: 1. 3.0cc/sample

2. Calculation of r_{405} and r_{595}, refer to Section

$r_{405} = \frac{R_s}{0.1075}$, $r_{595} = (R_s - 0.428) \times 10.101$

No.	E.V.	pH	p_{Cl}	405μ	595μ	r_{405}	r_{595}
1	5cc	7.58	1.55	-	-	-	-
2	10	7.60	1.58	0	0.433	0	0.050
3	15	7.60	1.59	-	-	-	-
4	20	7.60	1.58	0	0.432	0	0.040
5	23	7.64	1.58	-	-	-	-
6	26	7.64	1.58	0	0.432	0	0.040
7	29	7.62	1.57	0	0.430	0	0.020
8	32	7.62	1.57	0.001	0.432	0.0093	0.040
9	35	7.62	1.57	0.001	0.427	0.0093	0
10	38	7.70	1.48	0.012	0.444	0.1120	0.162
11	41	7.96	1.15	0.283	0.548	2.6330	1.212
12	44	7.68	0.95	0.169	0.552	1.5720	1.253
13	47	7.50	0.95	0.054	0.533	0.5020	1.060
14	50	7.45	0.95	0.016	0.484	0.1490	0.566
15	53	7.45	0.95	0.010	0.462	0.0930	0.343

No.	E.V.	pH	p_{Cl}	405μ	595μ	r_{405}	r_{595}
16	56cc	7.48	0.95	0.005	0.444	0.0465	0.162
17	59	7.45	0.95	0.004	0.433	0.0372	0.050
18	62	7.45	0.95	0.002	0.430	0.0186	0.020
19	65	7.45	0.94	0.004	0.426	0.0372	0
20	68	7.49	0.91	0.011	0.435	0.1023	0.070
21	71	7.52	0.82	0.013	0.440	0.1209	0.121
22	74	7.49	0.75	0.005	0.427	0.0465	0
23	77	7.45	0.75	0.002	0.425	0.0186	0
24	80	7.45	0.75	0.001	0.421	0.0093	0

Table 26

Run D-139

	Conc.	p_{Cl}	pH	405μ	595μ
Buffer	0.35M	1.00	7.4	-	0.426
	0.60M	0.75	7.4	-	0.426
Feed	0.10M	1.60	7.4	0.1155	0.548

Note: 1. 3.0cc/sample

2. Calculation of r_{405} and r_{595}, refer to Section

$r_{405} = \frac{R_s}{0.1155}$, $r_{595} = (R_s - 0.426) \times 8.1967$

No.	E.V.	pH	p_{Cl}	405μ	595μ	r_{405}	r_{595}
1	5cc	7.52	1.60	-	-	-	-
2	10	7.52	1.60	0	0.426	0	0
3	15	7.52	1.60	-	-	-	-
4	20	7.52	1.60	0.001	0.432	0.0087	0.0490
5	23	7.52	1.60	-	-	-	-
6	26	7.52	1.60	0.001	0.430	0.0087	0.0328
7	29	7.52	1.60	0.001	0.430	0.0087	0.0328
8	32	7.52	1.60	0.001	0.435	0.0087	0.0738
9	35	7.53	1.60	0.002	0.427	0.0173	0.0082
10	38	7.59	1.50	0.007	0.441	0.0606	0.1230
11	41	7.83	1.19	0.276	0.539	2.3900	0.9260
12	44	7.69	1.00	0.218	0.495	1.887	0.5930
13	47	7.50	1.00	0.066	0.471	0.571	0.3690
14	50	7.50	1.00	0.027	0.464	0.234	0.3110
15	53	7.49	0.99	0.017	0.470	0.147	0.3607

No.	E.V.	pH	p_{Cl}	405 μ	595 μ	r_{405}	r_{595}
16	56cc	7.49	0.98	0.011	0.463	0.0950	0.3030
17	59	7.49	0.98	0.007	0.459	0.0606	0.2700
18	62	7.49	0.98	0.007	0.455	0.0606	0.2377
19	65	7.49	0.95	0.006	0.450	0.0519	0.1967
20	68	7.50	0.91	0.027	0.479	0.2340	0.4340
21	71	7.55	0.80	0.052	0.543	0.4500	0.9590
22	74	7.51	0.75	0.015	0.454	0.1300	0.2295
23	77	7.48	0.74	0.006	0.437	0.0519	0.0902
24	80	7.48	0.75	0.003	0.431	0.0260	0.0410

Table 27

Run D-140

	Conc.	P_{Cl}	pH	405μ	595μ
Buffer	0.20M	1.20	7.4	-	0.413
	0.60M	0.75	7.4	-	0.413
Feed	0.10M	1.60	7.4	0.1145	0.4715

Note: 1. 3.0cc/sample

2. Calculation of r_{405} and r_{595}, refer to Section

$$r_{405} = \frac{R_s}{0.1145}, \quad r_{595} = (R_s - 0.413) \times 17.094$$

No.	E.V.	pH	P_{Cl}	405μ	595μ	r_{405}	r_{595}
1	5cc	7.48	1.60	-	-	-	-
2	10	7.48	1.60	0	0.409	0	0
3	15	7.48	1.60	-	-	-	-
4	20	7.48	1.60	0	0.410	0	0
5	23	7.48	1.60	-	-	-	-
6	26	7.48	1.60	0	0.414	0	0.0170
7	29	7.48	1.60	0.002	0.413	0.0175	0
8	32	7.49	1.60	0	0.414	-	0.0170
9	35	7.49	1.58	0.002	0.421	0.0175	0.1367
10	38	7.50	1.53	0.002	0.418	0.0175	0.0855
11	41	7.68	1.32	0.002	0.409	0.0175	0
12	44	7.70	1.30	0.003	0.418	0.0262	0.0855
13	47	7.64	1.27	0.005	0.432	0.0437	0.3248
14	50	7.49	1.22	0.009	0.430	0.0786	0.2906
15	53	7.45	1.20	0.016	0.425	0.1397	0.2051

No.	E.V.	pH	p_{Cl}	405μ	595μ	r_{405}	r_{595}
16	56cc	7.40	1.20	0.014	0.422	0.1222	0.1538
17	59	7.41	1.20	0.028	0.418	0.2440	0.0855
18	62	7.42	1.20	0.031	0.415	0.2707	0.0342
19	65	7.42	1.15	0.036	0.413	0.3144	0
20	68	7.42	1.10	0.172	0.431	1.5020	0.3077
21	71	7.60	0.90	0.315	0.590	2.7510	3.0260
22	74	7.42	0.75	0.055	0.455	0.4800	0.7180
23	77	7.40	0.75	0.012	0.419	0.1048	0.1026
24	80	7.40	0.75	0.005	0.418	0.0437	0.0855

Table 28

Run D-141

	Conc.	p_{Cl}	pH	405μ	595μ
Buffer	0.21M	1.21	7.4	-	0.408
	0.23M	1.14	7.4	-	0.408
	0.24M	1.13	7.4	-	0.408
	0.25M	1.12	7.4	-	0.408
	0.60M	0.75	7.4	-	0.408
Feed	0.10M	1.60	7.4	0.116	0.5245

Note: 1. 3.0cc/sample

2. Calculation of r_{405} and r_{595}, refer to Section

$r_{405} = \frac{R_s}{0.116}$, $r_{595} = (R_s - 0.408) \times 8.5837$

No.	E.V.	pH	p_{Cl}	405μ	595μ	r_{405}	r_{595}
1	5cc	7.45	1.62	-	-	-	-
2	10	7.45	1.62	0	0.410	0	0.0170
3	15	7.45	1.60	-	-	-	-
4	20	7.45	1.60	0	0.408	0	0
5	23	7.49	1.60	-	-	-	-
6	26	7.49	1.60	0.001	0.409	0.0086	0.0086
7	29	7.49	1.60	0.001	0.405	0.0086	0
8	32	7.49	1.60	0.003	0.407	0.0259	0
9	35	7.50	1.60	0	0.405	0	0
10	38	7.51	1.50	0.002	0.406	0.0172	0
11	41	7.69	1.32	0.002	0.412	0.0172	0.0343
12	44	7.71	1.25	0.003	0.419	0.0259	0.0944
13	47	7.63	1.23	0.005	0.456	0.0430	0.4120

No.	E.V.	pH	p_{Cl}	405μ	595μ	r_{405}	r_{595}
14	50cc	7.49	1.20	0.017	0.442	0.1470	0.2920
15	53	7.50	1.18	0.053	0.431	0.4570	0.1970
16	56	7.49	1.13	0.068	0.417	0.5860	0.0770
17	59	7.48	1.15	0.080	0.414	0.6900	0.0515
18	62	7.45	1.15	0.067	0.412	0.5780	0.0343
19	65	7.45	1.13	0.055	0.414	0.4740	0.0515
20	68	7.43	1.12	0.041	0.417	0.3530	0.0773
21	71	7.43	1.12	0.029	0.419	0.2500	0.0944
22	76	7.42	1.12	0.022	0.411	0.1900	0.0258
23	81	7.42	1.12	0.011	0.410	0.0950	0.0172
24	86	7.42	1.12	0.008	0.412	0.0690	0.0343
25	91	7.53	1.00	0.104	0.585	0.8970	1.5193
26	96	7.49	0.77	0.039	0.498	0.3360	0.7730
27	101	7.42	0.75	0.005	0.441	0.0430	0.2830

Table 29

Run D-142

	Conc.	p_{Cl}	pH	405 μ	595 μ
Buffer	0.60M	0.75	7.4	-	0.405
	1.00M	0.59	7.4	-	0.405
Feed	0.10M	1.60	7.3	0.0316	0.4128

Note: 1. 3.0cc/sample

2. Calculation of r_{405} and r_{595}, refer to Section

$$r_{405} = \frac{R_s}{0.0316} \quad , \quad r_{595} = (R_s - 0.405) \times 133.86$$

No.	E.V.	pH	p_{Cl}	405μ	595μ	r_{405}	r_{595}
1	5cc	7.35	1.60	-	-	-	-
2	10	7.35	1.60	0.001	0.406	0.0300	0.090
3	13	7.40	1.60	0.001	0.405	0.0300	0
4	16	7.48	1.50	0.029	0.408	0.9180	0.357
5	19	7.70	1.18	0.702	0.447	22.2150	5.580
6	22	7.62	0.90	0.396	0.431	12.5300	3.436
7	25	7.48	0.78	0.034	0.407	1.0760	0.223
8	28	7.40	0.75	0.006	0.402	0.1900	0
9	31	7.42	0.73	0.003	0.404	0.0950	0
10	34	7.42	0.72	0.004	0.404	0.1266	0
11	39	7.42	0.59	0.002	0.401	0.0630	0
12	44	7.42	0.59	0.001	-	0.0300	-

Table 30

Run D-143

	Conc.	p_{Cl}	pH	405μ	595μ
Buffer	0.19M	1.22	7.4	-	0.468
	0.30M	1.05	7.4	-	0.468
	0.60M	0.75	7.4	-	0.468
Feed	0.10M	1.60	7.4	0.116	0.5955

Note: 1. 3.0cc/sample

2. Calculation of r_{405} and r_{595}, refer to Section

$$r_{405} = \frac{R_s}{0.116} \quad , \quad r_{595} = (R_s - 0.468) \times 7.843$$

No.	E.V.	pH	p_{Cl}	405μ	595μ	r_{405}	r_{595}
1	5cc	7.45	1.55	-	-	-	-
2	10	7.45	1.55	0.001	0.464	0.0086	0
3	15	7.45	1.57	-	-	-	-
4	20	7.45	1.57	0	0.471	0	0.0235
5	23	7.47	1.58	-	-	-	-
6	26	7.51	1.60	0.001	0.473	0.0086	0.0392
7	29	7.55	1.60	0.002	0.470	0.0172	0.0157
8	32	7.55	1.60	0.001	0.475	0.0086	0.0549
9	35	7.55	1.55	0.001	0.473	0.0086	0.0392
10	38	7.60	1.55	0	0.474	0	0.0470
11	41	7.72	1.37	0.001	0.471	0.0086	0.0235
12	44	7.75	1.32	0	0.466	-	0
13	47	7.71	1.30	0.001	0.477	0.0086	0.0706
14	50	7.52	1.25	0.004	0.491	0.0345	0.1804

No.	E.V.	pH	p_{Cl}	405μ	595μ	r_{405}	r_{595}
15	53cc	7.41	1.24	0.003	0.0030	0.0259	0.18800
16	56	7.40	1.22	0.003	0.4960	0.0259	0.21960
17	59	7.40	1.22	0.003	0.4870	0.0259	0.14900
18	62	7.40	1.22	0.001	0.4830	0.0086	0.11760
19	65	7.42	1.21	0.030	0.4850	0.2590	0.13300
20	68	7.52	1.09	0.239	0.5000	2.0600	0.25100
21	71	7.51	1.02	0.143	0.4910	1.2330	0.18040
22	74	7.42	1.02	0.051	0.4850	0.4397	0.13300
23	77	7.41	1.02	0.017	0.4850	0.1466	0.13300
24	80	7.41	1.02	0.010	0.4750	0.0862	0.05490
25	83	7.41	1.02	0.006	0.4750	0.0517	0.05490
26	86	7.41	1.02	0.004	0.4780	0.0345	0.07843
27	89	7.41	0.99	0.004	0.4810	0.0345	0.10200
28	92	7.41	0.98	0.041	0.5160	0.3530	0.37600
29	95	7.52	0.83	0.116	0.7700	1.0000	2.36900
30	98	7.45	0.73	0.032	0.5440	0.2759	0.59600
31	101	7.41	0.73	0.009	0.4840	0.0776	0.12550
32	104	7.41	0.73	0.004	0.4750	0.0345	0.05490
33	107	7.40	0.73	0.002	0.4650	0.0172	0
34	112	7.40	0.73	0.002	0.4665	0.0172	0

Table 31

Run D-144

	Conc.	p_{Cl}	pH	405μ	595μ
Buffer	0.19M	1.22	7.4	-	0.410
	0.22M	1.17	7.4	-	0.410
	0.23M	1.16	7.4	-	0.410
	0.24M	1.15	7.4	-	0.410
	0.25M	1.13	7.4	-	0.410
	0.60M	0.75	7.4	-	0.410
Feed	0.10M	1.60	7.4	0.081	0.518

Note: 1. 3.0cc/sample

2. Calculation of r_{405} and r_{595}, refer to Section

$$r_{405} = \frac{R_s}{0.081}, \quad r_{595} = (R_s - 0.410) \times 9.259$$

No.	E.V.	pH	p_{Cl}	405μ	595μ	r_{405}	r_{595}
1	5cc	7.60	1.58	-	-	-	-
2	10	7.65	1.59	0	0.410	0	0
3	15	7.65	1.59	-	-	-	-
4	20	7.68	1.60	0.001	0.411	0.0123	0.0092
5	23	7.68	1.60	-	-	-	-
6	26	7.65	1.60	0	0.408	0	0
7	29	7.65	1.60	0.001	0.409	0.0123	0
8	32	7.65	1.59	0.001	0.412	0.0123	0.0185
9	35	7.69	1.59	0.001	0.411	0.0123	0.0092
10	38	7.70	1.55	0	0.409	0	0
11	41	7.80	1.39	0.002	0.412	0.0247	0.0185

No.	E.V.	pH	p_{Cl}	405μ	595μ	r_{405}	r_{595}
12	44cc	7.85	1.34	0.0010	0.407	0.0123	0
13	47	7.82	1.31	0.0010	0.413	0.0123	0.0278
14	50	7.63	1.29	0.0020	0.422	0.0247	0.1110
15	53	7.52	1.25	0.0020	0.424	0.0247	0.1300
16	56	7.50	1.24	0.0020	0.425	0.0247	0.1390
17	59	7.50	1.24	0.0020	0.420	0.0247	0.0930
18	62	7.50	1.24	0.0030	0.417	0.0370	0.0648
19	68	7.50	1.23	0.0020	0.415	0.0247	0.0463
20	71	7.50	1.23	0.0030	0.413	0.0370	0.0278
21	74	7.50	1.24	0.0040	0.413	0.0490	0.0278
22	77	7.50	1.24	0.0050	0.408	0.0615	0
23	80	7.52	1.23	0.0070	0.410	0.0860	0
24	83	7.51	1.21	0.0080	0.418	0.0990	0.0740
25	86	7.52	1.21	0.0080	0.418	0.0990	0.0740
26	89	7.58	1.20	0.0270	0.410	0.3300	0
27	92	7.58	1.17	0.0400	0.412	0.4940	0.0123
28	95	7.50	1.15	0.0450	0.410	0.5560	0
29	98	7.42	1.13	0.0590	0.414	0.7280	0.0370
30	101	7.42	1.12	0.0435	0.413	0.5370	0.0278
31	104	7.41	1.12	0.0310	0.410	0.3830	0
32	107	7.41	1.11	0.0260	0.410	0.3210	0
33	110	7.41	1.11	0.0160	0.409	0.2000	0
34	113	7.41	1.10	0.0105	0.413	0.1300	0.0278
35	116	7.41	1.10	0.0080	0.411	0.0990	0

No.	E.V.	pH	p_{Cl}	405μ	595μ	r_{405}	r_{595}
36	119cc	7.41	1.11	0.005	0.412	0.0615	0.0123
37	122	7.41	1.19	0.005	0.411	0.0615	0.0092
38	125	7.41	1.21	0.002	0.411	0.0247	0.0092
39	128	7.29	1.24	0.001	0.410	0.0123	0
40	131	7.29	1.26	0.001	0.410	0.0123	0
41	134	7.38	1.23	0.002	0.411	0.0247	0.0092
42	137	7.50	1.22	0	0.414	0	0.0370
43	140	7.54	1.20	0.002	0.411	0.0247	0.0092
44	143	7.52	1.18	0.002	0.145	0.0247	0.0463
45	146	7.52	1.18	0.002	0.411	0.0247	0.0092
46	149	7.45	1.17	0.002	0.410	0.0247	0
47	152	7.42	1.18	0.002	0.417	0.0247	0.0648
48	155	7.41	1.14	0.002	0.422	0.0247	0.1110
49	158	7.41	1.12	0.002	0.412	0.0247	0.0123
50	161	7.41	1.12	0.002	0.414	0.0247	0.0370
51	164	7.41	1.12	0.002	0.415	0.0247	0.0463
52	167	7.43	1.11	0.001	0.416	0.0123	0.0560
53	170	7.45	1.10	0.003	0.411	0.0370	0.0092
54	173	7.42	1.10	0.013	0.420	0.1600	0.0930
55	176	7.58	0.90	0.110	0.720	1.3580	2.8700
56	179	7.55	0.79	0.029	0.493	0.3580	0.7680
57	182	7.50	0.78	0.007	0.417	0.0860	0.0648
58	185	7.50	0.75	0.003	0.413	0.0370	0.0278
59	190	7.50	0.75	0.002	0.417	0.0247	0.0648

Table 32

Run D-145

	Conc.	p_{Cl}	pH	405μ	595μ
Buffer	0.60M	0.75	7.4	-	0.4095
	1.00M	0.59	7.4	-	0.4095
Feed	0.10M	1.60	7.4	0.096	0.523

Note: 1. 3.0cc/sample

2. Calculation of r_{405} and r_{595}, refer to Section

$r_{405} = \frac{R_s}{0.096}$, $r_{595} = (R_s - 0.4095) \times 8.8106$

No.	E.V.	pH	p_{Cl}	405μ	595μ	r_{405}	r_{595}
1	5cc	7.58	1.60	-	-	-	-
2	10	7.58	1.60	0.0010	0.4090	$1x10^{-2}$	0
3	15	7.58	1.60	-	-	-	0
4	20	7.58	1.60	0	0.4120	0	0.0220
5	23	7.59	1.60	0	0.4140	0	0.0400
6	26	7.59	1.60	0.0010	0.4100	$1x10^{-2}$	0
7	29	7.60	1.60	0	0.4120	-	0.0220
8	32	7.60	1.58	0.0010	0.4200	$1x10^{-2}$	0.0930
9	35	7.59	1.58	0.0010	0.4150	$1x10^{-2}$	0.0485
10	38	7.63	1.35	0.0150	0.4230	0.156	0.1190
11	41	7.93	1.05	0.4235	0.8130	4.410	3.5550
12	44	7.70	0.83	0.1070	0.6040	1.110	1.7140
13	47	7.50	0.78	0.0200	0.4390	0.208	0.2600
14	50	7.48	0.75	0.0050	0.4190	0.052	0.0837
15	53	7.50	0.75	0.0030	0.4150	0.031	0.0485

No.	E.V.	pH	p_{Cl}	405μ	595μ	r_{405}	r_{595}
16	56cc	7.49	0.75	0.002	0.4140	0.02	0.0400
17	59	7.50	0.75	0.001	0.4140	0.01	0.0400
18	62	7.50	0.75	0	0.4090	0	0
19	65	7.50	0.75	0.001	0.4100	0.01	0
20	68	7.50	0.72	0.002	0.4120	0.02	0.0220
21	71	7.52	0.65	0.002	0.4315	0.02	0.1940
22	74	7.48	0.61	0.002	0.4190	0.02	0.0837
23	77	7.45	0.60	0.001	0.4140	0.01	0.0400
24	80	7.45	0.60	0.001	0.4150	0.01	0.0485